ISSN 1980-9743

Soils and Rocks

An International Journal of Geotechnical and Geoenvironmental Engineering

Volume 41, N. 1
January-April 2018

Soils and Rocks
Volume 41, N. 1
2018

SOILS and ROCKS

An International Journal of Geotechnical and Geoenvironmental Engineering

Editor Paulo Scarano Hemsi - Aeronautics Institute of Technology, Brazil

Co-editor José Couto Marques - University of Porto, Portugal

"Ad hoc" Reviewers (2018)

Soils and Rocks is indebted to all "ad hoc" reviewers.
A complete list of reviewers that contributed to the current volume of Soils and Rocks will be published here in the December issue.

Soils and Rocks publishes papers in English in the broad fields of Geotechnical Engineering, Engineering Geology and Geoenvironmental Engineering. The Journal is published in April, August and December. Subscription price is US$ 90.00 per year. The journal, with the name "Solos e Rochas", was first published in 1978 by the Graduate School of Engineering, Federal University of Rio de Janeiro (COPPE-UFRJ). In 1980 it became the official magazine of the Brazilian Association for Soil Mechanics and Geotechnical Engineering (ABMS), acquiring the national character that had been the intention of its founders. In 1986 it also became the official Journal of the Brazilian Association for Engineering Geology and the Environment (ABGE) and in 1999 became the Latin American Geotechnical Journal, following the support of Latin-American representatives gathered for the Pan-American Conference of Guadalajara (1996). In 2007 the journal acquired the status of an international journal under the name of Soils and Rocks, published by the Brazilian Association for Soil Mechanics and Geotechnical Engineering (ABMS), Brazilian Association for Engineering Geology and the Environment (ABGE) and Portuguese Geotechnical Society (SPG). In 2010, ABGE decided to publish its own journal and left the partnership.

Soils and Rocks

1978,	1 (1, 2)
1979,	1 (3), 2 (1,2)
1980-1983,	3-6 (1, 2, 3)
1984,	7 (single number)
1985-1987,	8-10 (1, 2, 3)
1988-1990,	11-13 (single number)
1991-1992,	14-15 (1, 2)
1993,	16 (1, 2, 3, 4)
1994-2010,	17-33 (1, 2, 3)
2011,	34 (1, 2, 3, 4)
2012-2017,	35-40 (1, 2, 3)
2018,	**41 (1,**

ISSN 1980-9743 CDU 624.131.1

ISSN 1980-9743

SOILS and ROCKS

An International Journal of Geotechnical and Geoenvironmental Engineering

Publication of

ABMS - Brazilian Association for Soil Mechanics and Geotechnical Engineering

SPG - Portuguese Geotechnical Society

Volume 41, N. 1, January-April 2018

Table of Contents

Articles

Soils and Rocks
v. 41, n. 1

Laboratory Parameters of a Soft Soil Deposit in Macaé, Brazil

L.M.M. Póvoa, P.N.C. Nascimento, P.C.A. Maia

Abstract. This article presents the geotechnical parameters from a laboratory investigation of a Quaternary sedimentary deposit located in a low-lying area of Macaé, Rio de Janeiro (RJ), Brazil, and, when possible, compares these parameters with those from field tests and other Brazilian studies on soft soils. The deposit is described in terms of its geological origin, physical, chemical and mineralogical characterization, compressibility, consolidation and strength. To that end, a series of laboratory tests were performed, including physical, chemical and mineralogical characterization, conventional and special consolidation, and triaxial tests. The results obtained made it possible to determine the geotechnical properties considered essential for improving knowledge on the behavior of this layer. Differences between laboratory and field parameters were observed, and the geotechnical characteristics of the Macaé deposits were found to be similar to those of other Brazilian soft soils.

Keywords: laboratory tests, Macaé, soft soil.

1. Introduction

Soft soil sedimentary deposits formed in the Quaternary period are common along the Brazilian coast. These soils normally exhibit high compressibility, elevated organic matter content, low bearing capacity and low penetration resistance.

In Brazil, a number of studies on Quaternary soft soils have been conducted over the last 50 years in cities such as Santos, Rio de Janeiro, Porto Alegre, Recife and Belém. These studies resulted in a data bank on geotechnical characterization of soft deposits that has been systematically used by engineers in these regions.

In the Norte Fluminense mesoregion, particularly in the low-lying part of the city of Macaé, there is an extensive Quaternary sedimentary deposit, which has been used to expand the urban area, due mainly to the development of the oil and gas industry.

In contrast to the rest of the Brazilian coast, studies on the geotechnical parameters for these soils are scarce in the Norte Fluminense region, especially in Macaé, and constructive problems are observed in this region due to the lack of knowledge concerning the properties of the soft soils from Macaé.

In this respect, the present study shows the results (geotechnical parameters) from laboratory tests performed on the Quaternary sedimentary deposit located in a low-lying area of Macaé, Rio de Janeiro. When possible, the results are compared to parameters from field tests and other studies on soft soils.

2. Brazilian Sedimentary Deposits

The literature contains a number of studies on soft soil deposits aimed primarily at increasing knowledge on the behavior of geotechnical structures, including investigations in Rio de Janeiro state, such as Almeida & Marques (2002), Santos (2004), Crespo Neto (2004), Sandroni & Deotti (2008), Baroni (2010), Queiroz (2013), Marques (2008), Lima & Campos (2014), Lima (2007), Baldez (2013) and Carneiro (2014).

Some of these studies enabled Futai *et al.* (2001) to develop simple stratigraphic profiles to facilitate profile comparisons (Fig. 1). Additionally, Fig. 1 shows the profiles created in the present study, which complement those developed by Futai *et al.* (2001). It is important to underscore that the Sarapuí deposit is the main Brazilian reference in terms of soft soils. Several studies have been carried out in Sarapuí, including Ortigão (1975), Antunes (1978), Sayão (1980), Gerscovich (1983) and Sandroni (1993).

The profiles in Rio de Janeiro state demonstrate that layers of sand and sandy clay are usually just below the soft soil, and that the soft soil has a thickness ranging from 5 to 15 m. Costa Filho *et al.* (1985) found that the water table in clays in the low-lying regions of Guanabara and Sepetiba bays coincides with the level of the terrain in most profiles, with slight variations throughout the year.

In addition to the Quaternary sedimentary deposits of Rio de Janeiro state, other deposits along the Brazilian coast have been investigated, including Santos (SP), Porto Alegre (RS), Florianópolis (SC), Itajaí (SC), and Porto de

Luisa Muylaert de Menezes Póvoa, Ph.D. Student, Departamento de Engenharia Civil, Universidade Estadual do Norte Fluminense Darcy Ribeiro, Campos dos Goytacazes, RJ, Brazil. e-mail: lulumuylaert@hotmail.com.
Pedro Nolasco C. Nascimento, M.Sc., Departamento de Engenharia Civil, Universidade Estadual do Norte Fluminense Darcy Ribeiro, Campos dos Goytacazes, RJ, Brazil. e-mail: pedronascimento.civil@gmail.com.
Paulo César de Almeida Maia, D.Sc., Associate Professor, Departamento de Engenharia Civil, Universidade Estadual do Norte Fluminense Darcy Ribeiro, Campos dos Goytacazes, RJ, Brazil. e-mail: maia@uenf.br.
Submitted on January 3, 2017; Final Acceptance on January 31, 2018; Discussion open until August 31, 2018.
DOI: 10.28927/SR.411003

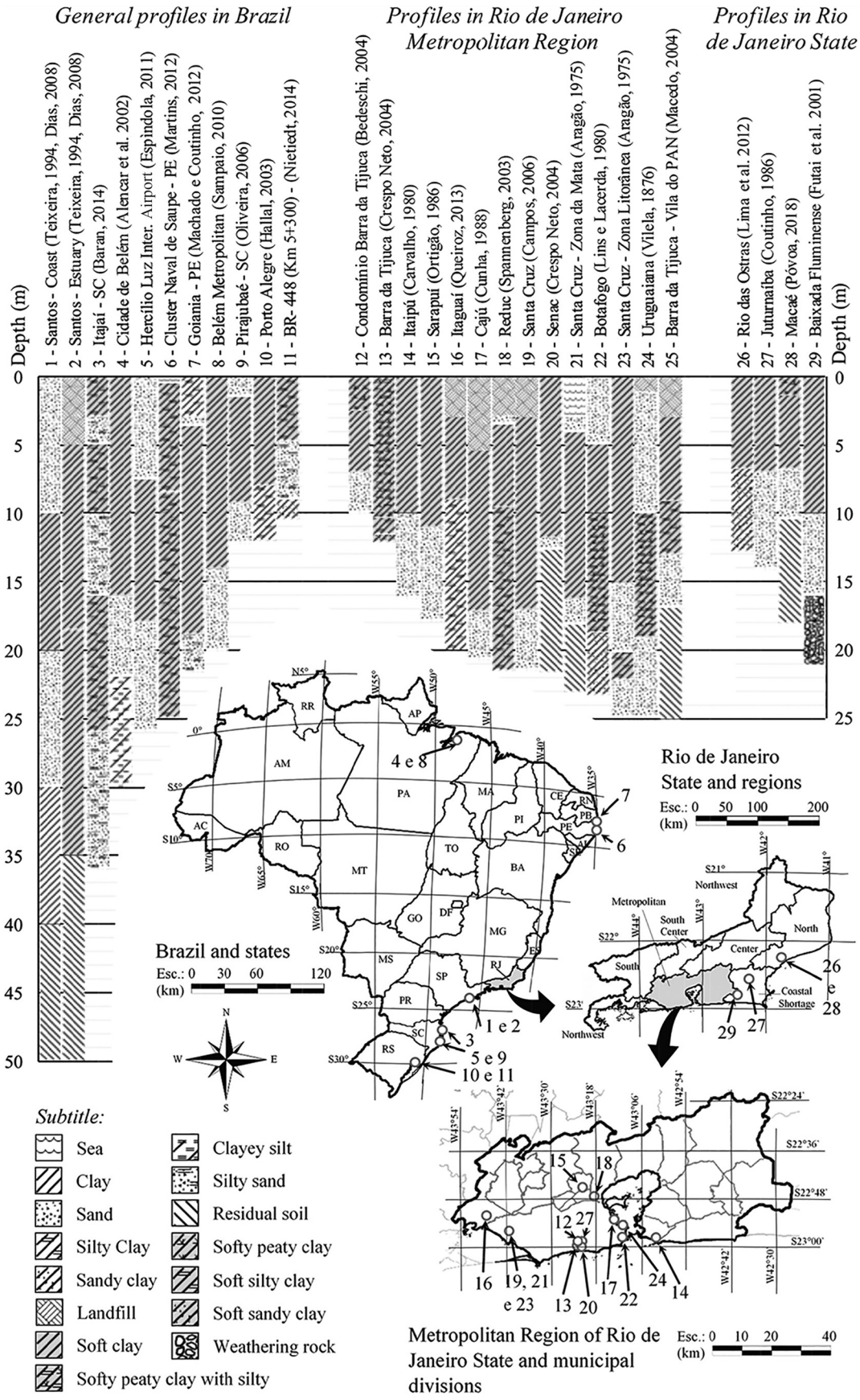

Figure 1 - Geotechnical Profiles of Soft Soils in different states in Brazil.

Saupe (PE), among others. General profiles in Brazil reveal that the clay layers may be thicker than those in Rio de Janeiro state and, once again, that the layers containing sand and silty sand are just below the soft layer. The soft soils in the stratigraphic profiles have been extensively investigated, and the geotechnical parameters are summarized in the Annex (Futai *et al.*, 2001).

3. Macaé Sedimentary Deposit

The study area is located in the sedimentary deposit on the low-lying region of Norte Fluminense, in the city of Macaé (Fig. 2). The study area is near the Macaé River, coming from the environmental protection area of Nova Friburgo, flowing for approximately 136 km and discharging in the Atlantic Ocean.

According to Martin *et al.* (1997), the study area is denominated by a coastal Quaternary cover that is related to the last cycles of marine transgression and regression, which occurred along the coast of Brazil.

Dantas *et al.* (1998) reported that the continental Quaternary sediments in this area may be the result of intense erosion, which dissected the Serra do Mar escarpment and elevated areas of the coastal lowland.

According to Dantas *et al.* (1998), the study region is part of the coastal plains domain of the coastal lowland, which contains marine and fluvial-lagoon plains of sedimentary origin, namely alluvial and colluvial soils.

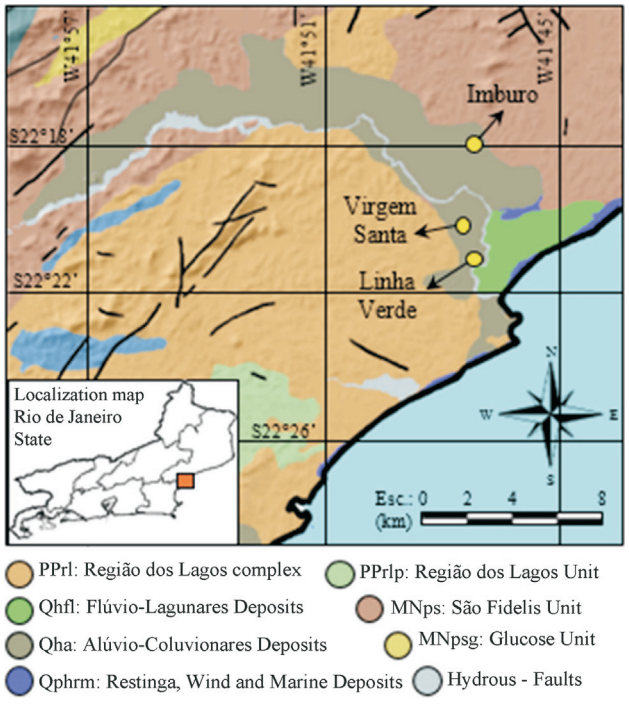

Figure 2 - Geographic location and Geological Map of the Norte Fluminense mesoregion, INEA, 2010.

Marine plains are formed by a succession of sub-horizontal sandy ridges, with a wavy microrelief of less than 5 m caused by marine sedimentation.

Fluvial-lagoon plains consist of organic clayey soil from paleolagoons, with flat, difficult-to-drain surfaces and a sub-outcrop phreatic zone.

4. Experimental Program

A battery of simple recognition probes was conducted to determine local stratigraphy. The investigation points are located in the Imburo, Linha Verde and Virgem Santa deposits (Fig. 2). The experimental program for each area is described in Table 1 and the typical stratigraphies obtained from the probes are shown in Fig. 3.

Table 1 - Experimental program.

Tests	Imburo	Linha Verde	Virgem Santa
SPT	6	12	4
Physical characterization	Complete		
Minerological characterization chemistry characterization	Complete		
Consolidation	7	-	-
Triaxial	2	-	-
CPTU	-	2	2
Experimental embankment	2	-	-

Obs: Field investigations are presented for discussion purposes and are not the objective of the study.

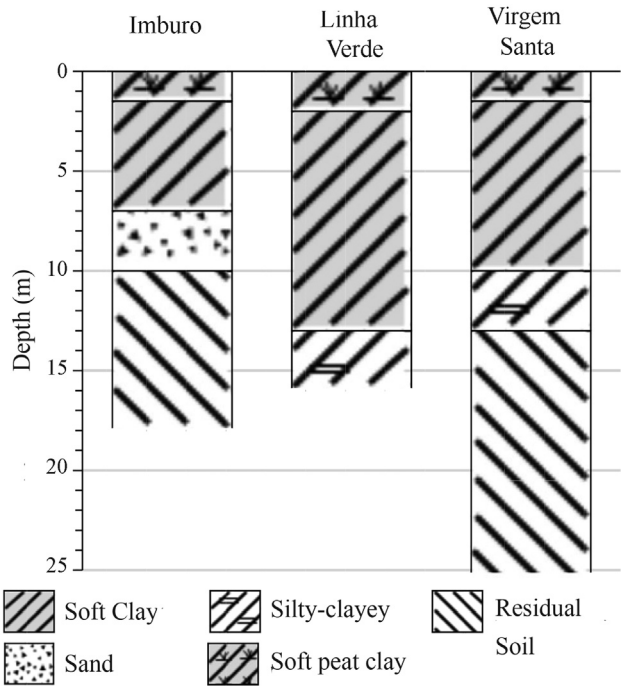

Figure 3 - Stratigraphic profile of the points investigated.

The undisturbed soft soil samples were collected using Shelby samplers (diameter = 100 mm and length = 600 mm) at maximum depths of 4.5 m. Although sampling was not performed at great depths, preliminary SPT and CPTu indicated a homogeneous layer and the samples are therefore considered representative.

The water table in general is quite shallow (about 0.5 m). Since these sites are surrounded by rivers or lagoons, the upper layer is peat, dredged material, or uncontrolled fills.

4.1. Mineralogical chemistry

The light grey odorless soft soil of Macaé has an organic matter content of approximately 7%. X-ray diffraction analyses at different deposit sites identified the presence of quartz, kaolinite and smectite.

Chemical and mineralogical analyses were conducted on samples from different depths of the sedimentary deposit. X-ray fluorescence spectrometry revealed that the soil contained a higher proportion of silicates (45.3%) and aluminates (28.1%) than the other samples, which likely indicates the existence of quartz and clay minerals such as kaolinite, smectite and illite.

Sorption complex analysis found a mean cation exchange capacity (CEC) of 83, suggesting that the samples exhibited reactivity. Moreover, associating CEC values with the clay minerals contained in the clay structure indicates the presence of smectite and vermiculite.

The mean indices of K_i and K_r, obtained by the molar ratios SiO_4/Al_2O_3 and $SiO_4/ (Al_2O_3 + Fe_2O_3)$ respectively, were 2.7 and 2.5, suggesting the presence of 2:1 clay minerals. The mean SiO_2 and Al_2O_3 contents were 26% and 16%, respectively, similar to the values reported by Campos (2006) for soft soil from the Industrial Zone of Santa Cruz, Rio de Janeiro.

Therefore, the mineralogical characterization of the soil is compatible with chemical analyses, since both indicated the presence of smectite.

The pH in water varies from 4.8 to 6, the range established by Coutinho (1986) for soft clays from Barragem de Juturnaíba, RJ. The mean value in electrical conductivity analyses was 4.5, corroborating the results of Lima *et al.* (2012) for soft clay in Rio das Ostras, RJ.

4.2. Physics

Soft soil from Macaé is composed, on average, of 65% clay, 34% silt and 1% sand. Figure 4 shows the profiles of liquidity limit (w_L), plasticity index (I_p), water content (w_n), initial void ratio (e_0) and natural specific weight (γ_{nat}). To determine the liquidity limit, the test was conducted using samples with their natural water content and no previous drying, in contrast to the standard. The decision not to dry the samples beforehand was based on the guidelines of Bjerrum (1973), who reported that liquidity limit and plasticity testing in silty clay with organic matter should be performed using samples in their natural state, since drying affects the plasticity of clay.

The water content of the surface layer (0.15 to 0.75 m deep) is 80.8%, with values ranging from 187.7% to 217.7% for the deeper layers.

The specific natural weight was approximately 12.6 kN/m^3; however, the specific weight of the surface

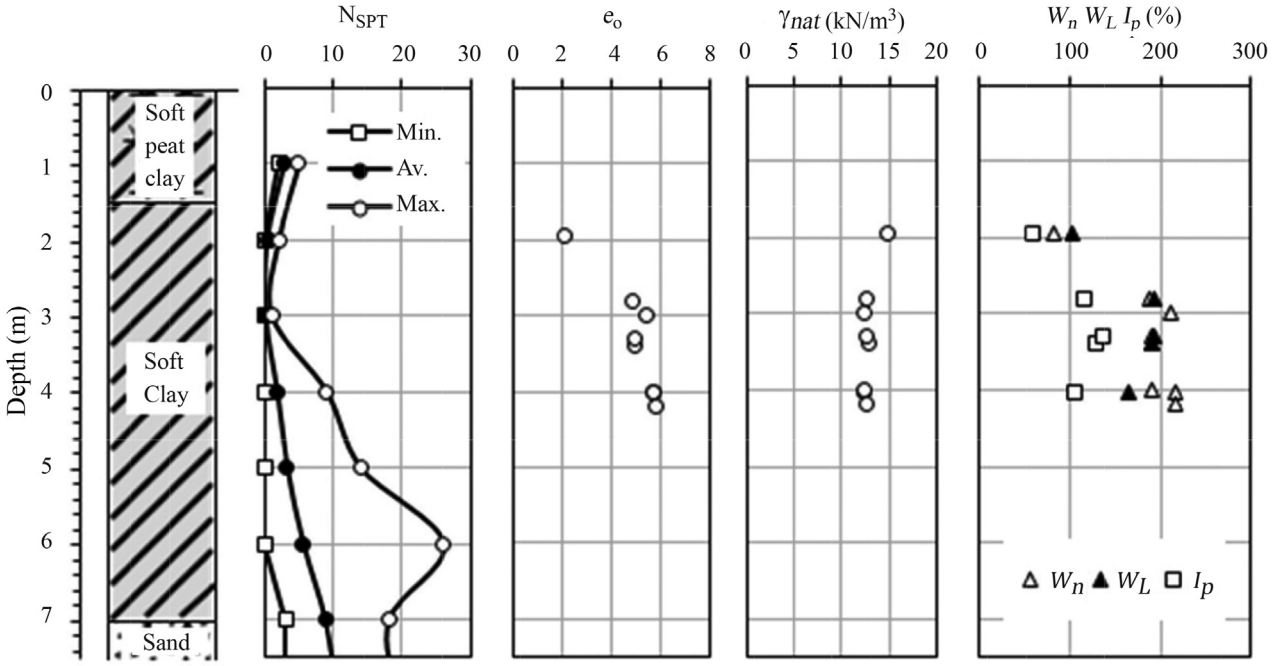

Figure 4 - Physical properties of soft clay.

layer was slightly higher than 14.9 kN/m^3. The differences in water content and specific weight in the surface layer can be explained by the seasonal water level variations in this layer.

The void index in the surface layer is 2, ranging from 4.8 to 5.7 in the rest of the soft soils, indicating that the deposit is composed of compressible soil (Póvoa *et al.*, 2016).

Relative grain density (G_s) was 2.6, showing a slight increase in depth. This behavior suggests there is no significant variation in minerology across the profile. The same observation was made by Lima & Campos (2014) for the region of Guaratiba, RJ.

The Skempton activity index classified all depths analyzed as active, except for the surface layer, which was classified as normal.

The geotechnical characterizations are compatible with chemical analyses, since cation exchange capacity (CEC) values were in line with Skempton activity indices.

4.3. Characterization of compressibility

Póvoa (2016) performed seven incremental oedometer consolidation tests (two types): conventional (AEI-1, AEI-2, AEI-3, AEI-4 and AEI-5), and with secondary compression (AEI -6 and AEI-7).

The conventional tests lasted 24 h for each loading stage and until readings stabilized at unloading. Consolidation with creep testing differed from conventional testing in that the loading stage lasted 72 h (AEI -6 and AEI-7).

Figure 5 shows that the consolidation curves of the 7 samples tested exhibit similar behavior. Two conventional tests (AEI-3, AEI-4) and one with creep measurement (AEI-7) for a depth between 2.1 and 2.7 m showed that the sample had a tendency to declining void indices if the loading stages were higher. This is also observed for depths between 1.3 and 1.9 m, where a test with a 24-h loading stage (AEI-5) and another lasting 72 h (AEI-6) were performed.

The behavior of the soft clays studied in laboratory may be affected by sample remolding. Coutinho (1976) was a pioneer in studying the quality of clay samples in Brazil. This was followed by other investigations, such as those by Ferreira (1982) and Martins & Lacerda (1994).

Technical studies conducted by Coutinho (1986), Mesri & Choi (1985), Ferreira and Coutinho (1988) and Martins & Lacerda (1994) reported that the virgin compression behaves curvilinearly rather than rectilinearly for good quality samples.

The findings of Martins & Lacerda (1994) agree with those of Coutinho (1986) for soft soil from Sarapuí I, in which the S-shaped curve is characteristic of a good quality sample. In order to validate the results of consolidation tests performed in the present study, the quality of test specimens was assessed based on the criteria of Lunne *et al.*

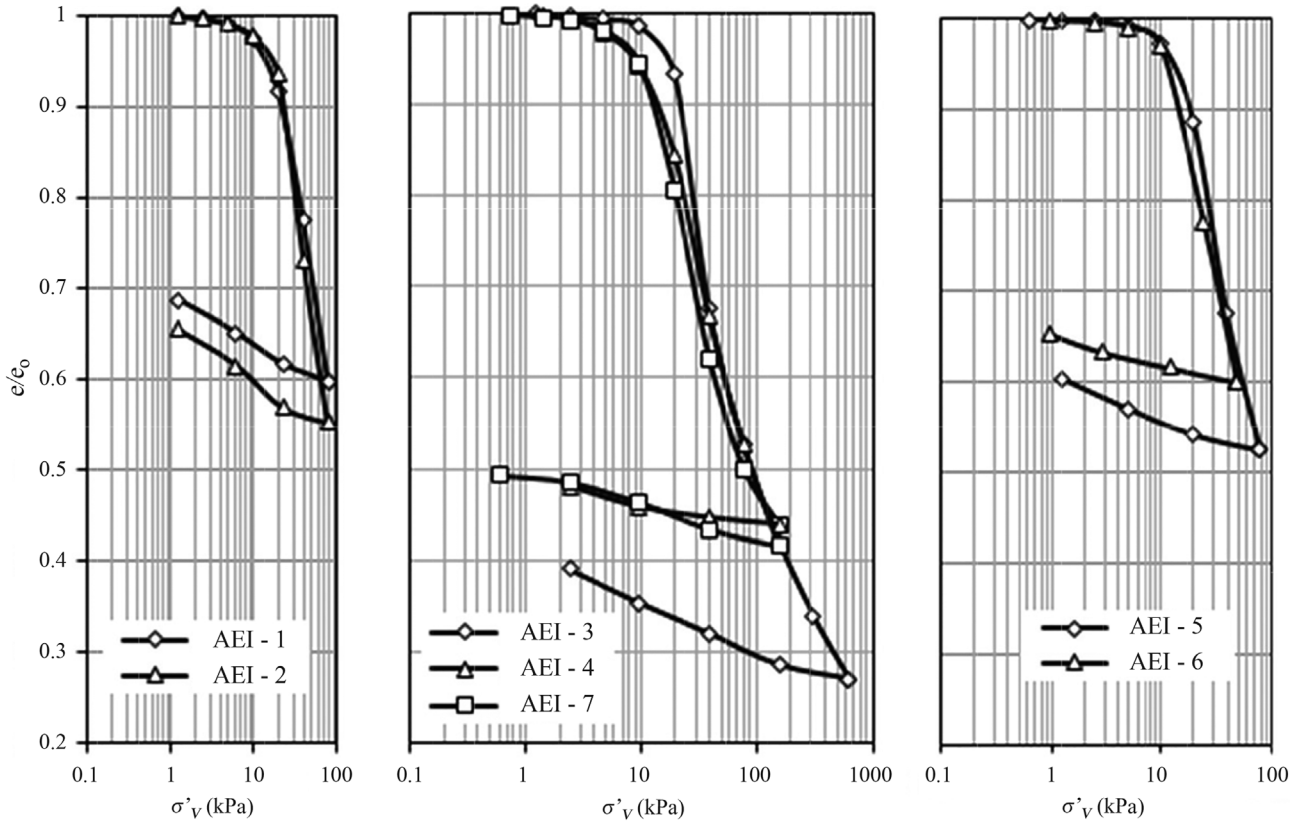

Figure 5 - Comparison between effective stress and void index curves.

(1997), Oliveira (2002), Coutinho (2007) and Andrade (2009). However, quality was only evaluated for consolidation tests with 24-h loading stages because the classification criteria considered the over consolidation ratio (*OCR*). This parameter depends on pre-consolidation stress which, in turn, is influenced by loading time. Five samples were classified as very good to excellent and one as good to fair, based on the criteria of Lunne *et al.* (1997) Oliveira (2002) and Coutinho (2007), and very good to good according to Andrade (2009).

4.3.1. C_s, C_c and C_a indices

Figure 6 shows a summary of some of the parameters obtained in oedometer tests, where C_s and C_c are the recompression and compression indices, respectively. Figure 6 also depicts C_s and C_c corrected using the method proposed by Schmertmann (1955), which takes remolding into account. In general, the corrected C_c parameters increased by an average of 19% and C_s parameters declined by an average of 12%, values similar to those reported by Oliveira (2002).

Soft soil compressibility is normally assessed using $C_c/1 + e_0$ values, given their much smaller dispersion and, according to Martins *et al.* (2006), should be considered representative of natural soft clay compressibility, rather than C_c.

Furthermore, the coefficient of secondary compression was obtained via the time *vs.* void index curve for each loading stage, based on the slope of the straight line at the end of primary consolidation, for samples AEI-6 and AEI-7. Their effective stress behavior is presented in Fig. 7. This graph shows that C_α increases with a rise in stress, reaching a peak and then declining. This behavior was also observed by authors such as Ladd (1973), Coutinho & Lacerda (1994) and Campos (2006). The variation in coefficient C_α was similar to that reported by Feijó (1991) for the coefficient of secondary compression of clay from Sarapuí. For the first loading stages, C_α values were very low, similar to those obtained by Campos (2006), who established a coefficient of secondary compression of 0.02% for the first stages. Andrade (2009) found a very small C_α value for effective vertical stress, which was half the pre-consolidation stress.

Mesri & Godlewski (1977) proposed that C_α/C_c is constant, whereas Mesri (1973) suggests that the coefficient of secondary consolidation declines with effective vertical stress.

Martins & Lacerda (1989) hypothesized that C_α should decrease over time and tend towards zero.

Secondary consolidation has been widely studied, but there is still no consensus concerning this phenomenon (Futai, 2010).

4.4. The c_v coefficient

According to Yu (2004), the coefficient of consolidation is one of the most difficult soil properties to measure in geotechnical engineering. It can be obtained from laboratory tests, *in situ* tests and retro analyses. In the present study, the coefficients of consolidation were measured in

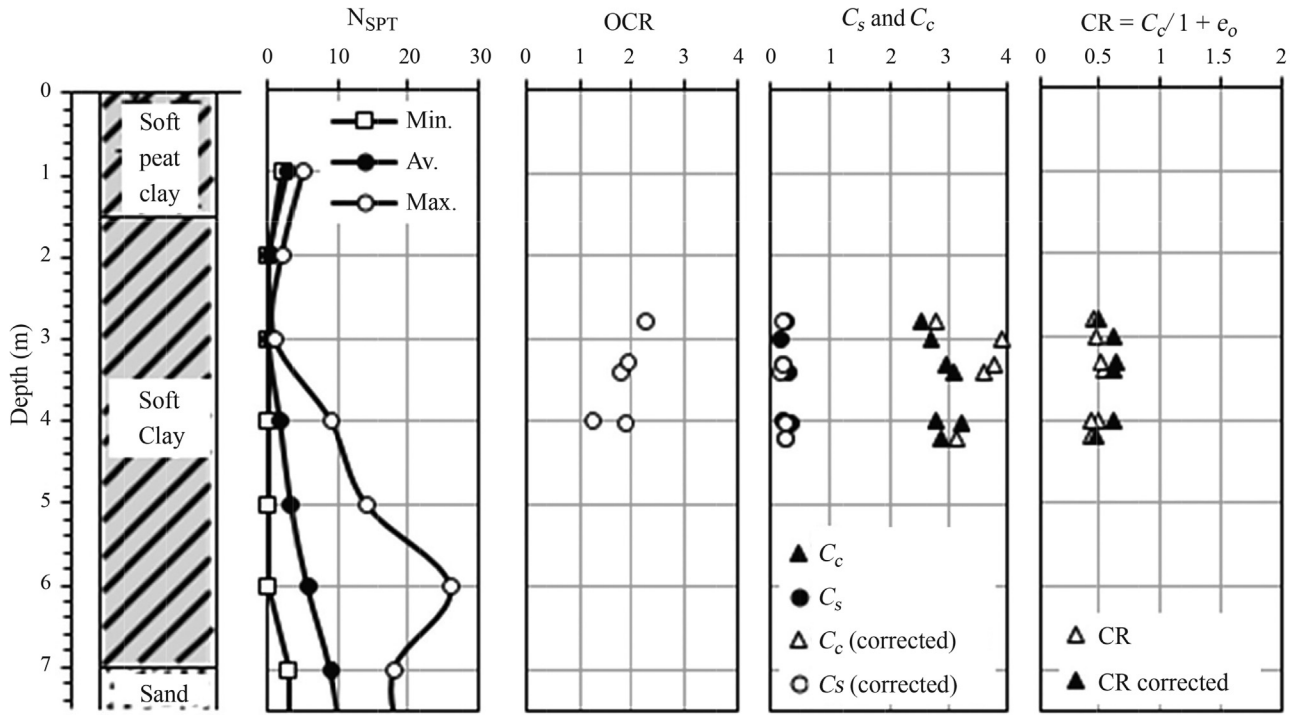

Figure 6 - Compressibility parameters of one-dimensional consolidation tests.

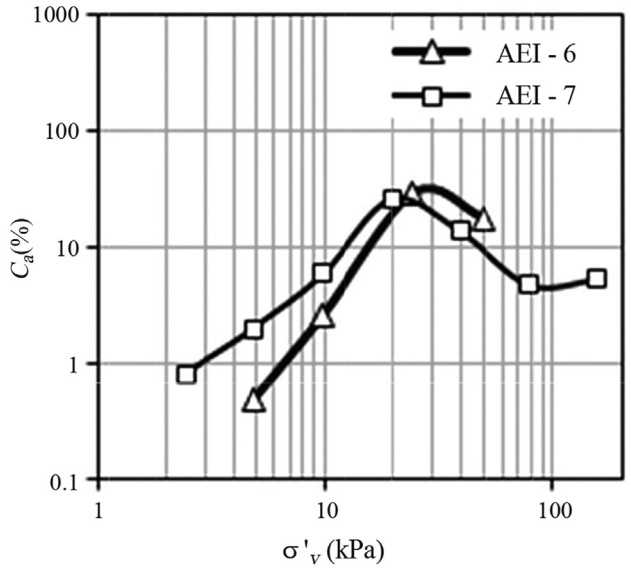

Figure 7 - log σ‘ *vs.* C_α curves of consolidation tests with creep measurement.

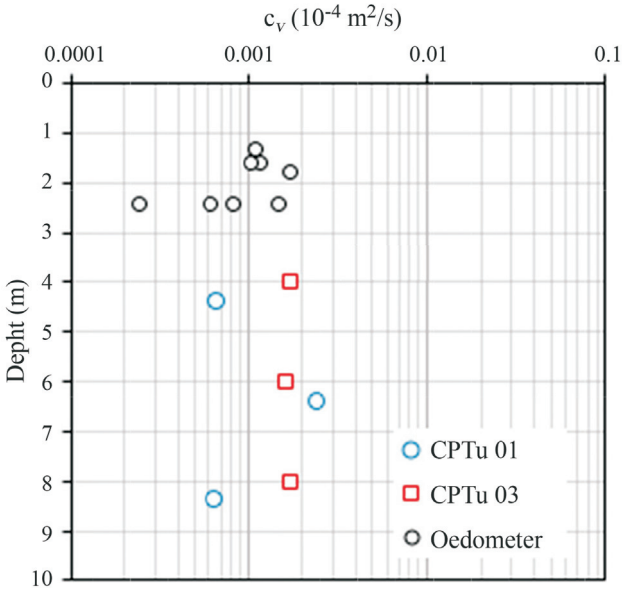

Figure 8 - Convergence of the vertical coefficients of consolidation, CPT 01 and CPT 03.

conventional oedometer consolidation tests and compared to values obtained in piezocone dissipation tests.

The horizontal coefficients of consolidation were estimated from the dispersion of excess pore-pressures in the piezocone tests and defined according to Houlsby and Teh's method (1988) and the standard procedures proposed in the literature (Lunne *et al.*, 1997; Schnaid, 2009).

These horizontal coefficients of consolidation (c_h) correspond to the soil properties in the preconsolidated range, since the material surrounding the cone is submitted to high strain levels during penetration, and then behaves like soil in recompression (Baligh & Levadoux, 1986). Coefficient of consolidation values in the overconsolidated range were calculated for 50% pore-pressure dissipation at the cone shoulder, and the t_{50} values were obtained from Δu *vs* log *t* curves using the time factor $T * 50 = 0.245$. Next, the method proposed by Jamiolkowski *et al.* (1985) was used to estimate c_h values in the normally consolidated range and transform them into the vertical coefficients of consolidation.

Figure 8 shows the vertical coefficient values estimated through consolidation and piezocone tests. The c_v values estimated using piezocone tests varied from 6.7 x 10^{-8} to 2.4 x 10^{-7} m²/s. The average c_v values estimated by consolidation tests in Imburo were similar to those estimated by piezocone tests. In addition, the overall average of the consolidation coefficients was 1.2 x 10^{-7} m²/s, which is in line with those found by Lima & Campos (2014) for the region of Guaratiba - RJ.

Figure 8 shows a difference between the c_v results obtained in the field using the CPTU test and those found in the laboratory applying the oedometer test. The ratio between coefficients c_v *in situ* and c_v in laboratory ranges from 6 to 15, corroborating the bibliography for similar soils. According to Lacerda & Almeida (1995) and Spotti (2000), this ratio for soft soil from Sesc/Senac-RJ varies between 20 and 30, the same as that observed by Gerscovich (1983) and Ortigão (1980) for clay from Sarapuí. Baroni (2010) recently obtained a relation of 6 for the Barra da Tijuca region.

One of the reasons suggested by Almeida *et al.* (2005) for the difference between c_v *in situ* and laboratory values is the influence of secondary consolidation. The authors subsequently agreed with Teixeira (2012), who reported that the fact test specimen deformability is not consistent with the real condition makes it difficult to assess the coefficient of consolidation in the laboratory and comparatively analyze the values.

4.5. The *K* coefficient

Figure 9 shows the permeability coefficient values obtained in consolidation and dissipation tests in the CPTU. It is important to underscore that Robertson's (2012), Eq. 1, was used to estimate the permeability coefficient via dissipation and piezocone tests:

$$k = \frac{c_v \gamma_n}{M} \quad (1)$$

where *M* is the oedometer modulus. As expected, the *k* coefficient declines with a rise in vertical stress (σ'_v) due to the decline in void index with an increase in σ'_v.

4.6. Characterization of undrained shear strength

The undrained shear strength of soil can be determined in laboratory tests, *in situ* tests and analyses in the same way as the vertical coefficient of consolidation. In the present study, undrained strength was measured in uncon-

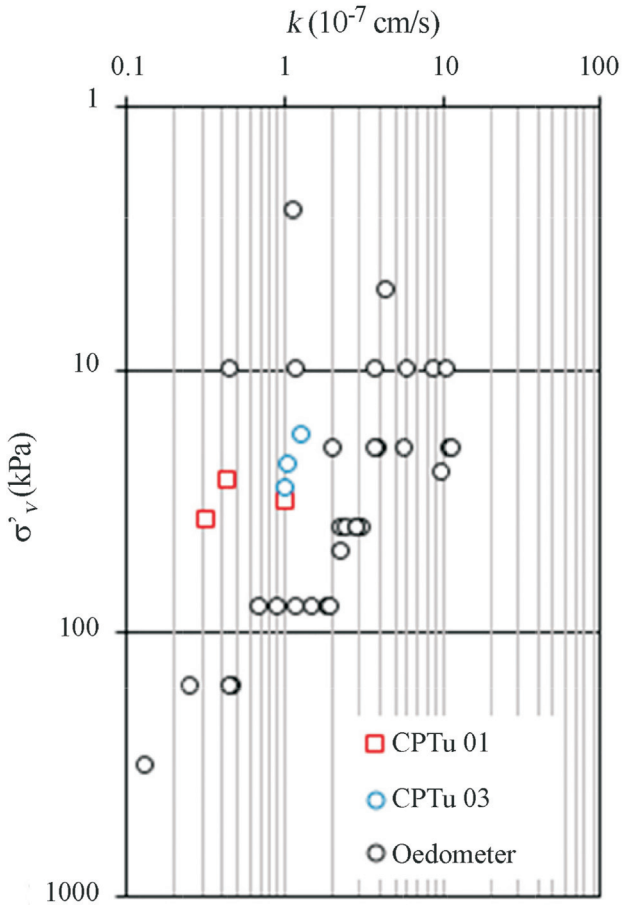

Figure 9 - Variation of the permeability coefficient *vs.* effective stress.

solidated undrained (UU) triaxial tests using a retroanalysis of an instrumented embankment in the same deposit induced to rupture, as described by Nascimento *et al.* (2016). This procedure was used to validate the estimated undrained shear strength calculated by a limited number of triaxial tests.

Undrained shear strength measured by UU triaxial tests varied between 6 and 7.5 kPa. When these results were related with the S_u of 8.8 kPa obtained by Nascimento *et al.* (2016) in a retroanalysis, a ratio between 1.2 and 1.5 was found between S_u *in situ* and S_u in laboratory. This field and laboratory ratio for undrained shear strength agrees with that obtained by different authors and deposits, as shown in Table 2.

Laboratory test results are generally lower than their field counterparts, corroborating the reports of Almeida *et al.* (2005) and Coutinho (2007). The latter associates this difference with sample disturbance, equipment conditions and the test procedures used.

The undrained shear strength values obtained for Macaé corroborate those reported by Spannenberg (2003) for Baixada Fluminense, Oliveira (2006) for Florianópolis and Sayão (1980) and Almeida *et al.* (2005) for Sarapuí.

Table 2 - Field and laboratory ratio of a number of embankments in Brazil.

Site	References	S_u *in situ*/S_u *lab*
Itaguaí - RJ	Queiroz (2013)	1.40
Sesc/Senac - RJ	Lacerda and Almeida (1995), Spotti (2000)	1.2-1.5
Sarapuí - RJ	Gerscovich (1983), Ortigão (1980)	0.77-2.30
Recife - PE	Bello (2004)	1.5
Juturnaíba - RJ	Coutinho (1986)	1.23
Macaé - RJ	Póvoa (2016), Nascimento (2016)	1.17

5. Summary of the Geotechnical and Mineralogical Properties of Macaé - RJ

The deposit is described in terms of its geological origin, physical characterization, compressibility, consolidation and strength. Table 3 presents a summary of the main geotechnical and mineralogical properties obtained for the compressible layer of Macaé - RJ. It is important to underscore that the surface layer parameters were not included in the average.

6. Conclusions

This study presented and discussed the geotechnical parameters from laboratory tests of a Quaternary sedimentary deposit located in a low-lying area of Macaé, Rio de Janeiro (RJ). The results led to the following conclusions:

- The sedimentary deposit, formed during the Quaternary period, is related to the last transgression and marine regression cycles. The thickness of the compressible layer varies between 5 and 12 m and the surface layer is signif-

Table 3 - Summary of the geotechnical and mineralogical properties of Macaé - RJ.

Minerals	Kaolini, smectite and quartz
w_n (%)	201 ± 13.7
w_L (%)	186 ± 14
Ip (%)	186 ± 14
% clay	121 ± 14
γ_{nat} (kN/m^3)	12.5 ± 0.1
% OM	7 ± 0.2
e_0	5.3 ± 0.4
*$CR = C_c/(1 + e_0)$	0.47 ± 0.04
c_v (m^2/s) x 10^{-7}	1.29 ± 0.6
Su (kPa)	7.5 ± 1.5

*Values not corrected by the Schmertmann (1955) method.

icantly affected by the natural variation in the water table in the area.

- The geotechnical and mineralogical characterizations of the soil are compatible with the chemical analyses, indicating the presence of smectite clay minerals.
- According to consolidation tests, the soft soils are slightly preconsolidated, with mean OCR of 1.8, the compression ratio (*CR*) varied from 0.42 to 0.52, considering Schmertmann's (1955) correction, and mean *CR* was 0.47, suggesting highly compressible soil.
- The behavior of log σ'_v x C_α curves of consolidation tests with creep measurement was also observed by authors such as Ladd (1973), Coutinho & Lacerda (1994) and Campos (2006).
- A comparison of the vertical coefficients of consolidation obtained from oedometer consolidation tests and CPTu tests indicates that the methods were adequate. The magnitude of c_v aaried from 2.45 x 10^{-8} to 2.4 x 10^{-7} m^2/s.
- The results of undrained shear strength, determined in UU triaxial tests, were satisfactory, since they were similar to those obtained in embankment retroanalyses. In this respect, the mean undrained shear strength estimated for the deposit was 8 kPa.
- The ratio between field and laboratory vertical coefficients of consolidation for undrained shear strength showed that the values obtained in field tests are higher than their laboratory counterparts, and that those for Macaé are compatible with the bibliography for similar soils.
- The main geotechnical and geological parameters found for soft soil from Macaé - RJ are summarized in Table 3 and suggest a close approximation with the experimental data reported in the literature for soft quaternary soils on the Brazilian coast.
- The present article is the first to characterize the Macaé deposit. As such, it does not eliminate the need for further laboratory and field investigations to better characterize the properties of the layer.

Acknowledgments

The authors would like to thank Carlos Chagas Filho Research Support Foundation of Rio de Janeiro State (FAPERJ) for financing.

References

Alencar, J.A.A.; Neto, S.F.; Saré, A.R. & Mendonça, T.M. (2002). Características geotécnicas de algumas argilas da cidade de Belém-PA. Proc. 12th Congresso Brasileiro de Mecânica dos Solos e Engenharia Geotécnica, COBRAMSEG, São Paulo, Brazil.

Almeida, M.S.S, & Marques, M.E.S. (2002). The behavior of sarapui soft organic clay. Proc. International Workshop on Characterization and Engineering Properties of Natural Soils.

Almeida, M.S.S.; Marques, E.S.; Lacerda, W.A. & Futai, M.M. (2005). Investigações de campo e de laboratório na argila do Sarapuí. Solos e Rochas, Revista Brasileira de Geotecnia, 28(1):3-20.

Alves, A.M.L. (2004). A Influência da Viscosidade do Solo e do Tempo Após a Cravação na Interação Dinâmica Estaca-Solo em Argilas. PhD Dissertation, Federal University of Rio de Janeiro, Rio de Janeiro, 350 p.

Andrade, M. (2009). Contribuição ao Estudo das Argilas moles da Cidade de Santos. MSc Dissertation, Federal University of Rio de Janeiro, Rio de Janeiro, 413 p.

Antunes, F. (1978). Ensaios Geológicos, Pedológicos e Mineralógicos nas Argilas Moles do Rio de Janeiro. Proc. Relatório IPR/DNER (2019-02.02-2/10/42).

Aragão, C.J.C. (1975). Propriedades Geotécnicas de Alguns Depósitos de Argila Mole da Área do Grande Rio. MSc Dissertation, Pontifical Catholic University of Rio de Janeiro, Rio de Janeiro.

Baldez, B. (2013). Avaliação dos Parâmetros de Compressibilidade da Camada de Argila mole da Baixada de Jacarepaguá, Após Longo Período de Sobrecarga de Aterro. MSc Dissertation, State University of Rio de Janeiro, Rio de Janeiro, 146 p.

Baligh, M.M. & Levadoux, J.N. (1986). Consolidation after undrained piezocone penetration. II: interpretation. Journal of Geotechnical Engineering, 112(7):727-745.

Baran, K.R. (2014). Propriedades Geotécnicas de Compressibilidade de uma Argila Mole de Itajaí-SC. MSc Dissertation, Federal University of Santa Catarina, Santa Catarina, 334 p.

Baroni, M. (2010). Investigação Geotécnica em Argilas Orgânicas Muito Compressíveis em Depósitos da Barra da Tijuca. MSc Dissertation, Federal University of Rio de Janeiro, Rio de Janeiro, Rio de Janeiro, 270 p.

Bedeschi, M.V. (2004). Recalques em Aterro Instrumentado Construído Sobre Depósito Muito Mole com Drenos Verticais na Barra da Tijuca, Rio de Janeiro. MSc Dissertation, Federal University of Rio de Janeiro, Rio de Janeiro, Rio de Janeiro, 184 p.

Bello, M.I.M.C.V. (2004). Estudo de Ruptura em Aterros Sobre Solos Moles Aterro do Galpão Localizado na BR-101 - PE. MSc Dissertation, Federal University of Pernambuco, Recife, 231 p.

Bjerrum, L. (1973). Problems of soil mechanics and construction on soft clays and structurally unsuitable soils (collapsible, expansive and others). State of the art report, session 4. Proc. 8th ICSMFE, Moscow, USRR, v. 3, pp. 109-159.

Campos, A.C. (2006). Características de Compressibilidade de uma Argila Mole da Zona Industrial de Santa Cruz, Rio de Janeiro. MSc Dissertation, Pontifical Catholic University of Rio de Janeiro, Rio de Janeiro, 175 p.

Carneiro, R.F. (2014). Previsão do Comportamento da Argila Mole da Baixada de Jacarepaguá: O Efeito da

Submersão e o Adensamento Secundário. MSc Dissertation, State University of Rio de Janeiro, Rio de Janeiro, 140 p.

Carvalho, J. (1980). Estudo da Compressão Secundária em Depósitos de Argila Mole de Itaipú. MSc Dissertation, Pontifical Catholic University of Rio de Janeiro, Rio de Janeiro.

Costa Filho, L.M.; Aragão, C.J.G. & Velloso, P.P.C. (1985). Características geotécnicas de alguns depósitos de argila mole na área do Rio de Janeiro, Solos e Rochas. 8(1):3-13.

Coutinho, R.Q. (1986). Aterro Experimental Instrumentado Levado à Ruptura Sobre Solos Orgânicos-Argilas Moles da Barragem de Juturnaiba. PhD Dissertation, Federal University of Rio de Janeiro, Rio de Janeiro, Rio de Janeiro, 646 p.

Coutinho, R.Q. (2007). Characterization and Engineering Properties of Recife Soft Clays-Brazil. Proc. 2th Workshop on Characterization and Engineering Properties of Natural Soils. Tan, Phoon, Higth and Leroueil (editors). Singapore, pp. 2049-2100.

Coutinho, R.Q. & Lacerda, W.A. (1994). Characterization and consolidation characteristics of Juturnaiba organic clays. Solos e Rochas, 17(2):145-154.

Coutinho, R.Q. (1976). Características de Adensamento com Drenagem Radial de uma Argila Mole da Baixada Fluminense. MSc Dissertation, Federal University of Rio de Janeiro, Rio de Janeiro, Rio de Janeiro, 206 p.

Crespo Neto, F.N. (2004). Aprimoramento do Equipamento de Palheta Elétrico Visando o Estudo do Efeito da Velocidade. MSc Dissertation, Federal University of Rio de Janeiro, Rio de Janeiro, Rio de Janeiro, 302 p.

Cunha, R.P. (1988). Análise de Ruptura de um Aterro Sanitário Sobre a Argila Mole do Caju. MSc Dissertation, Federal University of Rio de Janeiro, Rio de Janeiro, Rio de Janeiro, 253 p.

Dantas, M.E.; Ferreira, C.E.O.; Ferreira, P.P.O. & Silva, F.L.M. (1998). Domínios geomorfológicos do estado do Rio de Janeiro. Proc. 2th Simpósio Nacional de Geomorfologia, UGB, Florianópolis, Brazil, pp. 593-597.

Dias, M.S. (2008). Cidade de Santos: comparação entre as propriedades geotécnicos do subsolo de alguns trechos da orla de Santos. Proc. 6th SEFE, v. 2, pp. 331-342.

Espíndola, M.S. (2011). Análise dos Parâmetros Geotécnicos dos Solos Moles da Obra de Ampliação do Aeroporto Internacional Hercílio Luz, Florianópolis. MSc Dissertation, Federal University of Santa Catarina, Santa Catarina, 215 p.

Feijó, R.L. (1991). Relação entre a Compressão Secundária, Razão de Sobre-Adensamento e Coeficiente de Empuxo no Repouso. MSc Dissertation, Federal University of Rio de Janeiro, Rio de Janeiro, Rio de Janeiro, 182 p.

Ferreira, S.R.M & Coutinho, R.Q. (1988). Quantificação do efeito do amolgamento nas características de compressibilidade de argila mole, Rio de Janeiro e Recife. Proc. Simpósio Sobre Depósitos Quaternários das Baixadas Litorâneas Brasileiras: Origem, Características Geotécnicas e Experiências de Obras, v. 3, pp. 55-69.

Ferreira, S.R.M. (1982). Compressibilidade de Uma Argila Orgânica Mole do Recife. MSc Dissertation, Federal University of Rio de Janeiro, Rio de Janeiro, Rio de Janeiro, 235 p.

Francisco, G.M. (2004). Estudo dos Efeitos do Tempo em Estacas de Fundação em Solos Argilosos. PhD Dissertation, Federal University of Rio de Janeiro, Rio de Janeiro, Rio de Janeiro, 232 p.

Futai, M. M. (2010). Considerações Sobre a Influência do Adensamento Secundário e do Uso de Reforços em Aterros sobre Solos Moles. University of São Paulo, São Paulo, 197 p.

Futai, M.M.; Almeida, M.S.S. & Lacerda, W.A. (2001). Propriedades geotécnicas das argilas do Rio de Janeiro. Proc. Encontro Propriedades de Argilas Moles Brasileiras, Rio de Janeiro, pp. 138-165.

Gerscovich, D.M. (1983). Propriedades da Camada Ressecada do Depósito de Argila Mole de Sarapuí. MSc Dissertation, Pontifical Catholic University of Rio de Janeiro, Rio de Janeiro.

Hallal, R. (2003). Características de Depósitos de Argilas Moles no Estado do Rio Grande do Sul. MSc Dissertation, Federal University of Rio Grande do Sul, Porto Alegre, 150 p.

Houlsby, G.T. & Teh, C.I. (1988). Analysis of the piezocone in clay. Proc. ISOPT-1, Orlando, v. 2, pp. 777-783.

INEA (2010). Instituto Estadual Do Ambiente-INEA/ HD Consultoria - Relatório Final do Projeto da Estrutura Extravasora na Lagoa de Imboacica. Rio de Janeiro.

Jamiolkowski, M.; Ladd, C.C.; Germaine, J.T. & Lancellotta, R. (1985). New developments in field and laboratory testing of soils. Proc. 11th ICSMFE, San Francisco, v. 1, pp. 57-153.

Lacerda, W.A. & Almeida, M.S.S. (1995). Engineering properties of regional soils: residual soils and soft clays. Proc. 10th Panamerican Conference on Soil Mechanics and Foundation Engineering, Guadalajara, v. 4, p. 133-187.

Ladd, C.C. (1973). Estimating settlement of Structures on Cohesive Soils. Proc. MIT Soils Publication, n. 272, 99 p.

Lima, B. (2007). Modelagem Numérica da Construção de Aterro Instrumentado na Baixada Fluminense, Rio de Janeiro. MSc Dissertation, State University of Rio de Janeiro, Rio de Janeiro, 135 p.

Lima, B.; Almeida, R. & Barreto, E.C. (2012). Caracterização geotécnica de depósito de argila mole em Rio das Ostras-RJ. Proc. 16th Congresso Brasileiro de Me-

cânica dos Solos e Engenharia Geotécnica, COBRAMSEG, Porto de Galinhas, Brazil.

Lima. I. & Campos, T.M. (2014). Caracterização de um depósito de argila mole de Guaratiba-Rio de Janeiro-RJ. 17th Congresso Brasileiro de Mecânica dos Solos e Engenharia Geotécnica, COBRAMSEG, Goiânia, Brazil.

Lins, A.H.P. & Lacerda, W.A. (1980). Ensaios triaxiais de compressão e extensão na argila cinza do Rio de Janeiro em Botafogo. Solos e Rochas, Revista Brasileira de Geotecnia, 3(2):5-29.

Lunne, T.; Robertson, P.K. & Powell, J.J.M. (1997). Cone penetration testing. Proc. Geotechnical Practice, Spon Press,London, v. 20, pp. 23-35.

Macedo, E.O. (2004). Investigação da Resistência Não Drenada In Situ Através de Ensaios de Penetração de Cilindro. MSc Dissertation, Federal University of Rio de Janeiro, Rio de Janeiro, Rio de Janeiro, 120 p.

Machado, L. & Coutinho, R. (2012). Caracterização geotécnica das argilas moles na várzea de Goiana da BR-101/PE. Proc. 16th Congresso Brasileiro de Mecânica dos Solos e Engenharia Geotécnica, COBRAMSEG, Porto de Galinhas, Brazil.

Marques, M.E.S.; Lima, B.T.; Oliveira, J.R.M.; Antoniutti Netto, L. & Almeida, M.S.S. (2008). Caracterização geotécnica de um depósito de solo compressível de Itaguaí, Rio de Janeiro. Proc. 4th Congresso Luso-Brasileiro De Geotecnia, Coimbra, Portugal.

Martin, L.; Suguio, K.; Dominguez, J.M.L. & Flexor, J.M. (1997). Geologia do quaternário costeiro do litoral norte do Rio de Janeiro e Espírito Santo. Proc. CPRM; FAPESP, Belo Horizonte, Brazil, 104 p.

Martins, I.S.M. & Lacerda, W.A. (1994). Sobre a relação índice de vazios-tensão vertical efetiva na compressão unidimensional. Solos e Rochas, Revista Brasileira de Geotecnia, 17(3):157-166.

Martins, I.S.M. (2012). Ensaios de Solos em Laboratório das Amostras Retiradas no Local do Cluster Naval de Suape. Proc. Relatório PEC 16036, Fundação COPPETEC, Rio de Janeiro, RJ.

Martins, I.S.M.; Santa Maria, P.E.L. & Santa Maria, F. (2006). Investigações de campo e de laboratório na argila de Sarapuí. Solos e Rochas, 29(1):121-126.

Massad, F. (1994). Propriedades dos sedimentos marinhos. Proc. Solos do litoral de São Paulo. Mesa Redonda, ABM/ASSECOB, São Paulo, Brazil, pp. 99-128.

Mesri, G.; Kelly, W.E.; Vallee, R.P. & Andersland, O.B. (1973). Coefficient of secondary compression (discussion). Journal of Soil Mechanics & Foundations Div, v. 99, n. Proc Paper.

Mesri, G. & Choi, Y.K. (1985). Settlement analysis of embankments on soft clays. Journal of Geotechnical Engineering, 111(4):441-464.

Mesri, G. & Godlewski, P.M. (1977). Time-and stress-compressibility interrelationship. Journal of Geotechnical and Geoenvironmental Engineering, v. 103, n. ASCE 12910.

Nascimento, P.N.C.; Póvoa, L.M.M. & Maia, P.C.A. (2016). Retroanálise da ruptura de um aterro experimental instrumentado situado em Macaé-RJ. 18th Congresso Brasileiro de Mecânica dos Solos e Engenharia Geotécnica, COBRAMSEG, Belo Horizonte, Brazil.

Nietied, J.A. (2014). Aterros Instrumentados Sobre Solos Moles: Estudo de Caso na BR-448. Dissertação de Mestrado em Engenharia Civil. Rio Grande do Sul-RS, Universidade Federal do Rio Grande do Sul-UFRGS, 133 p.

Oliveira, J.T.R. (2002). A Influência da Qualidade da Amostra no Comportamento Tensão-Deformação-Resistência de Argilas Moles. PhD Dissertation, Federal University of Rio de Janeiro, Rio de Janeiro, Rio de Janeiro, 272 p.

Oliveira, J.T.R. (2006). Parâmetros geotécnicos da argila mole do Porto De Suape-PE. 13th Congresso Brasileiro de Mecânica dos Solos e Engenharia Geotécnica, COBRAMSEG, Curitiba, Brazil.

Ortigão, J.A.R. (1975). Contribuição ao Estudo de Propriedades Geotécnicas de um Depósito de Argila Mole da Baixada Fluminense. MSc Dissertation, Federal University of Rio de Janeiro, Rio de Janeiro, Rio de Janeiro, 101 p.

Ortigão, J.A.R. (1980). Aterro Experimental Levado à Ruptura Sobre Argila Cinza do Rio de Janeiro. PhD Dissertation, Federal University of Rio de Janeiro, Rio de Janeiro, Rio de Janeiro, 728 p.

Pinheiro, J.C.N. (1980). Ensaios Triaxiais em Depósito Mole Turfoso na Margem Oeste da Lagoa de Itaipú, Rio de Janeiro. MSc Dissertation, Pontifical Catholic University of Rio de Janeiro, Rio de Janeiro.

Póvoa, L.M.M. (2016). Caracterização Geotécnica de um Depósito de Solo Mole em Área de Baixada Localizada em Macaé-RJ. MSc Dissertation, State University of North Fluminense, Campos dos Goytacazes, 157 p.

Póvoa, L.M.M. & Nascimento, P.N.C. (2014). Projeto de Aterro sobre Solo Mole para Viabilizar a Ocupação em Área de Baixada Localizada em Macaé-RJ. Undergraduation Dissertation, State University of North Fluminense, Campos dos Goytacazes, 95 p.

Póvoa, L.M.M.; Nascimento, P.N.C. & Maia, P.C.A. (2016). Parâmetros físicos e de compressibilidade de um depósito de solo mole localizado em Macaé-RJ. 18th Congresso Brasileiro de Mecânica dos Solos e Engenharia Geotécnica, COBRAMSEG, Belo Horizonte, Brazil.

Queiroz, C.M. (2013). Propriedades Geotécnicas de um Depósito de Argila Mole da Região de Itaguaí-RJ. MSc Dissertation, Federal University of Minas Gerais, Belo Horizonte, 118 p.

Robertson, P.K. (2012). Proc. Guide to Cone Penetration Testing for Geotechnical Engineering.

Sampaio, J.L. (2010). Estudo da compressibilidade de uma argila mole da região metropolitana de Belém, por meio de ensaios de adensamento. 15th Congresso Brasileiro de Mecânica dos Solos e Engenharia Geotécnica, COBRAMSEG, Porto de Galinhas, Brazil.

Sandroni, S.S. & Deotti, L.O.G. (2008). Instrumented test embankments on piles and geogrid platforms at the panamerican village, Rio de Janeiro. Proc. 1th Pan American Geosynthetics Conference & Exhibition, Cancún Mexixo. (CD-ROM).

Sandroni, S.S. (1993). Sobre o uso dos ensaios de palheta no projeto de aterro sobre argilas moles. Solos e Rochas, 16(3):207-213.

Santos, H.M.C. (2004). Caracterização física, química, mineralógica e geotécnica dos gleissolos das baixadas de Jacarepaguá, Guaratiba e Santa Cruz do Município do Rio de Janeiro. Proc. Departamento de Geologia, CCMN/UFRJ, 244 p.

Sayão, A.S.F.J. (1980). Ensaios de Laboratório na Argila Mole da Escavação Experimental de Sarapuí. MSc Dissertation, Pontifical Catholic University of Rio de Janeiro, Rio de Janeiro, 201 p.

Schmertmann, J.H. (1955). The undisturbed consolidation behavior of clay. Proc. Trans. ASCE, v. 120, pp. 1201-1233.

Schnaid, F. (2009). In Situ Testing in Geomechanics. Proc. Taylor & Francis, 79 p.

Spannenberg, M.G. (2003). Caracterização Geotécnica de um Depósito de Argila Mole da Baixada Fluminense. MSc Dissertation, Pontifical Catholic University of Rio de Janeiro, Rio de Janeiro, 183 p.

Spotti, A. (2000). Monitoramento de Aterro Sobre Argila Orgânica Mole com Drenos Verticais. MSc Dissertation, Federal University of Rio de Janeiro, Rio de Janeiro, Rio de Janeiro, 195 p.

Teixeira, A.H. (1994). Fundações rasas na Baixada Santista. Proc. Solos do litoral de São Paulo. Mesa Redonda, ABM/ASSECOB, São Paulo, Brazil, pp. 137-154.

Teixeira, C.F. (2012). Análise dos Recalques de um Aterro Sobre Solos Muito Moles da Barra da Tijuca-RJ. PhD Dissertation, Pontifical Catholic University of Rio de Janeiro, Rio de Janeiro, 326 p.

Vilela, T.F. (1976). Determinação dos Parâmetros de Resistência, Creep e de Relaxação de Tensões de uma Argila Mole do Rio de Janeiro. MSc Dissertation, Federal University of Rio de Janeiro, Rio de Janeiro, Rio de Janeiro, 207 p.

Yu, H.S. (2004). In situ soil testing: from mechanics to interpretation. Proc. 2th Int. Conf. on Site Characterization ISC-2, Porto, v. 1, pp. 3-38.

List of Symbols

CEC: cation exchange capacity
CPTU: piezocone test
CR: compression ratio
M: oedometer modulus
N_{SPT}: blow count
OM: organic matter
SPT: Standard Penetration Test
C_c: compression index
c_h: horizontal coefficient of consolidation
C_s: recompression index
c_v: vertical coefficient of consolidation
C_α: Coefficient of secondary consolidation
e_0: initial void ratio
G_s: relative grain density
I_p: plasticity index (%)
k: permeability coefficient
K_i: molar ratios SiO_4/Al_2O_3
K_r: molar ratios $SiO_4/ (Al_2O_3 + Fe_2O_3)$
S_u: undrained clay strength (kPa)
w_L: liquidity limit
w_n: water content
σ'_v: vertical effective stress

Appendix

Table A - Geotechnical properties of soft soils in Brazil, modified from Futai *et al.*, 2001. (Part 1).

Site	Rio das Ostras	Juturnaiba	Itaipú	Cajú	Rua Uruguaiana	Botafogo
References	Lima *et al.* (2012)	Coutinho (1986)	Carvalho (1980) Pinheiro (1980)	Cunha (1988)	Vilela (1876)	Lins & Lacerda (1980)
Thicknesses (m)	1-6.8	7	10	12	9	6
w_n (%)	100-200	15495.6	240 ± 110	88	54.8 ± 1 9.5	35
w_l (%)	99-150	132 ± 44	175 ± 83	107	71 ± 30	38
Ip (%)	53-106	64 ± 22	74 ± 30	67	40 ± 22	11
% clay	47-66	60.7 ± 12.74			39.4 ± 10.11	28
γ_n (kN/m^3)	12-15	12.5 ± 1.87	12 ± 1.85	14.81	16.1 ± 1.39	17.04
% OM	7-11	19 ± 10.63	32.63 ± 20.46		2.56 ± 1.04	
e_0	2.6 -5.2	3.74 ± 1.98	6.72 ± 3.1	2.38	1.42 ± 0.36	1.1
$CR = C_c/(1 + e_0)$	0.4-0.46	0.31 ± 0.12	0.41 ± 0.12	0.267	0.31 ± 0.15	0.16
C_s/C_c	0.09 - 0.14	0.07 ± 0.06		0.21		0.19
c_v (cm^2/s) x 10^{-4}	1-9	1 - 10	5			30

Table A - Geotechnical properties of soft soils in Brazil, modified from Futai *et al.*, 2001. (Part 2).

Site	SESC/ SENAC	Baixada de Jacarepaguá	Duque de Caxias (REDUC)	Sarapuí	Sarapuí II	Itaguaí (RJ)
References	Crespo Neto (2004)	Cunha (1988)	Spannenberg (2003)	Almeida & Marques (2002)	Francisco (2004) and Alves (2004)	Queiroz (2013)
Thicknesses (m)	3- 12		11 - 13	12	6	2 - 7
w_n (%)	72 - 500	35.8 - 84.4	74.9 - 133.87	143 ± 21.7	183.5	84
w_l (%)	70 - 450	39 - 87	113.7	120 ± 18	158.2	70
Ip (%)	47- 250	12 - 49	85	73 ± 16	105.4	40
% clay	28 - 80	25 - 55	35	70	77	
γ_n (kN/m^3)	12.5		13 - 14.3	13.1 ± 0 49	12.1	14.7
% OM		5 - 13.9	6.6 ± 1			1.3 -15.8
e_0	1 - 11.1		1.94 - 3.55	3.71 ± 0.57		2
$CR = C_c/(1 + e_0)$	0.29 - 0.52		0.54	0.41 ± 0.07		0.25
C_s/C_c	0.17 - 80		0.1	0.15 ± 0.02		
c_v (cm^2/s) x 10^{-4}		1	2	9		1

Table A - Geotechnical properties of soft soils in Brazil, modified from Futai *et al.*, 2001. (Part 3).

Site	Santa Cruz (Coast)	Santa Cruz	Santa Cruz	PAN (Barra da Tijuca)	Western Region (RJ)	Eastern Region (RJ)
References	Aragão (1975)	Santos (2004)	Campos (2006)	Macedo (2004) Sandroni e Deotti (2008)	Bedeschi (2004)	Crespo Neto (2004)
Thicknesses (m)	15	5 - 15	5 - 15	5 - 16	7.5	2 - 11.5
w_n (%)	112	31 - 161.4	114 - 119	116 - 600	102 - 500	72 - 410
w_l (%)	60	18 - 161.4	56 - 121	100 - 370	97 - 368	23 - 472
Ip (%)	32	2.6 - 118	25 - 77	120 - 230	42 - 200	11 - 408
% clay		52 - 62	36.7 - 64.6			
γ_n (kN/m^3)	13.24		13.13	11.6 - 12.5	11.2 - 12.3	11 - 12.4
% OM		0.41- 10.4	1.2 - 4.13			
e_0	3.09	1.94 - 2.64	3.16 - 4.79	4.8 - 7.6	4.3 - 9	3.8 - 15
$CR = C_c/(1 + e_0)$	0.32	0.23 - 0.26	0.19 - 0.45	0.36 - 0.5	0.32 - 0.48	0.27 - 0.46
C_s/C_c	0.1		0.07 - 0.14			
c_v (cm^2/s) x 10^{-4}	0.2 - 18.2	62.5 - 80.3		0.4 -1.2		0.1 - 0.6

Table A - Geotechnical properties of soft soils in Brazil, modified from Futai *et al.*, 2001. (Part 4).

Site	Barra da Tijuca Recreio	Guaratiba	Hercílio Luz Airport, Florianópolis (SC)	Pirajubaé, Florianópolis (SC)	Municipality of Itajaí (SC)	Port of Santos SFL Clays
References	Baroni (2010)	Lima & Campos (2014)	Espíndola (2011)	Oliveira (2006)	Baran (2014)	Massad (1994)
Thicknesses (m)	2 - 21.8			10-20		< = 50
w_n (%)	191 - 670	34 - 184	75 - 93	120	93 -133	75 - 150
w_l (%)	147 -521	61.5 -148	38 - 87	105 - 165	37 - 54	40 - 150
Ip (%)	95 - 308	39 -100	20 - 54	60 -100	15 - 28	20 - 90
% clay	23 - 93		12 - 19	> 60		
γ_n (kN/m^3)	10.01 - 12.7	13.1-18.5	14 - 15	13.2 -14.2	13 - 16	13.5 - 16.3
% OM			2.8 - 6.2	5-6		
e_0	4 -12.4	0.85-4.69	2 - 2.4	3 - 4.5	1.9 - 3.6	2 - 4
$CR = C_c/(1 + e_0)$	0.31 - 0.54	0.11-0.46	0.03 - 0.04	0.26 -0.45	0.18 - 0.4	0.33 - 0.51
C_s/C_c		0.3	0.02 - 0.07	0.08 -0.14		8 - 12
c_v (cm^2/s) x 10^{-4}	0.018 - 19.8	1-10	0.14 - 0.89	1 - 5	0.28 - 39.10	

A Contingency Solution using Jet Grouting Barrier for a Dam under Risk of Piping in Brazil

S.M. Ludemann, R.S. Garcia, M.G.T. Barbosa, A.L.B. Cavalcante

Abstract. During routine inspection works in 2006 inspectors found resurgences of water at the toe of a small embankment dam named "Ribeirão do Gama", located at Brasília - DF. After technical visits, geotechnical engineers characterized these groundwater leakages as a piping process at an early stage. Intervention only began in 2015 due to obstacles that occasionally happen in public works. In consequence, the piping problem worsened. A geotechnical consultancy was contracted to design a solution. After analysis of field conditions, the consultancy decided to build overlapping columns by the Jet Grouting method. This paper presents a case study of the project and works treatment, detailing its design, construction, and monitoring.

Keywords: cut-off, earth dam, jet grouting, piping.

1. Introduction

According to the account of the oldest inhabitant of the region, the "Ribeirão do Gama" dam was constructed in the second half of the 1950s, simultaneously with the start of the construction of the federal capital of Brazil, Brasília. Brasília's government probably built this geotechnical structure to form a reservoir to serve as water supply for the necessary earthworks at the time. In this context, a dike was built with features of a temporary work and therefore had no sealing nor drainage devices, as would be normal in a permanent dam.

The dike formed a scenic lake of a considerable volume of water after the finalization of the main earthworks of Brasília. As there was a residential area near "Ribeirão do Gama", the dike was kept and later heightened, to allow the water surface also to increase, therefore configuring the dike as a small embankment dam. Later, already inserted in the "Fazenda Água Limpa", a property of the University of Brasília (UnB), the outlet water was used for agricultural purposes, providing water to the horticultural village "Vargem Bonita", and for human consumption downstream. Thus, the dam became a permanent structure.

"Ribeirão do Gama" dam has a length of 290 m and a height of 15 m. It has a concrete side channel spillway located in its right abutment and a volute siphon water intake in its left abutment, for Vargem Bonita's supply. Figure 1 presents the aerial view of the site.

After 60 years of the construction of the embankment dam, in a routine inspection carried out in 2006, the technicians from UnB noted several points of leaking water at the toe of the downstream dam slope and eroded soil particles. This fact, coupled with the advanced state of surface degradation of the upstream4 and downstream slopes, caused concern. A geotechnical engineering professor at UnB, Professor Pedro Murrieta, visiting the location, stated this situation had a high risk of developing a failure caused by piping, as had already occurred in many embankment dams in Brazil and abroad.

Because of difficulties in the contracting process, the recovery of the "Ribeirão do Gama" dam started only in 2015, when the risk of piping, which grew from six points of leakage in 2014 to fifteen in 2015, couldn't be ignored and a solution had to be implemented. The next sections present the main aspects of the design, and the construction works.

2. Treatment of a Dam with Risk of Piping Failure

Piping is a form of hydraulic failure, which is common in cases where erosion of soil by seepage forces occurs. Initially, it appears as a point of upwelling water, eroding the earth mass internally, carrying grains. The internal erosion results in the formation of a tube, usually in the form of a pipe. Hence this phenomenon was named piping.

These seepage forces are applied by unit volume, having the magnitude of $j = \gamma_w \cdot i$, where γ_w is the specific weight of water, and i is the hydraulic gradient, which is given by $i = \Delta H/\Delta L$, where ΔH is the hydraulic head loss along the length ΔL.

Sérgio Murari Ludemann, B.Sc., Technical Director, Ludemann Engenheiros Associados, São Paulo, SP, Brazil, e-mail: sergio@ludemann.com.br.
Robinson Siqueira Garcia, B.Sc., Civil Engineer, Ludemann Engenheiros Associados, São Paulo, SP, Brazil. e-mail: robin17sg@gmail.com.
Max Gabriel Timo Barbosa, M.Sc., Civil Engineer, Departamento de Engenharia Civil e Ambiental, Universidade de Brasília, Brasília, DF, Brazil. e-mail: maxtimo@gmail.com.
André Luís Brasil Cavalcante, Ph.D., Associate Professor, Departamento de Engenharia Civil e Ambiental, Universidade de Brasília, Brasília, DF, Brazil. e-mail: abrasil@unb.br.
Submitted on April 13, 2017; Final Acceptance on January 31, 2018; Discussion open until August 31, 2018.
DOI: 10.28927/SR.411017

Figure 1 - Aerial view of the site (yellow line represents the axis of the dam).

In earth dams, it is not uncommon to have regions where the permeability coefficient k_i is higher than the average permeability k_{eq}, making this region with higher permeability a preferential path to water flow. The flow velocity v is higher in this region and, therefore, the erosion of finer soil particles is more probable than in other regions. Consequently, the spacing between grains is higher, raising the maximum permeability of the region affected by this phenomenon.

When piping is progressing, the tendency is the upwelling of water in the dam's downstream surface and a point erosion, creating a hole into the affected volume of soil. As time goes by, the hole, resembling a pipe, progresses into the earth mass in a way opposite to the normal flow of the dam. As already described, this phenomenon is known as piping, generally defined as heave, internal erosion or backward erosion (Richards & Reddy, 2007). In earth dams, it mainly occurs in the middle section of the dam and also in its foundation. In recent history, there have been accidents due to piping in several earth dams. One of the most notorious episodes was in the Teton Dam, in the United States of America, in 1976 (Richards & Reddy, 2007).

As a reparation measure in similar occurrences, where there was evidence of a possible piping failure, an invasive ground improvement method is executed locally. The ground improvement methods applied in such situations consist in the alteration of the mechanical properties of the in-situ soil, giving to the earth mass and/or to the foundations better resistance, lower compressibility, and lower permeability.

Nevertheless, before the application of the most recommended techniques to obtain the desired results, such as Jet Grouting and Deep Soil Mixing, an assertive diagnosis of the problem was necessary. The diagnosis was performed using a detailed inspection of the upwelling water points, a topographic and bathymetric characterization of the dam slopes and the fulfillment of geotechnical surveys, lab and field tests which will allow to adequately typify the characteristics of the site underground and reduce risks (Lee & Ishihara, 2016).

3. *In Situ* Soil Geotechnical Description

Geologically, the Gama Hydrological basin is settled into the silty-slate unity Grupo Paranoá. Geotechnical investigations done in the dam showed its foundations consisted of peat of very soft consistency, with a thickness between 2.0 m to 5.0 m, on the main axis of the dam, overlaying a layer of a reddish clayey alluvium, of soft consistency, with a thickness between 1.0 m to 5.0 m. Downstream, into the clayey soil region, appears a layer of sandy alluvium, of loose consistency, which could contain gravels, with thickness up to 6.0 m. Below these alluvium layers existed a layer of residual soil, constituted by a variegated color sandy silt, of medium consistency, which could contain boulders, with thickness between 1.0 m (downstream and under the dam crest) to 6.0 m (upstream), overlying a layer of saprolite and the top of the rock matrix.

Regarding the dam, its foundation had different characteristics from the fill body, giving evidence that for its implementation the silty-sandy clay material was just dumped to allow the free traffic of the utilized equipment to construct the dam. Due to this procedure, the fill lower portion material had a soft consistency, with N values between 2-7 blow counts.

Also, due to the consolidation of the clayey alluviums, it is hypothesized there was a posterior complementation of the fill on the dam's crest. In Fig. 2 these observations are summarized in a typical section of "Ribeirão do Gama" dam, outlined based on the available borehole logs.

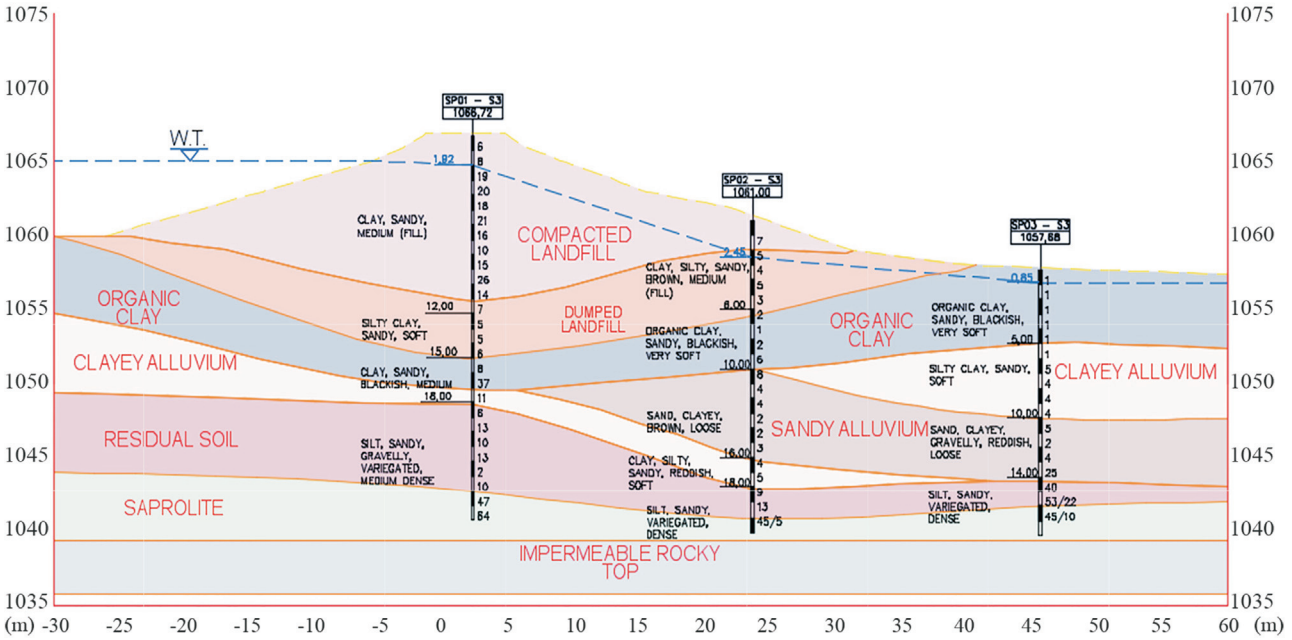

Figure 2 - Typical geotechnical section (Peg 9+00 m).

4. Diagnosis

4.1. Dam stability analysis

4.1.1. Geotechnical parameters

Piezocone field tests and laboratory tests (natural moisture, natural density, Atterberg limits, permeability and triaxial test CIU type) were necessary to obtain the geotechnical parameters of shear strength of the local underground layers. For the strength parameters of the cut-off columns, idealized as a possible solution for the flow problem, values were adopted from the literature (Nikbakhtan & Osanloo, 2009; Saurer *et al.*, 2011). Permeability parameters were firstly estimated from permeability values of previous projects; then they were calibrated with data obtained from piezometers already installed on site. Table 1 shows the values adopted in this design. Consolidation tests were also performed.

4.1.2. Adopted assumptions

The dam stability was studied by simulating the probable situation existent at the end of its construction to assess the adopted geotechnical parameters, considering at the time that the lower fill clayey layer was normally consolidated. Therefore, it had a lower resistance than noticed in tests conducted under the dam, probably similar to the resistance observed in the piezocone results on the dam downstream; also, it had a thickness higher than detected by surveys executed in the dam axis. Over the years, the clay layers were consolidated, making the dam foundation settle, for which an additional fill on the crest of the dam was necessary to maintain the original elevation.

4.1.3. Stability analysis

A stability analysis was performed since it was not clear if the dam would be stable in the long term. The Simplified Bishop method was used, aided by the software Slide 5.0 (Rocscience - Canada), with automatic search of the critical surface.

4.1.4. Initial state - End of construction

The graphical output of the stability analysis of the dam condition at the end of its construction is shown in Fig. 3, resulting in a safety factor of 1.06. It appears from this result that this dam was most likely built in stages, the first stage being the dumped landfill and the second stage the upper compacted embankment, confirming the chronology informed by locals.

4.1.5. Situation at the time of design

In the situation at the time of the design studies, the clayey and peaty soil under the soil structure was considered lightly consolidated. Thus, considering a gradation of resistances in the clay layers and estimating a critical phreatic line near the surface, the resulting safety factor is equal to 1.92, as shown in Fig. 4.

4.1.6. Conclusions about the stability analysis

The safety factor has undergone an increase in its value over time due to the strength gain caused by the consolidation of the clayey soil. Thus, considering the safety

Table 1 - Adopted geotechnical parameters.

Material	Specific weight γ (kN/m^3)	*Su* (kPa)	Cohesion *c*' (kPa)	Friction angle ϕ' (°)	Permeability *k* (m/s)
Compacted landfill	17.0	-	33.0	37.0	2.0 x 10^{-7}
Dumped landfill	16.0	-	17.0	37.0	6.0 x 10^{-6}
Sandy alluvium	16.5	-	5.0	25.0	5.0 x 10^{-5}
Residual soil	18.0	-	20.0	30.0	3.0 x 10^{-6}
Saprolite	19.0	-	30.0	35.0	2.0 x 10^{-6}
Sand filter drain	17.0	-	5.0	30.0	1.0 x 10^{-3}
Gravel toe drain	19.0	-	5.0	40.0	5.0 x 10^{-3}
Cut-off columns	18.0	-	40.0	30.0	1.0 x 10^{-12}
Normally consolidated organic clay	14.0	17.0	-	-	5.0 x 10^{-8}
Lightly consolidated organic clay 1	15.0	25.0	-	-	2.0 x 10^{-8}
Lightly consolidated organic clay 2	16.0	40.0	-	-	1.0 x 10^{-8}
Normally consolidated clayey alluvium	15.5	40.0	-	-	5.0 x 10^{-8}
Lightly consolidated clayey alluvium	16.0	60.0	-	-	2.0 x 10^{-8}
'Impervious' rock	-	-	-	-	1.0 x 10^{-12}

factor at the time of the design as satisfactory regarding the general stability of the dam, it was concluded that the main problem of the dam was water loss by the interface between the dumped landfill layer and the transition layers, with a potential risk of failure by piping.

Therefore, to reduce the flow of water significantly through the dam body, it was decided to make a cut-off. To make curtains with very low permeability in the studied dam, Slurry Walls, Deep Soil Mixing (DSM) and Jet Grouting techniques were considered, solutions much employed in this kind of work efficiently.

After analysis of field conditions, it was decided to build Jet Grouting columns. The reason for this choice stems from the fact that the solution in Jet Grouting would impose less critical stability conditions to the dam because of the lower weight of the necessary equipment and due to the fact that its execution method does not require much excavation in the dam body, aspects the solution in diaphragm walls did not meet. Further, supports the choice the fact Jet Grouting implementations, double fluid in the present case above, are efficient in forming columns in soil-cement with suitable permeability coefficients (AGI, 2012).

Croce & Modoni (2007) reviewed the subject and presented accounts of remediation of existing dams, furnishing the design and construction details. Moreover, Sembenelli & Sembenelli (1999) presented details of simi-

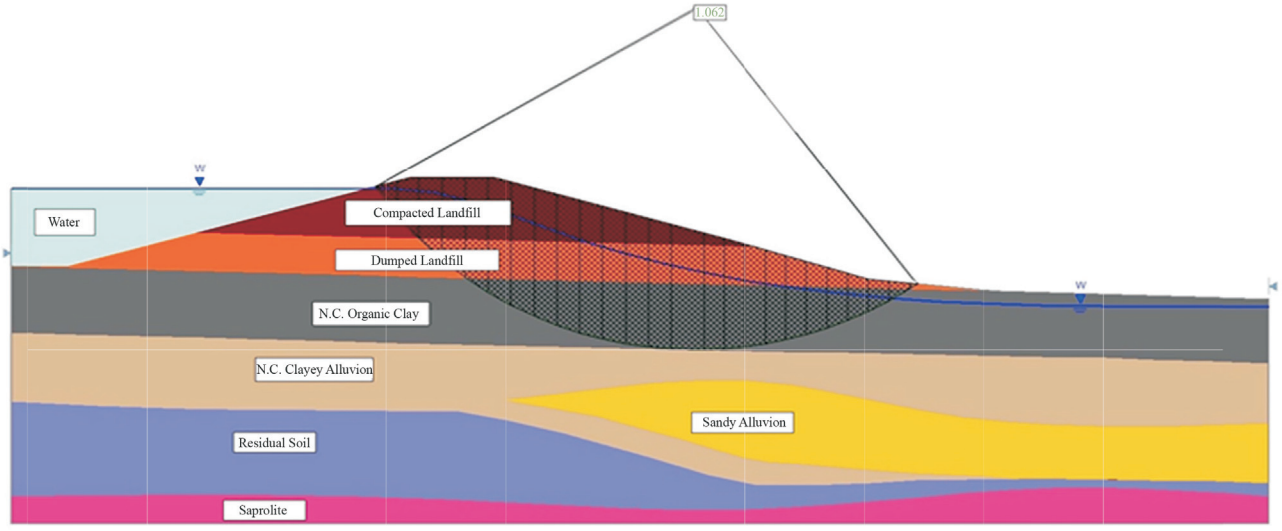

Figure 3 - End of construction stability analysis (FS = 1.062).

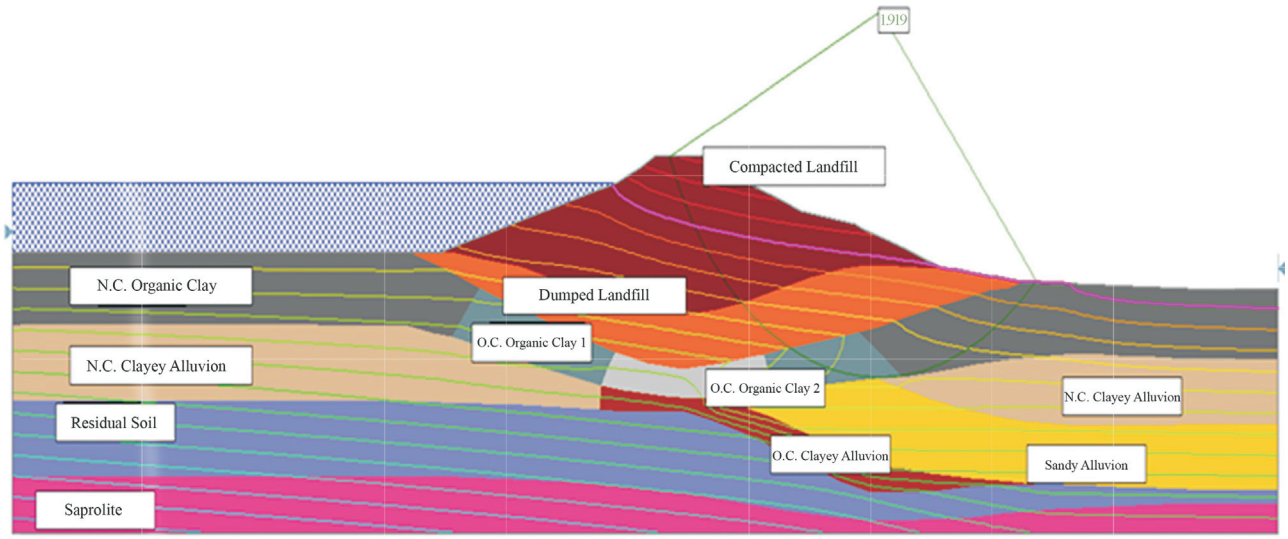

Figure 4 - Stability analysis of the dam's initial state (FS = 1.92).

lar cutoff projects, allowing to design the proposed Jet Grouting cut-off. The 706 columns, with 80 cm diameter each, were to be built 40 cm overlapped in a single continuous row, with depths ranging from 10 to 22 m, from the crest of the dam to its foundation. The single row cut-off design, running through the body of the dam, which is unprecedented in the author's knowledge of an advanced piping case in an existing dam, was possible due to the higher overlap of the columns (half of the diameter) than other cut-offs. Nevertheless, there was still a risk that the inherent variation of the diameters of the Jet Grouting columns would affect the overlapping and water tightness of the cut-off. The Jet Grouting cut-off was associated with a toe drainage system and the recovery of the downstream slope by a new fill to mitigate this risk.

4.2. Flow analysis of the proposed solution

As the main design concern was to assess the water flow through the body and foundation of the dam after the implementation of the Jet Grouting cut-off, the solution was analyzed by the Finite Element Method (FEM). FEM was assisted by the Slide software using the flow net calculation mode. Table 1 shows the coefficients of permeability adopted.

4.2.1. Permeability parameters calibration

As the permeability parameters were just estimated, it was decided to calibrate them with available field measurements of the dam's seepage flow. Fourteen Casagrande hydraulic piezometers were already installed prior to the start of the intervention, disposed as shown in Fig. 5. Table 2 presents the readings values.

With the data from Table 2, the flow nets of the embankment were drawn, adjusting some of the soil permeability parameters and the downstream headwater level to arrive at a combination that could best match the observed in situ water heads provided by the piezometers.

Table 2 - Piezometers readings before the intervention.

Piezometer	Peg (m)*	Piezometer depth (m)	Water level recorded (m)
P1	2+0.00	6.68	4.20
P2	5+0.00	15.33	2.90
P3	9+0.00	22.10	6.00
P4	N. I.	4.18	1.70
P5	N. I.	3.35	1.60
P6	N. I.	3.45	3.20
P7	15+0.00	7.70	2.90
P8	15+0.00	9.85	2.90
P9	9+0.00	10.00	4.20
P10	5+0.00	11.30	4.10
P11	2+10.00	3.75	2.00
P12	5+0.00	12.60	1.00
P13	9+0.00	16.20	1.14
P14	15+0.00	8.14	On top

Peg: Piezometer location, *e.g.* 2 + 0.00 m represents 40 m from datum.
N.I.: Not informed in Fig. 5.

4.2.2. Flow net for the situation at the time of design and for the proposed solution

With the calibrated parameters and the geotechnical sections drawn, the design and definition of flow nets for each peg of the dam (*i.e.*, each section 20.0 m spaced) was possible. Table 3 presents the estimated flow rates per dam section, before and after the imple-

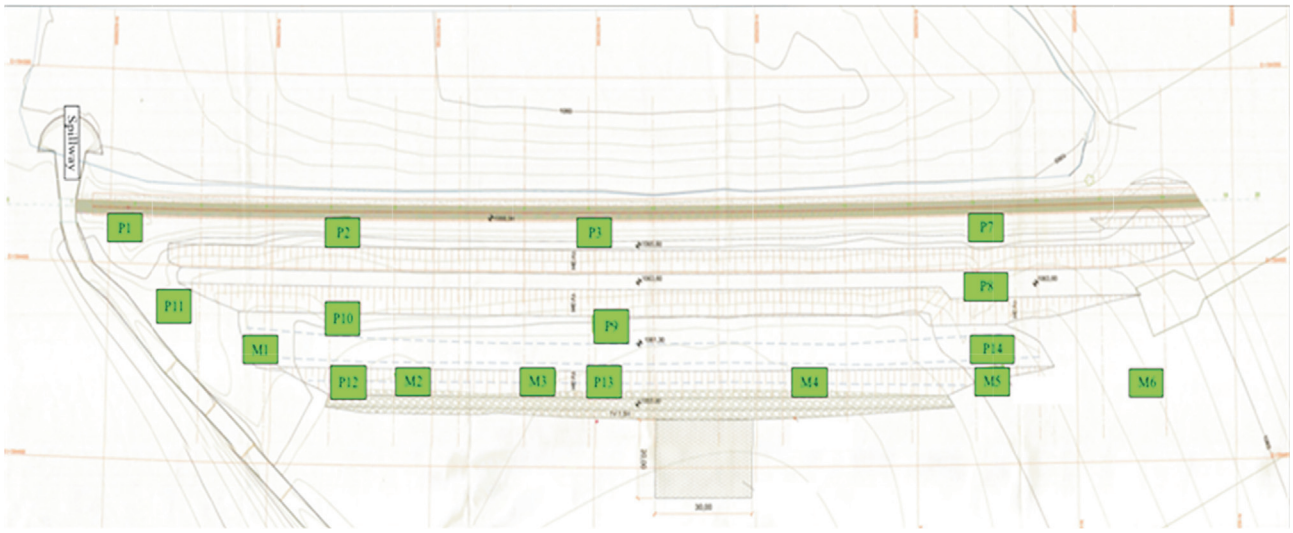

Figure 5 - Piezometers location in situ (P represents the piezometers and M the surface marks).

Table 3 - Flow rates estimate by the dam's sections in the condition at the time of design and the estimate after the project implementation.

Peg 9+00 m	Initial flow rate ($m^3/s/m$)			Design flow rate ($m^3/s/m$)		
	Input (I)	Output (O)	Δ	Input (I)	Output (O)	Δ
0	7.11×10^{-7}	7.11×10^{-7}	0.00	7.11×10^{-7}	7.11×10^{-7}	0.00
1	9.70×10^{-7}	7.14×10^{-7}	2.57×10^{-7}	7.10×10^{-7}	7.09×10^{-7}	7.70×10^{-10}
2	1.18×10^{-6}	1.16×10^{-6}	1.70×10^{-8}	8.96×10^{-7}	9.07×10^{-7}	0.00
3	1.67×10^{-6}	1.49×10^{-6}	1.77×10^{-7}	1.37×10^{-10}	8.83×10^{-11}	4.84×10^{-11}
4	2.03×10^{-6}	1.97×10^{-6}	6.10×10^{-8}	1.59×10^{-10}	9.67×10^{-11}	6.24×10^{-11}
5	2.68×10^{-6}	1.59×10^{-6}	1.10×10^{-6}	1.93×10^{-10}	1.87×10^{-10}	5.54×10^{-12}
6	2.79×10^{-6}	1.47×10^{-6}	1.32×10^{-6}	2.24×10^{-10}	2.24×10^{-10}	0.00
7	3.20×10^{-6}	1.47×10^{-6}	1.73×10^{-6}	4.56×10^{-7}	4.56×10^{-7}	0.00
8	4.33×10^{-6}	2.94×10^{-6}	1.40×10^{-6}	1.81×10^{-6}	1.81×10^{-6}	0.00
9	4.20×10^{-6}	2.37×10^{-6}	1.83×10^{-6}	1.52×10^{-6}	1.52×10^{-6}	0.00
10	4.67×10^{-6}	2.26×10^{-6}	2.41×10^{-6}	1.75×10^{-6}	1.68×10^{-6}	6.88×10^{-8}
11	4.68×10^{-6}	4.22×10^{-6}	4.54×10^{-7}	1.45×10^{-6}	1.41×10^{-6}	3.38×10^{-8}
12	5.36×10^{-6}	1.98×10^{-6}	3.37×10^{-6}	1.18×10^{-6}	9.65×10^{-7}	2.15×10^{-7}
13	5.11×10^{-6}	3.41×10^{-6}	1.70×10^{-6}	1.67×10^{-10}	1.38×10^{-10}	2.94×10^{-11}
14	3.90×10^{-6}	2.96×10^{-6}	9.36×10^{-7}	1.29×10^{-10}	1.01×10^{-10}	2.72×10^{-11}
15	1.97×10^{-6}	1.36×10^{-6}	6.10×10^{-7}	1.04×10^{-10}	7.13×10^{-11}	3.31×10^{-11}
16	1.39×10^{-6}	1.18×10^{-6}	2.10×10^{-7}	1.15×10^{-9}	5.68×10^{-11}	1.10×10^{-9}
17	8.12×10^{-7}	8.12×10^{-7}	3.00×10^{-11}	7.43×10^{-11}	2.85×10^{-11}	4.59×10^{-11}
18	4.50×10^{-7}	4.50×10^{-7}	0.00	4.87×10^{-11}	2.24×10^{-11}	2.63×10^{-11}
19	4.06×10^{-7}	4.06×10^{-7}	0.00	4.06×10^{-7}	4.06×10^{-7}	0.00
Total (m^3/s)	1.04×10^{-3}	6.88×10^{-4}	3.52×10^{-4}	2.07×10^{-4}	2.00×10^{-4}	$6.40.10^{-6}$

mentation of the proposed solution. The input flow rate (I) is the flow rate which occurs in the vertical section where the upstream piezometric elevation (+1,065.00 m) is the same as the reservoir level. The output flow rate (O) is the one that flows under the toe of the downstream slope. The outflow by the dam's downstream surface, called Δ, is the difference between the input and output flow rates, (I) and (O), not only in the previous condition, before the treatment, but also in the final condition of the project. In Fig. 6 the results are graphically presented,

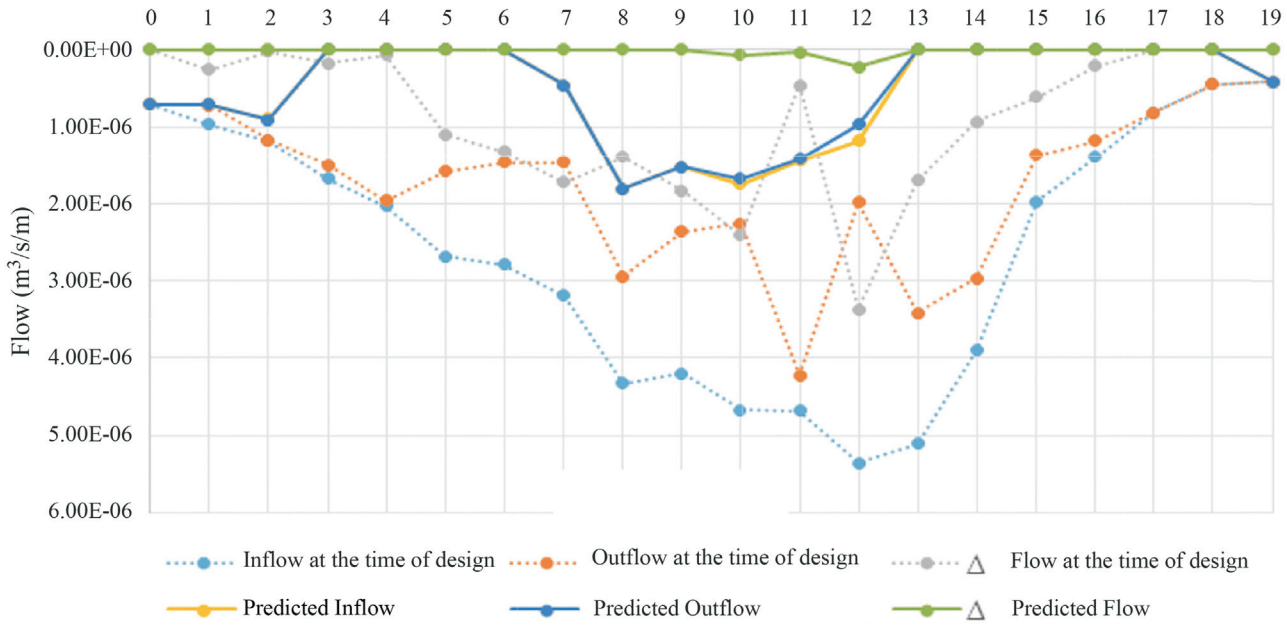

Figure 6 - Flow rates estimate per dam section.

and in Fig. 7 the input and output sections are presented schematically.

Figure 6 shows the proposed solution would substantially decrease the downstream water loss, almost eliminating the existent flow in the dam's foundation.

4.3. Stability analysis of the proposed solution

The most critical section refers to Peg 9 + 0.00 m, which is the location with the lowest downstream ground level and the highest thickness of organic peat.

Figure 7 presents the estimated flow net by that section. Adopting the strength parameters shown in Table 1, a stability analysis of the downstream slope at Peg 9 + 0.00 m was made. The graphical output of this stability analysis is presented in Fig. 8, resulting in a factor of safety FS = 2.00, considered satisfactory.

4.4. Conclusions regarding the proposed solution

According to design estimates, the Jet Grouting cut-off will decrease the leakage in the dam's foundations by 80% and the water flow near the dam's toe by 98%. The remaining water flow will be collected by the draining bed and by the toe drain. Thereby, the design controlled and hampered the downstream leakage problem and the piping process.

5. Solution Implementation

5.1. Implementation methodology

Despite the proven efficacy of the chosen solution for cut-offs, this solution was in a single row, not in two or three rows as in other projects (Sembenelli & Sembenelli, 1999; Croce & Modoni, 2007; Guatteri *et al.*, 2012). In "Ribeirão do Gama" dam the execution team was con-

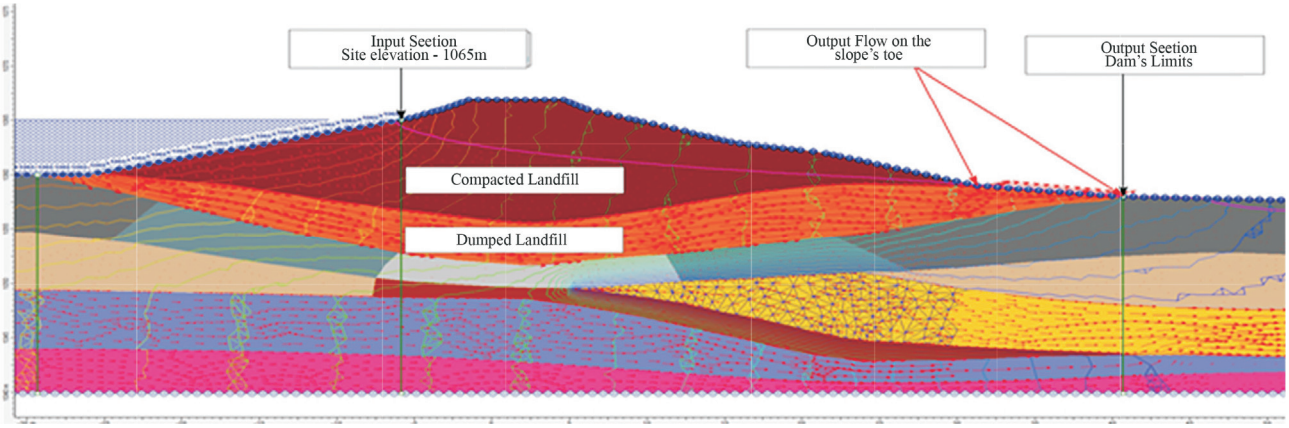

Figure 7 - Predicted flow net (Peg 9+00 m).

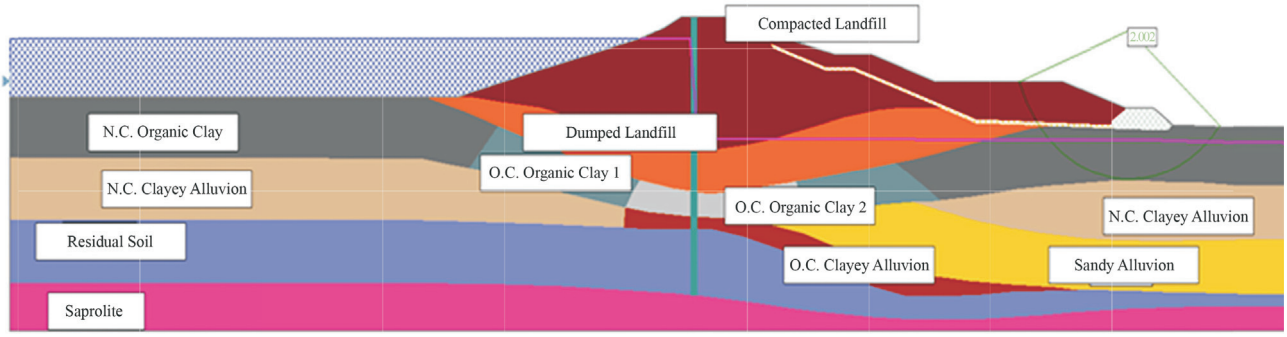

Figure 8 - Stability analysis of the dam's final state (FS = 2.00).

cerned mainly with two aspects, besides the recommended Jet Grouting control factors by AGI (2012):

- significant heterogeneity condition of the subsoil, with the presence of peat;
- possible lack of overlapping between columns.

It is added to these difficulties the existence of buried water intakes and tree roots in the dam body, additional triggering factors which can increase the probability of a failure by piping.

To surpass these aforementioned challenges, as whole soil-cement columns were formed with the parameters defined in the project, there was a need to follow rigorous methods of execution and control recommended by ABEF (2012) to avoid deviation and diameter variation of the columns, which can occur in Jet Grouting works (Croce & Modoni, 2007). Thus, the method of implementing Jet Grouting columns was analyzed to obtain sufficient information to achieve an engineering solution with high performance. The execution of Jet Grouting columns can be subdivided into three steps, as shown in Fig. 9.

- Ground drilling by rotation of the rods set, usually of 10 cm diameter, and triconed drill bit mandrel, parallel with the water flow (500 l / min) until the design depth. A metallic sphere closes the water injection nozzle;
- Grout injection at high pressures, which was enveloped by compressed air, to produce a high speed combined stream, eroding the ground and providing the interaction of cement grout with the earth mass;
- The rotational rise of the drill stem with step increase, rotation and speed calibrated to obtain columns with the desired parameters.

Several precautions are recommended to minimize instabilities of the Jet Grouting treatment of earth mass. Not only the parameters recommended by AGI (2012) must be considered, but also the diameter of the rod, the type of drill bit, the volume of the drilling water and the internal mechanism of the injection machinery to be used. These factors were considered for the choice of the Jet Grouting equipment.

Another aspect observed for the execution was the process of formation of columns. Because they are not formed immediately, as the Jet Grouting process forms columns with sufficient hardness to resist lateral injections only after a curing process of 48 hours, the execution method required columns spaced in a manner so that the execution of a column did not interfere with the curing of the other, as shown in Fig. 10.

According to AGI (2012), this method of making alternate boreholes, called "fresh in hard", shown in Fig. 10, requires special control. This caution is justified because of the possibility of the so-called "shadow effect" between the columns, a phenomenon caused by the difficulty of the jet to erode the earth mass outlining the primary columns (P), with the possibility of formation of secondary columns (S) with a diameter lower than desired. Then, after forming and curing the primary columns, the space between them, formed by secondary columns, was filled until achieving the design's desired overlapping. So sometimes the injection of secondary columns was done with slightly higher pressures than those used in primary columns.

5.2. Execution and control parameters

The technology parameters were monitored to obtain 0.8 m diameter columns with a permeability coefficient low enough to reduce the water flow through the dam foundation, besides presenting adequate compressive strength. For this it was considered the AGI (2012) and ABEF (2012) recommendations; also, the experience of the designer and

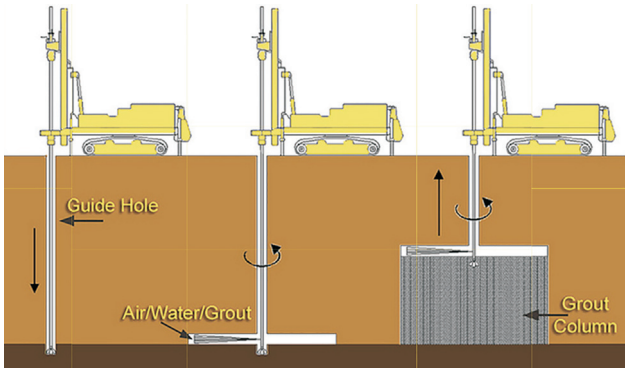

Figure 9 - Jet Grouting methodology (U.S. Army illustration by Todd Plain/Released).

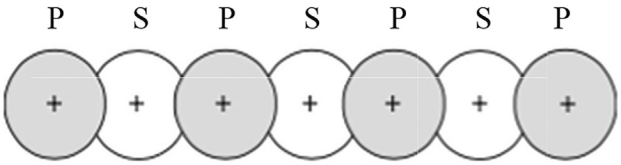

Figure 10 - "Fresh in hard" method, in which primary (P) columns are built first to the posterior closing of the Jet Grouting curtain with the implementation of secondary (S) columns (AGI, 2012).

the contractor in works of Jet Grouting was crucial. Thus, Table 4 presents the initial parameters.

After the establishment of these parameters, trial columns were made in a location with a similar geology of the dam site but unaffected by piping. The design predicted bentonite as an additive meant to improve the water tightness of the cut-off, as seen in Guatteri *et al.* (2012). Nevertheless, as the bentonite slowed the curing process, and there was a risk of washout of the mix, it was decided not to utilize the bentonite and lower the w/c ratio to 0.7. Thus, these corrected parameters were adopted to perform the work, yielding an average soil-cement column diameter of 0.8 ± 0.1 m, mitigating the washout of the mix, as shown in Fig. 11.

Due to the heterogeneity of the subsoil, the operation parameters were reassessed continuously and compared with the design parameters to ensure the Jet Grouting process formed columns with the desired diameter, permeability, strength, uniformity and spacing. The injection pressure was carefully monitored, so the inherent instability of the Jet Grouting process was minimized, reducing the risk of new communication paths between the upstream and the downstream of the dam.

Another object of observation in work was the reflux mud, arising from drilling with water since from the coloring of this mud was possible to estimate if the soil was found near those described in the geological investigations used in the preparation of the project.

Table 4 - Initial Jet Grouting parameters.

Parameter	
Rise step of the rods (m)	0.05
Rod rise velocity (m/s)	0.006
Rod rotation (rpm)	8
Rod rotations per step (rpm/step)	1.07
Nozzle diameter (m)	2.5
Nozzle number	2
Grout injection pressure (MPa)	15
Air pressure (MPa)	1
Grout flow rate (m^3/s)	1.2×10^{-3}
w/c - by weight	1.0
Bentonite addition by weight (%)	2.0

6. Monitoring and Instrumentation of the Implementation

6.1. Initial considerations

The recovery of "Ribeirão do Gama" earth dam, required particular attention, due to the exacerbated process of subsurface retro erosion and because during the dam construction works, at the end of the 1950s, the implementation wasn't carefully accompanied, a fact that led to formation of soil layers with improper parameters for an embankment dam. According to data from Perini (2009), 36% of zoned earth dams' failures are by piping.

In this case study, besides the fact the dam had shown several signs of subsurface retro erosion, the structure also had several trees downstream, with water intakes passing in its middle section, factors which could disturb its recovery. Furthermore, the design of the Jet Grouting cut-off constructed in a single continuous row for an advanced piping problem was unprecedented.

Thus, due to the high risk of the dam recovery solution implementation, adequate instrumentation and monitoring specifications were necessary. In this way designers and contractors could take expeditious technical decisions correctly and have greater confidence in the pace of work.

6.2. Instrumentation

Bassett (2012) classifies the instrumentation of geotechnical works into three types: passive monitoring, real-time monitoring for building control and monitoring for safety. In the case of "Ribeirão do Gama" dam, the instrumentation falls in the first two classes, since there were previous calculations concerning the behavior of the flow passing through the dam in the design phase and also a real-time instrumentation for adjustments of execution parameters based on data of piezometers and displacements. Consequently, if measurements from different field instruments were different from the input values previously calculated, remedial actions could be made.

Therefore, to provide monitoring with sufficiently accurate reporting provision for the evaluation of "Ribeirão do Gama" dam, electric vibrating wire piezometers, surface marks, and inclinometers were installed.

The design required the installation of piezometers for evaluating the performance of the work regarding the flow, so water passing through the dam had similar parameters of magnitude and direction provided by the project. Moreover, it was possible to assess if the intervention resulted in the expected water head drop, with the elimination of the piping process, also assessing if the constructed cut-off could stop the flow through the dam body. For this, the designers set with the topography team key points for installation of equipment: the abutments, the places where

Figure 11 - Trial Jet Grouting columns.

the points of piping manifested with more intensity and places near the water intakes.

Regarding the surface marks and inclinometers, they were installed to provide data related to the local and global stability of the dam.

The surface marks were sensitive enough for small movements of the downstream slope to be detected, so that the Jet Grouting works could be optimized. Thus, the surface marks provided data from the vertical movements of the dam embankments and propitiated the detection of unstable ground, which required extra caution.

Meanwhile, the inclinometers with two axes of measurements, monitored dam movements in the horizontal, normal and longitudinal directions, complementing the leveling of surface marks, allowing a three-dimensional analysis of displacements. The design required the installation of inclinometers in critical sections where stability was the main concern, especially those dam sections resting on peat.

Thus, through the analysis of the instrumentation data, collected twice daily, the monitoring and evaluation of the behavior of the dam were possible, and the execution team could make adjustments into the previously established executive sequence.

6.3. Monitoring

The design required constant monitoring of the dam to aid the continuation of the work. With the continuous evaluation of data generated by instruments, more confident technical decisions could be made. In Figs. 12 to 15, it is presented examples of plots generated by the monitoring at the time of the intervention.

These instruments generated necessary data for the accompaniment of the works. Nevertheless, since the Jet Grouting process leaves the object of its intervention momentarily less stable, by eroding a soil column before the strength of the JG column is fully set, it was required a careful observation of regions on the vicinity of the equipment, complementing the instrumentation.

The inclinometers sometimes displayed anomalous behavior. However, such behavior, as noticed by the execution and instrumentation team, originated from movements and activities of the equipment employed in the works. Some explanations of unexpected behaviors detected from the instrumentation data were made possible.

It was concluded that the effects reported were mainly due to the action of the Jet Grouting machine, as its execution sequence may induce small cracks and vibrations from the high pressures used in the injection process of this type of treatment.

From this continuous monitoring by the team involved in the recovery of “Ribeirão do Gama” dam, an abandoned anthill, of large dimensions, inside the dam body, was detected as a generator of instabilities. The discovery of the anthill led to detection of other voids nearby

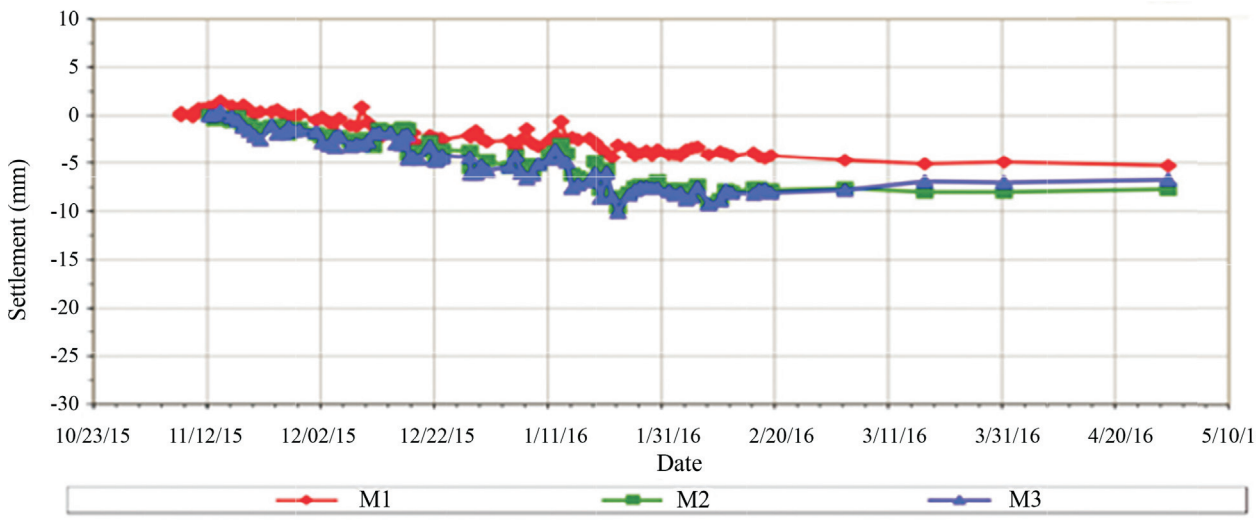

Figure 12 - Settlement (m) *vs.* Time (s) chart generated by surface marks M1, M2, and M3 data. Figure 5 shows these marks.

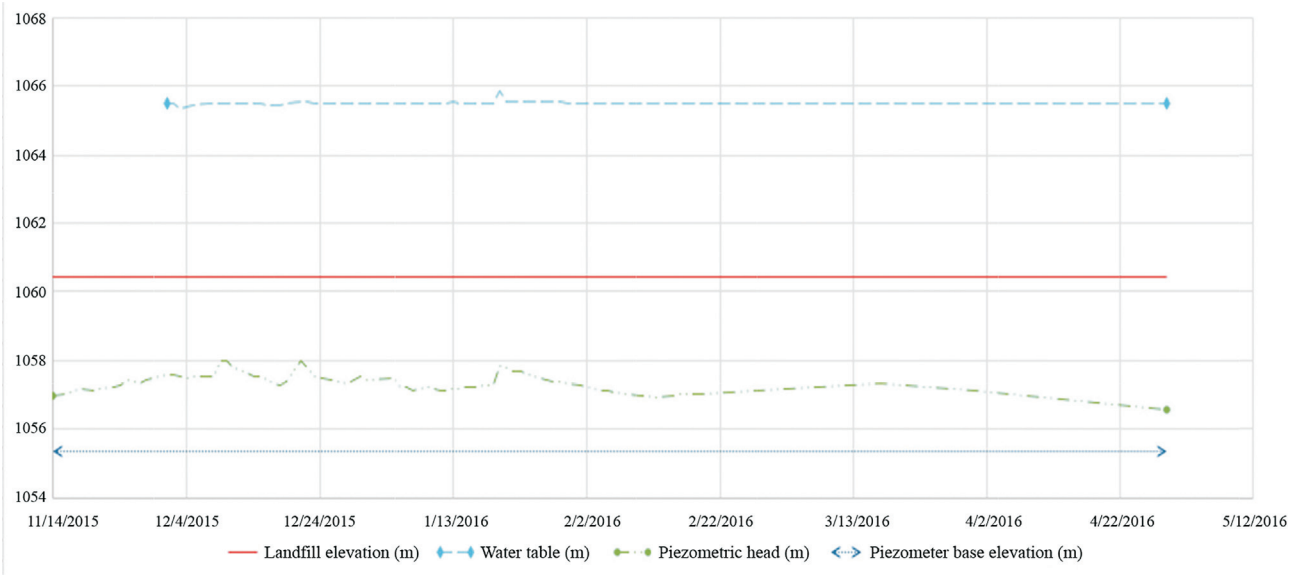

Figure 13 - Elevation (m) *vs.* Time (s) chart generated by the data collected by the electric piezometer 13 (P13), located on Peg 9+00 m.

due to long tree roots existing downstream of the dam. In addition to the concern regarding the anthill and the unpredicted voids, the peat layer presented thickness worryingly greater than forecasted by the geotechnical investigations.

Thus, regarding the analysis of these additional data which allowed to conclude that the original situation had worsened, the Jet Grouting treatment process had to be temporarily halted in this region, and consolidation grouting of the area was made. This consolidation was executed with a similar methodology to dams' foundations grout cut-offs to avoid possible new paths of preferential seepage and to fill the soil cavities in the affected stretch. The injections were composed of a cement slurry and injected at low pressures, as recommended by Zirlis *et al.* (2015).

To monitor the effect of the new treatment on the dam and the effectiveness of the grout injections, charts which correlated the volume of injected grout with the topography were made from the injection reports (Zirlis *et al.*, 2015), as illustrated in Fig. 16.

Upon visual observation of the work, from the instrumentation data analysis and the grout injections reports, it was possible to conclude that the treatment was effective; thus, the Jet Grouting intervention in this region was resumed, as it was, finally, enough consolidated.

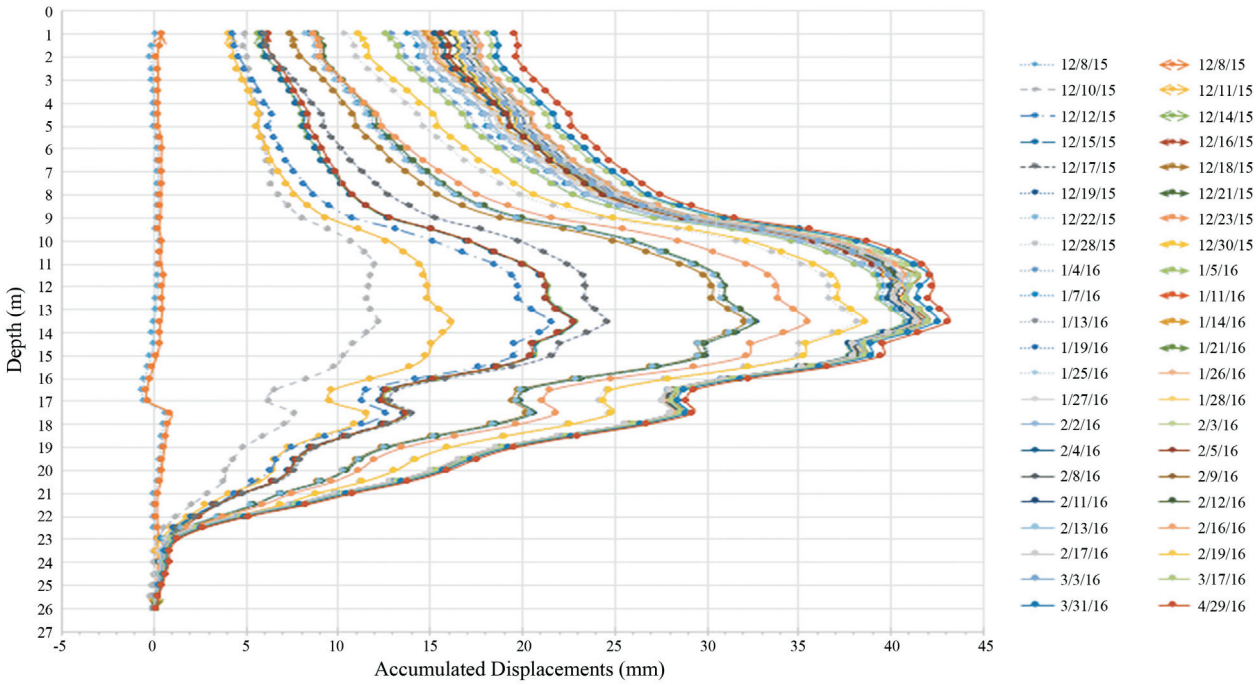

Figure 14 - Example of Depth (m) *vs.* Displacement (mm) chart from accumulated data generated by inclinometers in the longitudinal direction of the water flow. Different lines and symbols represent each measurement day.

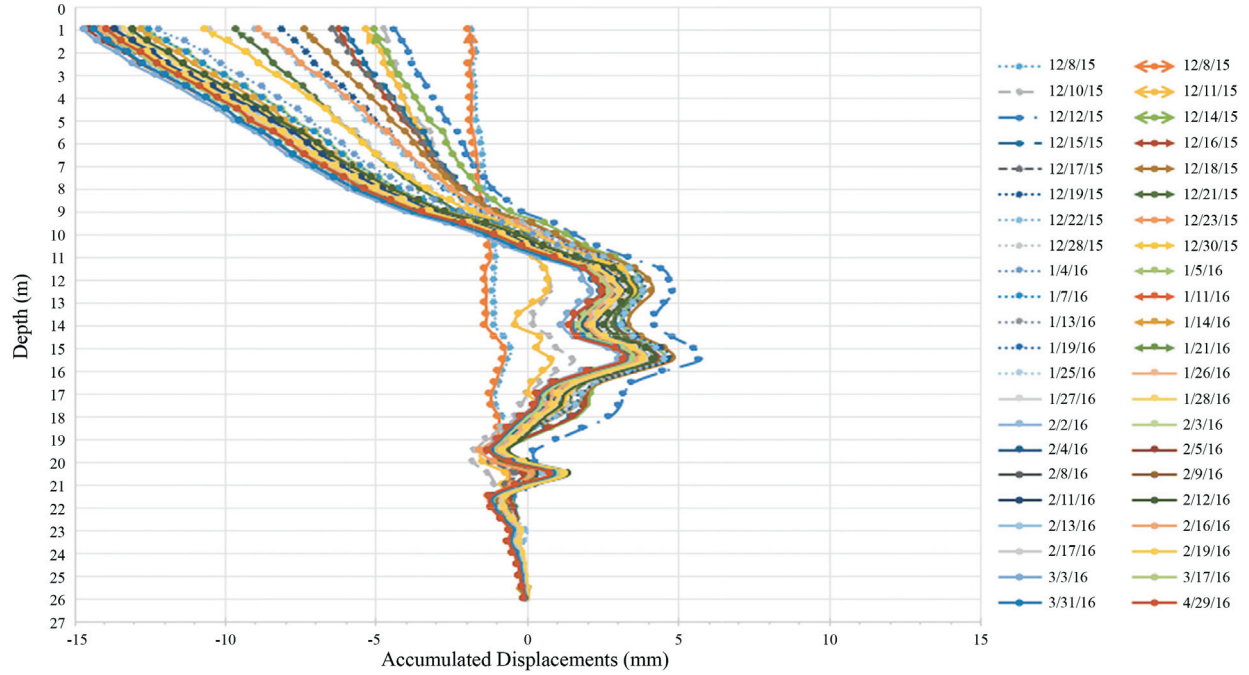

Figure 15 - Example of Depth (m) *vs.* Displacement (mm) chart from accumulated data generated by inclinometers in the normal direction of the water flow. Different lines and symbols represent each measurement day.

7. Results

7.1. Initial considerations

The success of geotechnical works is quite complex to be assessed. As ground is usually an anisotropic medium, heterogeneous, particulate and presenting non-linear behavior, obtaining genuinely representative parameters of the executed work would require a larger sample than financially allowed. Thus, the evaluation of the effectiveness of the recovery of "Ribeirão do Gama" dam assumes that a macroscopic analysis is sufficient for the problem.

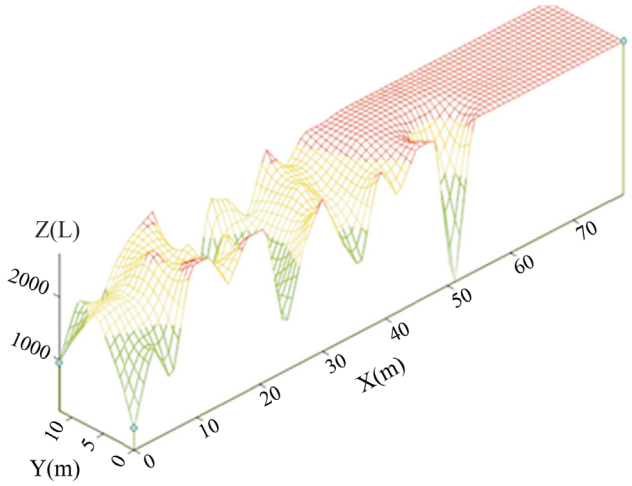

Figure 16 - Grout injection control. *Z* axis in total grout liters injected.

7.2. Obtained parameters evaluation

For assessing if the recovery of the "Ribeirão do Gama" dam was successful, the resulting parameters of the executed treatment were evaluated and compared with those previously estimated in the design phase. Thus, besides the observation of instrumentation data and a detailed visual analysis, samples of 15 m from four columns (1% of the total) were taken and analyzed regarding their degree of fracturing. In these four columns, which were selected in the passages in which there was more significant uncertainty regarding the formation and integrity of the soil-cement, tests of water loss were conducted, with methodology adapted from Porto (2002).

As for the instrumentation, the data collected by the electric VW piezometers provided the main indication of the effectiveness of the designed cut-off waterproofness. There were points in the dam, near the spillway, where the water level was below the depth of piezometer tips; therefore, the piezometers did not detect any water head. In other piezometers, hydraulic load values obtained were many times smaller than the expected in the design phase, a fact that attested to the proper overlapping of the Jet Grouting columns and the appropriate level of waterproofing provided by the treatment.

Surface measurements were made to assist the visual analysis, done with the main objective of evaluating the diameter of the column, expected to be 0.8 ± 0.1 m. Although the measurement of the surface diameter of the columns does not give a clear indication of the size of the lower portion of the columns, this information, along with the hydraulic load measured at the dam's downstream, was enough to indicate there was sufficient overlapping between the columns.

The design predicted the diameter of the lower portion of the columns would have sufficient size to provide overlapping between them. This expectation justifies itself due to the fact the earth mass, until the saprolite layer depth, had a resistance low enough for the Jet Grouting process to form columns of more than 0.8 m diameter. Still, there was doubt whether the executed columns had an appropriate degree of impermeability. For this, in addition to the analysis of piezometric data, the fracturing of the column cores and the results of the water loss tests performed in the four sampled columns were analyzed.

For the evaluation of the fracturing and quality of core samples from Jet Grouting columns, Yoshitake *et al.* (2003) proposed an alternative to the RQD method: the CRI (Core Recovery Index). This approach, idealized from the RQD classification, is based on visual examination of Jet Grouting column cores. Yoshitake *et al.* (2003) showed a correlation of uniaxial resistance to different types of cores. In this work, although our main concern was with the permeability coefficient, the presentation of the classification of the cores withdrawn is justified by the data generation for future CRI correlations with the permeability parameter of the sample and because the CRI also has a qualitative nature.

Therefore, from the analysis of four cored boreholes, one exemplified in Fig. 17, the quality of the samples with 0.1 m diameter extracted using rotary core drilling equipment was evaluated regarding the general appearance of the treatment.

The analysis, based on the CRI evaluation method, indicated high-quality treatment samples at a depth of 9.1 m, with a majority share of level 1 material (few cracks, solid and predominantly homogeneous) and level 2 material (presence of clay fractions). After this stretch, there is the peat layer; although the execution could make columns of the required diameter, there is the presence of material level 3, of fractured nature. Anyway, according to CRI criteria, the executed treatment can be characterized as high-quality.

However, for obtaining the permeability coefficient, the methodology adapted from Porto (2002) was used. The Jet Grouting columns were tested each 3 m, measuring water losses in 5 sections, totaling 15 m of depth. In each 3 m section, upward pressures, with a value multiple of 25 kPa, until obtaining a peak value of 150 kPa, were applied and then decreased to analogously correspondent pressures until reaching the previous minimum value of 25 kPa.

In the four tested drilled boreholes, the highest specific water loss was $1.98.10^{-6}$ m^3/s/m/kPa, in column 317, in the passage between 3 and 6 m, where peat occurred. Among the tested columns, the highest permeability had a magnitude of 10^{-6} m/s, again in the section where peat existed. In the piezometers, it is clear there was a load drop in the readings of instruments downstream of the executed Jet Grouting columns, but this fall was less than expected by the model adopted. Still, the executed treatment proved entirely satisfactory, having the resurgences of water down-

Figure 17 - Core sample from rotary drill borehole the Jet Grouting column number 186 (from the 706 executed).

Table 5 - Piezometer readings before and after the intervention.

Piezo meter	Peg (m)*	Piezometer depth (m)	Water level recorded before treatment (m)	Water level recorded after treatment (m)
P1	2+0.00	6.68	4.20	6.68 (Dry)
P2	5+0.00	15.33	2.90	N.A.
P3	9+0.00	22.10	6.00	N.A.
P4	N. I.	4.18	1.70	N.A.
P5	N. I.	3.35	1.60	N.A.
P6	N. I.	3.45	3.20	N.A.
P7	15+0.00	7.70	2.90	N.A.
P8	15+0.00	9.85	2.90	7.20
P9	9+0.00	10.00	4.20	7.05
P10	5+0.00	11.30	4.10	7.17
P11	2+10.00	3.75	2.00	N.A.
P12	5+0.00	12.60	1.00	N.A.
P13	9+0.00	16.20	1.14	N.A.
P14	15+0.00	8.14	On top	N.A.

Peg: Piezometer location, *e.g.* 2 + 0.00 m represents 40 m from datum.
N.I.: Not informed in Fig. 5.
N.A: Not available due to vandalism or obstruction.

stream ceased completely by the time of its completion in June 2016.

To complement the data and assess the current performance of the dam, further measurements were performed in the piezometers in October 2017, two years after the beginning of the treatment. Table 5 summarizes the results.

It is evident there was a further water head drop in the readings of instruments downstream of the executed Jet Grouting columns, even though the measurements were incomplete due to vandalism and obstructions in the piezometers. This further head drop is probably related to the slower dissipation of pore pressures in the peat layers.

8. Conclusion

It is advisable to inspect geotechnical works routinely after its implementation, especially dams as required by Brazilian laws. It was in one of these inspections the exposed problem was detected promptly, avoiding an accident which could have catastrophic consequences.

A successful geotechnical design depends fundamentally on proper diagnosis, which must be based on visual inspection and if possible in field and lab tests to obtain adequate constitutive parameters.

The execution of the proposed works must be monitored using the proper installation of specially selected monitoring and control instruments, allowing adjustments to the original design as soon as required to keep the execution phase safe and to minimize the probability of failure of the executed works.

In the present case study, the treatment of a piping process using a Jet Grouting cut-off with an adequate degree of waterproofing has shown to be satisfactory as the treatment eliminated downstream points of upwelling water.

The proposed solution also had a downstream toe drainage system which would be responsible for conducting the remaining flow by a proper path, after the completion of the treatment. This redundancy is necessary for situations like these because even if a failure occurred in the Jet Grouting impervious system, the resulting flow from this failure would be collected by the downstream drainage system, which would adequately conduct the flow to the natural bed of “Ribeirão do Gama”, without impacting the stability of the embankment.

Acknowledgments

The authors acknowledge the data provided by the companies Tüv Süd Bureau, Solotrat, and Trier. The authors also would like to give special thanks to the contracting engineer Max V. R. Barbosa, from Solotrat, for the execution guidance, details, and parameters. Finally, the authors acknowledge the support of the following institutions: the Brazilian National Council for Scientific and Technological Development (CNPQ) (Project

304721/2017-4), the Coordination for the Improvement of Higher Level Personnel (CAPES), and the University of Brasília for funding this research.

References

ABEF (2012). Manual de Execução de Fundações e Geotecnia - Práticas Recomendadas. Pini, São Paulo, pp. 441-466.

AGI (2012). Raccomandazioni Sul Jet Grouting. Ed. AGI, Roma, 74 p.

Bassett, R. (2012). A Guide to Field Instrumentation in Geotechnics: Principles, Installation and Reading. CRC Press, Boca Raton, pp. 3-5.

Croce, P. & Modoni, G. (2007). Design of Jet Grouting cut-offs. In Ground Improvement, 11(1):11-20.

Guatteri, G.; Koshima, A. & Pieroni, R.M. (2012). Challenges in execution of jet grouting curtains at the estreito HPP. In: Johnsen, L.F.; Bruce, D.A. & Byle, M.J. (eds.) Grouting and Deep Mixing 2012. Geotechnical Special Publication No. 228. American Society of Civil Engineers, Reston, pp. 2102-2111.

Lee, W.F. & Ishihara, K. (2016). Piping failure of a metro tunnel construction. In: Forensic Geotechnical Engineering, Developments in Geotechnical Engineering. Springer, New Delhi, pp. 433-450.

Nikbakhtan, B. & Osanloo, M. (2009). Effect of grout pressure and grout flow on soil physical and mechanical properties in jet grouting operations. International Journal of Rock Mechanics & Mining Sciences 46(3):498-505.

Perini, D.S. (2009). Estudo dos Processos Envolvidos na Análise de Riscos de Barragens de Terra. Master's Thesis, Publication G.DM-180/09, Civil and Environmental Engineering Department, University of Brasilia, 128 p.

Porto, E.C. (2002). Critério para Determinação de Vazões pela Fundação de Barragens com Base nos Ensaios de Perda d'água - O Caso da Usina Hidrelétrica de Itaipu. Master's Thesis, Federal University of Paraná, Graduate Program PPGCC/UFPR, 104 p.

Richards, K.S. & Reddy, K.R. (2007). Critical appraisal of piping phenomena in earth dams. Bulletin of Engineering Geology and the Environment, 66(4):381-402.

Saurer, E.; Marcher, Th. & Lesnik, M. (2011). Grid space optimization of jet grouting columns. In: Proc. 15th European Conference on Soil Mechanics and Geotechnical Engineering, 2(1):1055-1060.

Sembenelli, P. & Sembenelli G. (1999). Deep jet-grouted cut-offs in riverine alluvia for ertan cofferdams. Journal of Geotechnical and Geoenvironmental Engineering, ASCE, 125(2):142-153.

U.S. Army illustration by Todd Plain/Released (2016). Jet Grouting Process. 2016. Web. 20 Dec. 2016.

Yoshitake, I.; Mitsui, T.; Yoshikawa, T.; Ikeda, A. & Nakagawa, K. (2003). An evaluation method of ground improvement by jet grouting. Proceedings of the Japan Society of Civil Engineers, 735(1):215-220.

Zirlis, A.C.; Souza, G.J.T. & Pitta, C.A. (2015). Manual de Serviços Geotécnicos. Solotrat, São Paulo, 93 p.

One-Dimensional Consolidation Considering Viscous Soil Behaviour and Water Compressibility - Viscoconsolidation

P.E.L. Santa Maria, F.C.M. Santa Maria

Abstract. The aim of this paper is to draw attention to experimental evidence which may contribute to the understanding of the viscous behaviour of soft soils and, above all, present the equation for primary one-dimensional consolidation including the soil viscous resistance and the compressibility of water, with its analytical solution. Initially, a generic equation is presented, in which any constitutive relationship of viscous resistance *vs.* strain rate may be incorporated. This study, in particular, considers two constitutive relationships: the first, represented by a two-parameter hyperbola with a horizontal asymptote, and the second, represented by a linear relationship which characterizes the soil behaviour as Newtonian. The hyperbolic constitutive relationship was derived from consolidation test results where the viscous resistance was inferred. For this case, the equation was numerically integrated using the software MAPLE 2017. For the linear relationship (Newtonian behaviour), the equation was integrated analytically and its solution presented. Finally, the results of several analyses are presented and compared with results obtained experimentally as well as with classical results of Taylor (1942) and Terzaghi & Frölich (1936).

Keywords: compressibility of water, one-dimensional consolidation, pore pressure, two-parameter hyperbola, viscous resistance.

1. Introduction

The aim of this paper is to draw attention to experimental evidence that may contribute to the understanding of the viscous behaviour of soft soils (Taylor & Merchant, 1940; Taylor, 1942; Lacerda, 1976; Martins, 1992) and, most of all, to present an equation and its analytical solution for primary one-dimensional consolidation which considers the viscous resistance of the soil and the compressibility of the water in the voids. The drive behind this study surfaced during an experimental research performed at COPPE-UFRJ with the aim of understanding how the coefficient K_0 varies during secondary consolidation. The one-dimensional consolidation tests performed with a K_0 cell, designed by COPPE showed that at the beginning of each loading step, the pore pressure measured at the base of the sample was very low, increasing gradually with time until it reached a maximum, from which it decreased until finally reaching total dissipation. The solution proposed by Taylor (1942), which takes into account the viscous resistance component of the soil, was used to interpret the results, albeit this solution does not explain the initial pore pressure variation. The initial conjecture at that time was that this behaviour was due to the combined effect of the viscous resistance with the compressibility of water. For this to be true, it was believed that at the beginning of the test, the volumetric strain would lead to an increase in pore pressure with time, since the viscosity of the soil would prevent any process to occur instantly. Simultaneously, due to the high strain rates at this stage, the mobilized viscous resistance would be high, just sufficiently to alongside the resistance corresponding to pore pressure and effective frictional stress, satisfy the equilibrium condition. It is worth emphasizing that the component corresponding to the frictional effective stress would be, at this stage, much smaller than the pore pressure, since the stiffness of water is many orders of magnitude superior to that of the soil. With the progress of time, the drainage of the sample leads to a decrease in the pore pressure and an increase in the effective frictional stress. The strain rate, which has dropped monotonically, results in a reduction in the effective viscous stress. Thus, the growth rate of the pore pressure decreases, tending to zero (when the growth rate of the effective frictional stress equals the drop rate of the effective viscous stress) and, from then on, decreasing until the pore pressure is completely dissipated, at the end of the test.

Despite the existence of solutions which consider both the viscous resistance as well as the compressibility of the fluid in the study of one-dimensional consolidation, an analytical solution which considers both these mechanical phenomena combined could not be found within technical literature.

The solution proposed in this paper is able to predict reasonably well the pore pressure variation throughout the test during primary consolidation.

Paulo Eduardo Lima de Santa Maria, Ph.D., Engenheiro Sênior, SM Engenheiros Consultores, Rua Fernando Nogueira de Sousa 183, Barra da Tijuca, Rio de Janeiro, RJ, Brazil. e-mail: paulosm@smengenheiros.com.br.
Flavia Cristina Martins de Santa Maria, D.Sc., Engenheira Civil, Departamento de Análise de Tensões, Eletrobras Eletronuclear, Rua da Candelária 65, 7° andar, Rio de Janeiro, RJ, Brazil. e-mail: fsmaria@eletronuclear.gov.br.
Submitted on May 14, 2017; Final Acceptance on March 7, 2018; Discussion open until August 31, 2018.
DOI: 10.28927/SR.411033

2. Viscoconsolidation

In perfect analogy with disciplines which incorporate viscous behaviour to classical Solid Mechanics, such as Viscoelasticity and Viscoplasticity, in this paper the term viscoconsolidation is used to define the study of one-dimensional primary consolidation where the viscous and hydrodynamic behaviours occur simultaneously, including the effects of the compressibility of the water in the voids. In this case, both the viscous resistance and the hydrodynamic resistance work delaying the strain, making it occur as a function of time during primary consolidation until, at the end of the process, only the frictional resistance takes part in the process and the strain rate cancels out. Naturally, this is not precisely what is actually happening. It is known that the strain rate continues to exist after the end of primary consolidation, during secondary consolidation, until it finally comes to an end.

According to Tsytovich & Zaretsky (1969), the best way to assess the influence of viscous resistance of a soil, also called structural resistance by the authors and plastic structural resistance by Taylor (1942), is through the pore pressure measured in an undisturbed soil sample submitted to a compression test. For this purpose, a coefficient β_0 is defined as $\beta_0 = u_0/\Delta\sigma$, where u_0 is the initial pore pressure submitted to loading $\Delta\sigma$. These authors highlight the consideration of volumetric strain as a result of the unsaturation of the soil for cases with degrees of saturation above 90%. Figures 1 (a), (b) and (c) illustrate some experimental results of pore pressure variation with time in samples with degrees of saturation of 95% and 98%. It may be observed that, in most loading steps, there is an initial growth in pore pressure, up to a maximum value, followed by a decrease leading to total dissipation. Zaretsky (1972) observes that, although this behaviour was present in soils with degrees of saturation smaller than 100%, it was also verified in tests carefully prepared to guarantee total sample saturation.

Suklje (1969) presents curves for pore pressure *vs.* time obtained from consolidation of a normally consolidated lacustrine chalk with degrees of saturation of 96% and 92%, whose shapes resemble those of Tsytovich & Zaretsky (1969).

Due to its extremely low compressibility when compared to the compressibility of the soil structure, water is considered incompressible in most of the analyses of behaviour of saturated soils in Soil Mechanics. The bulk modulus of elasticity of degassed water at 20 °C is 2.15×10^3 MPa. It is also known that this modulus varies at different temperatures and pressures. However, when dealing with pore water in layers of soil below the water level, the situation is significantly different as, in these cases, not only may there be microscopic air bubbles, but also dissolved gases in the soil. According to Tsytovich (1987), a degree of saturation just under 100% increases significantly the compressibility of pore water and the bulk modulus of elasticity of water, K, in this case may be estimated with the equation:

$$K = \frac{p_a}{1 - S} \tag{1}$$

where: p_a = atmospheric pressure, S = degree of sample saturation.

It is easy to understand that a one-dimensional consolidation test performed on soil with viscous behaviour and compressible water in the voids may be elementarily represented by a rheological model composed of a Maxwell and a Kelvin model connected in parallel, as shown on Fig. 2.

The Kelvin model (a linear spring element and a linear viscous dashpot element connected in parallel) represents the soil with viscous behaviour and the Maxwell model (a linear spring element and a linear viscous dashpot element connected in series) represents the hydrodynamic behaviour of the compressible water under vertical drainage.

It is worth stressing that the time-dependent representation of the hydrodynamic behaviour by a linear function of its velocity, although a simplification, does not invalidate the purpose of this modelling, which is to present the aspect of the progress of the pore pressure with time.

The model's differential equation for a constant loading σ_0 obtained by the equilibrium of forces may be written as follows:

$$\frac{d}{dt}\varepsilon(t) + \frac{1}{\eta_2}\left[\frac{E\eta_3 + K\eta_3 + KEt}{\eta_3 + Kt}\right]\varepsilon(t) - \frac{\sigma_0}{\eta_2} = 0 \tag{2}$$

whose solution for the initial condition $\varepsilon(0) = 0$ is:

$$\varepsilon(t) = \left[\int_0^t \frac{\sigma_0 (K\tau + \eta_3)^{\frac{\eta_3}{\eta_2}} \cdot e^{\frac{E}{\eta_2}\tau}}{\eta_2} d\tau\right] e^{-\frac{E}{\eta_2}t} \cdot (Kt + \eta_3)^{-\frac{\eta_3}{\eta_2}} \tag{3}$$

The total resistance components may be represented as:
pore pressure:

$$u(t) = \frac{K\eta_3}{\eta_3 + Kt}\varepsilon(t) \tag{4}$$

frictional resistance:

$$\sigma'_f(t) = E\varepsilon(t) \tag{5}$$

viscous resistance:

$$\sigma'_v(t) = \eta_2 \frac{d}{dt}\varepsilon(t) \tag{6}$$

Figure 3 shows a result for the variation of pore pressure with time, obtained by Eqs. 3 and 4, for typical values of E, K, η_2 and η_3.

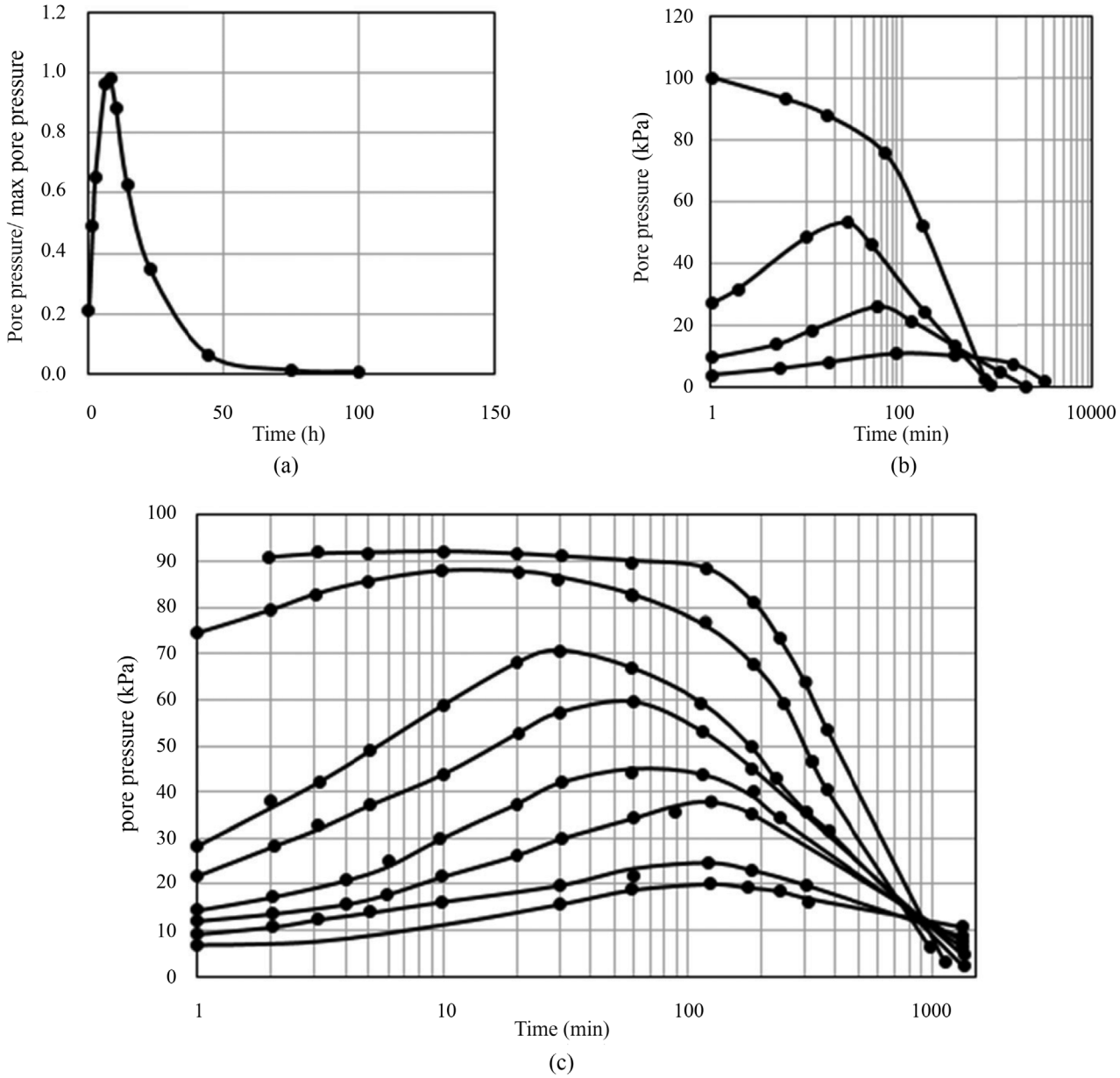

Figure 1 - (a)-Pore pressure dissipation for experiments of Sipidin (Cambrian clay, S = 98% and water content = 30%); (b)-Pore pressure dissipation for experiments of Ter-Martirosyan and Tsytovich (Saratov clay of a disturbed structure, S = 98%, with loading step q = 100 kPa, where curves correspond to the consecutive loading steps); (c)-Pore pressure dissipation for experiments of Kogan (Silty loam of an undisturbed structure, S = 95%, water content = 30%, with loading step q = 100 kPa) (after Zaretsky, 1972).

2.1. Relationship between viscous resistance and strain rate

According to Vyalov (1986), viscosity is a property of fluids (or gases) which causes resistance to the movement of elementary particles relative to one another. Newton (1687) was the first scientist to investigate viscosity. He observed that the resistance offered by a flowing liquid is proportional to its shear velocity.

Newton's law or rheological equation of state of a Newtonian liquid, which relates the shear stress τ_i with the shear strain rate $\dot{\gamma}_i$ is given by:

$$\tau_i = \eta \cdot \dot{\gamma}_i \quad (7)$$

The constant η is the viscosity or dynamic viscosity and its SI unit is *Pa.s*. The reciprocal of viscosity, $\Phi = 1/\eta$, is called fluidity.

Although the viscous phenomenon had been originally identified and defined for liquids, it is known to occur, with varying intensities, in virtually all solids found in Nature.

Thus, it may be written:

$$\sigma_{ij} = \eta_s \cdot \dot{\varepsilon}_{ij} \quad (\text{for } i \neq j) \quad (8)$$

$$\sigma_{ij} = \eta_n \cdot \dot{\varepsilon}_{ij} \quad (\text{for } i = j) \quad (9)$$

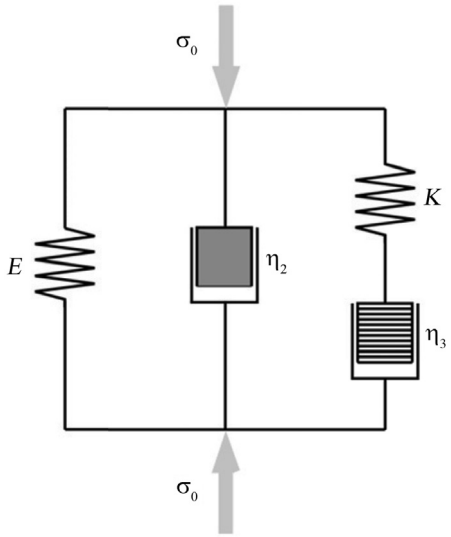

Figure 2 - Rheological model representing a one-dimensional consolidation test on viscous soil with compressible water in the voids.

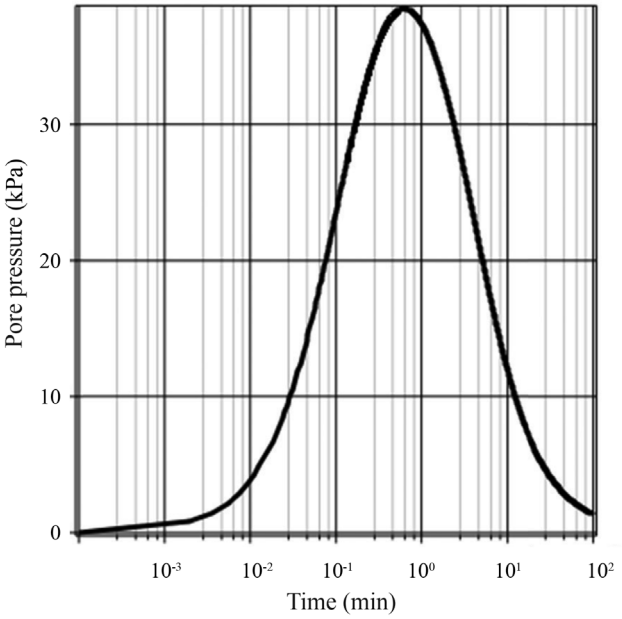

Figure 3 - Progress of pore pressure with time obtained from a rheological model (Maxwell and Kelvin in parallel) of a one-dimensional consolidation test on viscous soil with compressible water in the voids.

where η_c is the coefficient of viscosity for shear and η_n is the coefficient of viscosity for compression or tension, often called Trouton factor.

Many real solids have a viscous behaviour different from Newton's law. This distinct behaviour, known as anomalous viscosity, is manifested as a variation in the coefficient of viscosity as a function of the magnitude and direction of loading.

The dependency of parameter η on loading is equivalent to the non-linear relationship between the strain rate $\dot{\varepsilon}$ and the stress σ. This viscous behaviour is known as non-linear or non-Newtonian.

The rheological equation of state of a non-linear viscous solid may be presented as:

$$\sigma = f(\dot{\varepsilon}) \text{ or } \dot{\varepsilon} = \phi(\sigma) \tag{10}$$

Ostwald (1926), a pioneer in the study of anomalous viscous media, concluded that those media which have structure present a behaviour pattern distinct from those that are perfectly viscous (Newtonian). The explanation is that the structure changes with strain and, consequently, so does the viscosity. This variable viscosity is also known as structural viscosity.

Consolidation tests, either of one-dimensional or hydrostatic compression, have shown that the behaviour of clayey soils under compression is non-Newtonian. According to Alexandre (2000), the relationship between the effective viscous stress σ'_v and the rate of void ratio variation $\dot{e}$ may be presented as Ostwald's power function, as follows:

$$\sigma'_v = -a(\dot{e})^{\frac{1}{n}} \tag{11}$$

where $n > 1$, a = stress increment constant.

Santa Maria (2002) proposes adjusting the solution to fitted hyperbolas of two and three parameters, in addition to the power function. Although Santa Maria (2002) observes that the power function leads to better correlations, it is important to note that this was based only on the values of the correlation coeficients of the fitting. A qualitative assesment of the fitting with the three proposed functions indicates that the fitted two-parameter hyperbola presents results which best resemble the behaviour experimentally observed.

Comparing Fig. 4 with the behaviour observed by Santa Maria (2002), Taylor (1942) and Thomasi (2000), it may be stated that the viscous component of the resistance,

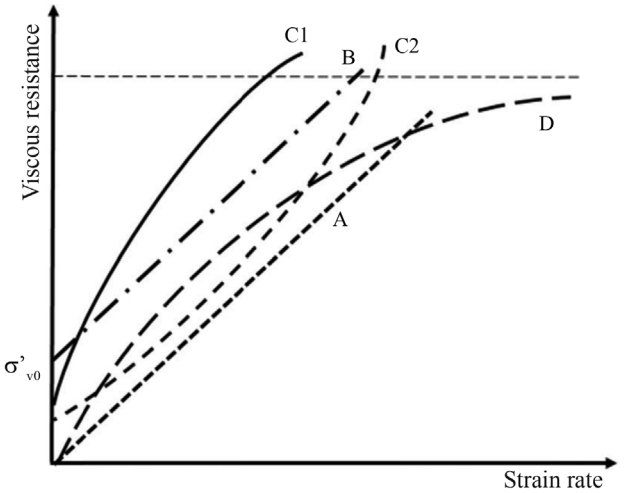

Figure 4 - Relationship between viscous resistance and strain rate. *A* = Newtonian viscous liquid; *B* = plastic viscous material; *C*1 and *C*2 = quasi-plastic viscous material; *D* = saturated clay under one-dimensional consolidation test.

either on one-dimensional or hydrostatic compression, does not display characteristics of either a purely viscous fluid (line *A*), or of a purely plastic one (line *B*), where the flow does not occur until a certain value of stress is reached. Likewise, it also does not present the behaviour of quasi-plastic materials (lines *C*1 and *C*2), but complies adequately with the behaviour described by the fitted two-parameter hyperbola, represented by line *D*.

Figures 5 to 8 regarding one-dimensional consolidation tests (Taylor, 1942; Santa Maria, 2002) and Fig. 9 regarding a hydrostatic consolidation test (Thomasi, 2000), show how the viscous component of the effective stress varies with the absolute value of the void ratio rate and the strain rate.

These figures also show the fitted two-parameter hyperbolas, adjusted visually to the experimental points. The equation for the hyperbolas is as follows:

$$\sigma'_v = \frac{\dot{e}}{\frac{1}{a_e} + \frac{\dot{e}}{b_e}} \text{ or } \sigma'_v = \frac{\dot{\varepsilon}}{\frac{1}{a_\varepsilon} + \frac{\dot{\varepsilon}}{b_\varepsilon}} \quad (12)$$

Parameters a_e and a_ε represent the angular coefficient of the tangent at the origin while b_e and b_ε represent the ordinate of the horizontal asymptote.

Figures 6 to 8 concern one-dimensional consolidation tests. It is worth drawing attention to the fact that the results presented were obtained for mean values of $\dot{e}$ and σ'_v.

As may be observed, the fitted two-parameter hyperbola represents reasonably well the viscous resistance variation with strain rate $\dot{\varepsilon}$, volumetric strain rate $\dot{\varepsilon}_v$, and void ratio rate $\dot{e}$. Figures 5 to 9 clearly indicate a trend for the viscous resistance to reach a maximum value when the strain rate increases. This evidence has an important implication.

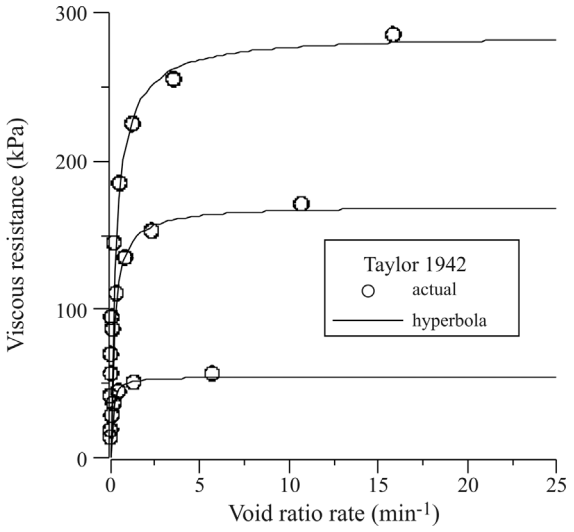

Figure 5 - Viscous component of the effective stress *vs.* void ratio rate – actual data from one-dimensional consolidation on a Boston Blue Clay sample (Taylor, 1942, after Alexandre, 2000) and fitted two-parameter hyperbolas.

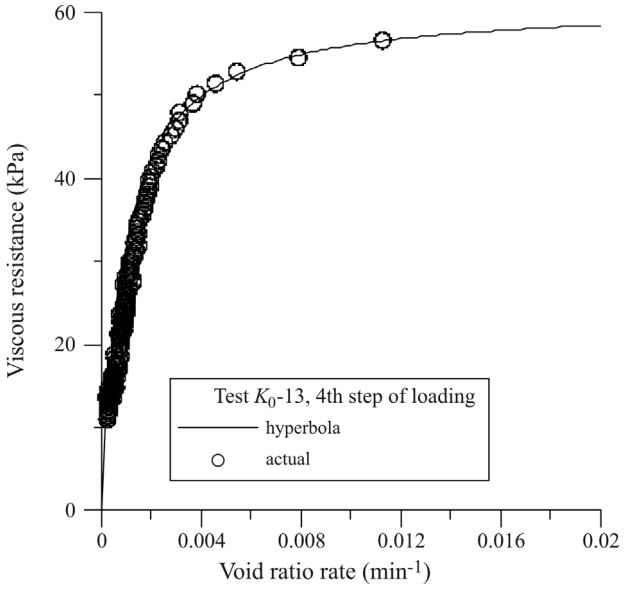

Figure 6 - Viscous resistance *vs.* void ratio rate – fitted two-parameter hyperbola compared with actual points obtained from one-dimensional consolidation test K_0-13 / 4th loading step (Santa Maria, 2002).

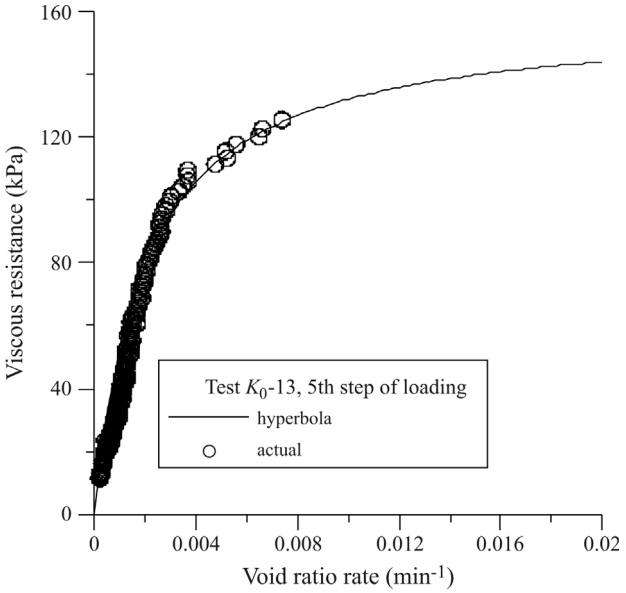

Figure 7 - Viscous resistance *vs.* void ratio rate – fitted two-parameter hyperbola compared with actual points obtained from one-dimensional consolidation test K_0-13 / 5th loading step (Santa Maria, 2002).

Experimental results from consolidation tests have shown that there is an infinite set of void ratio *vs*. effective stress curves defining the behaviour of a clayey soil, one for each void ratio rate $\dot{e}$ (Bjerrum, 1967; Martins & Lacerda, 1985). Naturally, this set of curves features a limit to the left, characterized by the curve e *vs*. σ' for $\dot{e} = 0$. In this curve, the resistance to strain is exclusively frictional in origin as the viscous component is not mobilized ($\dot{e} = 0$). The new evidence indicates the existence of a limit to the right also,

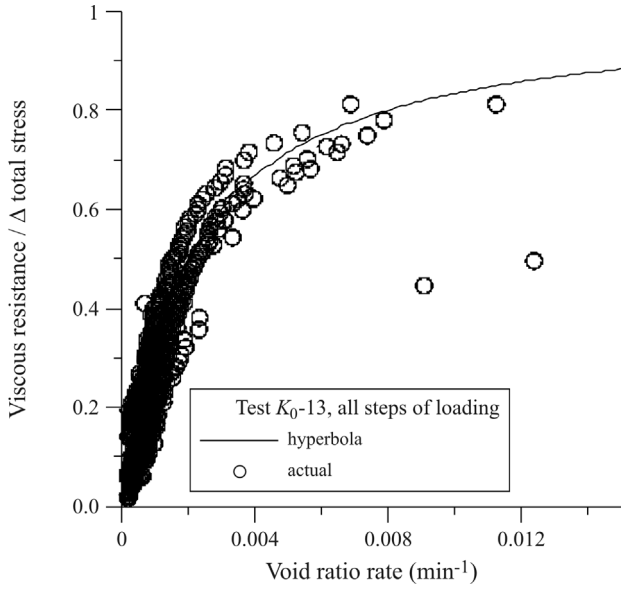

Figure 8 - Normalized viscous resistance *vs.* void ratio rate – fitted two-parameter hyperbola compared with actual points obtained from one-dimensional consolidation test K_0-13 / all loading steps (Santa Maria, 2002).

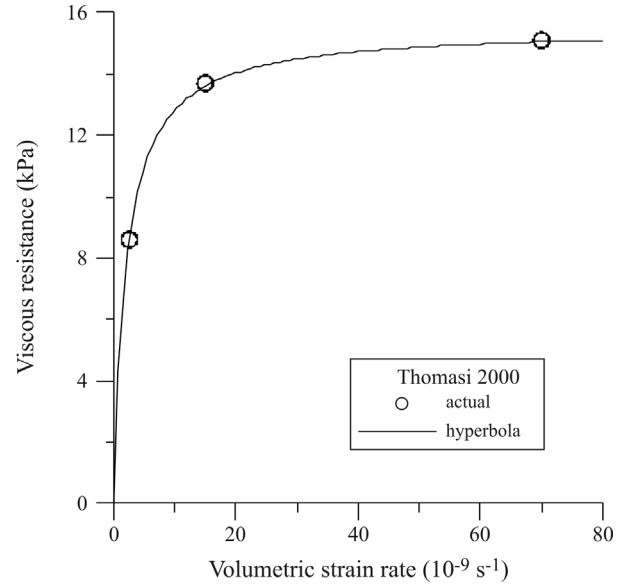

Figure 9 - Viscous component of the effective stress *vs.* volumetric strain rate during a hydrostatic consolidation test – actual data (Thomasi 2000) and fitted two-parameter hyperbola.

corresponding to $\dot{e} \geq \dot{e}_{lim}$ (Fig. 10). This means that after mobilizing all the available resistance (frictional and viscous), any subsequent load increment would result in an incresase in pore pressure, so that the condition of equilibrium is satisfied.

2.2. General equation

The general equation for one-dimensional viscous consolidation considering the compressibility of water may be written as (Appendix A):

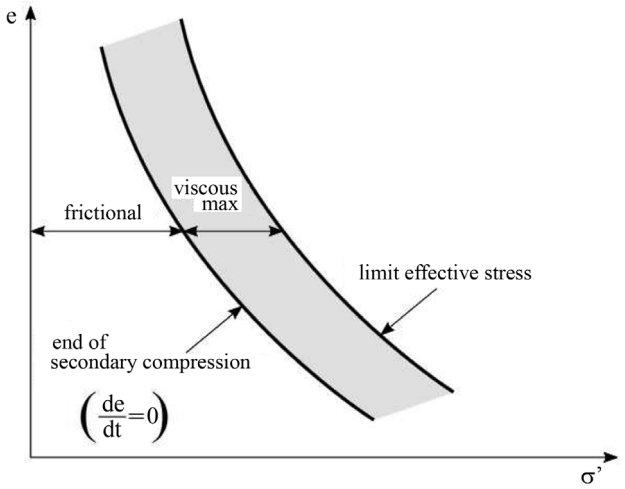

Figure 10 - Schematic representation of the two boundaries of the region where the pattern of behaviour is possible.

$$\frac{\partial e}{\partial t} = -C_k \frac{\partial}{\partial t}(e - a_v \cdot \sigma'_v) + C_v \frac{\partial^2}{\partial z^2}(e - a_v \cdot \sigma'_v) \quad (13)$$

where e = void ratio, function of t and z, $C_k = \frac{\bar{e}}{K \cdot a_v}$, $C_v = \frac{k \cdot (1+\bar{e})}{\gamma_w \cdot a_v}$, $\bar{e}$ = average void ratio, K = bulk modulus of elasticity of water, a_v = coefficient of compressibility, γ_w = unit weight of water and k = coefficient of permeability.

The following hypotheses are admitted:

- soil is homogeneous;
- soil particles are incompressible;
- vertical soil drainage and strain;
- Darcy's law is valid;
- small strains;
- water is considered as an elastic compressible fluid;
- the bulk modulus of elasticity of water is constant for the existing pressure range;
- C_k and C_v are constant for existing stress range and with time;
- the viscous resistance σ'_v is a function of $\bar{e}$ and $\frac{\partial e}{\partial t}$;
- the total applied stress is constant with time.

2.2.1. Numerical solution and experimental results

Admitting that the viscous resistance σ'_v was defined by the fitted two-parameter hyperbola, expressed by Eq. 14 and illustrated in Fig. 11, Eq. 13 is numerically integrated using the software MAPLE 2017.

$$\sigma'_v = \frac{\dot{e}}{\frac{1}{a_e} + \frac{\dot{e}}{b_e}} \quad (14)$$

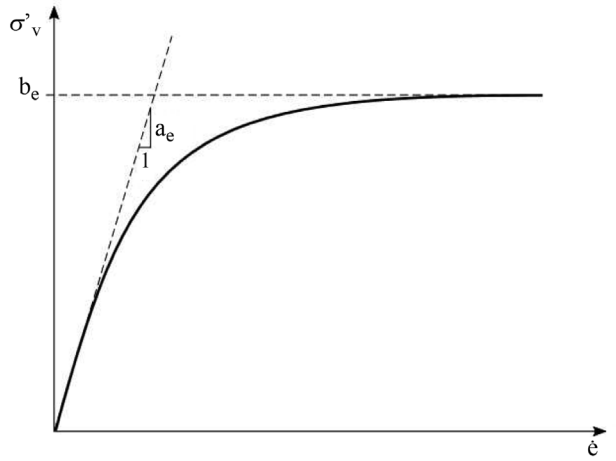

Figure 11 - Definition of limit viscous resistance (b_e) and initial coefficient of viscosity (a_e) for one-dimensional consolidation tests.

The solution requires two boundary conditions in z and two initial conditions in t:

(1) $z = 0, \forall t$ - solution of equation:

$$\frac{-\frac{de}{dt}}{\frac{1}{a_e}-\left(\frac{1}{b_e}\times\frac{de}{dt}\right)} = \sigma - \frac{e_0 - e}{a_v};\quad e(t=0) = e_0$$

(2) $z = 2h, \forall t$ - solution of equation:

$$\frac{-\frac{de}{dt}}{\frac{1}{a_e}-\left(\frac{1}{b_e}\times\frac{de}{dt}\right)} = \sigma - \frac{e_0 - e}{a_v};\quad e(t=0) = e_0$$

(3) $e(\forall z, t=0) = e_0$

$$(4)\ \frac{\partial e}{\partial t}(\forall z, t=0) = -\frac{\frac{\sigma}{a_e}}{1-\left(\frac{\sigma}{b_e}\right)}$$

where σ represents the total stress applied.

Eq. 15 is obtained by equilibrium and allows the evaluation of the pore pressure.

$$u = \sigma - \frac{\Delta e}{a_v} + \frac{\dot{e}}{\frac{1}{a_e}-\frac{\dot{e}}{b_e}} \qquad (15)$$

Santa Maria (2002) performed one-dimensional consolidation tests with remolded clay samples from the Sarapuí river using a K_0 cell designed by COPPE-UFRJ, illustrated in Fig. 12. The instrumentation comprises three load cells (one for each of the two lateral windows, to study the K_0 coefficient, and a third at the base, to determine the friction on the walls), three LVDT's, one for each window and one to measure the vertical displacement of the top cap, and a pore pressure transducer at the base.

The results presented in this paper refer to the incremental test K_0-13. Figure 13 shows the variation of the pore pressure from the beginning of the test up to 2000 min, at the last two loading steps (4th and 5th steps), alongside the values obtained from the integration of Eq. 13, performed using MAPLE 2017. The data and parameters regarding these two steps, obtained by Santa Maria (2002), are presented in Table 1. As mentioned before, k, a_v, a_e and b_e represent mean values for each step.

It may be seen that from minute 0.6 onwards the theoretical curve is very representative of the behaviour obtained experimentally. Nevertheless, before this moment, there is a significant discrepancy owing to the initial conditions of the theoretical solution where, for time $t = 0^+$, the vertical strains and, consequently, the pore pressures are null. On the 5th step of the test, for instance, the first pore pressure measurement occurs at 0.001 min, with a value of 28.5 kPa. Thus, it is thought that the best explanation for this high value of pore pressure at such a small fraction of time may be the inertial effect resultant from the load increment applied with weights on the yoke at the centre of the top cap of the oedometric cell. Naturally, this loading was performed with the utmost care to minimize the effects which are inherently associated with the manual loading process.

2.3. Equation for linear relationship between σ'_v and $\frac{\partial e}{\partial t}$

When the functional relationship between σ'_v and $\frac{\partial e}{\partial t}$ is linear, it may be written as:

$$\sigma'_v = -\eta \cdot \frac{\partial e}{\partial t}$$

For this condition, Eq. 13 becomes (Appendix A):

$$C_{k1}\frac{\partial e}{\partial t} + C_{kt}\frac{\partial^2 e}{\partial t^2} - C_v\frac{\partial^2 e}{\partial z^2} - C_{vt}\frac{\partial^3 e}{\partial z^2 \partial t} = 0 \qquad (16)$$

Table 1 - Data and parameters regarding the 4th and 5th loading steps.

Parameter	4th step	5th step
k (m.min^{-1})	6.20×10^{-9}	4.20×10^{-9}
K (kPa)	8.25×10^{3}	9.00×10^{3}
a_v (kPa^{-1})	3.32×10^{-3}	1.79×10^{-3}
h (mm)	33.1	29.5
σ (kPa)	69.8	167.5
e_0	2.11	1.80
a_e (kPa.min)	38000	70000
b_e (kPa)	73.7	173

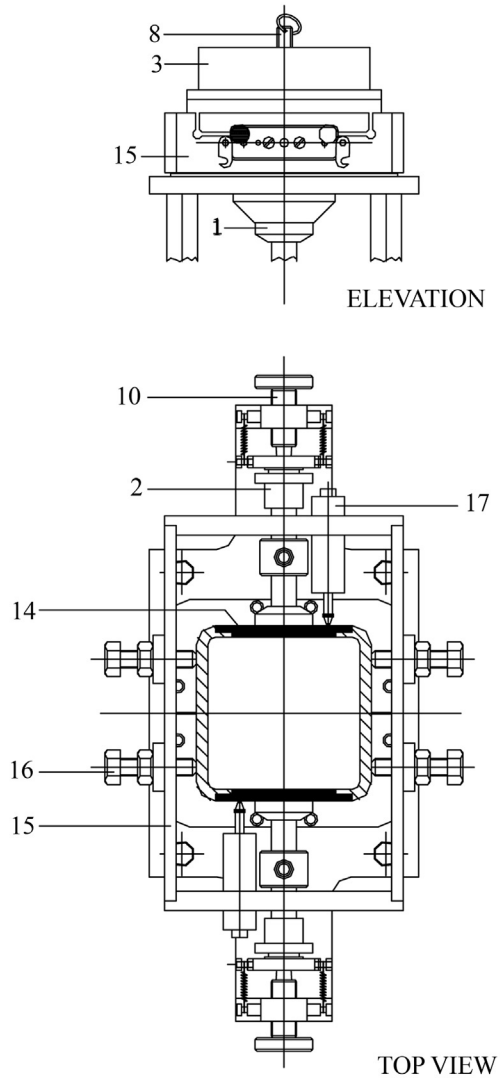

1 - vertical load cell

2 - horizontal load cell

3 - extension part

4 - screws to fix the extension part

5 - cell where the soil sample is placed

6 - top cap

7 - plate of sinterized bronze attached to the top cap

8 - handles to place the top cap in position

9 - steel sphere

10 - screw-spring system for fixing and adjusting the load cells

11 - socket to fit pore pressure transducer or drainage plastic hose

12 - base cell window

13 - socket for the sinterized bronze disc

14 - lateral cell window

15 - horizontal LVDTs holder

16 - screws to fix the horizontal LVDTs holder

17 - horizontal LVDTs

Figure 12 - Detail of the K_0 cell with the LVDTs holder.

where η = coefficient of viscosity

$$C_{k1} = \frac{\bar{e} + Ka_v}{Ka_v}$$

$$C_{kt} = \frac{\eta \bar{e}}{K}$$

$$C_v = \frac{k(1+\bar{e})}{\gamma_w \cdot a_v}$$

$$C_{vt} = \frac{k(1+\bar{e})\eta}{\gamma_w}$$

Eq. 16 is a third-order linear partial differential equation with t and z as independent variables.

To derive this equation, the following assumptions were considered:

- soil is homogeneous;
- soil particles are incompressible;
- vertical soil drainage and strain;
- Darcy's law is valid;
- small strains;
- water is considered as an elastic compressible fluid;
- the bulk modulus of elasticity of water is constant for the existing pressure range;
- C_{k1}, C_{kt}, C_v and C_{vt} are constant for the existing stress ranges and with time;
- the total applied stress is constant with time.

2.3.1. Analytical solution and experimental results

The solution to the equation requires two boundary conditions in z and two initial conditions in t, as shown below:

(1) $z = 0$, $\forall t$ - solution for equation:

$$-\eta \frac{de}{dt} = \sigma - \frac{e_0 - e}{a_v}; \quad e(t=0) = e_0$$

(2) $z = 2h$, $\forall t$ - solution of equation:

$$-\eta \frac{de}{dt} = \sigma - \frac{e_0 - e}{a_v}; \quad e(t=0) = e_0$$

(3) $e(\forall z, t=0) = e_0$

$$(4)\ \frac{\partial e}{\partial t}(\forall z, t=0) = -\frac{\sigma}{\eta}$$

where σ is the total applied stress.

Considering that the solution for the differential equation presented in conditions (1) and (2) is

$$e = e_0 - a_v \sigma \left(1 - e^{-\frac{t}{\eta a_v}}\right),$$

the integration of Eq. 16 for the above conditions leads to the following solution (Appendix B):

$$e = e_0 - \sigma \cdot a_v \left\{1 - \sum_{m=0}^{n} \left[\frac{(B_{m2} - C_c)}{M\sqrt{A_m}} e^{-\frac{1}{2}\frac{B_{m1}\cdot t}{C_{kt}\cdot h^2}} - \frac{(B_{m1} - C_c)}{M\sqrt{A_m}} e^{-\frac{1}{2}\frac{B_{m2}\cdot t}{C_{kt}\cdot h^2}} \right] \cdot \sin\left(\frac{M\cdot z}{h}\right) \right\} \quad (17)$$

$$u = \sigma \left\{ \sum_{m=0}^{n} \left[\frac{(B_{m2} - C_c)\cdot(C_{kt}h^2 - \frac{1}{2}\frac{B_{m1}C_{vt}}{C_v})}{M\sqrt{A_m}C_{kt}h^2} e^{-\frac{1}{2}\frac{B_{m1}\cdot t}{C_{kt}\cdot h^2}} - \frac{(B_{m1} - C_c)\cdot(C_{kt}h^2 - \frac{1}{2}\frac{B_{m2}C_{vt}}{C_v})}{M\sqrt{A_m}C_{kt}h^2} e^{-\frac{1}{2}\frac{B_{m2}\cdot t}{C_{kt}\cdot h^2}} \right] \cdot \sin\left(\frac{M\cdot z}{h}\right) \right\} \quad (18)$$

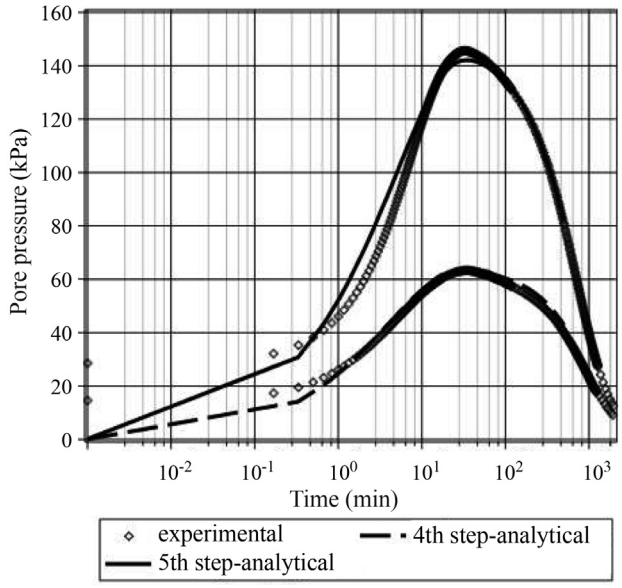

Figure 13 - Comparison between pore pressures predicted from Eq. 13 and obtained experimentally (Santa Maria, 2002).

where

$$A_m = C_{k1}^2 \cdot h^4 + 2C_{k1} \cdot C_{vt} \cdot M^2 \cdot h^2 - 4C_{kt} \cdot C_v \cdot M^2 \cdot h^2 + C_{vt}^2 \cdot M^4$$

$$B_{m1} = C_{k1} \cdot h^2 + C_{vt} \cdot M^2 - \sqrt{A_m}$$

$$B_{m2} = C_{k1} \cdot h^2 + C_{vt} \cdot M^2 + \sqrt{A_m}$$

$$C_c = \frac{2C_{kt} \cdot C_v \cdot h^2}{C_{vt}}$$

It can be easily shown that Eq. 17 becomes Taylor's solution (1942) when $K \to \infty$.

Figures 14 and 15 present the results of a comparative analysis between the solution proposed in this study and that presented by Taylor for the same parameter values corresponding to the 5th step of test K_0-13 (Table 1)

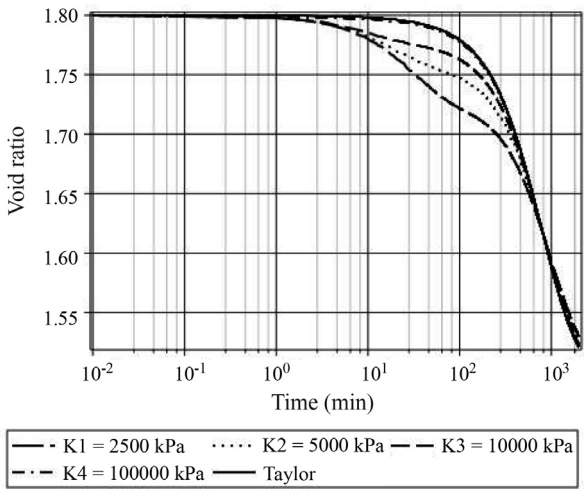

Figure 14 - Comparison of void ratio values determined by Eq. 17 for several values of K and by Taylor's solution (1942).

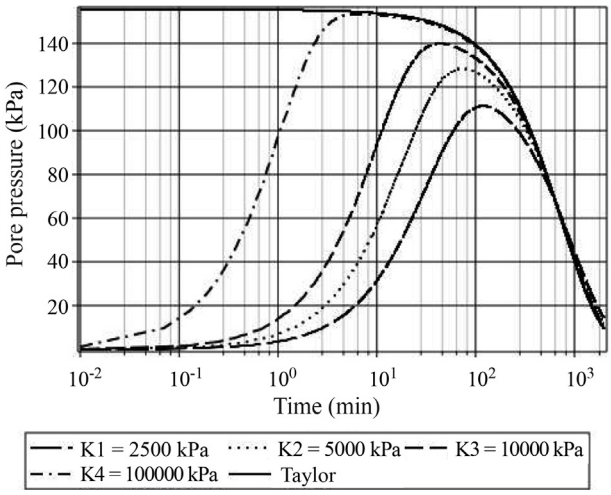

Figure 15 - Comparison of pore pressure values determined by Eq. 18 for several values of K and by Taylor's solution (1942).

It becomes clear that, as the bulk modulus of elasticity of water increases, the curves get closer to the curve corresponding to Taylor's solution (1942), as expected.

With the aim of comparing and verifying the consistency between analytical and numerical results, Fig. 16 presents the curves obtained by means of Eq. 17 and through numerical integration of Eq. 16 using MAPLE 2017, for the parameter values corresponding to the 5th step of test K_0-13 (Table 1).

As a perfect match was obtained, to distinguish the numerical result from the analytical the former was multiplied by a factor of 0.999.

Figure 17 presents the progress of pore pressure with time for the same parameters presented in Table 1, where the coefficients of viscosity, η, are considered equal to the angular coefficient of the tangent, a_e, of the two-parameter hyperbola at the origin. As expected, the match between the theoretical and experimental curves is not as good as the one obtained by the general equation with function σ'_v represented by a fitted two-parameter hyperbola.

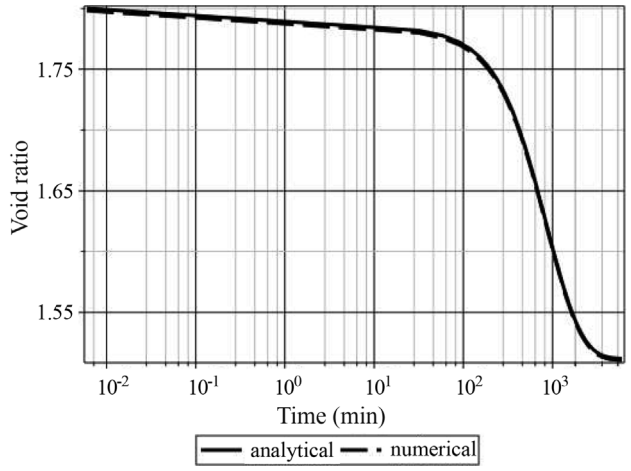

Figure 16 - Comparison between numerical and analytical solutions of Eq. 16, suggesting a perfect match (an offset was introduced in the curves, otherwise only one line would be seen).

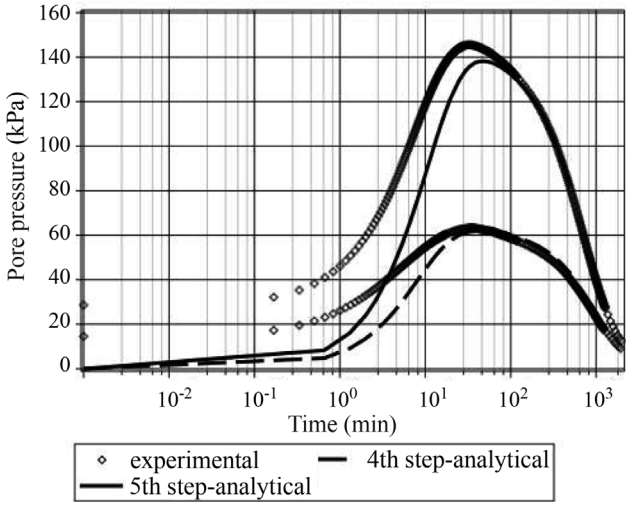

Figure 17 - Comparison between pore pressures predicted from Eq. 18 and obtained experimentally (Santa Maria, 2002).

To fully envision the importance of the coefficient of viscosity in the behaviour of a soil during one-dimensional consolidation, the curves for void ratio *vs.* time and pore pressure *vs*. time are plotted for various values of η, as well as the curve for the Terzaghi & Frölich's solution (1936), which does not contemplate this effect (Figs. 18 and 19). The values of the remaining parameters are those presented in Table 1. It is worth noting that, for numerical convenience, in this case hour has been adopted as a unit of time.

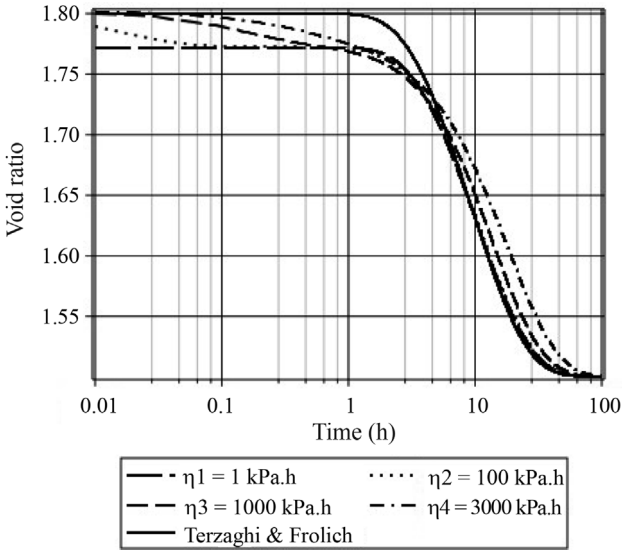

Figure 18 - Void ratio *vs.* time comparison between values determined by Eq. 17 for various values of η and by Terzaghi & Frölich's solution (1936).

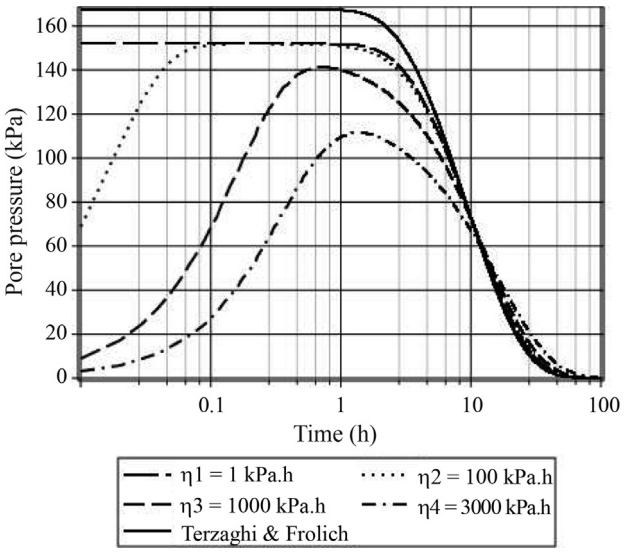

Figure 19 - Pore pressure *vs.* time comparison between values determined by Eq. 18 for various values of η and by Terzaghi & Frölich's solution (1936).

It becomes evident that as η increases, the values of the maximum pore pressure decreases, with the peaks displacing to the right. Additionally, as expected, the more the η value decreases, the more the pore pressure curves approach in aspect to that of Terzaghi & Frölich's solution (1936). With respect to the void ratio, it is observed that the lower the value of η, the more the curve moves away from that of Terzaghi & Frölich's solution (1936) in the initial branch. In the final branch of the curve, exactly the opposite occurs.

As a final analysis, the condition of applying a loading while the drain is closed is considered to predict the progress of pore pressure growth. In this case, except for the coefficient of permeability, all test parameters refer to the 5th step in Table 1. To simulate the effect of closed drainage, a coefficient of permeability of 1×10^{-50} m.min^{-1} is considered.

Figure 20 shows that, as expected, the higher the stiffness of water, the faster the pore pressure reaches its maximum and the closer it gets to the applied load (167.5 kPa). The difference between the maximum pore pressure value and the applied load represents the effective stress resisted by the soil, since it is submitted to the same volumetric strain as the water.

3. Conclusions

The study that resulted in this paper allows to highlight the following main conclusions:

(i) For the soils investigated by Taylor (1942) and Santa Maria (2002) in one-dimensional consolidation tests and by Thomasi (2000) in hydrostatic consolidation tests, the relationship between the mean values of the viscous component of the effective stress and the strain (or void ratio) rate is characterized by a curve which may be satisfactorily represented by a two-parameter hyperbola going through the origin and featuring a horizontal asymptote.

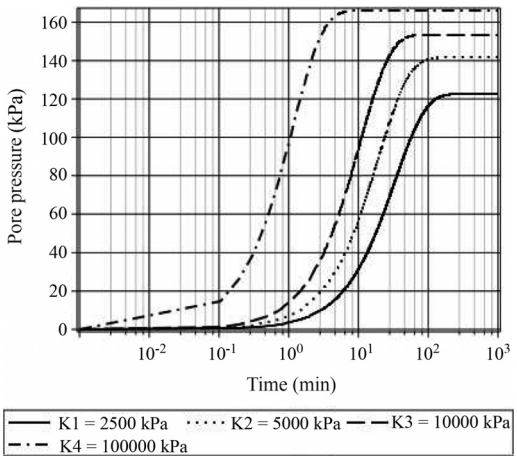

Figure 20 - Pore pressure growth with time in an undrained soil sample with viscous behaviour considering several values of *K*.

(ii) For these soils, the shape of the curve viscous resistance *vs.* strain (or void ratio) rate suggests the existence of a limit value, represented theoretically by the ordinate of the fitted two-parameter hyperbola's horizontal asymptote.

(iii) For one-dimensional consolidation of a soil with viscous behaviour and compressible water in the voids, both the general Eq. 13, where the viscous resistance *vs*. void ratio rate is represented by a two-parameter hyperbola (Eq. 14), and and Eq. 16, where the soil behaviour is considered Newtonian, can predict the pore pressure variation with time.

(iv) As expected, the general Eq. 13 with the viscous resistance defined by Eq. 14 presents better results than Eq. 16, where viscous behaviour is linear (Newtonian).

(v) The analytical solution obtained assuming Newtonian behaviour for the soil was succesfully verified (a) by the fact that it becomes Taylor's solution (1942) when $K \rightarrow \infty$ and (b) by the perfect match between their results and those obtained by numerical integration of Eq. 16 using the software MAPLE 2017.

(vi) Although the assumptions for both of the solutions presented lead to a condition of null pore pressure at the $t = 0^+$ instant, the initial values measured are approximately 20% of the total applied stress and may be accounted for as a result of dynamic effects inherently associated to the application of the load increment at the beginning of each step.

Acknowledgments

The authors are grateful to Igor Santa Maria for having kindly translated the original text into English and for his valuable comments and suggestions on the work.

References

Alexandre, G.F. (2000). A Fluência Não Drenada Segundo o Modelo de Martins. MSc Dissertation, Programme of Civil Engineering, COPPE-UFRJ, Rio de Janeiro (In Portuguese).

Bjerrum, L. (1967). Engineering geology of Norwegian normally-consolidated marine clays as related to settlements of buildings. Géotechnique, 17(2):81-118.

Lacerda, W.A. (1976). Stress Relaxation and Creep Effects on Soil Deformation. PhD Dissertation, University of California, Berkeley.

Martins, I.S.M. & Lacerda, W.A. (1985). A theory of consolidation with secondary compression. Proc. 11th Int. Conf. on Soil Mech. and Found. Engn., ISSMFE, San Francisco, v. 1, pp. 567-570.

Martins, I.S.M. (1992). Fundamentals of Behavioural Model of Saturated Clays. DSc Dissertation, Programme of Civil Engineering, COPPE-UFRJ, Rio de Janeiro (In Portuguese).

Newton, I.S. (1687). Philosophiæ Naturalis Principia Mathematica. London (in Latin).

Ostwald, W. (1926). Ueber die Viskosität Kolloider Lösungen in Struktur Laminar und Turbulezgebiet, Kolloid-Z., 38:261-280.

Santa Maria, F.C.M. (2002). Estudo Teórico-Experimental do Coeficiente de Empuxo no Repouso, K_0. DSc Dissertation, Programme of Civil Engineering, COPPE-UFRJ, Rio de Janeiro. (In Portuguese).

Suklje, L. (1969). Rheological Aspects of Soil Mechanics. Ed. Wiley-Interscience, Madison.

Taylor, D.W. & Merchant, W. (1940). A theory of clay consolidation accounting for secondary compression, Journal of Mathematics and Physics, 19(3):167-185.

Taylor, D.W. (1942). Research on Consolidation of Clays. Department of Civil and Sanitary Engineering, MIT, Serial 82, 147 p.

Terzaghi, K. & Frölich, O.K. (1936). Theorie der Setzung von tonschichten; eine einfürhrung in die analytische tonmechanik. Leipzig, Franz Deuticke, 265 p.

Thomasi, L. (2000). Sobre a Existência de uma Parcela Viscosa na Tensão Normal Efetiva. MSc Dissertation, Programme of Civil Engineering, COPPE-UFRJ, Rio de Janeiro (In Portuguese).

Tsytovich, N.A. & Zaretsky, Y.K. (1969). The development of the theory of soil consolidation in the USSR, 1917-1967. Géotechnique, 19(3):357-375.

Tsytovich, N.A. (1987). Soil Mechanics. Mir Publishers, Moscow.

Vyalov, S.S. (1986). Rheological Fundamentals of Soil Mechanics. Developments in Geotechnical Engineering n. 36. Elsevier, Amsterdam.

Zaretsky, Y.K. (1972). Theory of Soil Consolidation (Teoriya konsolidatsii gruntov). Edited by N.A. Tsytovich. Izdatel 'stvo "Nauka". Moskva. Translated from Russian. Israel Program for Scientific Translations, Jerusalem.

List of Symbols

a_e, a_ε = first parameter of the two-parameter hyperbola
a_v = coefficient of compressibility of the soil
b_e, b_ε = second parameter of the two-parameter hyperbola
e = void ratio
e_0 = initial void ratio
$\overline{e}$ = average void ratio
$\dot{e}$ = void ratio rate
C_k, C_v = coefficients of the general equation - Eq. 13
C_{k1}, C_{kt}, C_v and C_{vt} = coefficients of the equation for Newtonian behaviour - Eq. 16
h = half sample thickness
K = bulk modulus of elasticity of water
K_0 = coefficient of lateral stress at rest
k = coefficient of permeability of the soil
n = porosity of the soil
p_a = atmospheric pressure
S = degree of sample saturation
t = time coordinate
u = pore pressure
v = apparent seepage speed
v_e = average value of the true seepage speed
$\dot{v}$ = apparent velocity of grains related to the gross-section area of the soil
z = position coordinate
η = coefficient of viscosity
ϕ = fluidity
ε = linear strain
$\dot{\varepsilon}$ = linear strain rate
$\dot{\gamma}$ = shear strain rate
γ_w = unit weight of water
σ = normal stress
σ'_f = frictional component of the effective stress
σ'_v = viscous component of the effective stress
τ = shear stress

Appendix A - General consolidation equation and its particular form for Newtonian behaviour

Considering:

(i) viscous resistance $\sigma'_v = f\left(\bar{e}, \frac{\partial e}{\partial t}\right)$ and $\sigma'_v = -\eta \frac{\partial e}{\partial t}$,

(ii) compressibility of water

1. If the drainage velocity v increases with *z*, the quantity of pore water leaving a volume *dxdydz* over an interval of time *dt*, neglecting the infinitesimal contribution, is

$$\frac{\partial v}{\partial z} dz\, dxdydt$$

2. Volume variation for the same time interval *dt* is

$$-\frac{\partial n}{\partial t} dxdydz\, dt$$

where *n* is the porosity of the soil.

3. Continuity equation for the liquid phase

element volumetric variation – volume of water leaving the element = volumetric variation of water contained in the element

3.1. Volumetric variation of water for time interval *dt*

$$\frac{1}{K}\frac{\partial u}{\partial t} dt\, ndxdydz$$

where:

$$K = \frac{\Delta u}{\varepsilon_v}$$

3.2. Equation

$$-\frac{\partial n}{\partial t} - \frac{\partial v}{\partial z} = \frac{n}{K}\frac{\partial u}{\partial t} \tag{A.1}$$

or

$$\frac{\partial n}{\partial t} + \frac{\partial v}{\partial z} = -\frac{n}{K}\frac{\partial u}{\partial t}$$

4. Continuity equation for the solid phase (incompressible)

$$\frac{\partial \dot{v}}{\partial z} + \frac{\partial (1-n)}{\partial t} = 0 \tag{A.2}$$

where $\dot{v}$ is the apparent velocity related to the gross cross-sectional area of the soil.

5. Derivation of the equation

Adding Eqs. A.1 and A.2

$$\frac{\partial v}{\partial z} + \frac{\partial \dot{v}}{\partial z} = -\frac{n}{K}\frac{\partial u}{\partial t} \tag{A.3}$$

Having in mind that

$$h = \frac{u}{\gamma_w} \text{ and } i = -\frac{\partial h}{\partial z} \therefore i = -\frac{1}{\gamma_w}\frac{\partial u}{\partial z} \text{ and } v_e = \frac{v}{n}$$

thus

$$v_e = -\frac{k}{\gamma_w n}\frac{\partial u}{\partial z} \quad \left(v = ki \text{ and } v_e = \frac{ki}{n}\right)$$

The particle-liquid relative velocity must then be considered

$$v_e - \dot{v}_e = -\frac{k}{\gamma_w n}\frac{\partial u}{\partial z} \text{ or } \frac{v}{n} - \frac{\dot{v}}{1-n} = -\frac{k}{\gamma_w n}\frac{\partial u}{\partial z}$$

Since $e = \frac{n}{1-n}$, then

$$v - e\dot{v} = -\frac{k}{\gamma_w}\frac{\partial u}{\partial z} \tag{A.4}$$

Differentiating Eq. A.4 with respect to *z*

$$\frac{\partial v}{\partial z} - e\frac{\partial \dot{v}}{\partial z} - \dot{v}\frac{\partial e}{\partial z} = -\frac{\partial}{\partial z}\left(\frac{k}{\gamma_w}\frac{\partial u}{\partial z}\right)$$

Considering Eq. A.3, one obtains

$$\frac{\partial v}{\partial z} - e\left(-\frac{n}{K}\frac{\partial u}{\partial t} - \frac{\partial v}{\partial z}\right) - \dot{v}\frac{\partial e}{\partial z} = -\frac{\partial}{\partial z}\left(\frac{k}{\gamma_w}\frac{\partial u}{\partial z}\right)$$

or

$$\frac{\partial v}{\partial z}(1+e) + \frac{e^2}{(1+e)K}\frac{\partial u}{\partial t} - \dot{v}\frac{\partial e}{\partial z} = -\frac{\partial}{\partial z}\left(\frac{k}{\gamma_w}\frac{\partial u}{\partial z}\right)$$

Admitting $\dot{v}\frac{\partial e}{\partial z} \cong 0$ the following can be written

$$\frac{\partial v}{\partial z}(1+e) = -\frac{e^2}{(1+e)K}\frac{\partial u}{\partial t} - \frac{\partial}{\partial z}\left(\frac{k}{\gamma_w}\frac{\partial u}{\partial z}\right)$$

Considering Eq. A.1

$$\left(-\frac{n}{K}\frac{\partial u}{\partial t} - \frac{\partial n}{\partial t}\right)(1+e) = -\frac{e^2}{(1+e)K}\frac{\partial u}{\partial t} - \frac{\partial}{\partial z}\left(\frac{k}{\gamma_w}\frac{\partial u}{\partial z}\right)$$

or

$$-\frac{n}{K}\frac{\partial u}{\partial t} - \frac{\partial n}{\partial t}(1+e) = -\frac{\partial}{\partial z}\left(\frac{k}{\gamma_w}\frac{\partial u}{\partial z}\right)$$

or

$$-\frac{\partial n}{\partial t}(1+e) = \frac{n}{K}\frac{\partial u}{\partial t} - \frac{\partial}{\partial z}\left(\frac{k}{\gamma_w}\frac{\partial u}{\partial z}\right) \tag{A.5}$$

Since $n = \frac{e}{1+e}$ and, therefore,

$$\frac{\partial n}{\partial t} = \frac{1}{(1+e)^2}\frac{\partial e}{\partial t}$$

then

$$\frac{1}{(1+e)}\frac{\partial e}{\partial t}=-\frac{e}{(1+e)K}\frac{\partial u}{\partial t}+\frac{\partial}{\partial z}\left(\frac{k}{\gamma_w}\frac{\partial u}{\partial z}\right) \quad (A.6)$$

The Expanded Principle of Effective Stress (EPES) (Martins, 1992) may be written as

$$\sigma=\underbrace{\sigma'_f+\sigma'_v}_{\sigma'}+u$$

or

$$u=\sigma-\sigma'_f-\sigma'_v \text{ and } \frac{\partial u}{\partial z}=\frac{\partial \sigma}{\partial z}-\frac{\partial \sigma'_f}{\partial z}-\frac{\partial \sigma'_v}{\partial z}$$

Admitting k = constant and, by equilibrium, $\frac{\partial \sigma}{\partial z}=0$

$$\frac{\partial e}{\partial t}=-\frac{e}{K}\frac{\partial u}{\partial t}+\frac{k(1+e)}{\gamma_w}\frac{\partial^2 u}{\partial z^2}$$

or

$$\frac{\partial e}{\partial t}=-\frac{e}{K}\frac{\partial u}{\partial t}+\frac{k(1+e)}{\gamma_w}\left(-\frac{\partial^2 \sigma'_f}{\partial z^2}-\frac{\partial^2 \sigma'_v}{\partial z^2}\right) \quad (A.7)$$

Applying the chain rule

$$\frac{\partial \sigma'_f}{\partial z}=-\frac{1}{a_v}\frac{\partial e}{\partial z}$$

and

$$\frac{\partial^2 \sigma'_f}{\partial z^2}=-\frac{1}{a_v}\frac{\partial^2 e}{\partial z^2}$$

Substituting the equations above in Eq. A.7, one obtains

$$\frac{\partial e}{\partial t}=-\frac{e}{K}\frac{\partial u}{\partial t}+\frac{k(1+e)}{\gamma_w}\left(\frac{1}{a_v}\frac{\partial^2 e}{\partial z^2}-\frac{\partial^2 \sigma'_v}{\partial z^2}\right)$$

Differentiating the EPES with respect to t

$$\frac{\partial u}{\partial t}=\frac{\partial \sigma}{\partial t}-\frac{\partial \sigma'_f}{\partial t}-\frac{\partial \sigma'_v}{\partial t}$$

Admitting

σ = constant with time, then

$$\frac{\partial u}{\partial t}=\frac{1}{a_v}\frac{\partial e}{\partial t}-\frac{\partial \sigma'_v}{\partial t}$$

Thus

$$\frac{\partial e}{\partial t}=-\frac{e}{K}\left(\frac{1}{a_v}\frac{\partial e}{\partial t}-\frac{\partial \sigma'_v}{\partial t}\right)+\frac{k(1+e)}{\gamma_w}\left(\frac{1}{a_v}\frac{\partial^2 e}{\partial z^2}-\frac{\partial^2 \sigma'_v}{\partial z^2}\right)$$

$$\frac{\partial e}{\partial t}=-\frac{e}{Ka_v}\left(\frac{\partial e}{\partial t}-a_v\frac{\partial \sigma'_v}{\partial t}\right)+\frac{k(1+e)}{\gamma_w a_v}\left(\frac{\partial^2 e}{\partial z^2}-a_v\frac{\partial^2 \sigma'_v}{\partial z^2}\right)$$

Defining

$$\begin{cases} C_k=\dfrac{e}{Ka_v} \\ C_v=\dfrac{k(1+e)}{\gamma_w a_v} \end{cases}$$

Now, assuming by simplification that $e=\bar{e}$ (mean value of e), then

$$\frac{\partial e}{\partial t}=-C_k\frac{\partial}{\partial t}(e-a_v\sigma'_v)+C_v\frac{\partial^2}{\partial z^2}(e-a_v\sigma'_v) \quad (A.8)$$

For the particular case where the soil behaviour is Newtonian $\sigma'_v=-\eta\left(\frac{\partial e}{\partial t}\right)$, Eq. A.8 assumes the following aspect

$$\frac{\partial e}{\partial t}=-C_k\frac{\partial}{\partial t}\left(e+a_v\eta\frac{\partial e}{\partial t}\right)+C_v\frac{\partial^2}{\partial z^2}\left(e+a_v\eta\frac{\partial e}{\partial t}\right)$$

It can be further developed in the following way

$$(1+C_k)\frac{\partial e}{\partial t}+C_k a_v\eta\frac{\partial^2 e}{\partial t^2}-C_v\frac{\partial^2 e}{\partial z^2}-C_v a_v\eta\frac{\partial^3 e}{\partial z^2\partial t}=0$$

Denoting

$$\begin{cases} C_{k1}=(1+C_k)=\dfrac{\bar{e}+Ka_v}{Ka_v} \\ C_{kt}=C_k a_v\eta=\dfrac{\eta\bar{e}}{K} \\ C_{vt}=C_v a_v\eta=\dfrac{k(1+\bar{e})\eta}{\gamma_w} \end{cases}$$

Leading finally to

$$C_{k1}\frac{\partial e}{\partial t}+C_{kt}\frac{\partial^2 e}{\partial t^2}-C_v\frac{\partial^2 e}{\partial z^2}-C_{vt}\frac{\partial^3 e}{\partial z^2\partial t}=0 \quad (A.9)$$

Appendix B - Analytical solution of the one-dimensional consolidation Eq. A.9

The boundary conditions are

(1) $(z=0, \forall t)$ - equation solution: $-\eta\frac{de}{dt}=\sigma-\frac{e_0-e}{a_v}$; $e(t=0)=e_0$

(2) $(z=2h, \forall t)$ - equation solution: $-\eta\frac{de}{dt}=\sigma-\frac{e_0-e}{a_v}$; $e(t=0)=e_0$

(3) $e(\forall z, t=0)=e_0$

(4) $\frac{\partial e}{\partial t}(\forall z, t=0)=-\frac{\sigma}{\eta}$

where the solution of the differential equation indicated in conditions (1) and (2) is

$$e=e_0-a_v\sigma\left(1-e^{-\frac{t}{\eta a_v}}\right) \quad (B.1)$$

Taking into account that this equation is linear, its solution may be written as

$$e = e_f + f(z,t) \tag{B.2}$$

where $e_f = e_0 - a_v \sigma\left(1 - e^{-\frac{t}{\eta a_v}}\right)$, which represents the void ratios at boundaries $z = 0$ and $z = 2h$.

Differentiating Eq. B.1 twice with respect to t, it comes to

$$\frac{de_f}{dt} = -\frac{\sigma}{\eta} e^{-\frac{t}{\eta a_v}}$$

$$\frac{d^2 e_f}{dt^2} = \frac{\sigma}{\eta^2 a_v} e^{-\frac{t}{\eta a_v}}$$

Differentiating Eq. B.2 twice with respect to t, twice with respect to z and once with respect to t and twice with respect to z, it becomes

$$\frac{\partial e}{\partial t} = \frac{de_f}{dt} + \frac{\partial f}{\partial t} = -\frac{\sigma}{\eta} e^{-\frac{t}{\eta a_v}} + \frac{\partial f}{\partial t}$$

$$\frac{\partial^2 e}{\partial t^2} = \frac{d^2 e_f}{dt^2} + \frac{\partial^2 f}{\partial t^2} = \frac{\sigma}{\eta^2 a_v} e^{-\frac{t}{\eta a_v}} + \frac{\partial^2 f}{\partial t^2}$$

$$\frac{\partial^2 e}{\partial z^2} = \frac{\partial^2 f}{\partial z^2}$$

$$\frac{\partial^3 e}{\partial z^2 \partial t} = \frac{\partial^3 f}{\partial z^2 \partial t}$$

Substituting the above equations in Eq. A.9, it leads to:

$$C_{k1} \frac{\partial f}{\partial t} + C_{kt} \frac{\partial^2 f}{\partial t^2} - C_v \frac{\partial^2 f}{\partial z^2} - C_{vt} \frac{\partial^3 f}{\partial z^2 \partial t} = \left(\frac{\bar{e} + K a_v}{K a_v} \frac{\sigma}{\eta} - \frac{\eta \bar{e}}{K} \frac{\sigma}{\eta^2 a_v}\right) e^{-\frac{t}{\eta a_v}}$$

which, by simplification, can be written as

$$C_{k1} \frac{\partial f}{\partial t} + C_{kt} \frac{\partial^2 f}{\partial t^2} - C_v \frac{\partial^2 f}{\partial z^2} - C_{vt} \frac{\partial^3 f}{\partial z^2 \partial t} = \frac{\sigma}{\eta} e^{-\frac{t}{\eta a_v}} \tag{B.3}$$

The boundary conditions for $f(z,t)$ are

(1) $f(0,t) + \eta a_v \frac{\partial f}{\partial t}(0,t) = 0$

(2) $f(2h,t) + \eta a_v \frac{\partial f}{\partial t}(2h,t) = 0$

(3) $f(z,0) = 0$

(4) $\frac{\partial f}{\partial t}(z,0) = 0$ (because $\eta \frac{\partial e}{\partial t}(z,0) = -\sigma$)

According to Taylor (1942), the aspect of Eq. B.3 and the boundary conditions above suggest that the solution may be written as

$$f = \sum_{m=0}^{\infty} F_m(t) \sin\left[\frac{(2m+1)\pi}{2} \frac{z}{h}\right] \tag{B.4}$$

Considering $M = (2m+1)\pi/2$, substituting Eq. B.4 in Eq. B.3 and having in mind that $\sum_{m=0}^{\infty} \frac{2}{M} \sin\left(\frac{Mz}{h}\right) = 1$ for $0 < z < 2h$, the following equation is obtained

$$C_{k1} \sum_{m=0}^{\infty} \sin\left(\frac{Mz}{h}\right) \frac{dF_m(t)}{dt} + C_{kt} \sum_{m=0}^{\infty} \sin\left(\frac{Mz}{h}\right) \frac{d^2 F_m(t)}{dt^2} + C_v \sum_{m=0}^{\infty} \left(\frac{M}{h}\right)^2 F_m(t) \sin\left(\frac{Mz}{h}\right) + C_{vt} \sum_{m=0}^{\infty} \left(\frac{M}{h}\right)^2 \frac{dF_m(t)}{dt} \sin\left(\frac{Mz}{h}\right)$$
$$= \sum_{m=0}^{\infty} \frac{2}{M} \sin\left(\frac{Mz}{h}\right) \frac{\sigma}{\eta} e^{-\frac{t}{\eta a_v}}$$

and, by simplification, it can be written as

$$\sum_{m=0}^{\infty} C_{kt} \sin\left(\frac{Mz}{h}\right) \frac{d^2 F_m(t)}{dt^2} + \sum_{m=0}^{\infty} \left[C_{k1} + C_{vt}\left(\frac{M}{h}\right)^2\right] \sin\left(\frac{Mz}{h}\right) \frac{dF_m(t)}{dt} + \sum_{m=0}^{\infty} C_v \sin\left(\frac{Mz}{h}\right)\left(\frac{M}{h}\right)^2 F_m(t) = \sum_{m=0}^{\infty} \frac{2}{M} \sin\left(\frac{Mz}{h}\right) \frac{\sigma}{\eta} e^{-\frac{t}{\eta a_v}}$$

Admitting

$$O_m = \frac{C_{kt}}{C_{k1} + C_{vt}\left(\frac{M}{h}\right)^2}; P_m = \frac{C_{vt}\left(\frac{M}{h}\right)^2}{C_{k1} + C_{vt}\left(\frac{M}{h}\right)^2}; Q_m = \frac{2\sigma}{M\eta\left[C_{k1} + C_{vt}\left(\frac{M}{h}\right)^2\right]}$$

the following equation is obtained

$$O_m \frac{d^2 F_m(t)}{dt^2} + \frac{dF_m(t)}{dt} + P_m F_m(t) = Q_m e^{-\frac{t}{\eta a_v}}$$

whose solution is

$$F_m(t) = C_1 e^{-\frac{1}{2}\left(\frac{B_{m1} + 2\sqrt{A_m}}{C_{kt} h^2}\right) t} - C_2 e^{-\frac{1}{2}\left(\frac{B_{m2} - 2\sqrt{A_m}}{C_{kt} h^2}\right) t} - 2\sigma \frac{C_{vt}}{C_v M \eta} e^{-\frac{C_v}{C_{vt}} t} \tag{B.5}$$

where

$$\begin{cases} A_m = C_{k1}^2 h^4 + 2C_{k1} C_{vt} M^2 h^2 - 4C_{kt} C_v M^2 h^2 + C_{vt}^2 M^4 \\ B_{m1} = C_{k1} h^2 + C_{vt} M^2 - \sqrt{A_m} \\ B_{m2} = C_{k1} h^2 + C_{vt} M^2 + \sqrt{A_m} \end{cases}$$

Differentiating Eq. B.5 once, it becomes

$$\frac{dF_m(t)}{dt} = C_1 \left[-\frac{1}{2} \left(\frac{B_{m1} + 2\sqrt{A_m}}{C_{kt} h^2} \right) \right] e^{-\frac{1}{2}\left(\frac{B_{m1} + 2\sqrt{A_m}}{C_{kt} h^2} \right) t} - C_2 \left[-\frac{1}{2} \left(\frac{B_{m2} - 2\sqrt{A_m}}{C_{kt} h^2} \right) \right] e^{-\frac{1}{2}\left(\frac{B_{m2} - 2\sqrt{A_m}}{C_{kt} h^2} \right) t} + \frac{2\sigma}{M\eta} e^{-\frac{C_v}{C_{vt}} t}$$

Having in mind that, for

$$f(z,0) = 0 \Rightarrow F_m(0) = 0$$

$$\frac{\partial f}{\partial t}(z,0) = 0 \Rightarrow \frac{dF_m}{dt}(0) = 0$$

the following system that determines the integration constants is obtained

$$\begin{cases} C_1 - C_2 - 2\sigma \dfrac{C_{vt}}{C_v M \eta} = 0 \\ C_1 \left[-\dfrac{1}{2} \left(\dfrac{B_{m1} + 2\sqrt{A_m}}{C_{kt} h^2} \right) \right] - C_2 \left[-\dfrac{1}{2} \left(\dfrac{B_{m2} - 2\sqrt{A_m}}{C_{kt} h^2} \right) \right] + \dfrac{2\sigma}{M\eta} = 0 \end{cases}$$

whose solution provides the following results

$$C_1 = \frac{(C_{vt} A_m - C_{k1} C_{vt} \sqrt{A_m} h^2 + 2C_{kt} C_v \sqrt{A_m} h^2 - C_{vt}^2 M^2 \sqrt{A_m})\sigma}{M A_m C_v \eta}$$

$$C_2 = \frac{(C_{vt} A_m + C_{k1} C_{vt} \sqrt{A_m} h^2 - 2C_{kt} C_v \sqrt{A_m} h^2 + C_{vt}^2 M^2 \sqrt{A_m})\sigma}{M A_m C_v \eta}$$

Admitting:

$$C_c = \frac{2C_{kt} C_v h^2}{C_{vt}}$$

Eq. B.6 is then obtained

$$F_m(t) = e^{-\frac{B_{m1}}{2C_{kt} h^2} t} (B_{m2} - C_c) \frac{\sigma a_v}{M\sqrt{A_m}} - e^{-\frac{B_{m2}}{2C_{kt} h^2} t} (B_{m1} - C_c) \frac{\sigma a_v}{M\sqrt{A_m}} - \frac{2\sigma a_v}{M} e^{-\frac{C_v}{C_{vt}} t} \tag{B.6}$$

Considering Eqs. B.2, B.4 and B.6, the final result is obtained

$$e = e_0 - \sigma a_v \left\{ 1 - \sum_{m=0}^{n} \left[\frac{e^{-\frac{1}{2}\frac{B_{m1} t}{C_{kt} h^2}} (B_{m2} - C_c)}{M\sqrt{A_m}} - \frac{e^{-\frac{1}{2}\frac{B_{m2} t}{C_{kt} h^2}} (B_{m1} - C_c)}{M\sqrt{A_m}} \right] \sin\left(\frac{Mz}{h} \right) \right\}$$

Interaction Factor Between Piles: Limits on Using the Conventional Elastic Approach in Pile Group Analysis

M.M. Sales, T.S. Curado

Abstract. Analyses of load settlement behavior for pile groups must consider the interaction of nearby piles. In small pile groups, the key factor for evaluating load-settlement behavior is single-pile stiffness, but when analyzing large pile groups and piled rafts, the importance of induced settlements due to neighboring piles increases. This paper reviews the most commonly used approaches that consider the interaction between piles and notes some aspects that can result in important differences in foundation settlement predictions. Topics including soil heterogeneity, the presence of other piles, and large pile groups are presented using both the conventional approach and finite element method analysis, showing that for large piled foundations, such aspects can result in considerable differences.

Keywords: pile group, piled raft, pile-to-pile interaction factor, settlement analysis.

1. Introduction

Currently, most piled foundation designs are based only on the load capacity of the pile group, and the main challenge in a project is the definition of how many piles would be necessary to support the applied load. Since the emblematic paper of Burland *et al.* (1977), who primarily noted the use of piles as settlement reducers, many authors have reinforced this idea (Randolph, 1994; Mandolini & Viggiani, 1997; Poulos 2001; and others). Randolph (2003) stated that the trend towards design based on allowable deformations may be appropriate for both large and small pile groups, such as those used to support bridge piers.

The load settlement behavior of a pile group results from the individual characteristics and the piles arrangement. Each pile in a group, regardless of its similarity to the neighboring piles, has its individual stiffness (relation between load and settlement of the pile) influenced by the presence of other piles. Mandolini (2003) noted that in large pile groups, in which different piles would be in different stages of mobilized loads, the nonlinear pile behavior should be considered. Moreover, at some distance from a loaded pile, the elastic displacements would prevail.

The additional settlement suffered by one pile near another pile has been studied by many authors. Poulos (1968) and Cooke *et al.* (1980), in a very similar way, labeled the relation between the induced settlement to a nearby pile and the self-settlement of a loaded pile the *"interaction factor"*.

The focus of the present paper is to evaluate how the interaction factor α can be calculated, the similarities of the available theories, and how they affect the final prediction of piled foundations.

2. Existing Theories

Poulos (1968) considered soil to be an elastic continuum and developed a solution based on a boundary element method to evaluate the two-pile interaction factor, as defined in Eq. 1. Some of the charts presented in that paper allowed a "manual prediction", in which the final interaction factor α would be estimated by Eq. 2. This method was well detailed by Poulos & Davis (1980).

$$\alpha_{ji} = \frac{w_{ji}}{w_i} \tag{1}$$

where α_{ji} is the interaction factor between loaded pile *"i"* and its neighboring pile *"j"*; w_{ji} is the induced settlement on the pile *"j"* due to the loaded pile *"i"*; and w_i is the settlement of pile *"i"* due to its own load.

$$\alpha = \alpha_F . N_h . N_b . N_v \tag{2}$$

where α is the final two-pile interaction factor; α_F is the interaction factor for a semi-infinite soil using "0.5" for Poisson's ratio (the presented curves are for specific values of K_p and relative spacing - *S/D*); N_h is the correction for the finite soil layer; N_b is the correction for the presence of a stiffer soil layer below the pile tip; N_v is the correction for other Poisson's ratios; K_p is the pile stiffness (P/w = load/top settlement); S is the center-to-center distance between piles; and D is the pile diameter.

Poulos (1989) highlighted that α decreases with increasing pile-to-pile distance, or as the distribution of the Young's modulus of the soil becomes less uniform with depth. Considering K to be the relative stiffness of a pile ($= E_p/E_s$ = pile Young's modulus/soil Young's modulus),

Maurício Martines Sales, D.Sc., Full Professor, Escola de Engenharia Civil e Ambiental, Universidade Federal de Goiás, Av. Universitária 1488, Qd 86, Bl A, Setor Universitário, Goiânia, GO, Brazil. e-mail: sales.mauricio@gmail.com.
Tallyta da Silva Curado, M.Sc., Assistant Professor, Escola de Engenharia Civil e Ambiental, Universidade Federal de Goiás, Av. Universitária 1488, Qd 86, Bl A, Setor Universitário, Goiânia, GO, Brazil. e-mail: tallytacurado@gmail.com.
Submitted on July 28, 2017; Final Acceptance on March 18, 2018; Discussion open until August 31, 2018.
DOI: 10.28927/SR.411049

for floating piles, the interaction factor α increases with increasing relative stiffness; in contrast, α decreases with increasing relative stiffness for end-bearing piles.

Randolph & Wroth (1979) presented a simpler approach based on Winkler approximation. The resulting analytical solutions consider that shear stresses around the pile would decay inversely with radius, leading to a logarithmic decay in vertical displacements, all limited to a maximum radius of influence (r_m). The interaction between two piles is calculated separately in terms of shaft and base induced displacements. Eqs. 3 and 4 present the final shaft and base settlements of two similar rigid neighboring piles. Adding the effects of shaft and base displacements, the overall load-settlement ratio could be expressed as Eq. 5. Thus, the interaction factor α can be obtained from Eq. 6.

$$w_S = w_1 + w_2 = \frac{\tau_0 r_0}{G_{l/2}}\left[\ln\left(\frac{r_m}{r_0}\right) + \ln\left(\frac{r_m}{S}\right)\right] \quad (3)$$

$$w_b = w_1 + w_2 = \frac{Pb(1-v)}{4r_0 G_1}\left(1 + \frac{cr_0}{S}\right) \quad (4)$$

$$\left(\frac{P_t}{G_l r_0 w_t}\right) = \frac{4}{1-v}\frac{S}{r_0 c + S} + \frac{2\pi\rho}{\zeta + \ln\left(\frac{r_m}{S}\right)}\frac{L}{r_0} \quad (5)$$

$$\left(\frac{G_l r_0 w_t}{P_t}\right)_2 = (1+\alpha)\left(\frac{G_l r_0 w_t}{P_t}\right)_1 \quad (6)$$

where w_s, w_b and w_t are the shaft, base and total settlements, respectively; w_1 and w_2 are the settlements of Piles 1 and 2, respectively; τ_0 is the shear stress at the pile shaft; $G_{l/2}$ and G_l are the values of the shear modulus at the pile mid-depth and pile base, respectively; r_0 is the pile radius; r_m is the limiting radius of influence of the pile; S is the center-to-center distance between piles; P_b and P_t are the base and total loads acting on the pile, respectively; ν is the Poisson's ratio of the soil; c is a constant (= 2/π); L is the pile length; ρ is the degree of homogeneity (= $G_{l/2}/G_l$); and ζ is calculated as $\ln(r_m/r_0)$.

El Sharnouby & Novak (1990) presented a method based on boundary element analysis. The authors noted that the longer the pile, the larger the number of discretized points at the pile-soil interface should be. They suggested at least 30 points for shorter piles (relative length L/D < 50) and 50 points for longer piles (L/D > 50). El Sharnouby & Novak (1990) recalled that the charts presented by Poulos & Davis (1980) featured only 10 points at the pile-soil interface, so discrepancies could arise when applying the method for longer piles. Another interesting point of the same paper is that the influence of intermediary piles was mentioned for the first time. Figure 1 shows one particular example (K = 1000, L/D = 50, ν = 0.5) for 3-in-line piles with the tips resting on a much stiffer layer. The curves in Fig. 1 represent the effect of the presence of Pile 2 or the lack thereof between Piles 1 and 3. When Pile 2 is considered, Pile 3 suffers a lower influence from Pile 1, resulting in a lower interaction factor. The authors also explored an example for a 5-in-line pile group, and presented results in a dimensionless format. In this situation, α_{21} is the interaction factor on Pile 2 due to the load on Pile 1 but considers the presence of all five piles and so on for α_{31}, α_{41}, and α_{51}.

Southcott & Small (1996) presented some analyses based on the finite layer method that can solve three-dimensional (3D) problems but in a much easier way (computational effort). The authors mentioned that for a floating pile, the interaction factor of many two-pile theories are in reasonable agreement but that for non-uniform soils, the differences can be relevant. The paper explained the method and revisited some examples from previous theories.

Mylonakis & Gazetas (1998) developed a general analytical formulation based on the Winkler model of soil reaction to study the two-pile interaction problem, especially for piles embedded in multilayered soils. In addition to the induced displacements on neighboring piles, the authors presented an approach to consider the generated stresses along the shaft on nearby piles. The paper shows that a loaded pile will induce a soil displacement field around itself. However, if there is another pile inside this free-displacement field, the axial stiffness of that pile tends to reduce the settlement of any other neighboring piles. To incorporate this physical behavior an attenuation function was suggested for the original free-displacement field, as in the following equation.

$$\alpha = \psi(S).\zeta(h\lambda, \Omega) \quad (7)$$

$$\psi(S) = \frac{\ln\left(\frac{r_m}{S}\right)}{\ln\left(\frac{r_m}{r_0}\right)} \quad (8)$$

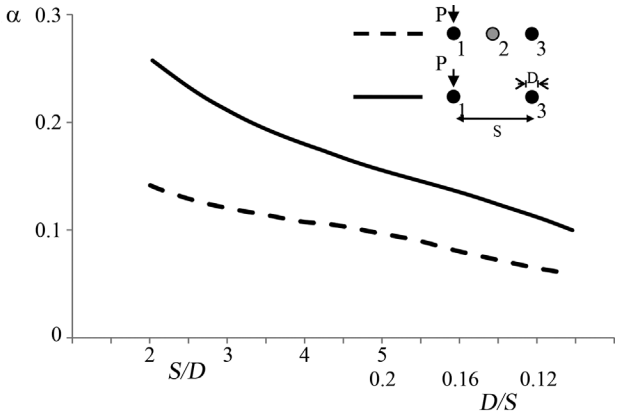

Figure 1 - Interaction factor for two piles with the presence or lack of another pile between them. K = 1000, L/D = 50 (El Sharnouby & Novak, 1990).

$$\zeta(h\lambda,\Omega)=\frac{2h\lambda+\sinh(2h\lambda)+\Omega^2\left[\sinh(2h\lambda)-2h\lambda\right]+2\Omega\left[\cosh(2h\lambda)-1\right]}{2\sinh(2h\lambda)+2\Omega^2\ \sinh(2h\lambda)+4\Omega\cosh(2h\lambda)} \quad (9)$$

where α is the final interaction factor; $\psi(S)$ is the free displacement field (as presented by Randolph & Wroth, 1979); $\zeta(h\lambda,\Omega)$ is the attenuation factor due to the self-stiffness of the neighboring pile; h is the layer thickness crossed by the pile (in a homogeneous soil, $h = L$); λ is the Winkler load transfer parameter ($=\sqrt{\left(\frac{\delta G_S}{E_p A_p}\right)}$); Ω is the dimensionless pile base stiffness ($=\frac{K_b}{E_p A_p \lambda}$); δ is the relation between spring stiffness and soil shear modulus in the Winkler model proposed by Randolph & Wroth (1978); G_s is the soil shear modulus; E_p is the pile Young's modulus; A_p is the pile cross-sectional area; and K_b is the pile load/settlement relation at the pile base.

Mylonakis & Gazetas (1998) reported that the attenuation process occurs mainly along the pile shaft and the parcel due to the pile base interaction could be disregarded. Therefore, the total value of $\zeta(h\lambda,W)$ could be presented as shown in Fig. 2.

Cao & Chen (2008) presented an interesting analytical method for calculating the interaction factor between two identical piles subjected to vertical loads. The solution starts from the point at which the continuum medium (original loaded piles) is decomposed into two parts (Fig. 3): an "extended soil" mass and "two fictitious piles". The former is the soil, which is considered a three-dimensional elastic material (E_s and ν) loaded with the difference of stresses, defined as the total applied stress minus the stresses on the piles ($\sigma = (P_0\text{-}P^*)/pile\ area$), at the positions where the piles should be. The "two fictitious piles" consist of one-dimensional material for which the Young's modulus (E^*) would be the difference between the pile material Young's modulus (E_p) and soil Young's modulus (E_s). The pile should be discretized in parts to solve the equations and the authors claimed that four or more segments would be sufficient. Plotted data with the interaction factors are presented for different values of relative spacing (S/D), the relation of the base soil and shaft soil Young's modulus (E_b/E_s) and different relative lengths (L/D).

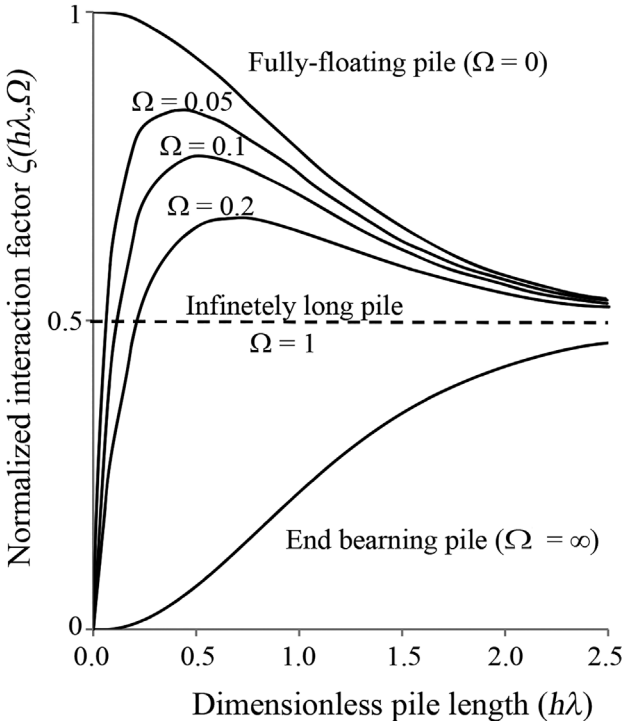

Figure 2 - Attenuation factor $\zeta(h,W)$, after Mylonakis & Gazetas (1998).

In all presented methods, once the interactions between two piles are estimated, the total settlement of any pile situated in a pile group can be calculated as the sum of every two-by-two induced settlements, as expressed in the following equation.

$$w_j=\sum_i^n w_{ji}=\sum_i^n \alpha_{ji} w_i \quad (10)$$

where w_j and w_i are the settlements of piles j and i, respectively; w_{ji} is the induced settlement in pile j due to the loaded pile i; and α_{ji} is the interaction factor between piles i and j.

The presented analysis of the aforementioned methods indicate that the original and most commonly used method presented by Poulos (1968) had an important role in stating a mathematical and logical way to predict the settlement of pile groups and that the simple two-pile interaction factor would be more effective for homogeneous soil and small pile groups, but divergences could emerge in other contexts. The following items will attempt to focus on the last points.

3. Comparing the Different Theories

To discuss the similarities of the presented theories, an analysis was performed using the finite element method (FEM) to establish a benchmark for what should be the "reference value". Despite the importance of nonlinear analysis for pile settlement predictions, the interaction factors between two piles using a simple elastic approach are widely accepted (Mandolini, 2003). The soils used in all of the following examples were considered a continuous elastic medium, and the piled foundations were subjected to "project loads" (serviceability limit state - SLS).

The chosen program for FEM Analyses was DIANA (TNO, 2012), which has already been described in Hemada *et al.* (2014), Tradigo *et al.* (2015), and many other papers.

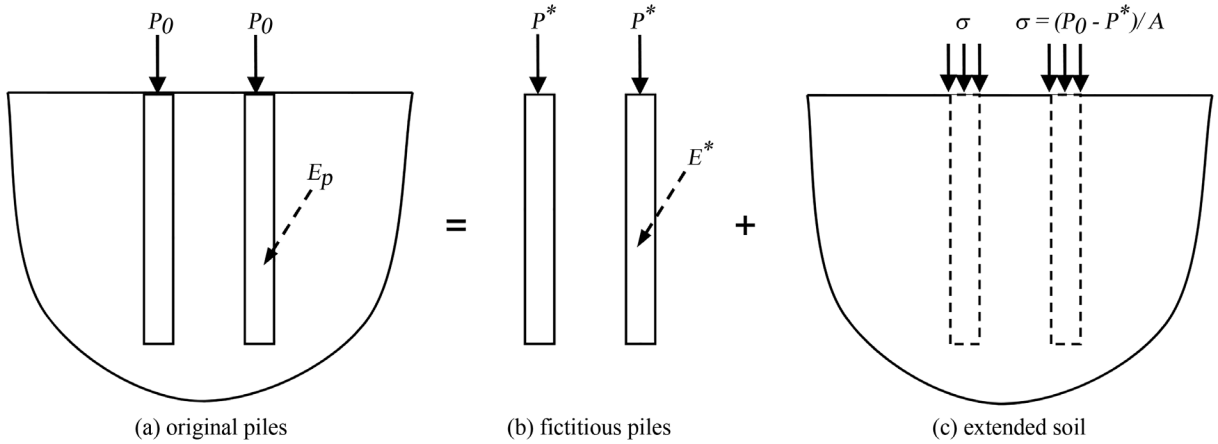

Figure 3 - Cao & Chen's (2008) hypothesis of foundation decomposition in: (a) original problem; (b) fictitious piles; (c) extended soil.

A typical mesh used in the following examples is presented in Fig. 4. Lateral and vertical boundary limits of *3L* and *5L* (*L* is the pile length), starting from the superficial center load point, were considered. Three different solid isoparametric elements (4faces/10nodes, 5faces/15nodes or 6faces/20nodes) were applied to better represent different geometries, always with a quadratic interpolation.

Figures 5 and 6 present comparisons of a two-pile interaction factor predicted from the different described theories. The exemple piles had relative lengths (*L/D*) of 25 and 50 with a relative stiffness (*K*) of 1000. For the methods of El Sharnouby & Novak (1990), Mylonakis & Gazetas (1998), Cao & Chen (2008), the presented values were taken from the original papers on each theory. Poulos &

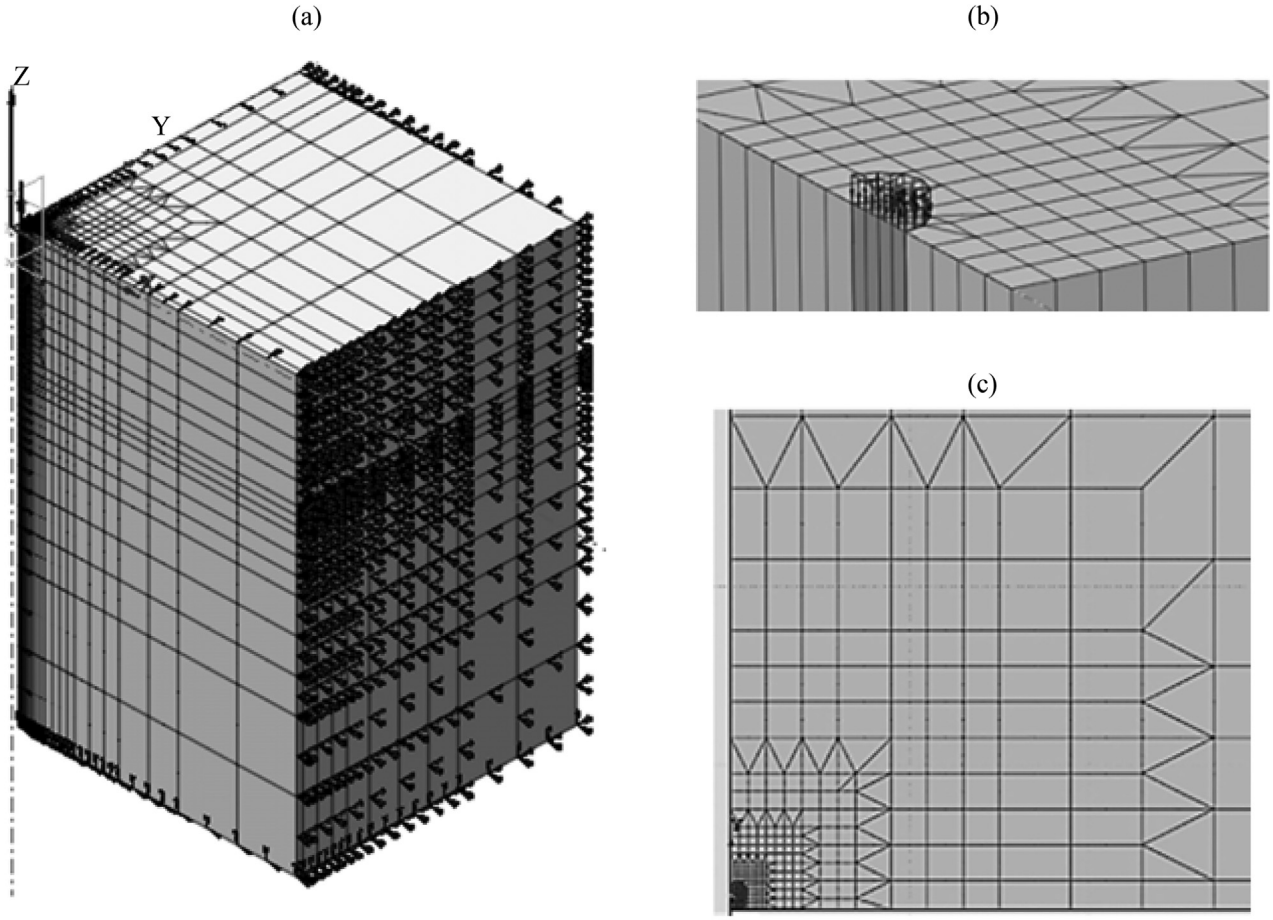

Figure 4 - Example of FEM analysis. (a) general view, (b) zoom close to the pile, (c) zoom of the more refined mesh near the pile.

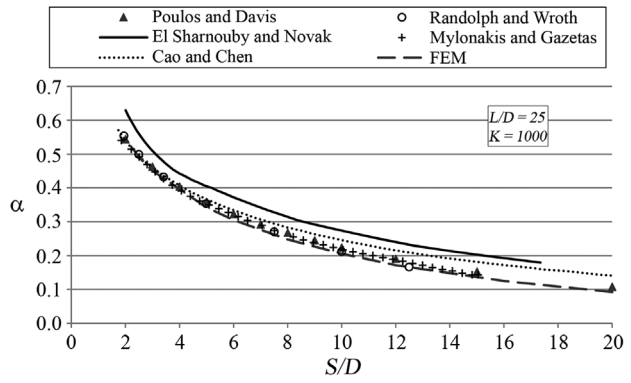

Figure 5 - Two-pile interaction factor predictions from different theories. Piles with L/D = 25 and K = 1000.

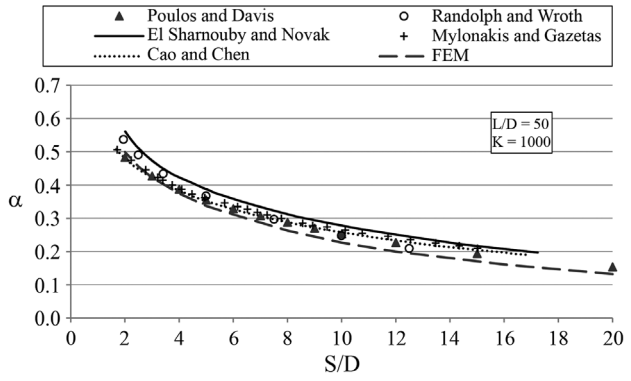

Figure 6 - Two-pile interaction factor predictions from different theories. Piles with L/D = 50 and K = 1000.

Davis (1980) interaction values were calculated using the DEFPIG software application (Poulos, 1980), which is the original program used to prepare the book charts, but with more than 20 elements to discretize the pile. The values for Randolph & Wroth's (1979) method were obtained by using Eq. 3 through 6. In a general view, all results are in reasonable agreement.

The presented results are in general agreement with many other analyses presented by Curado (2015) and demonstrate that the solution of El Sharnouby & Novak (1990) tends to produce higher values of α. The results of Randolph & Wroth's (1979) theory present marginally higher values for longer piles (L/D = 100). It must be noted that in these examples, homogeneous soil was assumed.

4. Stiffness of the Neighboring Piles

Almost all theories define the interaction factor α_{21} based on the induced settlement on Pile 2 due to the loading on Pile 1, generally considering similar piles. In other words, the induced settlement is calculated using only the material properties of Pile 1 and the soil characteristics where this pile is embedded. The real stiffness of Pile 2 is not considered. Figure 7 presents the results of FEM analysis for two hypothetical limits of Pile 2 stiffness. The Young's modulus for the Pile 2 material was varied from a very low value (same as the soil) up to the same value of Pile 1 modulus (similar concrete piles). The Pile 2 settlement is not the same if its stiffness changes. The longer the piles are, the larger the difference in induced settlement is. Figure 8 highlights that for end-bearing piles, the differences would be even larger. In these examples, E_b represents the Young's modulus of a stiffer soil layer below the pile tip. Based on these figures, it is possible to note that the interaction problem depends on the behavior of both piles. Poulos & Davis (1980) and Wong & Poulos (2005) have studied the interaction-factor problem for dissimilar piles and presented simplified approaches in attempts to incorporate correction factors into the original value of α for similar piles.

5. Interference of Other Piles

Some examples are presented to evaluate the effect of the presence or lack of other piles between the two analyzed piles. Figures 9 and 10 compare the interaction factor

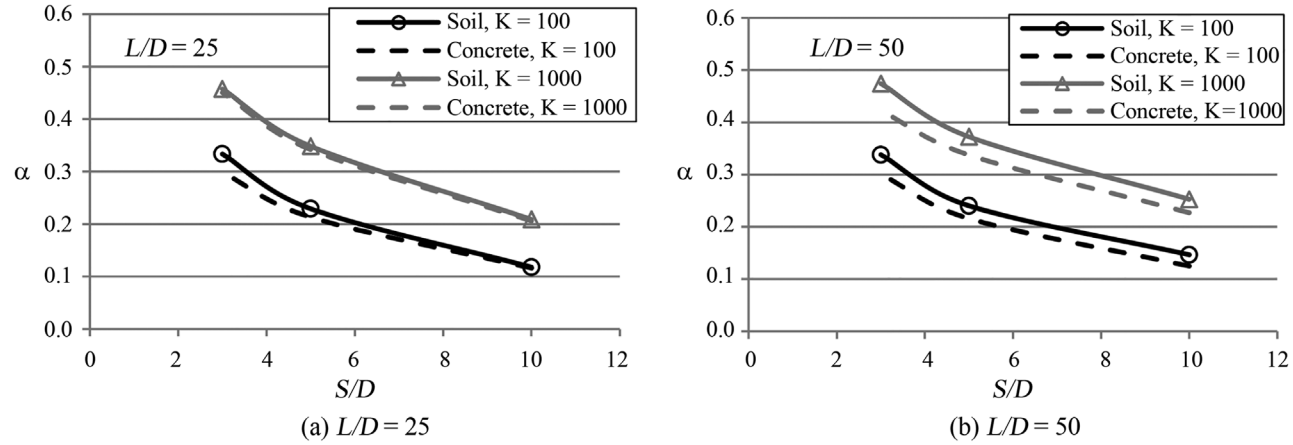

Figure 7 - Interaction factors behavior under different pile materials for the affected pile (Pile 2). Piles embedded in a homogeneous soil.

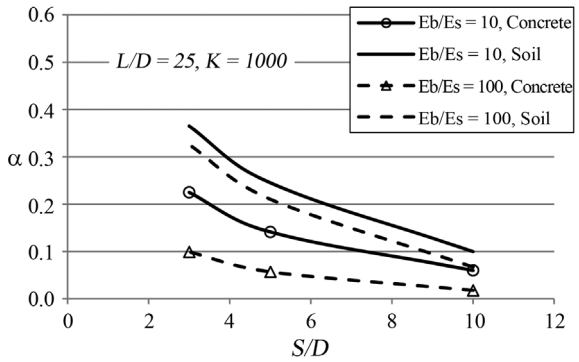

Figure 8 - Interaction factors behavior under different pile materials for the affected pile (Pile 2). Piles resting on a stiffer layer with Young's modulus E_b.

among piles 1-2 and 1-4, respectively. Figure 9 presents the factor α_{21}, which represents the interaction of two neighboring piles, with a separation of $S = x$, a relative length (L/D) of 25 and a relative stiffness (K) of 1000. For Poulos & Davis's (1980) method, this is the two-pile interaction factor; *i.e.*, only these two piles exist. The El Sharnouby & Novak (1990) curve was obtained from the problem of the 5-in-line pile group, where Piles 1 and 2 are the two leftmost piles, separated by a distance of x, but now with the presence of three piles at the right-hand side of Pile 2. Four different values of x were considered (S/D = 2.5, 3, 4 and 5) along with different relations for the base and shaft soil Young's modulus (E_b/E_s = 1, 10, 100 and 1000).

Figure 10 presents a similar analysis for α_{41}. For Poulos & Davis's (1980) theory, the piles were a distance of $3x$ apart, but only the two piles existed. For El Sharnouby & Novak (1990), α_{41} is the interaction between the first and fourth piles in a group of five piles. For this figure, the interaction factors were calculated for center-to-center spacings of 7.5, 9, 12 and 15 diameters. In both figures, Poulos & Davis's (1980) theory achieved better predictions for homogeneous soils (E_b/E_s = 1), whereas for end-bearing piles, the interaction factors from ElSharnouby & Novak (1990) were similar to the FEM analysis.

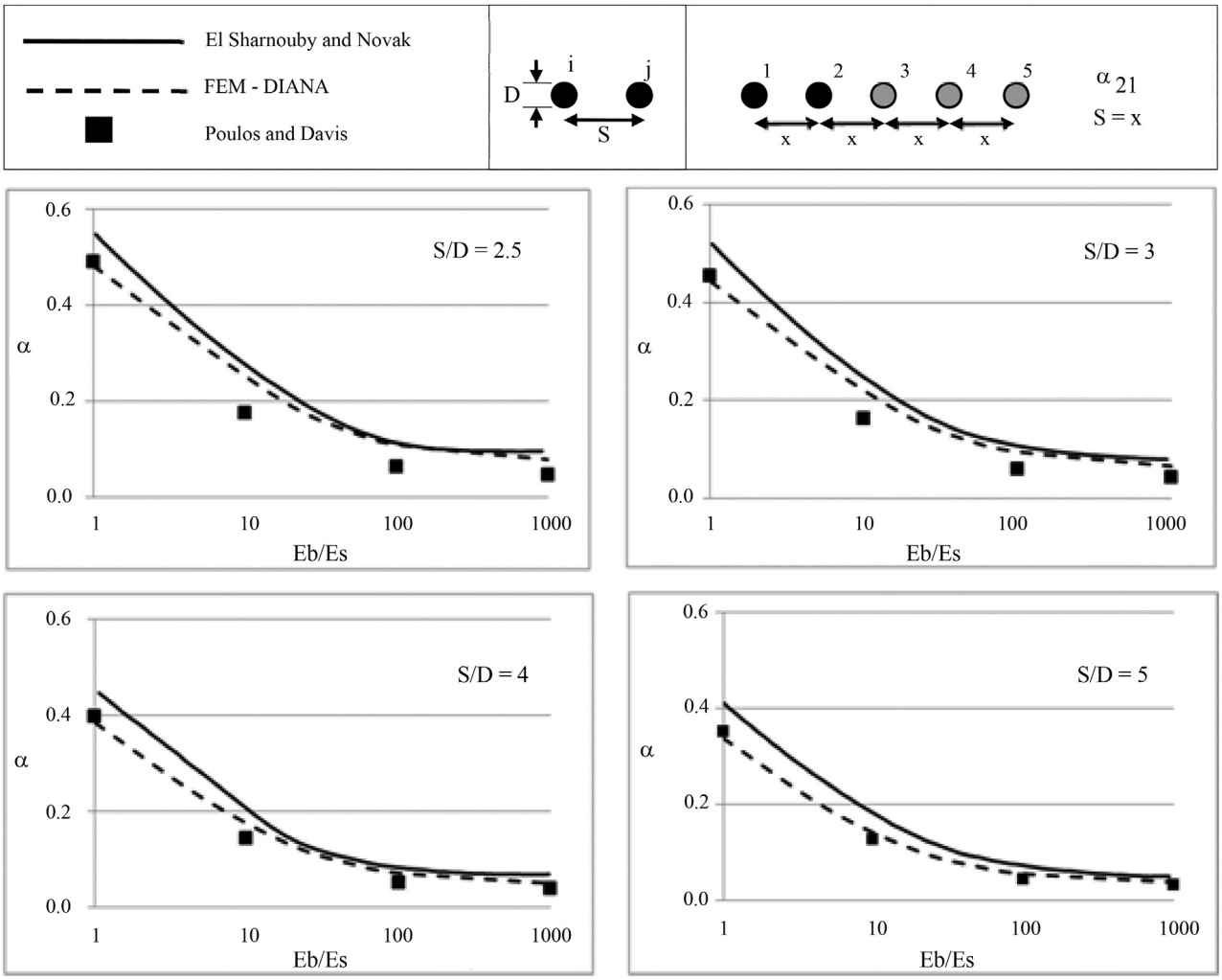

Figure 9 - Interaction factor α_{21} for two piles in groups of two and five piles (L/D-25, K = 1000).

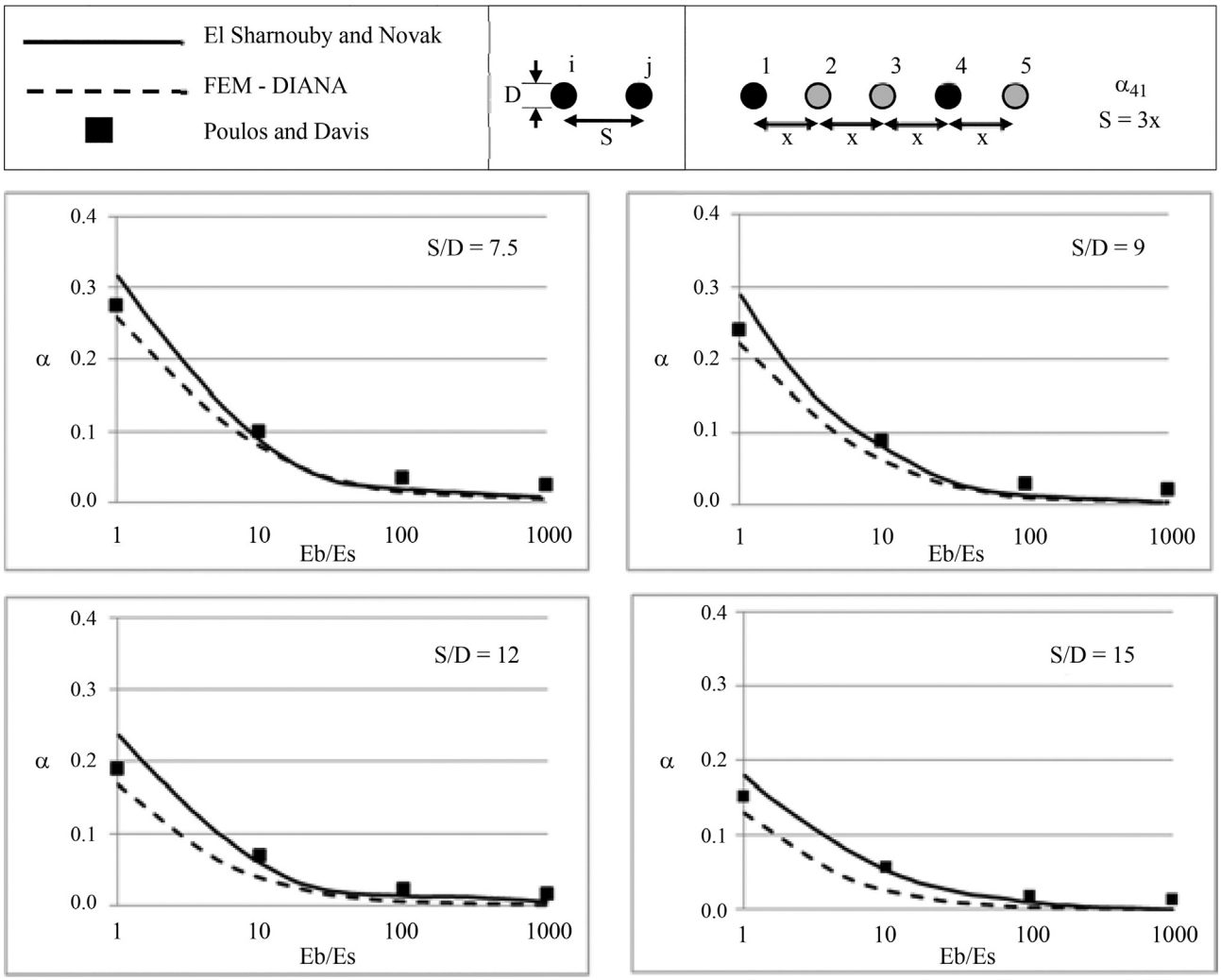

Figure 10 - Interaction factor α_{41} for two piles in groups of two and five piles (*L*/*D*-25, *K* = 1000).

Mylonakis & Gazetas (1998) mentioned that intermediate piles would provoke a reduction in the induced settlement to a neighboring pile, this direct correlation was not confirmed by the results, as could be inferred from the presented data in Fig. 10 for the homogeneous soil case. Values of α_{41} (with two other piles between the loaded and the analyzed piles) from El Sharnouby & Novak (1990) were higher than the factors predicted by Poulos & Davis's (1980) theory. To further examine this result, four different pile groups were studied using FEM. Figure 11 presents the results for groups with 2, 3, 5, 9 and 25 piles. The only loaded pile is represented with an arrow, and all other piles were unloaded. No cap was considered in these cases, and the interaction factor was calculated for the pile represented by a hatched area (target pile). These examples are not found in practice, but this is the manner to exclude all other factors that affect the pile settlement prediction. Therefore, in all groups with three or more piles, there was always one pile between the loaded and the studied piles. A relative stiffness (*K*) of 1000 and different spacings were considered in this analysis. Figures 11a and 11b show the results for piles with relative lengths of 25 and 50, respectively.

Some remarks can be drawn from Fig. 11:

- By comparing the groups with 3 and 5 piles, we can observe that not only did the pile placed between the studied piles result in lower values of α, but the other piles in the same line still contributed to reduce the settlement in the target pile;
- Other nearby piles also contributed to reduce the interaction factor between the two studied piles, as seen for the 9- and 25-pile groups.

With all of these comments, we can see that the interaction factor is not simply a two-pile problem. The presence of other nearby piles can interfere in the total pile stiffness. Thus, the nearby piles would hamper the soil movement around the pile that is receiving the influence of the loaded pile.

6. Pile Position in the Foundation

Returning to Fig. 11, one point stands out. Comparing the groups with 5 and 9 piles, the 9-pile group has a lower

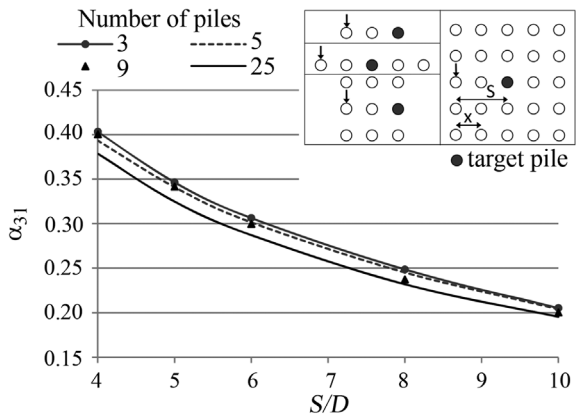

(a) $L/D = 25$, $K = 1000$, $S = 2x$.

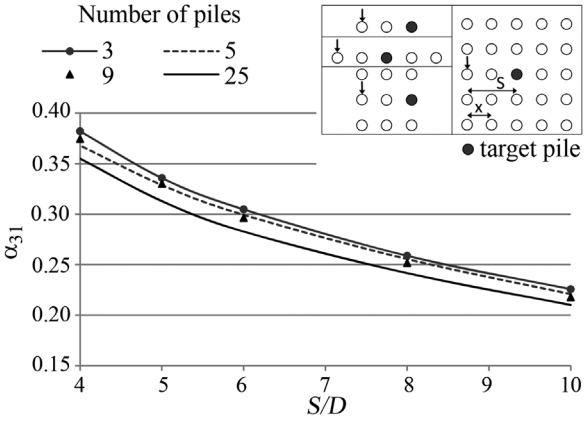

(b) $L/D = 50$, $K = 1000$, $S = 2x$.

Figure 11 - Interaction factor for two piles with another intermediate pile in groups of 3, 5, 9 and 25 piles. (a) piles with $L/D = 25$, (b) piles with $L/D = 50$.

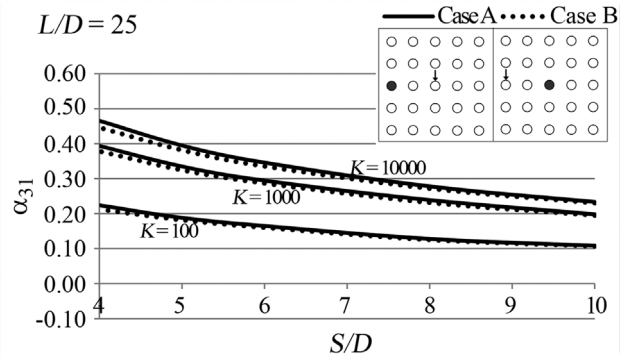

(a) $L/D = 25$

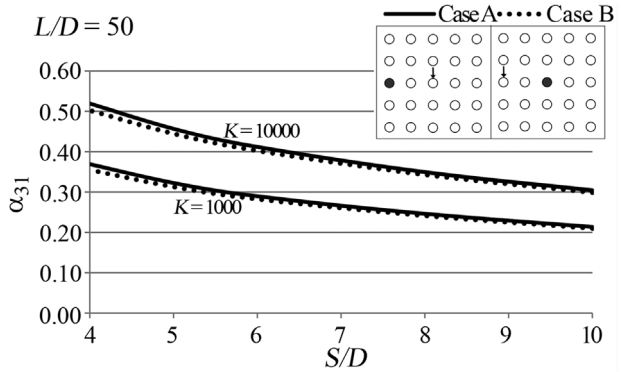

(b) $L/D = 50$

Figure 12 - Comparing the interaction factor α_4 inside a 25-pile group with different loaded pile positions. (a) $L/D = 25$, (b) $L/D = 50$.

interaction factor for all spacings and both pile lengths, except when $S/D = 4$ (distance from loaded and studied piles, recalling that another pile was between them). For some reason, the trends were reversed at this point. To explore this fact, a 25-pile group was analyzed with a finite element software program DIANA (TNO, 2012), and Fig. 12 presents the interaction factor between 2 piles. Two different relative pile lengths were explored: $L/D = 25$ (Fig. 12a) and $L/D = 50$ (Fig. 12b), changing the spacings between piles (S/D). In this group, only one pile was loaded, and the settlement was evaluated in other pile (filled circle). In Case A, the loaded pile was in the center, and the studied pile (target pile) was the leftmost lateral one. Conversely, in Case B, the loaded pile was in the lateral position, and the central pile was receiving settlement influence. As shown in Fig. 12, for all situations, Case A resulted in the higher settlement of the neighboring pile because the settlement receiving pile was in the lateral position; thus, the less confined situation allowed this pile to experience a higher movement. In contrast, when the target pile (filled circle) was in the center (Case B), the most confined position, the induced settlement was lower.

This example shows that a two-pile interaction is not a reciprocal problem. Despite all similitudes between piles, the interaction factors were different ($\alpha_{21} \neq \alpha_{12}$), showing that pile position and group geometry do matter.

For the reason mentioned previously, the studied pile in the 9-pile group (Fig. 11 with $S/D = 4$) was "less confined" than the corresponding 5-pile group, so the influenced pile had a higher settlement. When the pile spacing increased, the confinement started to change, and the interaction factor gradually decreased.

7. Large Pile Groups and Piled Rafts

All previous comparisons presented differences that could be classified as "not so relevant". This is partially true for groups with only a few piles. For a large piled foundation (pile groups or piled rafts), as used in an increasing number of tall building foundations, the cumulative differences due to lower interaction factors can result in a considerable difference in the final elastic settlement prediction.

Figure 13 compares the predictions for three different pile groups with different approaches: one calculated as a full three-dimensional (*3D*) pile group problem (ρ_{FEM}) and the other using a theoretical method based on the superposi-

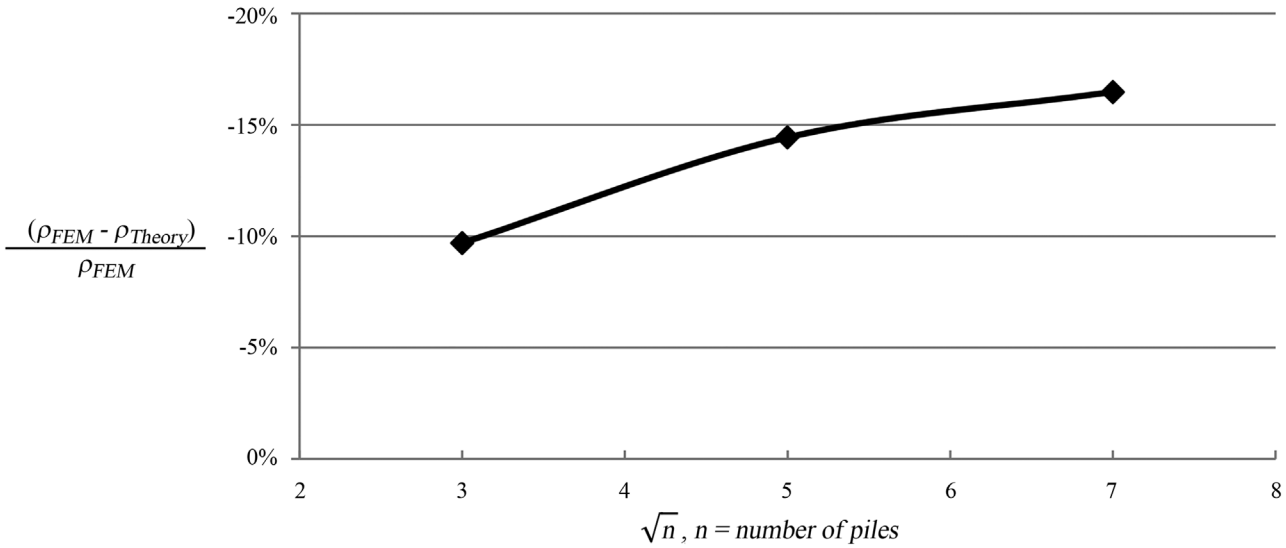

Figure 13 - Influence of different concepts for interaction factors in a homogeneous soil for groups with different numbers of piles.

tion of interaction factors (ρ_{Theory}). In the theoretical case, the individual two-pile interaction was also pre-calculated with the same software (as in Fig. 5). Square pile groups with 9(3×3), 25(5×5) and 49(7×7) piles are presented, and the reduction factor is defined here as the relation between the settlement difference (true 3D FEM analysis minus the conventional superposition of interaction factors) and the considered more realistic approach (3D FEM analysis). In this example, the soil was considered as a homogeneous profile with K = 1000 and L/D = 25, all piles had the same load, and the spacing of three diameters between the piles (center-to-center) was considered for all of these groups. The figure shows an increasing difference becoming more than 15% for the largest group. The reduction ratio is non-linear because the number of interactions increases with increasing pile number, which results in lower interaction factors for even more distant piles. For heterogeneous soils, the differences can be even larger.

To exemplify this situation, the problem proposed by TC-18 in 1998 (Matsumoto *et al.*, 1998) of a 16-pile group resting in a heterogeneous profile is presented here. The elastic soil modulus distribution was considered to be similar to Frankfurt clay, as suggested by Amman (1975) and explored in Sales *et al.* (2010). Some authors were invited to present predictions of the settlement and distribution of pile loads. Figure 14 presents the soil, piles and raft data, and a total load of 80MN was uniformly spread over the raft. Table1 compares some returned predictions and a new 3D FEM analysis using the software application DIANA (TNO, 2012). We clearly have two different sets of predictions: the first group (Horikoshi & Randolph, 1998; Matsumoto, 1998 and Sales, 2000) contains the predictions based on hybrid methods using the two-pile interaction concept (not considering the other piles when calculating the pile interactions), and the second group uses 3D FEM software. Inside each group of predictions, the results are very similar; however, the difference between the average values for the predicted settlements (42 mm and 28.7 mm, respectively) is greater than 30%. The procedure of considering all sets of piles in a 3D analysis resulted in a lower foundation settlement than using the conventional superposing two-pile process. The presented example indicates that for a heterogeneous soil, the difference in pile group settlement predictions can still be higher than the values shown in Fig. 13. Considering the remarks of Fig. 13 and Table1, it should be pointed out that for large pile groups (more than 9 piles) and piled rafts, especially for a heterogeneous soil, a more rigorous analysis on settlement predictions would be necessary.

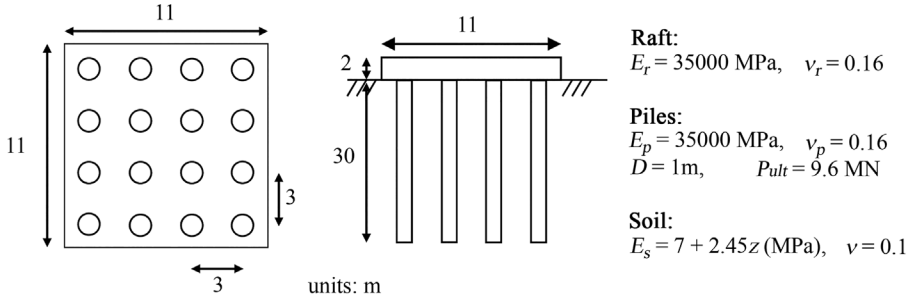

Figure 14 - 16-pile group in a heterogeneous soil proposed by TC-18.

Table 1 - Settlement Predictions for the 16-piled raft of TC-18.

Author	Software	Interaction Method	Maximum Settlement (mm)
Horikoshi and Randolph(1998)	HyPR (HM*)	Two-piles	41-43
Matsumoto (1998)	KURP (HM*)	Two-piles	42
Sales (2000)	GARP (HM*)	Two-piles	42
Yamashita (1998)	NA (FEM)	Full Interaction	29
Sales (2000)	ALLFINE (FEM)	Full Interaction	27
This Paper	DIANA (FEM)	Full Interaction	30

*HM = Hybrid Method, FEM = Finite Element Method, NA = name not available.

Conclusions

This paper discussed methods used to evaluate the interaction between piles in a piled foundation under a vertical load. The conventional process of superposing interaction factors, which is a consequence of induced settlements of two neighboring piles, was compared with a three-dimensional finite element analysis in foundations with different pile configurations; and the following aspects can be noted:

1) The factor α, proposed by Poulos (1968) to evaluate the interaction between two piles, is the basis of many other theories. The superposing principle of two-pile interaction to study pile group settlements achieves good results mainly for small pile groups and homogeneous soils;

2) Some theories, including El Sharnouby & Novak (1990) and Mylonakis & Gazetas (1998), note that if another pile is between the other two considered piles, the settlement field and the interaction factor will be affected;

3) The presented examples showed that, in a pile group, the position of all other piles will interfere with the induced settlements. Thus, the two-pile interaction is not a perfect "reciprocal problem" because the pile position and group geometry change the factor α.

4) When comparing a complete 3D FEM analysis with the conventional approach of superposing interaction factors, a smaller pile group settlement is found. This difference can exceed 15% for homogeneous soils but can be much larger for heterogeneous soils and a large number of piles (over 9-pile groups).

5) This paper analyzed the process of induced settlements on nearby piles. Only elastic examples were presented to clarify and simplify the comparisons. The authors, however, recognize that many other aspects can contribute to pile interaction factors, including nonlinear behavior, and pile installation method.

Acknowledgments

The authors acknowledge CNPq, the Brazilian National Research Council, for financial support. Grateful Acknowledgments are made to Rodrigo Salgado and Monica Prezzi for their support during the first author stay at Purdue University.

References

Amman, P. (1975). Verformungsverhalten des Baugrundes beim Baugrubenaushub und anschlieβendem Hochhausbau am Beispiel des Frankfurtes Tons. Mitteilungen des Institutes fur Grundbau, Boden und Felsmechanik, Technische Hochschule Darmstadt, Heft 15, Darmstadt, Germany. (in German).

Burland, J.B.; Broms, B.B. & Mello, V.F.B. (1977). Behavior of foundation and structures. Proc. of the 9th International Conference Soil Mechanics and Foundation Engineering, Tokyo, v. 2, pp. 495-546.

Cao, M. & Chen, L.Z. (2008). Analysis of interaction factor between two piles. Journal of Shanghai Jiao Tong University (Science), 13(2):171-176.

Cooke, R.W.; Price, G. & Tarr, K.W. (1980). Jacked piles in London clay: Interaction and group behavior under working conditions. Géotechnique, 30(2):449-471.

Curado, T.S. (2015). Comparisons of Pile Interaction Theories. M.Sc. Thesis. School of Civil and Environmental Engineering, Federal University of Goiás, Goiânia, 151p. (in portuguese).

El Sharnouby, B. & Novak, M. (1990). Stiffness constants and interaction factors for vertical response of pile groups. Canadian Geotechnical Journal, 27(6):813-822.

Hemada, A.A.; Abdel-Fattah, T.T. & Abdel-Fattah, M.T. (2014). Application of FEM to evaluate pile loading test in some special situations. Tunneling and Underground Construction GSP 242, ASCE, Shangai, pp. 790-801.

Horikoshi, K. & Randolph, M.F. (1998). Analyses of piled raft model provided by ISSMGE TC-18 – Part3: Estimation by simple approach and hybrid method HyPR. Proc. TC-18 Japanese Geotechnical Society Member's meeting on Piled Raft, Tokyo, pp. 3.1-3.16.

Mandolini, A. (2003). Design of piled raft foundations: practice and development. Proc. Deep Foundation on Bored and Auger Piles – BAP IV, Ghent, Belgium. W.F. Van Impe (ed.), Millpress, Rotterdam, the Netherlands, pp. 59-80.

Mandolini, A. & Viggiani, C. (1997). Settlement of piled foundations. Géotechnique, 47(4):791-816.

Matsumoto, T., Yamashita, K. & Horikoshi, K. (1998). Analyses of piled raft model provided by ISSMGE

TC-18 – Part5: Summary and comparisons of results. Proc. TC-18 Japanese Geotechnical Society Member's meeting on Piled Raft, Tokyo, pp. 5.1-5.2.

Matsumoto, T. (1998). Analyses of piled raft model provided by ISSMGE TC-18 – Part4: Analyses of piled raft subjected to vertical loading and horizontal loading. Proc. TC-18 Japanese Geotechnical Society Member's meeting on Piled Raft, Tokyo, pp. 4.1-4.7.

Mylonakis, G. & Gazetas, G. (1998). Settlement and additional internal forces of grouped piles in layered soil. Géotechnique, 48(1):55-72.

Poulos, H.G. (1968). Analysis of the settlement of pile groups. Géotechnique, 18(4):449-471.

Poulos, H.G. (1980). DEFPIG – users' guide. Centre for Geotechnical Researches, University of Sydney, Australia.

Poulos, H.G. (1989). Pile behaviour - theory and application. Géotechinique, 39(3):365-415.

Poulos, H.G. (2001). Piled raft foundations: Design and applications. Géotechinique, 51(2):95-113.

Poulos, H.G. & Davis, E.H. (1980). Pile foundations analysis and design. John Wiley and Sons Inc, New York, 397 p.

Randolph, M.F. (1994). Design methods for pile groups and piled rafts. Proc. of the 13th International Conference Soil Mechanics and Geotechnical Engineering, New Delhi. India, Balkema, Rotterdam, the Netherlands. v. 5, pp. 61-82.

Randolph, M.F. (2003). Science and empiricism in pile foundation design. Géotechnique, 53(10):847-875.

Randolph, M.F. & Wroth, C.P. (1978). Analysis of deformation of vertically loaded piles. Journal of Geotechnical Engineering Division, ASCE, 104(GT12):1465-1488.

Randolph, M.F. & Wroth, C.P. (1979). An analysis of the vertical deformation of pile groups. Géotechnique, 29(4):423-439.

Sales, M.M. (2000). Behavior analysis of piled footings. PhD. thesis. Faculty of Technology, University of Brasilia, Brasília, 229 p. (in portuguese).

Sales, M.M.; Small, J.C. & Poulos, H.G. (2010). Compensated piled rafts in clayey soils: Behavior, measurements, and predictions. Canadian Geotechnical Journal, 47(3):327-345.

Southcott, P.H. & Small, J.C. (1996). Finite layer analysis of vertically loaded piles and pile groups. Computers and Geotechnics, 18(1):47-63.

TNO (2012). DIANA Finite Element Analysis: User's Manual – Release 9.4.4. TNO Diana BV, Delft, the Netherlands.

Tradigo, F.; Castelazza, R.; Patrovi, M. & Shreppers, G. (2015). Calibration procedure for embedded pile modeling based on in situ pile load tests. Proc. of the 16th ECSMGE, Edinburgh, pp. 3771-3776.

Wong, S.C. & Poulos, H.G. (2005). Approximate pile-to-pile interaction factors between two dissimilar piles. Computers and Geotechnics, 32(8):613-618.

Yamashita, K. (1998). Analyses of piled raft model provided by ISSMGE TC-18 – Part2: Estimation by three dimensional finite element analysis. Proc. TC-18 Japanese Geotechnical Society Member's meeting on Piled Raft, Tokyo, pp. 2.1-2.8.

List of Symbols

A_p: pile cross-sectional area
c: a constant
D: pile diameter
E^*: "fictitious pile" Young's modulus
E_b: Young's modulus of a stiffer soil layer below the pile tip
E_p: pile Young's modulus
E_r: raft Young's modulus
E_s: soil Young's modulus
FEM: Finite Element Method
$G_{l/2}$, G_l: values of the shear modulus at the pile mid-depth and pile base, respectively
G_s: soil shear modulus
h: layer thickness crossed by the pile
K: relative stiffness of a pile
K_b: pile load/settlement relation at the pile base
K_p: pile stiffness
L: pile length
n: number of piles
N_b: correction for the presence of a stiffer soil layer below the pile tip
N_h: correction for the finite soil layer
N_v: correction for other Poisson's ratios
P: load
P^*: applied load on the "fictitious piles"
P_0: total applied load on the original piles
P_b, P_t: base and total loads acting on the pile, respectively
P_{ult}: ultimate load
r_0: pile radius
r_m: limiting radius of influence of the pile
S: center-to-center distance between piles
w: top settlement
w_1, w_2: settlements of Piles 1 and 2, respectively
w_b: base settlement
w_{ji}: induced settlement on the pile *"j"* due to the loaded pile *"i"*
w_j: settlement of pile *"j"* due to its own load
w_s: shaft settlement
w_t: total settlement
x: center-to-center distance between piles, in 5-in-line pile group
α: two-pile interaction factor
α_{21}, α_{31} , α_{41} , α_{51}: interaction factor on pile number "n" due to the load on Pile 1 but considers the presence of all five piles

α_F: interaction factor for a semi-infinite soil using "0.5" for Poisson's ratio

α_{ji}: interaction factor between loaded pile *"i"* and its neighboring pile *"j"*

δ: relation between spring stiffness and soil shear modulus in the Winkler model

λ: Winkler load transfer parameter

ρ: degree of homogeneity

ρ_{FEM}: predictions for pile groups calculated as a full three-dimensional (3D) pile group problem

ρ_{Theory}: predictions for pile groups using a theoretical method based on the superposition of interaction factors

σ_z soil stress load

τ_0: shear stress at the pile shaft

ν: Poisson's ratio of the soil

ν_p: Poisson's ratio of the pile

ν_r: Poisson's ratio of the raft

Ω: dimensionless pile base stiffness

$\psi(S)$: free displacement field

ζ: calculated as $\ln(r_m/r_0)$

$\zeta(h\lambda, W)$: attenuation factor due to the self-stiffness of the neighboring pile

Geotechnical Aspects of Weak Sandstone from Recife/Brazil

O.M. Oliveira, R. Bim, G.B. Nunes, R.A.R. Higashi

Abstract. Diagenetic processes acting on the sandy sediments of the marine plains from the city of Recife/Brazil formed different types of sandstones. Two blocks of the sandstone formed in the Pleistocene epoch were collected to perform characterization tests and determine their mechanical properties. This sandstone is present in a depth between 0.3 and 4.5 m and with a thickness between 0.5 and 4.5 m. The average values obtained for their specific dry weight and porosity are respectively equal 16.5 kN/m^3 and 30%. In the unconfined compressive strength tests were obtained mean values of resistance and deformability module respectively, equal to 2 MPa and 162 MPa, classifying this sandstone as weak rock. An isotropic behavior was observed when performing direct shear tests in the direction parallel and perpendicular to the level of the terrain. The sandstone block collected at a greater depth presented higher resistance parameters in these tests with cohesion of 393 kPa and a friction angle of 55.6°. A case study is presented where the geological and geotechnical characteristics of these sandstones were explored as support for a building foundation, and a good performance was observed.

Keywords: marine plain, weak rock, weak sandstone.

1. Introduction

The two marine transgressions occurring within the Pleistocene and Holocene Epoch of the Quaternary Period, formed in the Metropolitan Region of the city of Recife/Brazil, a marine terrace with distinct geological characteristics. The sandy deposits of these terraces were submitted to diagenetic processes that allowed the formation of sandstones with different cementing agents.

It is of fundamental importance to understand the role of marine transgressions in the formation of these marine terraces, due to the great amount of sediments brought to the continent and its peculiar form of deposition. The advancement of the sea by the receding coastline (transgression) occurs due to fluctuations of its relative level, as a result of complex interactions between the surface of the ocean and the continent. Deglaciations and changes in the volume of ocean basins due to plate tectonics and the local level changes of the continent are factors of change in these relative positions (Suguio *et al.*, 1985). Marine transgression breaks the dynamic balance of coastal regions due to its high energy in the wave front, causing sediment erosion, deposition in deeper regions and lower transport energy. During the process of marine regression, the erosive process is reversed. The wave front erodes the sediments deposited during the transgressive process with transport and deposition of the same to the post-beach. In the regressive phase, the formation of beach ridges occurs -which together form the plain of marine sediments.

The transformations imposed by natural elements, such as marine transgressions, rivers, mangroves and man, resulted in the formation of several geological units in the metropolitan region of the city of Recife, with very different geotechnical properties. The units deposited in the Quaternary Period are Pleistocene, Undifferentiated and Holocene marine terraces, alluvial and mangrove deposits.

The sandstones studied here are present in the marine terrace formed in the penultimate transgression occurring 120.000 years ago, display an altimetric level varying between 7 and 11 m, and a small slope on the coastline. The sediments deposited during the regression of the sea are formed by quartz grains with dimensions ranging from fine to coarse sand, incoherent in surface and of white color. With increasing depth, these sediments are consolidated by a cementing agent that gives it a brown coloration. These weak sandstones are present in practically all the extension of this marine terrace in the form of a slab, located near the surface that has been little explored as a foundation support in the construction of buildings. This type of sandstone is a common occurrence in the coastal plains of the coastal region of Brazil. The lack of knowledge of its geological and geotechnical properties leads engineers to design deep foundations for the buildings, which are common practice in the metropolitan area of the city of Recife. When used for surface foundation purposes in buildings, its deformability and strength parameters are framed within conservative models (Gusmão Filho, 1998). This article has as main ob-

Orlando Martini de Oliveira, D.Sc., Associate Professor, Departamento de Engenharia Civil, Universidade Federal de Santa Catarina, Florianópolis, SC, Brazil. e-mail: oliveiraorlando@hotmail.com.
Rodrigo Bim, Ph.D. Student, Universidade Federal de Santa Catarina, Florianópolis, SC, Brazil. e-mail: fale_com_ro@yahoo.com.br.
Gabriel Bellina Nunes, Ph.D. Student, Universidade Federal de Santa Catarina, Florianópolis, SC, Brazil. e-mail: gabrielbnunes@gmail.com.
Rafael Augusto dos Reis Higashi, D.Sc., Associate Professor, Departamento de Engenharia Civil, Universidade Federal de Santa Catarina, Florianópolis, SC, Brazil. e-mail: rrhigashi@gmail.com.
Submitted on August 24, 2017; Final Acceptance on February 21, 2018; Discussion open until August 31, 2018.
DOI: 10.28927/SR.411061

jective to demonstrate that these weak sandstones could be adequate as a support for shallow foundations.

During the characterization studies of these sandstones, their physical properties were obtained, in addition to their coefficient of permeability and aspects related to texture and structure. Its resistance parameters were determined in direct shear tests and uniaxial compression tests. For the determination of its area of occurrence, depth and thickness, the database of drilling of the geotechnical chart of the city of Recife was used.

2. Materials and Methods

2.1. Determination of the occurrence area of sandstones

The Geotechnical Chart of the Metropolitan Region of Recife was prepared in 1990 based on geotechnical drilling data, among other types of results. From this database, the drillings of the coastal region were selected, where two marine plains are inserted and were constructed by process of variations of the relative sea level occurring in the Holocene and Pleistocene epochs. The results of the analyses of 41 drillings indicated that the weak sandstones are present only in the marine plain formed during the Pleistocene Epoch, denominated in the geotechnical chart as Quaternary Pleistocene Unit (QP). These sandstones were identified in 22 drillings. The other 19 drillings, where the presence of the sandstone was not found, were concentrated in the Holocene Marine Terrace (QH) and in the Pleistocene Marine Terrace, whose sediments of marine origin were reworked by the river action being denominated as Quaternary Undifferentiated Unit (QU). The region of study with identification of the drilling sites is shown in Fig. 1. The drillings where the presence of the sandstone was identified are presented in this figure by circles. Beside these circles, the depth of the surface of this sandstone followed by its thickness are indicated in parentheses. The points indicated by triangle correspond to drillings where these sandstones were not found. The weak sandstones present in the QP unit are found in depths ranging from 0.3 to 4.5 m, with a thickness between 0.5 and 4.5 m.

Two geological profiles were determined using the survey data. The A-A' profile, shown in Fig. 2, is substan-

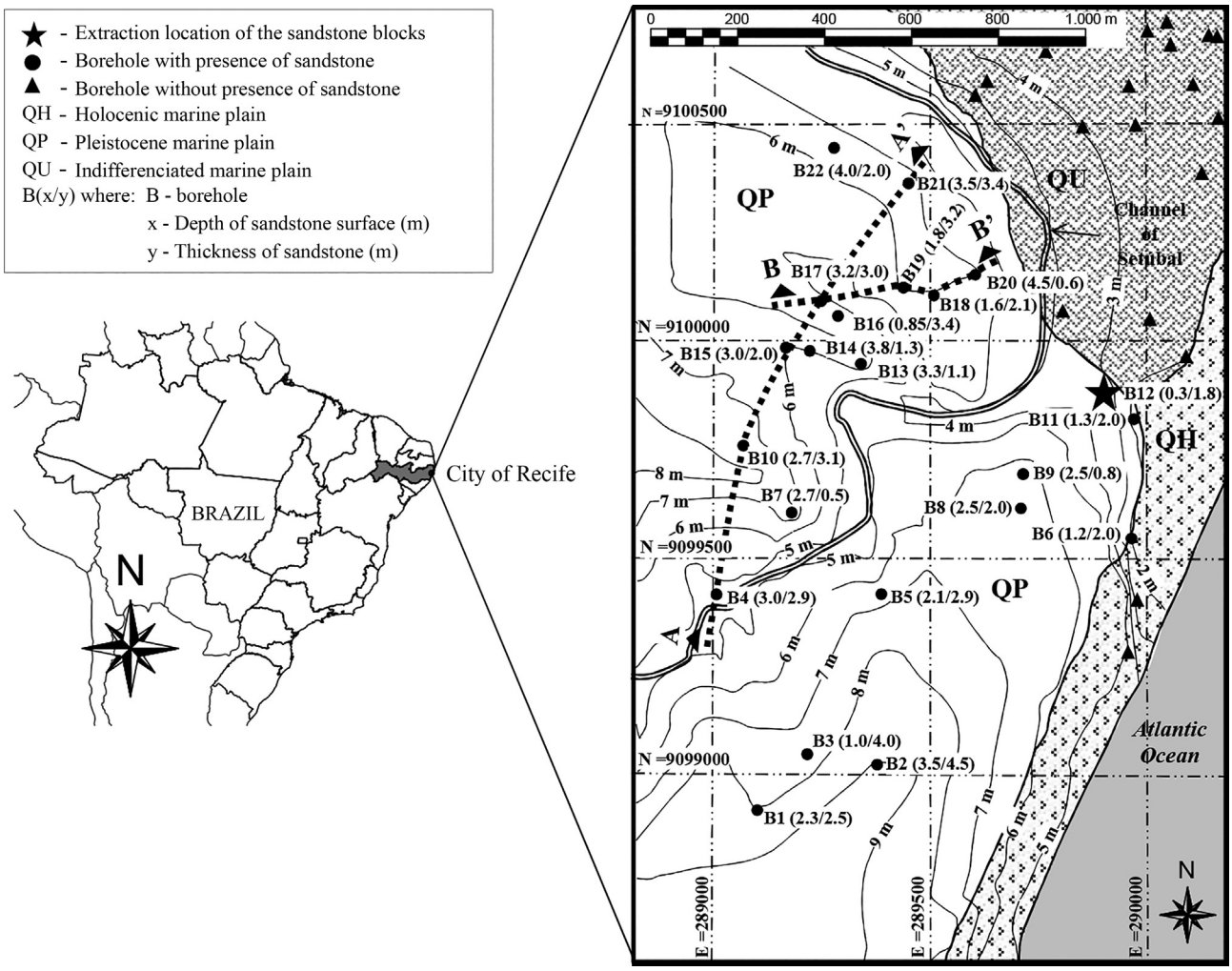

Figure 1 - Location of the drillings in the geotechnical chart of the city of Recife/Brazil.

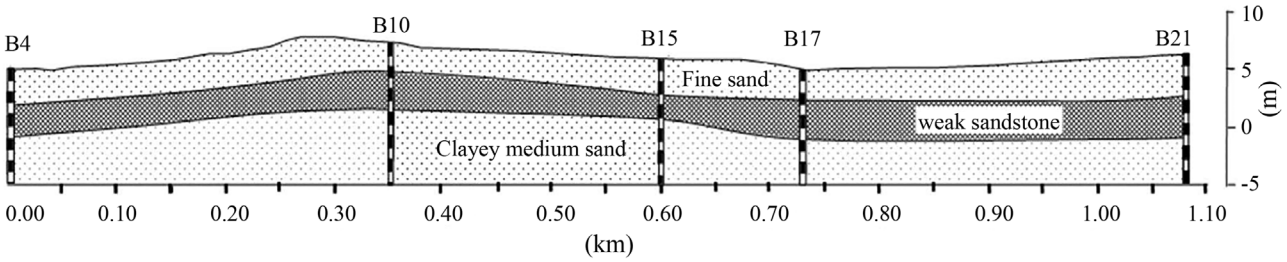

Figure 2 - Geological profile A-A'.

tially parallel to the coastline. This profile was plotted with the use of boreholes B4, B10, B15, B17 and B21. The profile B-B' represents a different direction being shown in Fig. 3. In this figure, a reduction in the thickness of the sandstone can be observed as it approaches the boundary of its marine terrace in the borehole B20. Figures 2 and 3 demonstrate that these sandstones are present in the shape of a stone slab. This spatial arrangement and proximity to the ground surface are what gives these sandstones great potential as support material for buildings having shallow foundations.

2.2. Sampling procedures

The removal of weak sandstone samples for performing laboratory tests involves some difficulties. When found during engineering projects, they are often avoided due to lack of knowledge of their geotechnical behavior (Dobereiner, 1984). The extraction of samples with rotary probe presents great difficulty due to the mechanical stresses transmitted and the circulation of water that causes the disaggregation of this weak rock (Kanji, 2014). The solution for the removal of blocks presents another difficulty, related to the difficulties of finding a place without buildings, given that it is a densely populated region, where this sandstone is not so deep and is above the level of the water table. The equipment generally used for the removal of soil blocks is not appropriate for working on weak rocks. The results presented here were obtained from 2 cubic blocks, with 0.3 m side, removed from the same excavation. In order to verify possible variations of physical and mechanical properties, the blocks were removed from different depths. Block 1 represents the depth of 0.3 to 0.6 m and block 2 represents the depth of 0.7 to 1.0 m. Figure 4 shows the place of the executed excavation for removal of weak sandstone blocks. The lack of local experience, as these are the first blocks removed from this rock formation, leads to improvisation in the use of available equipment such as hoe, shovel, pick, mallet, slitter and saw. Initially, a cube block with a 0.4 m edge was molded with the aim to avoid any disturbance caused by the impact of the tool (Fig. 4a). The finishing work, with a reduction of the length of the edge of the block to 0.3 m, was executed with the use of mallet and slicer (Fig. 4b). The process of removing only 1 block required a time of 5 h, and the labor of 3 workers. The 2 blocks were removed from the upper sandstone region, and they were representative of the settlement place of the buildings surface foundations.

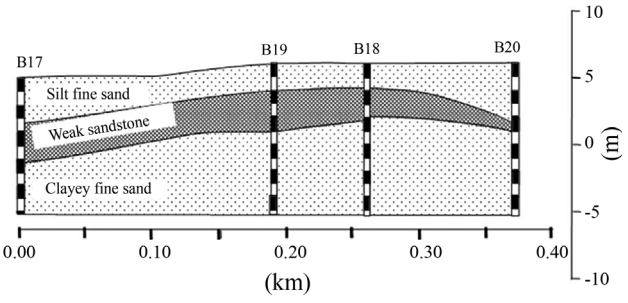

Figure 3 - Geological profile B-B'.

The profile presented in Fig. 5, obtained from two boreholes executed at the removal site of blocks 1 and 2, indicates that the soil is composed of a small layer of fine and medium sand, of around 0.2 m, with presence of organic matter, passing to unconsolidated white sand with an average thickness of 0.5 m, followed by a transition to the brown sandstone, which presents a thickness ranging from 1.5 to 2 m. The level of the water table, located at a depth of 1.8 m, presents the same coloration of the sandstone and characteristic smell of organic matter. The Nspt values, indicated in Fig. 5, correspond to the number of blows given for the nailing of the last 0.3 m of the standard sampler. The blows are given by a standard hammer with 65 kg with a free fall height of 0.75 m (ABNT, 2001). The region of Fig. 5, defined as sandstone, shows Nspt higher than 40 which characterizes it, according to ABNT (2001), as a very compact sediment. The layer of clayey sand, located just below the sandstone, is classified as a compact to soft sediment. The values of the Nspt only begin to increase from the depth of 14 m where the sediments are from compact to very compact.

The execution of works where there is a need to excavate these sandstones are also problematic. In another place, belonging to the same marine terrace, located 3 km from the location where the 2 blocks were removed, great difficulty was found in the excavation of a drainage channel. The lack of research and local knowledge have led to serious implementation difficulties, resulting in excavation machines breaking down due to excessive efforts.

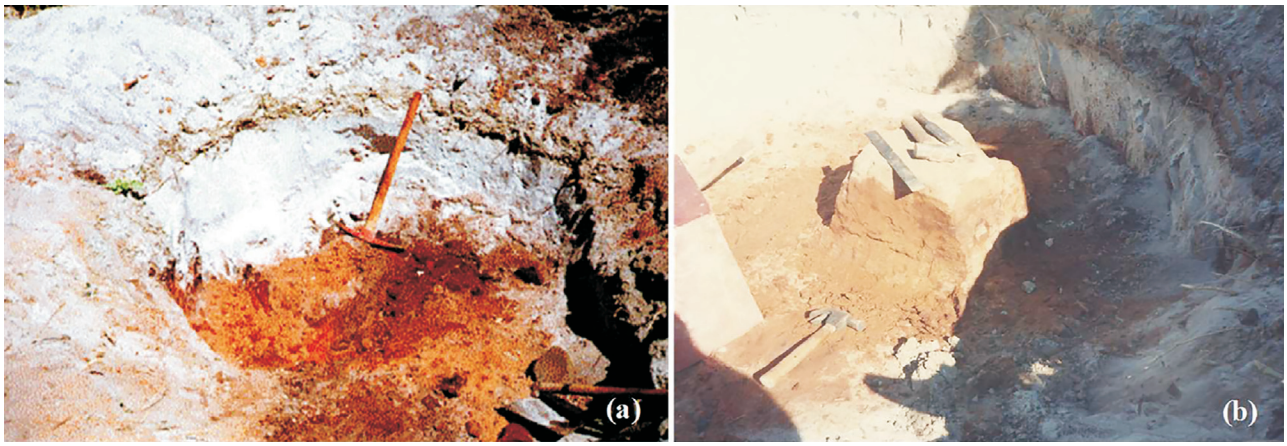

Figure 4 - Place of the executed excavation for removal of weak sandstone blocks.

2.3. Geotechnical characterization

For the determination of the physical indices, 10 specimens of each block were molded with cylindrical shape on a manual lathe. The volume was obtained with a pachymeter using for this the average of 4 determinations of height and diameter. The determination of the natural moisture contents (ABNT, 2016a), porosity and the density of the solid particles (ABNT, 2016b) allowed the definition of the physical properties that are presented in Table 1. The values of these parameters are indicated by their range and the average value placed in parentheses.

The physical properties of blocks 1 and 2 are practically the same, being indicative of their homogeneity. In relation to block 1, it can be observed that the sandstone sample from block 2 shows a darker brown tonality. During work visits to superficial foundations executed on this sandstone, it can be observed that the sandstones present two shades of brown. The workers involved in the excavation project claim that the region of the sandstone that has a darker shade of brown is more difficult to excavate. To verify this aspect tests were carried out to determine the organic material content using the method of burning (ABNT, 1996). In these tests it was verified that the darker sandstones present organic material content of 3.9% and in the sandstones with a lighter tonality this value is 3.5%. This is probably one of the factors that justifies the greater resistance to excavation presented by the darker sandstone. The presence of organic material is associated with humus which is composed of fulvic acids, humina and humic acid, considered as one of the cementing agents of these sandstones (Assis, 1990). In order to obtain the samples for grain size analysis, the sandstones were moistened since in these conditions they are more easily disaggregated. Due to the weak cementation of the sandstones, their disaggregation occurs with translation of the grains, possibly resulting in the breaking of more intemperate grains. However, it is assumed that this breakage occurs in a limited way without altering the results. Dobereiner (1984) found that grain breakage occurs in sandstones with resistance greater than 20 MPa, thus extrapolating the limit of weak rocks. The grain size analyses (ABNT, 2016c), presented in Fig. 6, were determined for the sand layer located above the sandstone, and for the sandstones of blocks 1 and 2. It can be observed that the three particle size analyses represent a poorly selected sediment with great predominance of the sandy fraction. The percentages by weight of each type of sediment, obtained from Fig. 6, are presented in Table 2. There is a great similarity between the grain size analyses

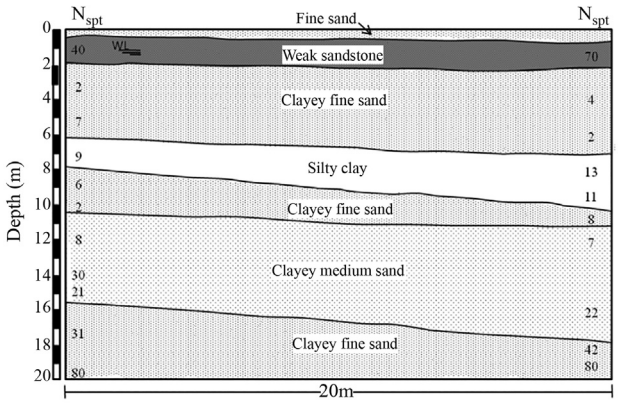

Figure 5 - Geological profile of the place where the soft sandstone blocks were removed.

Table 1 - Results of characterization tests of the sandstone blocks 1 and 2.

Block	Depth (m)	γ_s (kN/m^3)	γ_d (kN/m^3)	$w_{ant.}$ (%)	n (%)
1	0.3-0.6	26.0	15.6-17.4 (16.4)	9.1-11.8 (9.8)	33-40 (37)
2	0.7-1.0	26.0	15.5-17.2 (16.6)	8.5-13.3 (10.4)	34-41.5 (37)

γ_s - density of the solid particles; γ_d - specific dry weight; w_{nat} - natural moisture content; n - porosity.

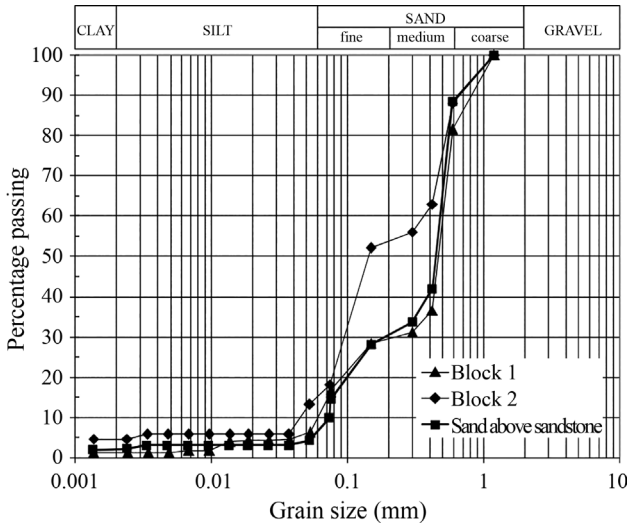

Figure 6 - Grain size distribution of sand and sandstone of blocks 1 and 2.

of the sand and the sandstone of block 1 which are closer to the surface of the terrain. However, it is shown in Table 2 that there is a reduction in the amount of medium sand and increase in the amount of fine sand and silt as the depth increases. In this way it is verified that in block 1 there is predominance of medium sand and in block 2 a predominance of fine sand.

3. Results and Discussion

3.1. Aspects related to composition, texture and cementation

The aspects related to the composition and texture of these sandstones and determination of the probable type of cementation were investigated through scanning electron microscopy images JEOL JSM-6390LV. Figure 7 shows some of the images obtained with enlargements between 50 and 1000 times. These images demonstrate that the grains of medium sand are wrapped in a matrix of fine sand. The grains of medium sand are not in contact with each other which implies a mechanical behavior commanded by fine sand (Figs. 7a and 7b). The presence of bioclasts (shell and algae) were not observed, indicating that these were probably dissolved by the action of humic acid present in solution in the groundwater. The sandy sediments are poorly selected, presenting angular to sub-angular shape and have low sphericity (Fig. 7c).

In the image with enlargement of 1000 times, shown in Fig. 6, the presence of a thin film is observed, which surrounds the grains of medium and fine sand, that probably corresponds to the cementing agent (Fig. 7d).

The analysis of X-rays emitted by the sample bombarded with a fine electron beam allows to quantify the chemical elements present in its constitution. The chemical elements present in the film covering the sand particles and their percentage by weight obtained from two different points of the sample are presented in Table 3. The large amount of carbon shown in Table 3 is an indicator of the presence of products derived from the decomposition of organic matter, such as humic acid. Energy dispersive spectroscopies (EDS) of these two points of analysis are shown in Fig. 8.

The diagenetic processes that formed the sandstones present in the Pleistocene Marine Terrace require more detailed investigations to identify its type of cementation. The cementation of these sandstones has been cited by some researchers as resulting from the precipitation of iron and the presence of humic acid. The action of humic acid as a cementing agent has been studied by several researchers and its ability to form aggregations of soil particles has been recognized (Baver, 1968; Tisdall & Oades, 1982). Research carried out by Andrade & Dominguez (2002), in the soft sandstones of the Caravelas region, located in the state of Bahia, concluded that iron oxide and humic acid are the cementing agents. Manso *et al.* (2003) reached the same conclusion when studying the sandstones of Ipojuca, located in the state of Pernambuco/Brazil. The sandstones investigated by these researchers are present on Pleistocene Marine Terrace.

During the formation of the marine terrace of the city of Recife, resulting from the oscillations of the middle sea level, lagoons were formed that later became brackish marshes, whose plant species contributed to the enrichment of the soil in organic matter (Suguio *et al.*, 1985).

The humic acids resulting from the decomposition of organic matter, are very aggressive and capable of reducing iron oxides making them more soluble and transporting them in solution over long distances by lateral movement of groundwater (Bigarella *et al.*, 2007). The iron oxides back to precipitate by oxidation reactions, where deposition occurs on the water level oscillation region, providing a brown coloration to the soil (Bigarella *et al.*, 2007).

From the previously mentioned aspects it is very probable that the Pleistocene sandstones studied here pres-

Table 2 - Granulometric fractions of sand and sandstone of blocks 1 and 2.

Material	Depth (m)	Clay (%)	Silt (%)	Fine sand (%)	Medium sand (%)	Coarse sand (%)
Sand	0-0.3	2.4	4	30	52	11.6
Block1	0.3-0.6	1.2	8.2	29.4	42.7	18.5
Block2	0.7-1.0	4.3	12.2	53.5	18	12

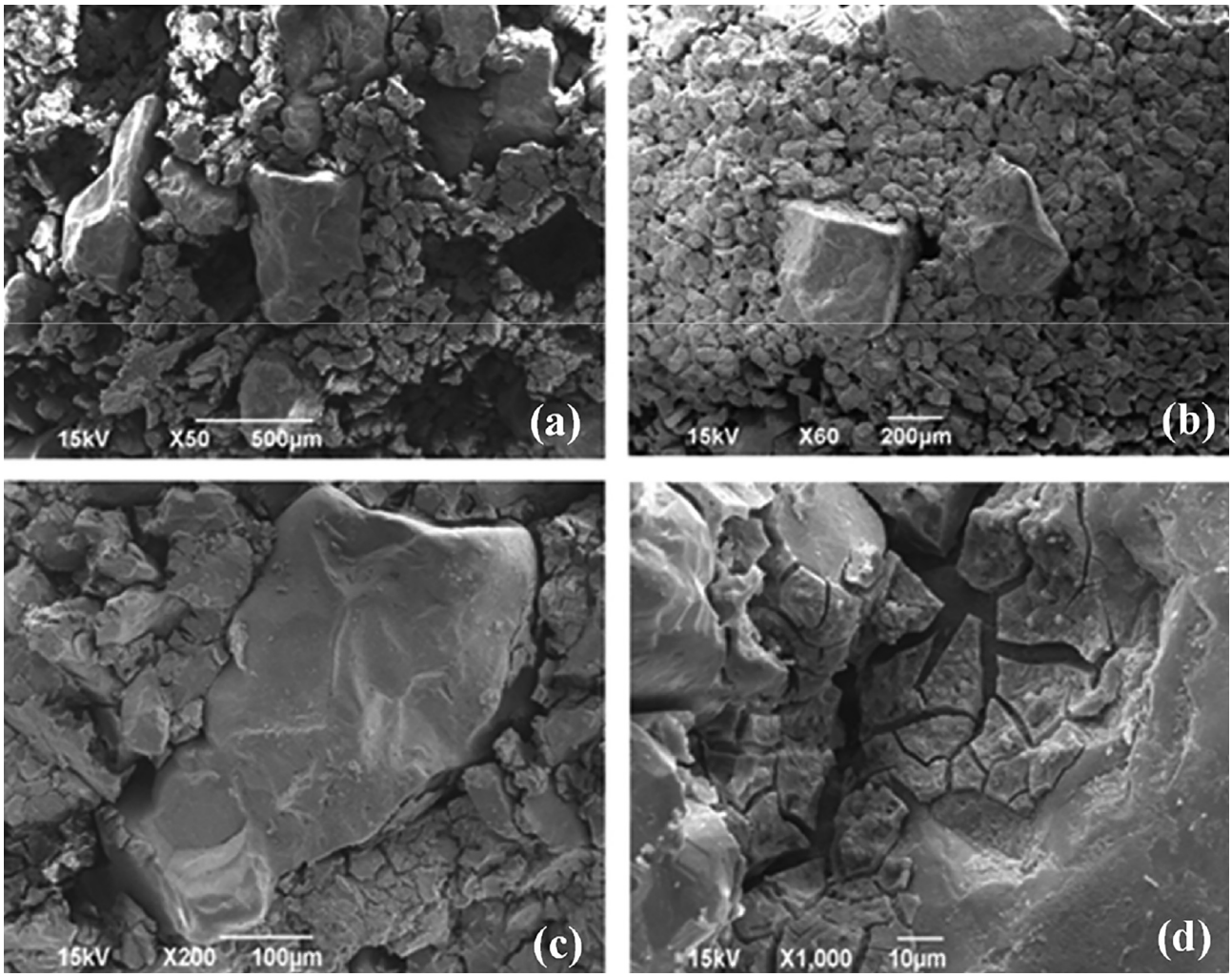

Figure 7 - Scanning electron microscopy images of the sandstone.

ent a cementation by iron oxide and by humic acid. However, the iron oxide plays a predominant role in the mechanical resistance of these sandstones. The iron source is probably associated with the sediments of the Barreira Group, represented by cliffs bordering the marine plain where these sandstones are found. Mabesoone (1967) affirms that the Barreira Group is the main source of iron that cemented the beach sediments of the coastal strip from the city of Recife - located in the state of Pernambuco - to the city of João Pessoa, -located in the state of Paraíba. Following this line of reasoning, these ferruginous solutions originated from the Barreira Group, migrated laterally in solution inside the sandy sediments of the Pleistocene Terrace,

Table 3 - Percentage by weight of the chemical elements present in the cementation of the sandstone.

Point	C-K	N-K	O-K	Al-K	Si-K	Tc-L
1	32.53	30.87	15.51	5.56	8.98	6.55
2	48.25	-	13.06	3.63	35.06	-

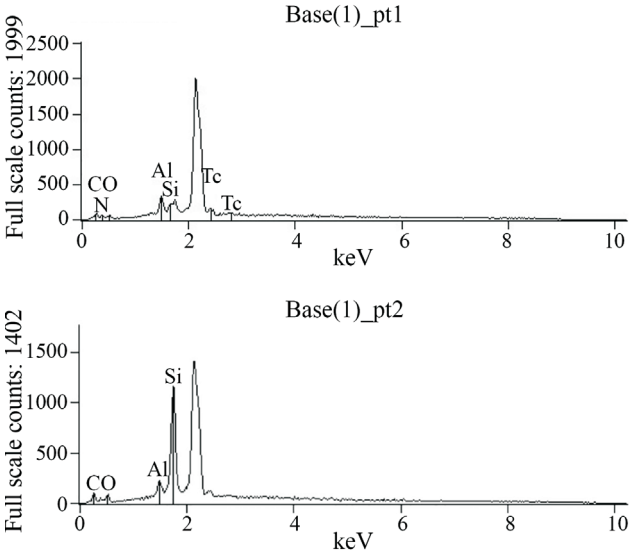

Figure 8 - Energy dispersive spectroscopy (EDS) of the film covering the sand particles.

resulting in the oxidation of the iron in the oscillating region of the water table, forming a horizon of weak sandstone near the ground surface.

3.2. Direct shear and permeability test

A more detailed study conducted for the determination of resistance parameters and verification of a probable anisotropic behavior of these values was carried out in direct shear tests, performed on specimens molded with surface parallel and perpendicular to the ground surface. For these tests a common use equipment of the soil mechanics laboratory was used. The specimen is inserted into a split cell being ruptured in its medium horizontal plane. In order to obtain the shear stress, a dynamometric ring was used installed in its lower half. The vertical displacements were obtained with the use of an extensometer installed on the top of the specimen. All tests were performed in saturated conditions, with the specimens remaining submerged for 48 h prior to their start. The shear stage was performed at a constant velocity of 2.5E-6 m/s.

The results of the variation of the shear strength and the vertical displacement of the direct shear tests, performed in blocks 1 and 2, are shown respectively in Figs. 9- and 10. In these figures it is observed that a reduction occurs in the value of the shear strength right after reaching its maximum value. However, this reduction occurs more abruptly in sandstone samples from block 2 (Fig. 10), thus presenting a more brittle behavior. In all tests the shear strength tends to stabilize at a residual value after reaching its maximum value. The measures of height variation of the specimens during the shear stage indicate that all ruptured with larger volume than the initial one. As the normal stress of the test is increased, these volumetric variations become smaller. In the tests performed in block 1 (Fig. 9) it was observed that there are no reductions in the vertical displacement of the specimens after reaching the maximum shear strength. Vertical displacements tend to stabilize as the horizontal displacement value increases. A different behavior was observed for the test specimens of block 2 (Fig. 10). The vertical displacements increase until the rupture, followed by an abrupt reduction in value followed by an increase according as to which horizontal displacement increases. This again shows a more brittle behavior of the sandstone of block 2. The increase in volume is related to the rolling of one grain of sand on the other along the shear plane. It can be observed during tests the sound of grain breaking.

In Table 4 are the values of the peak and residual shear strength of each of the tests presented in Figs. 9 and 10. These values are plotted in Fig. 11 depending on the normal pressure applied during the test. It can be seen in this figure that the results of the tests performed on each of the blocks, in parallel and perpendicular condition to the surface of the terrain, define the same rupture envelope. This indicates an isotropic behavior regarding the shear strength. In this way, only one rupture envelope was determined for each of the sandstone blocks and one shear envelope for the residual shear strength. These 3 rupture envelopes are plotted in Fig. 11. The strength parameters associated with the envelopes and their correlation coefficients (R^2) are shown in Table 5.

The rupture envelope obtained for the sandstone of block 2 shows cohesion of 393.2 kPa and angle of friction equal to 55.6°. These values are higher than the results found for block 1, whose cohesion is 240 kPa and angle of friction is 47.8°. The residual strength values of all the tests, represented by unfilled symbols, defined a single rupture envelope with an angle of friction equal to 41.7°.

It is seen in Table 5 that the shear strength parameters of the sandstone of block 2 are larger and have a better correlation coefficient (R^2 = 0.96). This is related to the fact that the specimens from block 2 have been molded from a region of the block which has a darker brown coloration. During field work, it was observed that this region offers a higher resistance to excavation and therefore is more resistant. The high values of the friction angle must be related to

Table 4 - Results of the direct shear tests performed on blocks 1 and 2 specimens.

Sample and shear direction	Shear strength (kPa)	Normal Pressure (kPa)					
		100	200	300	400	500	600
Block1 (Parallel)	τ_{peak}	-	478.5	659.5	-	796.5	903.5
	$\tau_{residual}$	-	221.3	247.1	-	424.1	540.1
Block1 (Perpendicular)	τ_{peak}	-	385.5	592.4	-	676.8	951.2
	$\tau_{residual}$	-	87.4	251.8	-	381.6	539.2
Block 2 (Parallel)	τ_{peak}	601.3	712.3	-	1039.3	-	1247.6
	$\tau_{residual}$	109.1	192.2	-	405.8	-	526.3
Block2 (Perpendicular)	τ_{peak}	447.6	681.2	-	954	-	-
	$\tau_{residual}$	109.1	204.6	-	424.6	-	-

τ_{peak}- peak shear strength; $\tau_{residual}$- residual shear strength.

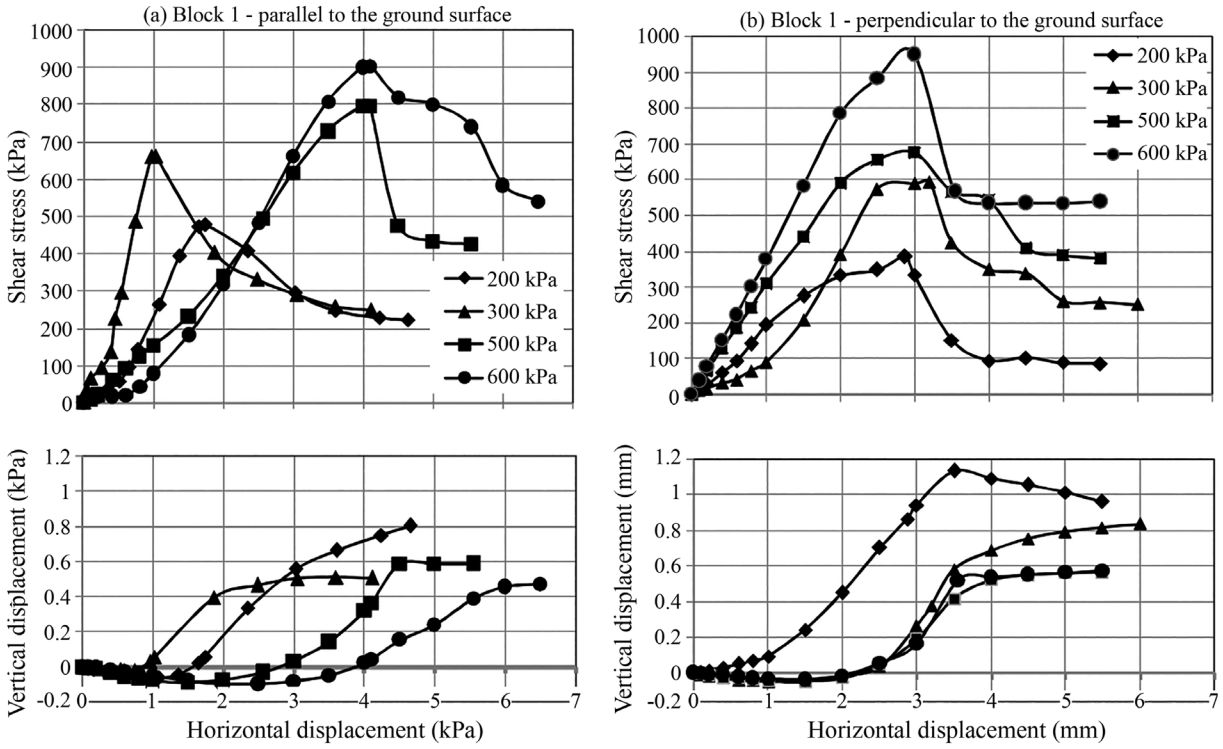

Figure 9 - Results of the direct shear tests performed on molded specimens of block 1 with a direction perpendicular and parallel to the ground surface.

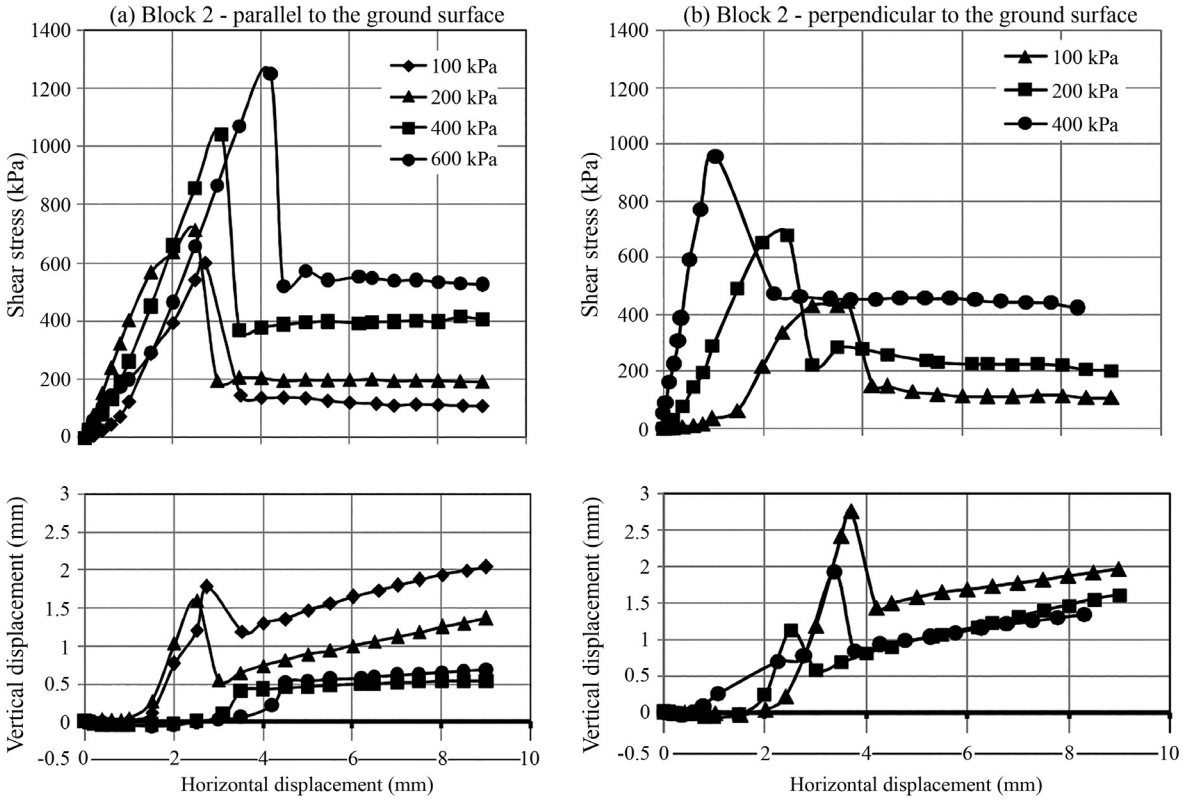

Figure 10 - Results of the direct shear tests performed on molded specimens of block 2 with a direction perpendicular and parallel to the ground surface.

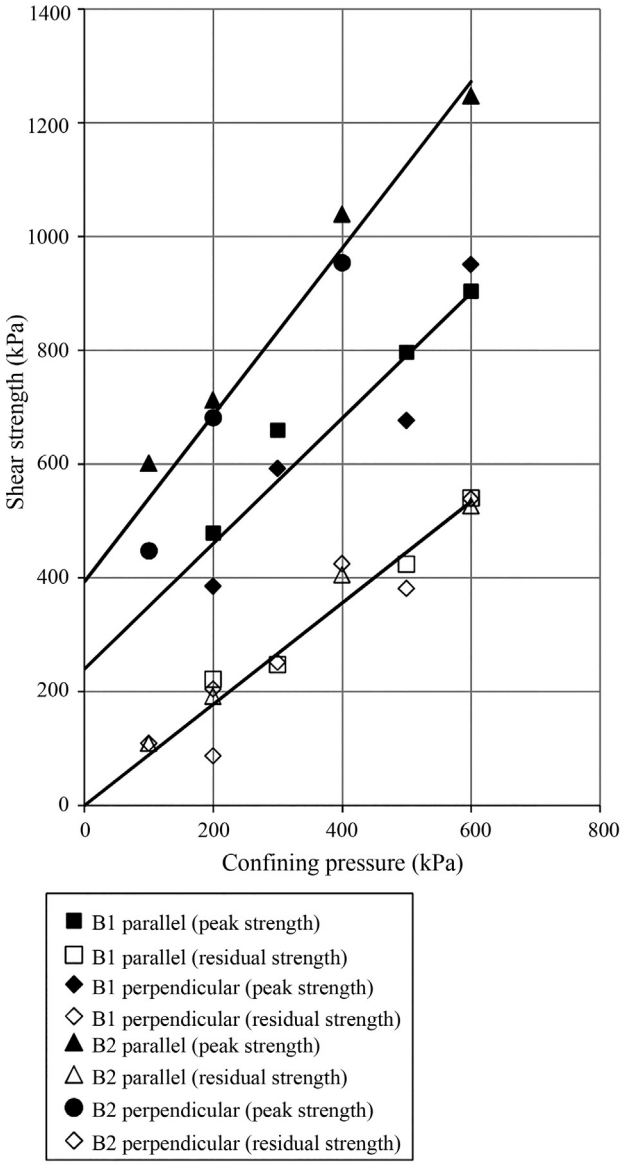

Figure 11 - Results of the direct shear tests performed in the flooded condition.

the interlocking between the sediment particles that compose the sandstone. The sandy sediments are the predominant granulometric fraction in the sandstones of blocks 1 and 2. The angular to sub-angular shape with low sphericity of these sandy particles, identified in the scanning electron microscopy, allow a good interlocking between them. Barton (1993) found, for a sand of the Grantham Formation (United Kingdom), a friction angle of 58.4°, provided by the mesh between the grains. Direct shear tests perpendicular to the stratification planes, performed by Ferraz *et al.* (1981) in the Bauru Group sandstones, belonging to the Caiuá Formation, provided values similar to the values of the sandstones of blocks 1 and 2. The tests performed on specimens with natural moisture, showed a friction angle of 53° and cohesion of 560 kPa. Fernandes (1981), studying the landslide in the Botucatu sandstone (Botucatu Formation), in the Serra da Esperança (PR), verified in direct shear test, a cohesion of 490 kPa and friction angle of 64°. In the case of studies performed by Fernandes (1981), the high value of the friction angle is attributed to the low levels of normal stresses used in the tests, which should decrease to higher levels of stress. This same justification can also be applied to the sandstones of blocks 1 and 2 as a second factor related to the high friction angle found. The maximum normal stress applied in the direct shear tests performed in the sandstones of blocks 1 and 2 was 600 kPa, which is a low value, however, representative of the tensions transmitted by building foundations. The values of the friction angle should decrease with the increase of the normal stress due to non-linearity of the rupture envelopes.

Table 5 - Strength parameters obtained from the direct shear tests.

Block	c' (kPa)	φ'	R^2
1 (peak)	240.0	47.8°	0.89
2 (peak)	393.2	55.6°	0.96
1 and 2 (residual)	0	41.7°	0.93

To verify the hydraulic conductivity of these sandstones, permeability tests were performed using the TRIFLEX 2 equipment manufactured by Soil Moisture. Using two specimens of block 1, molded with a diameter and height of 10 cm, tests were performed in the direction parallel and perpendicular to the ground surface. For these tests the specimens were saturated by backpressure. Inside the test cell the specimen was wrapped in a rubber membrane and subjected to a confining pressure of 230 kPa. For saturation was applied at its top a pressure of 220 kPa and at its base a pressure of 200 kPa, remaining under this hydraulic gradient for a period of 48 h. Due to the limited number of samples, this test could not be performed on the sandstone of block 2.

In the parallel and perpendicular direction, the permeability values were respectively 4.8E-6 and 5.6E-6 m/s. These values are within the range of variation obtained by Dobereiner and Freitas (1996) when testing soft sandstones of Portugal, England, Brazil and Turkey. In their experiments they obtained values of permeability ranging from 1.8E-5 m/s to 8.9E-6 m/s. The results of direct shear tests and permeability tests indicate that Pleistocene sandstones exhibit isotropic behavior in relation to their mechanical and hydraulic properties.

3.3. Unconfined compressive strength test

The equipment used in soil mechanics is inadequate for the molding of specimens of this sandstone. The weak sandstone was first sawed in a prismatic shape with a square base. The refining, leaving the specimens of 4 cm in diameter and 8 cm in height, was given by a scraping process using a molding lathe. The specimens from block 1

were allowed to air dry. In this condition, the values of the degree of saturation varied between 20.4 and 27.2%. In order to verify the influence of the moisture content on the resistance values, the molded specimens of block 2 were submerged for a period of 3 days. In this procedure the samples were initially submerged in water up to 1/3 of their height, remaining there for a period of two hours. After this initial stage the water level was raised to 2/3 of its heights, remaining in this condition for the same time interval. In the final stage they remained submerged until completing a period of 3 days. The purpose of this procedure is to saturate the sample by capillarity. After the period of 3 days, the values of the degree of saturation varied between 60.7% and 68.3%. These values were lower than expected. This fact is probably associated with the presence of hydrophobic organic compounds (Mataix-Solera *et al.*, 2007; Wallach *et al.*, 2005; Dekker *et al.*, 1998). The presence of organic material in the sandstones of blocks 1 and 2 was verified in the analysis of scanning electron microscopy and method of burning.

The unconfined compressive strength tests were performed with a strain rate of 0.1 mm/min, adopting the recommendations established in standard D 2938-71 (ASTM). For these tests a press was used in the laboratory of soil mechanics. To obtain the values of the normal stress applied at the top of the specimen during the test a dynamometric ring was used. To avoid loss of moisture, the specimens were sealed in plastic film. Due to the difficulties to glue strain gauges to the surface of the weak rocks (Almisned *et al.*, 2011; Chen & Hu, 2003), the axial strains were obtained by using an extensometer placed on top of the compression cell. The values of the physical indices of the specimens and the results of the unconfined shear tests are presented in Tables 6 and 7. The variations of the stress as a function of the axial deformations are presented in Fig. 12.

Comparing Tables 6 and 7, it can be seen that the mean values of the unconfined shear strength of the specimens of blocks 1 and 2 are similar. However, the mean value of the modulus of deformability of the test specimens of block 1 is 33% greater than the value found for the tests of block 2. The values of the unconfined compressive strength tests and the modulus of deformability are shown in Figs. 13 and 14 as a function of the water moisture content. In Fig. 13 it is observed that the values of the unconfined compressive strength tests of block 1 have a greater dispersion when compared to the values of block 2. This same conclusion is also valid for the values of the tangent deformability modules presented in Fig. 14. However, it is observed that the results of block 2, presented in Figs. 13 and 14, vary within the range of the results of the tests performed in the sandstone of block 1. The greater dispersion of the results of block 1 is probably related to the fact that it is located in a transition region between the sandy sediments and the sandstone (Fig. 5).

In the results of direct shear tests, presented in Table 5, it was also observed a greater dispersion in the results

Table 6 - Results of the unconfined compressive strength tests of Block 1.

Specimens	γ_d (kN/m^3)	w (%)	S (%)	n (%)	σ_c (MPa)	E_{tg} (MPa)
1B1	17.10	4.08	20.40	34.20	2.06	157.00
2B1	16.70	3.76	17.60	35.90	2.69	265.80
3B1	17.40	4.21	22.30	32.90	1.93	263.40
4B1	16.50	5.31	24.20	36.30	2.58	190.60
5B1	16.80	5.76	27.20	35.50	1.44	74.30
Average value	16.90	4.62	22.34	34.96	2.10	190.22

γ_d - specific dry weight; w_{nat} - water moisture content; S - degree of saturation; n - porosity; σ_c - Unconfined compressive strength; E_{tg} - tangent deformability modulus.

Table 7 - Results of the unconfined compressive strength tests of Block 2.

Specimens	γ_d (kN/m^3)	w (%)	S (%)	n (%)	σ_c (MPa)	E_{tg} (MPa)
1B2	16.90	14.05	68.30	34.60	2.04	116.80
2B2	17.20	12.86	65.40	33.80	2.36	136.60
3B2	16.60	14.20	65.40	35.90	1.66	136.70
4B2	16.60	13.25	60.70	36.30	1.48	115.20
Average value	16.83	13.59	64.95	35.15	1.90	126.33

γ_d - specific dry weight; w_{nat} - water moisture content; S - degree of saturation; n - porosity; σ_c - Unconfined compressive strength; E_{tg} - tangent deformability modulus.

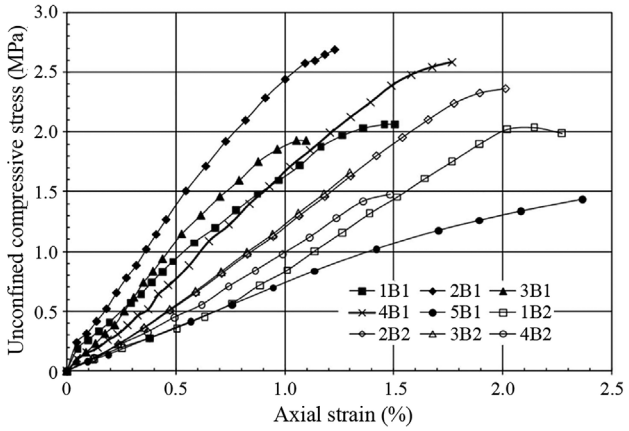

Figure 12 - Stress-strain curve of the unconfined compressive strength tests performed on the weak sandstone of blocks 1 and 2.

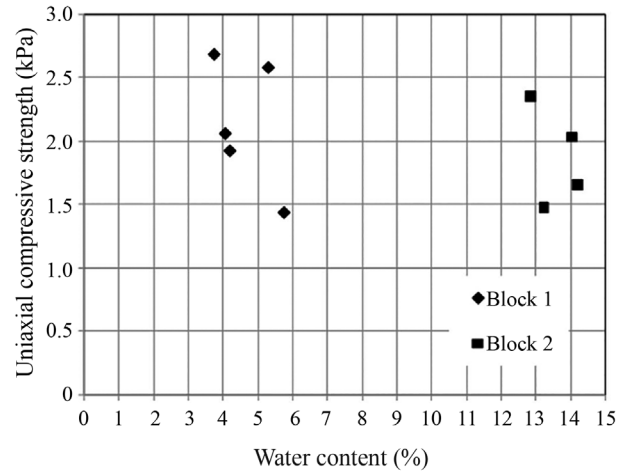

Figure 13 - Relation between the unconfined compressive strength tests and water moisture content.

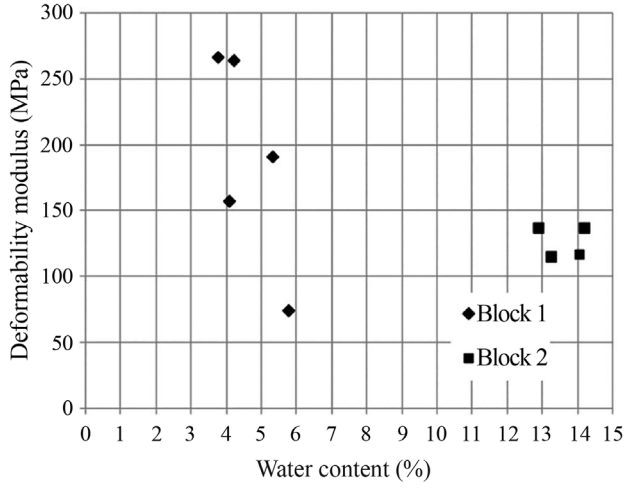

Figure 14 - Relation between the tangent deformability modulus and water moisture content of the unconfined compressive strength tests.

obtained from block 1. However, in the unconfined compressive strength tests a new variable was introduced. The specimens from block 1 were tested with a lower moisture content than the specimens from block 2. This difference in moisture content had a considerable influence on the results of simple compression tests. Comparing the results of Tables 6 and 7, it can be observed that a reduction in the moisture content causes an increase in the value of the unconfined compressive strength and deformability modulus. Dobereiner & Dyke (1986) also obtained the same type of result when testing three types of sandstone with different moisture contents.

Armaghani *et al.* (2016) and Kim *et al.* (2017) present several correlations between simple compression strength and some sandstone properties, including the Schmidt hammer rebound number, point load test and wave velocity.

The mechanical and hydraulic properties of the weak rocks determined in laboratory tests are important because they represent values of the rock mass (Oliveira, 1993). Due to the plasticity of the weak rocks, which do not allow relevant fractures, it is almost always possible to consider the deformability of the rock mass as approximately equal to that obtained in laboratory tests (Rocha, 1975). Therefore, for the purpose of classification, the average values of unconfined shear test results presented in Tables 6 and 7 will be considered as representative parameter of the sandstone rock mass.

The values of the unconfined compressive strength, presented in the Tables 6 e 7, varied between 1.5 and 2.7 MPa, with an average value of 2 MPa, and the values of the modulus of deformability varied between 115 and 266 MPa, with an average value of 162 MPa. These ranges of unconfined compressive strength values and deformability modulus are compatible with porous rocks, such as sandstones that have heterogeneous mechanical behavior evidenced by dispersion in the values of their mechanical properties (Gama, 1994).

In Fig. 15, some proposals for the classification of rocks that use the value of unconfined shear strength are presented. Using the average value of 2 MPa as representative of the sandstones studied here, it is observed that this rock is classified as a weak rock according to the proposal of the Geological Society of London (1970) and as very weak by the ISRM (1978) and Dobereiner (1984).

Figure 16 shows the relationship between the modulus of deformability and the resistance to simple compression, obtained by Dobereiner (1984), when investigating 11 different types of weak sandstones. Point 12 indicated in this figure corresponds to the results obtained for the soft sandstones of this research, represented by the uniaxial compressive strength of 2 MPa and tangential deformability modulus of 162 MPa. It can be seen in Fig. 16 that point 12 shows a good correlation with the results obtained by Dobereiner (1984).

4. Use of Sandstone as a Foundation Material

In the region located 300 m from the site of removal of the two blocks of sandstones, a concrete building with 16 floors was built. The Fig. 17 photo illustrates the excavation for execution of the shallow foundation. It can be observed in this figure that the soil profile is formed by sandy sediments followed by abrupt transition to weak sandstone. The structural system of this building has reduced rigidity due to the distances between the pillars.

The terrain is inserted in the Pleistocene marine terrace, being its geological profile presented in Fig. 18a. The shallow foundations were designed to be built directly on the sandstone (depth of 3.8 m), and the value of 100 MPa was adopted for its tangential deformability modulus. The pillars were instrumented and the displacement monitored from the beginning of the construction, for 16 months. The maximum settlement was of the order of 30 mm. The representative curves of the same settlement value (Fig. 18b) indicate that the building presented a small slope of 1/2250 to the east. The parallelism of these curves indicates that the weak sandstone worked as a rigid plate reducing the differential settlement. The performance of the shallow founda-

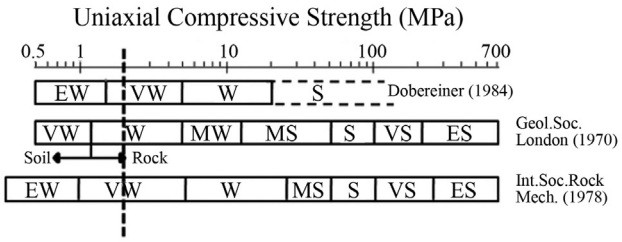

Figure 15 - Proposals for classification of rocks as a function of unconfined shear strength modified from Dobereiner & Freitas (1986) (EW, extremely weak; VW, very weak; W, weak; MW, moderately weak; MS, moderately strong; S, strong; VS, very strong; ES, extremely strong).

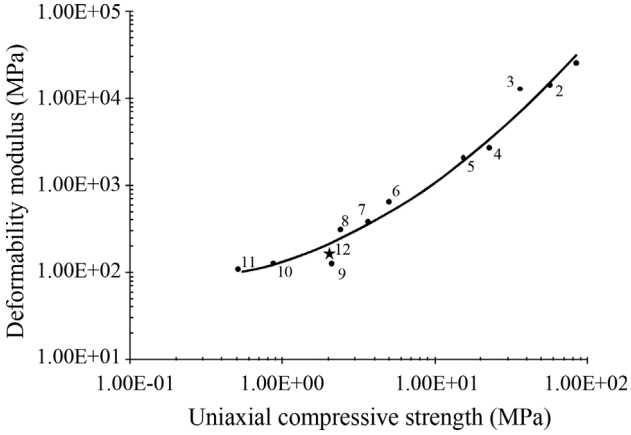

Figure 16 - Correlation between the tangential deformability modulus and the unconfined shear strength obtained by Dobereiner, 1984.

Figure 17 - Excavation for the execution of a superficial foundation on the sandstone.

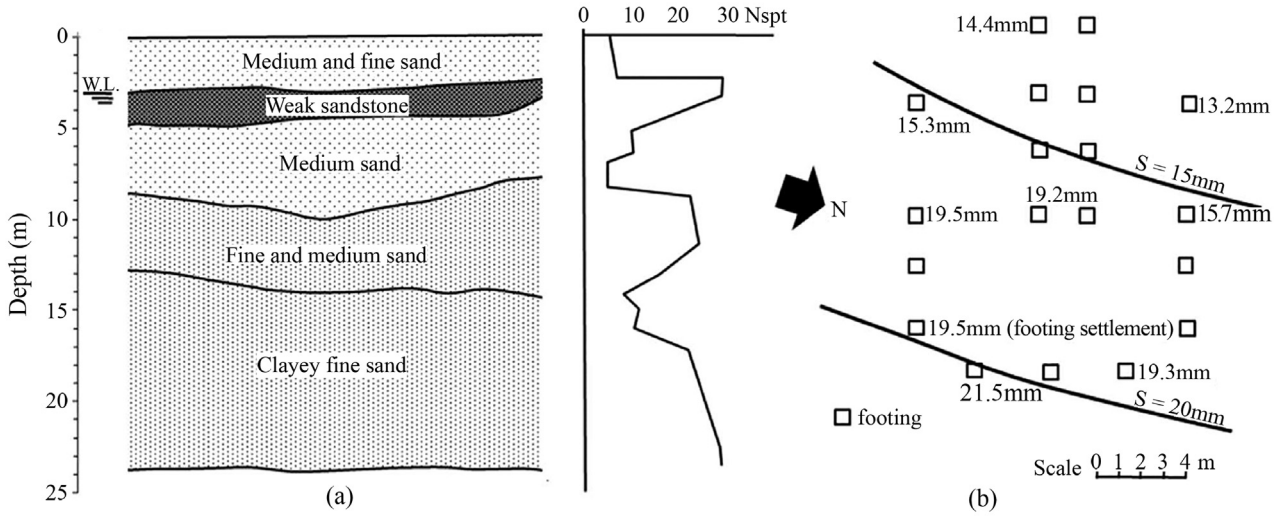

Figure 18 - (a) Geotechnical profile of the ground where a superficial foundation was executed on the sandstone. (b) Curves of the same displacement (Gusmão Filho, 1998).

tions built directly on these sandstones has been excellent, allowing for more economical solutions (Gusmão Filho, 1998).

5. Conclusions

The sandy sediments of the Pleistocene Marine Terrace, located in the Metropolitan Region of the City of Recife/Brazil, were submitted to diagenetic processes that resulted in the formation of a layer of sandstone, cemented by humic acid. Analyzing the boring database, used in the elaboration of the Geotechnical Chart of the City of Recife, it was found that these sandstones are located near the ground surface forming a horizontal slab with thicknesses ranging from 0.5 to 4.5 m, being present at a depth of 0.3 to 4.5 m. Based on the classifications proposed by ISRM (1978) and by Dobereiner (1984), these sandstones are classified as very weak rock with mean values of unconfined compressive strength and modulus of deformability, respectively, equal to 2 MPa and 162 MPa. The results of the hydraulic conductivity and direct shear tests conducted in the direction parallel and perpendicular to the ground surface indicate that these sandstones present as isotropic material. This rock formation is present in a large part of the coastal region of Brazil and its good performance, observed in a case study, indicates that this material may be suitable as support to shallow foundations of buildings.

References

ABNT (1996). Brazilian Association of Technical Standards. NBR 13600: Determination of Organic Material Content by Igniting at 400 °C - Method of Test. Rio de Janeiro, 2 p. (in portuguese)

ABNT (2001). Brazilian Association of Technical Standards. NBR 6484: Soil - Standard Penetration Test - SPT - Soil Sampling and Classification: Test Method. Rio de Janeiro, 17 p. (in portuguese)

ABNT (2016a). Brazilian Association of Technical Standards. NBR 6457: Soil Samples - Preparation for Compactation and Characterization Tests. Rio de Janeiro, 9 p. (in portuguese)

ABNT (2016b). Brazilian Association of Technical Standards. NBR 6458: Gravel Grains Retained on the 4.8 mm Mesh Sieve: Determination of the Specific Gravity, of the Apparent Specific Gravity and of Water Absorption. Rio de Janeiro, 6 p. (in portuguese)

ABNT (2016c). Brazilian Association of Technical Standards. NBR 7181: Grain Size Analyses. Rio de Janeiro, 13 p. (in portuguese)

Almisned, O.A., Somerville, J. & Smart, B.G.D. (2011). Difficulties in Laboratory Characterization of Weak Sandstone. Proc. 45th US Rock Mechanics/Geomechanics Symposium, San Francisco, United States, pp. 1-4.

Andrade, A.C.S. & Dominguez, J.M.L. (2002). Geological-geomorphological information as subsidies to the environmental analysis: the example of the marine terrace of Caravelas-Bahia. Bulletin Paranaense de Geosciences, 51:9-17.

Armaghani, D.J., Amim M. F.M., Yagiz, S., Faradonbeh, R.S. & Abdullah, R.A. (2016). Prediction of the uniaxial compressive strength of sandstone using various modeling techniques. International Journal of Rock Mechanics & Mining Sciences, 85(5):174-186.

Assis, H.M.B. (1990). Beach Rocks Studies of the South Coast of Pernambuco Based on Petrographic and Isotopic Evidence, MSc. Dissertation, Federal University of Pernambuco, Recife (PE), 91 p. (in portuguese)

ASTM (1971). Standard Test Method for Unconfined Compressive Strength of Intact Rock Core Specimens - D2938. ASTM International, West Conshohocken, Pennsylvania, USA, 4 p.

Barton, M.E. (1993). Cohesive sands: The natural transition from sands to sandstones. Proc. Geotechnical Engineering of Hard Soils-Soft Rocks. Anagnostopoulose *et al.* (eds), Balkama, Rotterdam, pp. 367-374.

Baver, L.D. (1968). The effect of organic matter on soil structure. In: Study Week on Organic Matter and Soil Fertility. John Wiley & Sons, New York. pp. 383-413.

Bigarella, J.J.; Becker, R.D. & Passos, E. (2007). Structure and Origin of Tropical and Sutropical Landscapes. Vol. 2. 2nd Edition. Publisher of UFSC. 875 p. (in portuguese)

Chen, H. & Hu, Z. (2003). Some factors affecting the uniaxial strength of weak sandstones. Bull. Eng. Geol. Env., 62(4):323-332.

Dekker, L.W.; Ritsema, C.J.; Oostindie, K.; Ziogas, A.K. & Boersma, O.H. (1998). Effect of drying temperature on the severity of soil water repellency. Soil Science, 163(10):780-796.

Dobereiner, L. & Dyke, C. (1986). Characteristics of the deformability of sandstones in function of the variation of the moisture content. Proc. 2th South American Symposium on Rock Mechanics, Porto Alegre / RS, pp. 57-65. (in portuguese)

Dobereiner, L. (1984). Engineering Geology of Weak Sandstones. PhD Dissertation, Department of Geology, Imperial College, 471 p.

Dobereiner, L. & Freitas, M.H. (1986). Geotechnical properties of weak sandstones. Geotechnique, 36(1):79-94.

Ferraz, J.L.; Minicucci, L.A. & Armelin, J. A. (1981). Preliminary geotechnical characterization of caiuá sandstone occurring at Pontal do Paranapanema. Proc. 3th Brazilian Congress on Engineering Geology, Itapema/SP, v.3, pp 55-88. (in portuguese)

Fernandes, C.E.M. (1981). Geological-geotechnical studies for the stabilization of cutting slopes in BR-277 - Serra da Esperança (PR). Proc. 3th Brazilian Congress on Engineering Geology, Itapema/SP, v.3, pp 33-54. (in portuguese)

Gama, E.M. (1994). High technology in mechanical testing laboratory with rocks. Journal Soils and Rocks, 17(2):131-143.

Geological Society of London (1970). The logging of rock cores for engineering purposes. Quarterly Journal of Engineering Geology and Hydrogeology, 3(1):1-24.

Gusmão Filho, J.A. (1998). Foundations: from Geological Knowledge to Engineering Practice. Recife: University Publishing House- Federal University of Pernambuco/UFPE, 345p. (in portuguese)

ISRM (1978). Suggested methods for the quantitative descriptions of discontinuities in rock masses. Int. J. Rock. Min. Sci., 15(6):319-368.

Kanji, M.A. (2014). Critical issues in soft rocks. Journal of Rock Mechanics and Geotechnical Engineering, 6(3):186-195.

Kim, E.; Stine, M.A.; Oliveira, D.B.M. & Changani, H. (2017). Correlations between the physical and mechanical properties of sandstones with changes of water content and loading rates. International Journal of Rock Mechanics & Mining Sciences, 100:255-262.

Mabessone, J.M. (1967). Sedimentology of the coastline between Recife-João Pessoa, Bulletin of the Brazilian Society of Geology, 16(1):57-72.

Manso, V.A.V.; Motta, J.A.; Guerra, N. C. & Soares Júnior, C.F.A. (2003). Final Report - Definition of the contour points of the maximum tidal line of the coast of the municipality of Ipojuca / PE. Reference term MMA / PNMA II - SECTMA No 249. (in portuguese)

Mataix-Solera, J.; Arcenegui, V.; Guerrero, C.; Mayoral, A.M..; Morales, J.; González, J.; García-Orenes, F. & Gómez; I. (2007). Water repellency under different plant species in a calcareous forest soil in a semi arid Mediterranean environment. Hydrological Processes, Bristol, 21(17):2300-2309.

Oliveira, R. (1993). Weak rock materials. Proc. 26th Annual Conference of the Engineering Group of the Geological Society. United Kingdom. A.A. Balkema, pp. 5-15.

Rocha M. (1975). Some problems related to the rock mechanics of low strength natural materials. Proc. 5th Pan-American Conference on Soil Mechanics and Foundation Engineering, Buenos Aires; pp. 489-514. (in portuguese)

Suguio, K.; Martin, L.; Bittencourt, A.C.S.P.; Dominguez, J.M.L.; Flexor, J.M. & Azevedo, A.E.G. (1985). Relative sea level Fluctuations During the quaternary period along the brazilian coast and its implications on coastal sedimentation. Brazilian Journal of Geosciences, 15(4):273-286.

Tisdall, J.M. & Oades, J.M. (1982). Organic matter and water-stable aggregates in soil. J. Soil Sci., 33:141-163.

Wallach, R.; Ben-Arie O. & Graber E.R. (2005). Soil water repellency induced by long-term irrigation with treated sewage effluent. J. Environ. Qual., 34(5):1910-1920.

List of Symbols

c': cohesion intercept
E_{tg}: tangent deformability modulus
φ' : friction angle
$\varphi'_{resid.}$: residual friction angle
γ_d : specific dry weight
γ_s: density of solid particles
n: porosity
QH: quaternary Holocene Unit
QP: quaternary Pleistocene Unit
QU: quaternary Undifferentiated Unit
S: degree of saturation
σ_c: unconfined compressive shear strength
τ_{peak}: peak shear strength
$\tau_{residual}$: residual shear strength
w: water moisture content
$w_{nat.}$: natural water moisture content

Maximum Envelope of Lateral Resistance through Dynamic Increasing Energy Test in Piles

R.M. Valverde, F. Massad

Abstract. The traditional dynamic load test, based on the one-dimensional wave propagation theory consists in applying a sequence of constant energy blows and making measurements using deformation and acceleration sensors installed on top of the pile, as a function of time. The traditional method has evolved with the development of a numerical model that simulates the Static Load Test (SLT) of a pile dynamically tested. Another evolution was the introduction of the Dynamic Increasing Energy Test (DIET) created and proposed by Aoki (1997). The present study is an initiative to deepen the increasing energy method focusing on the definition of the maximum lateral resistance envelope, allowing the recovery of the mobilized resistance along the shaft, lost in blows prior to the maximum applied energy, especially in layers close to the top of the pile. This procedure is called the Maximum Envelope of Lateral Resistance. Two case studies are presented, in which static and dynamic tests were performed on the same pile. The application of the Maximum Envelope of Lateral Resistance, also referred to as Maximum Envelope Method, led to a definition of higher load capacities through the CAPWAP analysis, with simulated load-displacement curves with good correlations in comparison with the Static Load Tests (SLT). When performed after several rest periods, the Maximum Envelope Method allows an assessment of the "set up" development over time.

Keywords: dynamic load test, increasing energy, lateral resistance, load capacity, maximum envelope.

1. Introduction

The PDA ("Pile Driving Analyzer") signal of the hammer blow associated to the highest pile capacity during the dynamic load test is the one chosen to be analyzed by CAPWAP (Case Pile Wave Analysis Program). This program provides a simulation of the Static Load Test (SLT) and allows determining the mobilized shear and toe resistances as if the pile had received only that single blow since the end of its installation, without considering changes in soil properties caused by earlier blows of lower energies. However, at each applied blow, the shear and toe resistances change due to effects on the soil, particularly on those with high sensitivity. Therefore, to consider only the last blow as the one in which the maximum capacity occurs is a practice that generates simplified interpretations regarding the pile load capacity and the lateral friction along the pile shaft. The Maximum Envelope Method has the objective of evaluating the whole Dynamic Increasing Energy Test (DIET), considering the effects of the blows applied prior to the one with the maximum mobilization of static resistance. This allows recovering as much information as possible about the load capacity in a Dynamic Increasing Energy Test (DIET), including: a) a top load-settlement curve simulated through the mathematical model of Coyle and Reese (1966); and b) an assessment of the "set up" development over time in sensitive soils.

2. Dynamic Load Test and CAPWAP

The dynamic load test consists in applying a sequence of blows on the pile and measuring values of specific deformation and acceleration over time through force transducers and high sensitivity accelerometers. These instruments are installed at a minimum distance from the top established by standard. After applying the blows, the recorded data are sent to the PDA, which calculates the force and velocity curves of the recorded blows. The data acquired in the field can later be analyzed by CAPWAP, a computer program whose results include a simulated static analysis of the load-set curve and the distribution of resistances along the pile shaft and toe. The wave equation is solved using one variable as input (velocity or force) and computing the other variable. The results are based on the quality of the match between the curves of the calculated and the measured variables, called "*Match Quality*". CAPWAP allows calculating tensions and movements by dividing the pile into segments of known properties (elastic modulus and mass density). The propagations of the descending and ascending waves ("*Wave down*" and "*Wave Up*") are recorded and their superposition is done according to the wave equation, in which the ascending and descending forces are summed and the velocities are equal to their differences divided by the impedance of the pile in each segment. The displacement and velocity of each pile segment

Rafael Marin Valverde, M.Sc., PDI Engenharia e Departamento de Engenharia Civil, Escola Politécnica da Universidade de São Paulo, São Paulo, SP, Brazil. e-mail: rafael.valverde@gmail.com
Faiçal Massad, Ph.D., Full Professor, Departamento de Engenharia Civil, Escola Politécnica da Universidade de São Paulo, São Paulo, SP, Brazil. e-mail: faical.massad@usp.br.
Submitted on September 26, 2017; Final Acceptance on March 21, 2018; Discussion open until August 31, 2018.
DOI: 10.28927/SR.411075

are the basis for determining the soil resistance. The soil model, introduced by Smith (1960), consists in an elasto-plastic spring and a linear dashpot. The total static load capacity is the sum of the static resistances of the shaft and pile toe segments.

Figure 1 illustrates the association between the basic static resistance and the pile shaft displacement. In the loading phase, as a pile segment moves downward, the static resistance increases linearly over a quake distance q_s up to the maximum shaft resistance value R_u, and then it remains constant until the maximum displacement u_{px} on this element is reached. Next is the unloading phase, with a slope defined by the "unloading quake" q_u up to a negative ultimate resistance level R_{nu}, which is the minimum limit defined by the product of R_u and an unloading multiplier U_n (Rausche *et al.*, 2010).

For the static pile toe resistance, there is a similar association except for the unloading phase, in which the toe resistance is zero (U_n value is 0). As the pile toe moves downward, the resistance may eventually remain zero due to some existing gap ("Resistance toe gap"), represented by t_g and then increases linearly over a quake distance q_t ("loading toe quake") until it reaches the maximum toe resistance R_{ut}, and remains constant up to a maximum displacement u_t (Fig 2). For total toe resistance activation, the pile toe displacement must be greater than the sum of the quake q_t and the toe gap t_g.

This model even allows considering a soil mass embedding on the shaft or pile toe. In order to be able to match certain signals, it was necessary to include an extension of the soil model called "Radiation Damping", necessary in cases when displacements are small and the soil practically moves with the pile. An example is a pile partially embedded on hard rock. As the pile exerts compression forces

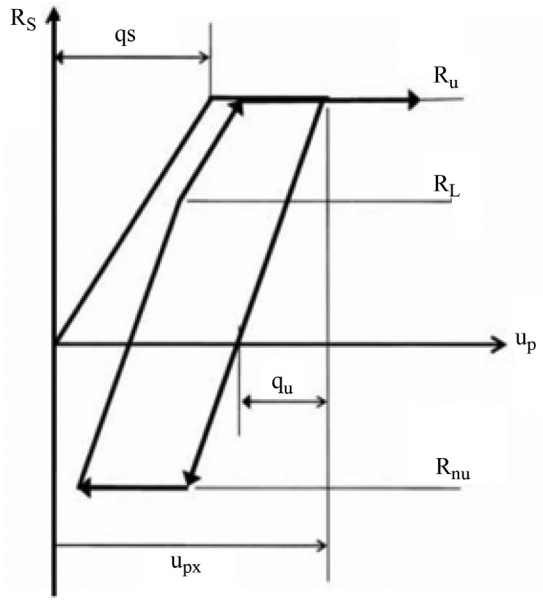

Figure 1 - Static shaft resistance-displacement - CAPWAP soil model (Pile Dynamics 2006).

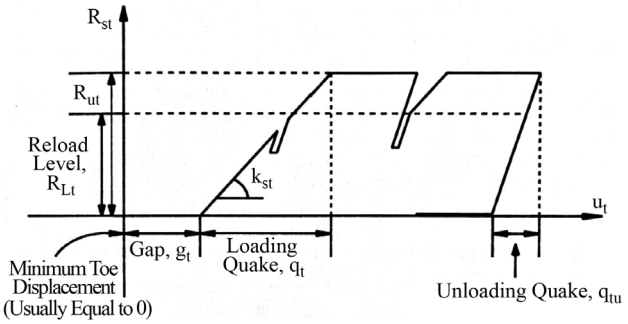

Figure 2 - Toe static resistance-displacement - CAPWAP soil model (Pile Dynamics 2006).

against the rock, a wave is generated in the rock and the soil resistance appears to be a function of the velocity rather than the displacement (Pile Dynamics, 2006).

The balance of forces and displacements at the top is computed by ignoring the viscous effects of the soil (Rausche *et al.*, 1994). The results of the CAPWAP signal matching process are primarily ultimate resistance values and quakes (and therefore soil stiffness). Together with the pile stiffness, CAPWAP produces a simulated static load-set curve. Such procedure yields important limitations that should be considered:

(i) the simulated static load-set curve represents a load test that was performed during a fraction of a second; for that reason, the result cannot include displacements caused by consolidation of soil layers below or around the pile;

(ii) the calculated static load-set curve refers to the time of the dynamic testing and may differ from the Static Load Test (SLT) curve with longer waiting time; and

(iii) for concrete piles, the elastic modulus used in the calculation of the static load-settlement curve is the same as that determined by the PDA. Static elastic moduli are generally lower than the dynamic moduli and the static analysis options allow for an input of pile modulus reduction factor, as stated in the CAPWAP manual (Pile Dynamics, 2006).

3. Maximum Envelope Method

The main objective of the Maximum Envelope Method is to analyze all the blows applied during the Dynamic Increasing Energy Test (DIET). Rausche *et al.* (1994) state that the distribution of ultimate shaft resistance forces of all segments can be directly determined from the record portion between the time of impact and the time of the first wave return. This procedure is applied to all blows of the DIET allowing to calculate the maximum envelope of the shaft resistance distribution and, additionally, the maximum toe resistance. These results, together with soil profile, make it possible to estimate elasto-plastic load transfer functions for each soil layer, also known as q-z and t-z functions, as shown in Figs. 1 and 2. In this paper only the loading phase will be considered.

The authors applied the Coyle-Reese method to simulate the static load-set curve using these elasto-plastic load transfer functions, in order to validate the results obtained through the Maximum Envelope Method. The validation is accomplished comparing the resulting curve with the Static Load Test (SLT) curve. In the Coyle-Reese method the pile is divided into segments with their respective load transfer functions. Its application initiates from the last element of the pile assuming that the pile toe has moved a small displacement y_t downward. Through the pile toe load transfer function, the toe resistance Q_p is determined. Then, forces and displacements of upper segments are calculated iteratively up to the top using the lateral load transfer functions and considering the elastic shortening of the pile together with the balance of acting forces, in order to obtain one point of the load-settlement curve. This process is iteratively repeated, assuming different pile toe displacements y_t, to obtain several points of the load-set curve until the maximum lateral friction (determined by the Maximum Envelope Method) of all soil segments is reached.

The number of segments in the Coyle-Reese method should be the same or greater than the number of soil layers determined by local geotechnical tests, like the Standard Penetration Test (SPT). Each blow applied during the Dynamic Increasing Energy Test (DIET) indicates different values of lateral resistance and, therefore, different skin friction f_s and quake q_s values. According to Fig. 3, the maximum skin friction value f_{max} of each soil layer is the average of the greatest f_s values calculated through the CAPWAP, considering all applied blows during the DIET, in accordance with the Maximum Envelope Method, described above.

4. First Case: Port Terminal - Santos, SP - Brazil

4.1. Pile and subsoil profiles

The first case studied refers to a pile (EC1304) of a terminal port at the Santos Coastal Plain ("Baixada Santista"), Brazil. It was a precast concrete pile, circular, with an outer diameter of 80 cm, a wall thickness of 15 cm and a nominal cross-sectional area of 3062.05 cm2. The pile had a total length of 52.0 m, in which 43.4 m have penetrated in the soil. These and other characteristics are shown on Table 1.

The pile was driven offshore, on May 29th, 2012, using a 160 kN Junttan HHK hydraulic hammer. During the initial 20 m, the pile penetrated the soil with an approximately constant rate of 50 cm for every 20 blows applied and, from this point on, with the same number of blows, the penetration reduced to 20 cm until reaching the final depth with 43.4 m of its length.

The soil profile was determined from several field tests 6 m below sea water level. The subsoil is composed

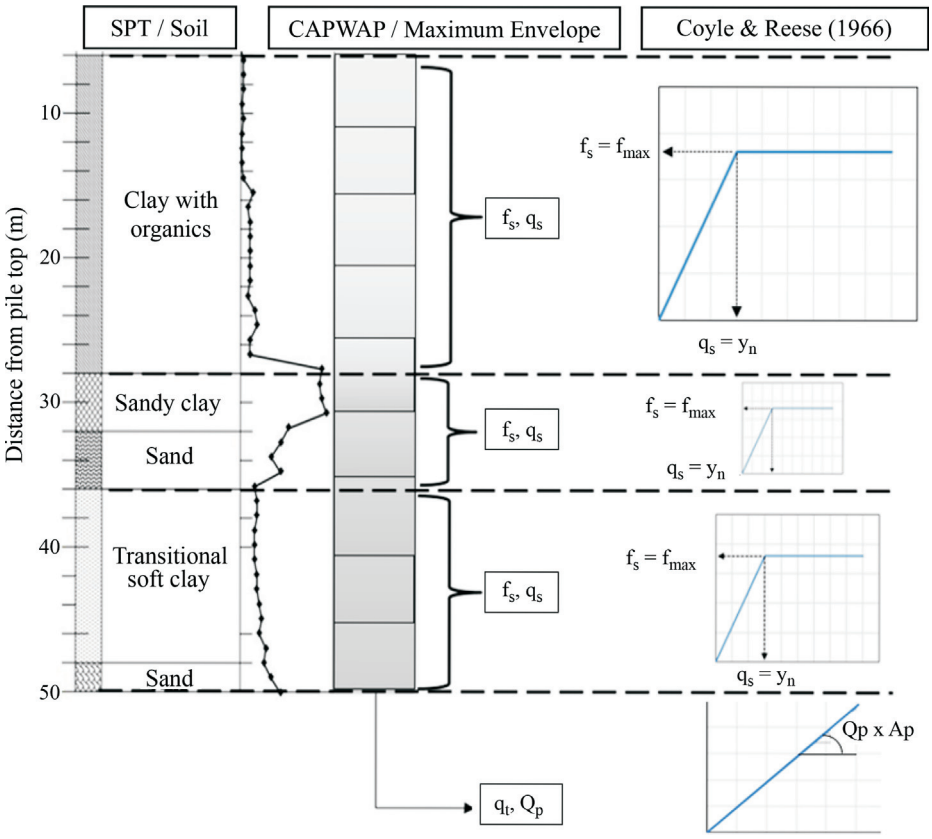

Figure 3 - Relationship between soil profile, maximum envelope results and Coyle-Reese load transfer functions.

Table 1 - EC1304 pile profile and PDA data.

Pile name	Diameter		Length			Wave speed	Dynamic modulus
	Outside (cm)	Inside (cm)	Total (m)	Below sensors (m)	Embedded (m)	(m/s)	(GPa)
EC1304	80.0	50.0	52.0	50.8	43.40	3700	34.2

initially by a 20 m thick very soft organic marine clay, locally known as SFL Clay (Fluvio Lagunar Sediment), which is generally slightly overconsolidated (OCR~1.1 to 1.5), followed by a medium to compact clayey sand (SPT ranging from 7 to 33 blows), about 8 m thick. These soils overlie 4 m of an overconsolidated clay, with OCR greater than 2.5 due to a great sea level lowering during the last glaciation, known locally as Transitional Clay (AT), with SPT higher than 5. Finally, at depth greater than 32 m below seabed occur thin to thick layers of compact sand, with SPT of the order of 10. More detailed information about the origin and composition of these soils can be found in Massad (2009).

4.2. Static Load Test (SLT)

The Static Load Test (SLT) was performed on August 7 and 8, 2012, about 70 days after pile installation, using a set of pumps, hydraulic jack and pressure gauge supported on a block of concrete and 4 reaction piles. Known as Mixed Maintained Load, the test consisted of slow applications of load increments during the loading phase and quick unload during the unloading phase, according to NBR 12131 (2006). The maximum load and displacement in the Static Load Test (SLT) were 8407 kN and 34 mm, respectively, without indication of failure and the permanent set was 6 mm, as shown in Fig. 4.

4.3. Dynamic Increasing Energy Test (DIET) and CAPWAP

Pile EC1304 was dynamically tested on June 6, 2012, therefore about 8 days after its installation. Blows with the following hammer drop heights were applied: 20; 40; 60; 80; 100; 120; 120; 120 and 120 cm. The last applied blow corresponding to the highest mobilized resistance was used for the first CAPWAP analysis. Table 2 provides some of the numerical results obtained from the "best match quality" of CAPWAP analysis.

Figure 4 shows visually an excellent correlation between the curve simulated by the CAPWAP and the curve obtained from Static Load Test (SLT).

4.4. Maximum envelope of lateral resistance - EC1304

Figure 5 shows the lateral resistance in pile segments distributed along depth given by the CAPWAP for each applied blow. It is possible to notice that in the first half of the pile the maximum values of lateral friction are associated with lower energy blows. In the lower half, such maximum lateral resistances are reached with higher energy blows.

After each new applied blow, the soil undergoes changes and loses part of the resistance recovered during the "set up". Figure 5 allows to compare the lateral resistance of the last blow ($120^{(3)}$ cm) with the Maximum Envelope, highlighted in dashed line. The envelope of lateral resistance of EC1304 pile allows some considerations regarding lateral resistance: (i) blows with hammer drops of 20 cm to 80 cm indicate greater static lateral resistances up to approximately 24 m; (ii) the first 20 m show a gradual reduction of lateral resistance as the hammer drop heights increase, up to a minimum limit of lateral resistance; (iii) the last blow ($120^{(3)}$ cm), represented with a full black line, is at the minimum limit of the mobilized lateral resistance in the upper segments, until approximately 22 m.

Using the dashed line of Fig. 5, *i.e.*, the Maximum Envelope of Lateral Resistance, associated with the highest mobilized toe resistance (blow $120^{(3)}$ cm), the total pile capacity was estimated as 10085 kN. Figure 6 shows the curves simulated by CAPWAP considering as the starting

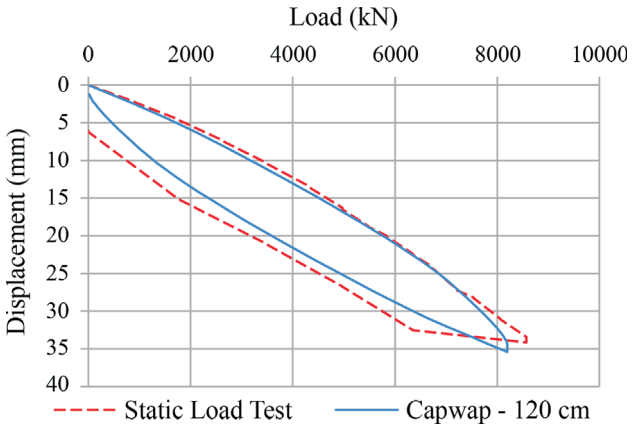

Figure 4 - Simulated CAPWAP and Static Load Test curves - blow 120 cm - EC1304.

Table 2 - CAPWAP analysis results - Pile EC1304.

Pile name	Total capacity	Lateral resistance		Toe resistance		Shaft quake	Toe quake
	(kN)	(kN)	(%)	(kN)	(%)	(mm)	(mm)
EC1304	8044	6206	77	1838	23	2.31	3.32

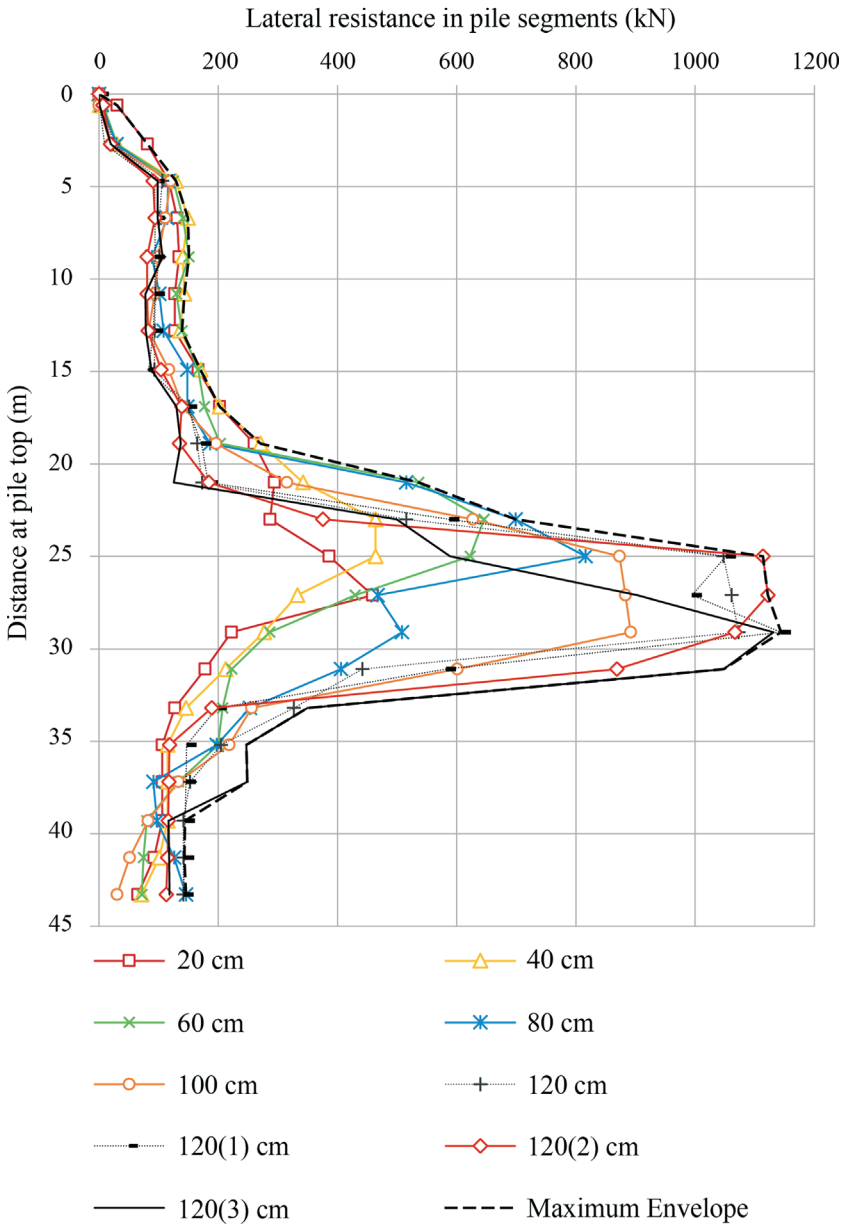

Figure 5 - Lateral resistance distribution - EC1304.

point of each applied blow the final point of the precedent blow, like a cyclic monotonic test. The set of simulated CAPWAP curves maintain a good visual correlation with the Static Load Test (SLT). It is possible to notice that there was no evidence of failure, as emphasized previously.

4.5. Coyle-Reese method using the last applied blow (120$^{(3)}$ cm)

For the application of the Coyle-Reese method to the last blow (120$^{(3)}$ cm) using CAPWAP results, the part of the pile embedded in the soil was divided into 5 segments, the same number of layers identified in the soil profile, as shown in Table 3. In this table, the shaft quake q_s was assumed constant indicating the full activation of lateral resistance throughout the pile length. Furthermore, the toe quake was figured out as 3.3 mm with 1838 kN of toe resistance. The static elastic modulus of the pile was figured out as 27.8 GPa, *i.e.*, 86% of the dynamic modulus (see Table 1), according to Lydon and Balendran (1986) empirical relation. The last column of Table 3 shows the "elastic" parameter B of each load transfer function. The pile length above ground was 8.6 m.

The result of Coyle-Reese method is shown in Fig. 7. The total capacity by the Coyle-Reese method was estimated at 8029 kN with 38 mm of displacement. The load-set curve was adjusted considering the elastic shortening of the part of the pile above the sea bed in order to simulate the same conditions of the Static Load Test (SLT), which added 10 mm in the last point of the curve. The Coyle-Reese curve of Fig. 7 is close to the curves of the static load

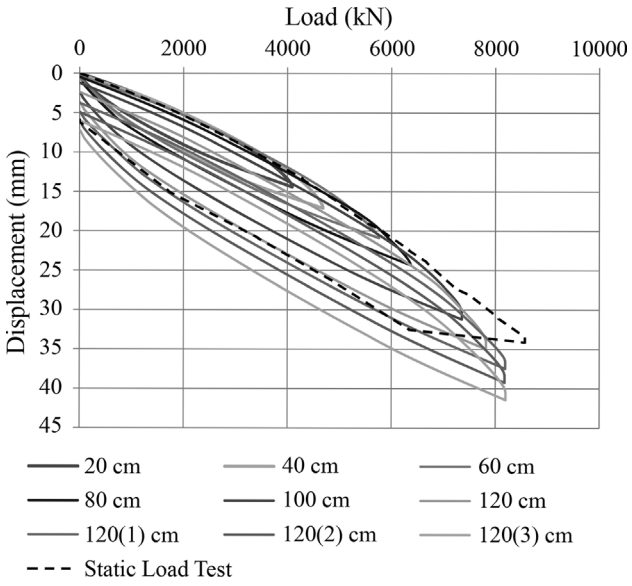

Figure 6 - Simulated static curves from CAPWAP vs Static Load Test - EC1304.

test and the simulated static curve from CAPWAP, at least up to the 4000 kN load.

4.6. Coyle-Reese method using maximum envelope results

For this new Coyle-Reese application, the mean lateral friction of each soil layer was determined using the dashed line of Fig. 5 and is shown in Table 4, together with the values of the mean shaft quakes. The result is presented in Fig. 8, which reveals excellent correlation between the Coyle-Reese simulated curve using Maximum Envelope results and the Static Load Test (SLT). In addition, the total capacity from the Coyle-Reese curve was 9863 kN with 45 mm of displacement. This total capacity is close to

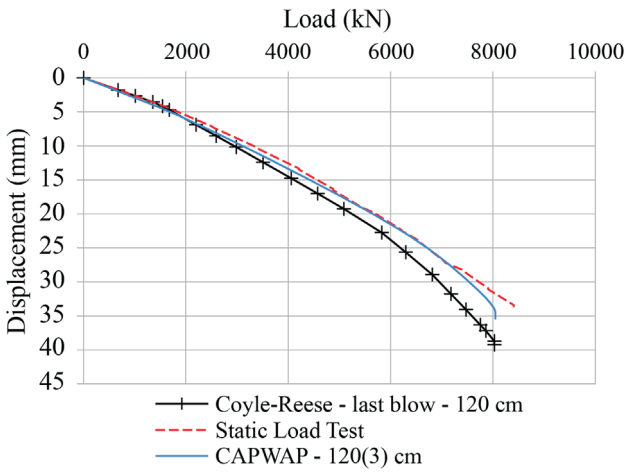

Figure 7 - Simulated load-set curves *vs.* Static Load Test - EC1304.

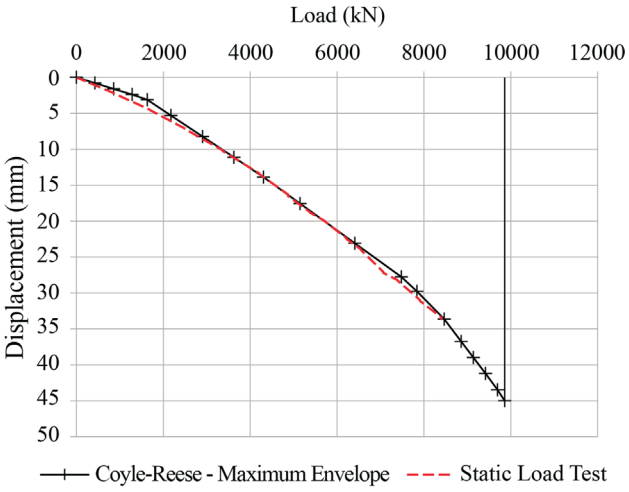

Figure 8 - Simulated load-set curve *vs.* Static Load Test - EC 1304.

Table 3 - Input data for the Coyle-Reese method - last applied blow ($120^{(3)}$ cm) - EC1304.

No.	Soil Layer	ΔH (m)	f_{max} (kPa)	y_n (mm)	$B = f_{max}/y_n$ (kPa/mm)
1	SFL Clay	20	17.7	2.308	7.7
2	Clayey sand	4	60.0	2.308	26.0
3	Transitional clay	8	176.3	2.308	76.4
4	Medium sand	10	41.5	2.308	18.0
5	Compact sand	2	22.7	2.308	9.8

Table 4 - Input data for the Coyle-Reese method - Maximum Envelope - EC1304.

No.	Soil layer	ΔH (m)	f_{max} (kPa)	y_n (mm)	$B = f_{max}/y_n$ (kPa/mm)
1	SFL Clay	20	28.8	1.25	23.1
2	Clayey sand	4	116.4	1.7	68.5
3	Transitional clay	8	208.8	2.46	84.9
4	Medium sand	10	42.3	1.75	24.2
5	Compact sand	2	27.9	0.234	119.3

10085 kN, estimated in section 4.4, using the Maximum Envelope of Lateral Resistance.

In order to show the difference of the unit skin friction values of the SFL Clay layer between the CAPWAP of the last blow and the Maximum Envelope method, Fig. 9 shows the average load transfer function calculated with CAPWAP results of all applied blows during the dynamic load test. The peak of the curve, with unit skin friction of 28.8 kPa and displacement of 1.25 mm, corresponds to the values of f_{max} and y_n of Table 4. For displacements above roughly 2.3 mm, the curve tends to a residual value indicating a condition close to a remolded soil; this value was used in the Coyle-Reese method for the last applied blow ($120^{(3)}$ cm).

4.7. Summary of static resistance results - EC1304

Table 5 summarizes the results obtained for the first case, related to the static resistances. Notice that the toe resistance has the same value, determined by CAPWAP applied to the last blow ($120^{(3)}$ cm). The total static resistances from this single blow (CAPWAP $120^{(3)}$) and from the Static Load Test (SLT) differ by no more than 8044/8407-1 ≅ 4%. Moreover, compared with CAPWAP $120^{(3)}$ cm, the Maximum Envelope Method allows estimating a lateral resistance increment of 8247 - 6206 = 2041 kN.

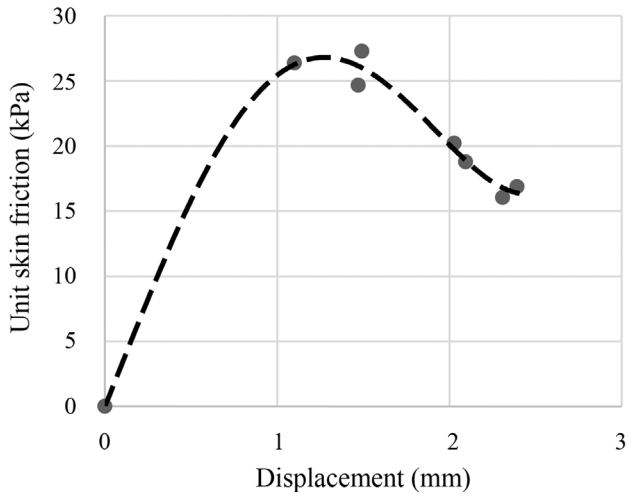

Figure 9 - Average load transfer function for the SFL Clay from Max. Envelope Method.

Table 5 - Final results - EC1304.

Test/method	Static resistance (kN)		
	Shaft	Toe	Total
Static Load Test (SLT)	-	-	8407
CAPWAP - $120^{(3)}$	6206	1838*	8044
Maximum envelope	8247	1838*	10085
Coyle-Reese - $120^{(3)}$	6191	1838*	8029
Coyle-Reese - maximum envelope	8025	1838*	9863

5. Second Case: Steel Tube Pile in Port - Santos, SP - Brazil

5.1. Pile properties

The second case refers to a test pile for the construction of a pier in the Piaçaguera Chanel, close to Cubatão City in the Santos Coastal Plain ("Baixada Santista"), Brazil. The tests were performed on a steel tube driven pile, with external diameter of 91.4 cm and wall thickness equal to 16 mm, resulting in a section steel area of 451.4 cm^2. The pile (PC01) was submitted to Static Load Test (SLT) and to Dynamic Increasing Energy Tests (DIET) and its characteristics are detailed in Table 6.

The pile was installed on February 11, 2015, using a 90 kN Junttan HHK hydraulic hammer. Dynamic load tests were performed after the end of driving (EOD) and after several rest periods: 3 h, 6 h, 24 h, 48 h and 216 h (9 days). The objective was to analyze the "set up" effect of the soil and to estimate the long term lateral resistance, applying the Maximum Envelope Method. The Static Load Test was performed three months after the DIETs, using the Slow Maintained Load procedure in accordance to NBR 12131 (ABNT 2006).

The subsoil profile is composed initially by a 6 m fill layer of clayey sand m (SPT~1 to 10), followed by (i) a soft layer of the SFL Clay (18 m thick and SPT~2 to 4), and (ii) 6 m of fine to coarse sand, with gravel, SPT ranging from 15 to 30. Below about 30 m there is a layer of fine to coarse clayey sand, 8 m thick (SPT~12 to 30), overlying gneiss. The SFL Clay layer may be subdivided in two sublayers, half with SPT ≅ 2 and half with SPT ≅ 4.

5.2. Dynamic Increasing Energy Tests (DIET) and CAPWAP - 216 h

Dynamic Increasing Energy Tests (DIETs) were performed at the end of driving and in all "set up" periods. Blows with the following hammer drop heights were applied: 20; 40; 60; 80; 100 and 120 cm. The results of the CAPWAP analysis of the last blow after the 216 h "set up" time are shown in Table 7 and in Fig. 10.

Table 6 - PC01 pile profile and PDA data.

Pile name	Diameter		Length			Wave speed (m/s)	Dynamic modulus (GPa)
	Outside (cm)	Inside (cm)	Total (m)	Below sensors (m)	Embedded (m)		
PC01	91.4	88.2	40.1	36.14	33.30	5123	210.9

This test was performed on 02/20/2015, three months before the Static Load Test (SLT), which justifies the difference between the maximum displacements shown in Fig. 10: 28 mm in the Static Load Test (SLT) against 35 mm in the dynamic test.

5.3. Maximum envelope of lateral resistance - 216 h

The Maximum Envelope result for the 216 h "set up" period is shown in dashed line in Fig. 11, together with the distribution of lateral resistance in pile segments along depth for various hammer drop heights. It can be noticed the same behavior of the first case, *i.e.*, as the applied energy increases, lower values of lateral static resistances are gradually mobilized in segments of the pile close the top, in contrast to higher values in segments close the pile toe.

Table 8 summarizes the static resistances and reveals an increase of 5252/4647 - 1 ≅ 13% in the lateral resistance estimated with the Maximum Envelope Method compared to the single 120 cm CAPWAP analysis. Note that, maintaining the same value for the pile toe, this amount drops to 10164/9559 - 1 ≅ 6% for the total static resistance.

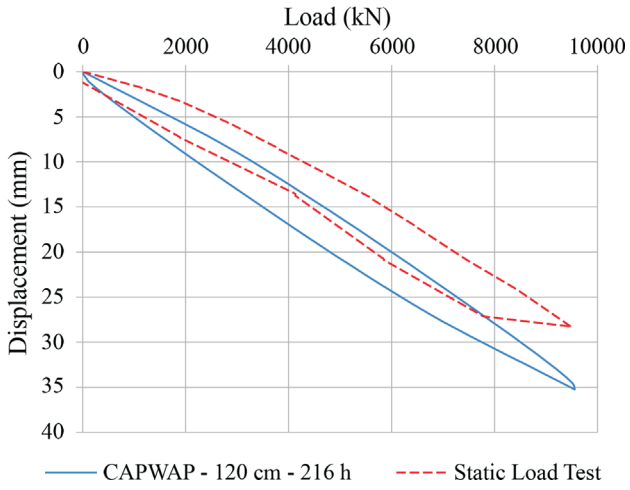

Figure 10 - Simulated CAPWAP and Static Load Test curves - 216 h "set up" - PC01.

Figure 12 allows comparing the Maximum Envelope with the lateral resistance distributions obtained by the CAPWAP on the last blow (120 cm) at the end of driving and after 216 h rest period. At the end of the driving, a lateral resistance of 1381 kN was estimated by the CAPWAP. Using the data shown in Table 8, it may be concluded that the lateral resistance increased 4647/1381 - 1 ≅ 336% for the last blow (120 cm) after the 216-h period (9 days) compared to 5252/1381 - 1 ≅ 380% related to the Maximum Envelope.

5.4. "Set up" evaluation using the Maximum Envelope of Lateral Resistance - PC01

Dynamic load test results at all "set up" periods, presented in Table 9, indicate lateral and total resistance gains over time. This is also evident with the Maximum Envelope results.

The decreasing toe resistance values over time, observed in Table 9, indicate that the pile toe was not fully mobilized due to the lateral resistances increase along the pile shaft. Based on these results, Figs. 13 and 14 show variations of the Q/Q_0 ratio for the lateral resistance and for the total capacity over time. In this relation, Q and Q_0 are lateral resistance (Fig. 13) or load capacity (Fig. 14) after a certain period of rest and at the end of driving (EOD), respectively.

It is possible to notice that the lateral resistance increases significantly during the first 48 h and, after that, the increments are smaller and practically linear. An important factor to consider when evaluating the "set up" is the activation of all skin frictions during the dynamic test. Therefore, it is necessary to evaluate the shaft quake q_s of the last blow (120 cm) for each period of rest. If the result of the CAPWAP shows that the shaft quake does not remain constant and that from a certain depth it decreases, it may be

Table 7 - CAPWAP Analysis results - PC01-120 cm blow and 216 h "set up" time.

Pile name	Total capacity	Lateral resistance		Toe resistance		Shaft quake	Toe quake
	(kN)	(kN)	(%)	(kN)	(%)	(mm)	(mm)
PC01	9559	4647	48	4.912	52	5.73	1.75

Table 8 - Distribution of resistance along the pile - PC01-216 h "set up" time.

Static resistances	Hammer drop heights (cm)						Maximum envelope
	20	40	60	80	100	120	
Lateral (kN)	3063	3644	3867	3993	3938	4647	5252
Toe (kN)	753	2390	2528	4085	4530	4912	4912
Total (kN)	3816	6034	6395	8078	8468	9559	10164

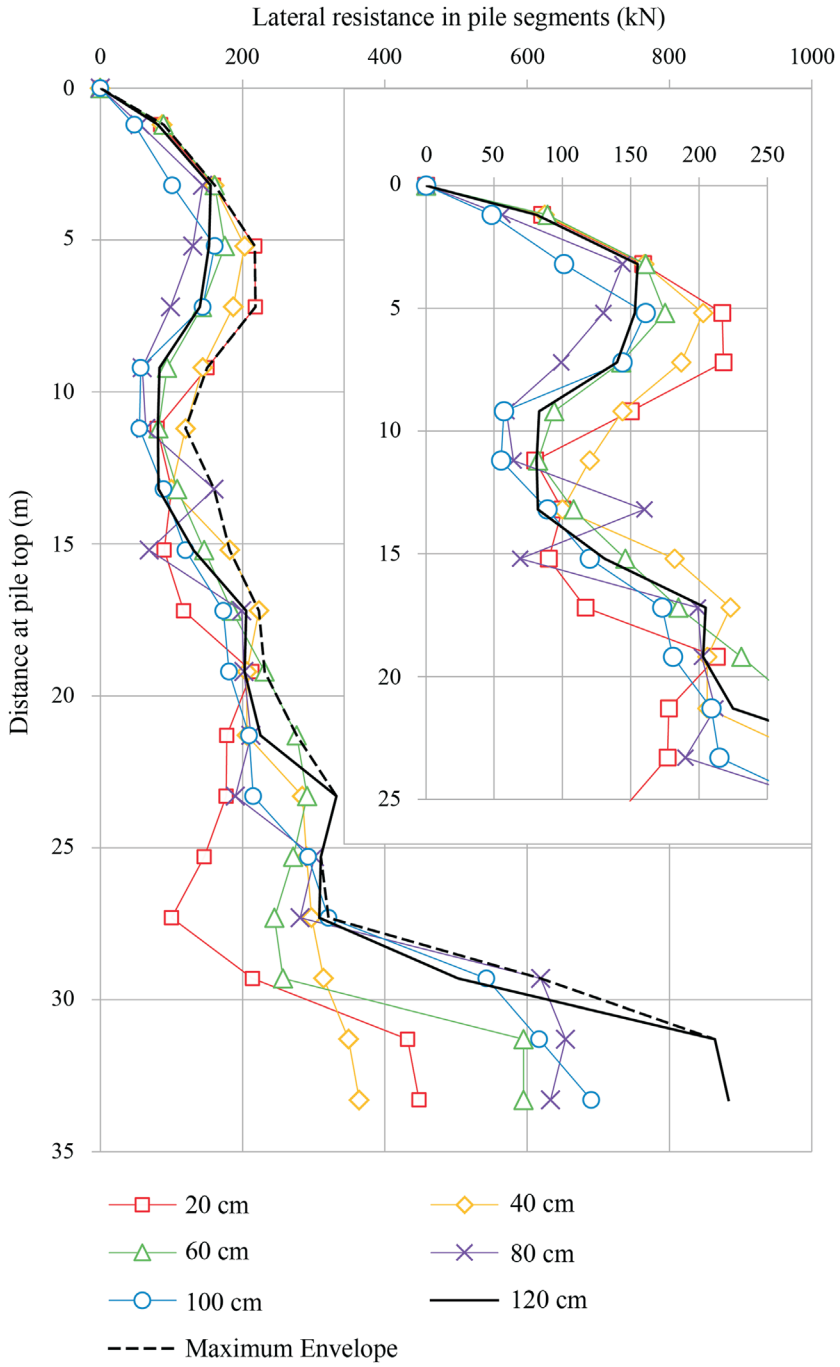

Figure 11 - Lateral resistance distribution - 216 h "set up" time- PC01.

concluded that the applied energy was not enough to activate all lateral resistance. The shaft quake remained constant only within the EOD and the 3 h rest period. On longer periods, q_s decreased on segments near the pile toe. Thus, the results obtained for the evaluation of the "set up" can be considered underestimated, mainly in the last segments of the pile-soil system.

A more detailed and accurate evaluation of the skin friction gain can be achieved specifically for the SFL Clay, the predominant soil layer along the pile shaft. According to the soil profile described, this layer lies between depths of -4.0 m and -24.0 m. Another important observation is that the shaft quake remained constant in all rest periods in this depth interval, which indicates that there was maximum skin friction mobilization. Figs, 15 and 16 show the f/f_0 ratio over time only of the SFL Clay layer for both the Maximum Envelope and the blow of 120 cm. The f and f_0 values refer to unit skin friction after a certain period of rest and at the end of driving (EOD), respectively.

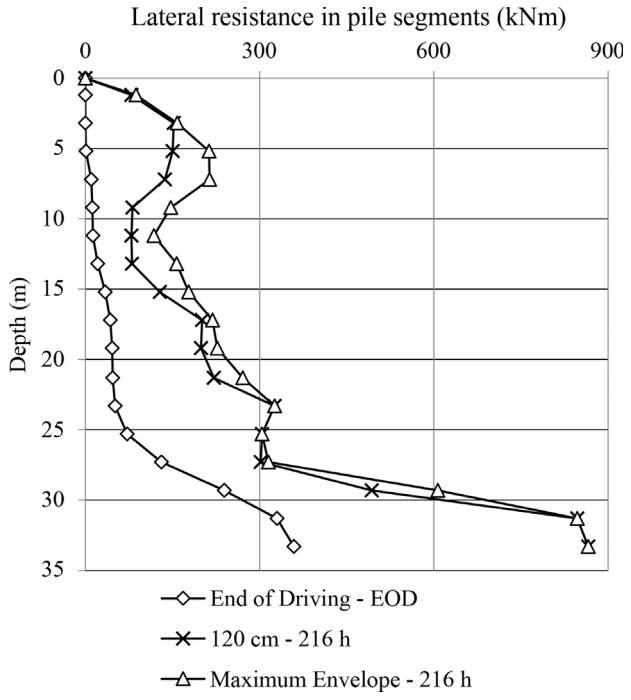

Figure 12 - Lateral resistance distribution -Max. Envelope, EOD and 216 h - PC01.

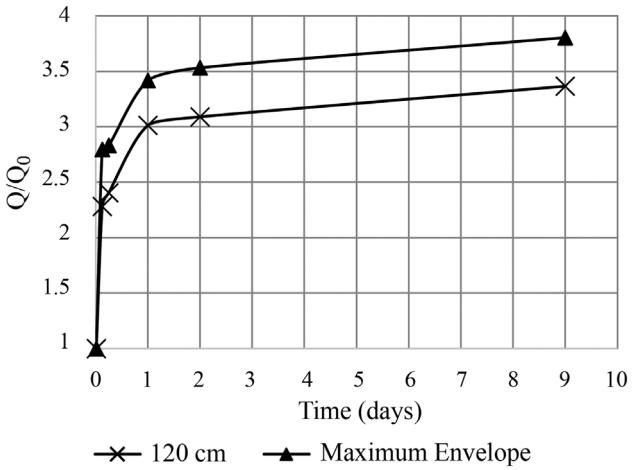

Figure 13 - Results of lateral "set up" - 120 cm and Maximum Envelope - PC01.

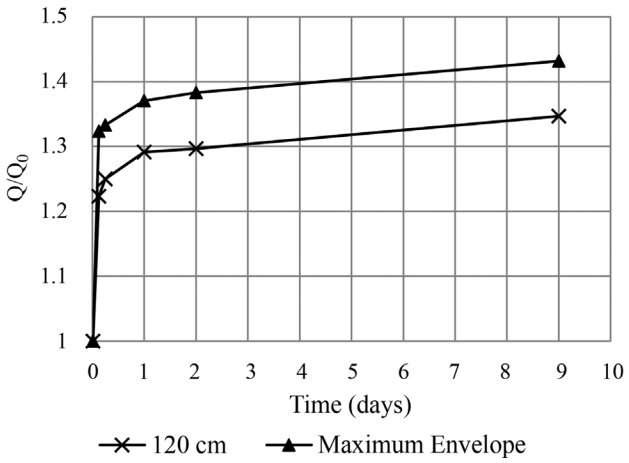

Figure 14 - Results of total "set up" - 120 cm and Maximum Envelope - PC01.

Based on the results of the Maximum Envelope, it is possible to determine the parameter "A" of Bullock *et al.* (2005), which depends on the soil type, through the linear regression coefficients obtained in Fig. 15. This analysis shows that for the whole shaft the parameter "A" is equals to 0.98 and, for the SFL Clay layer alone, 1.6. This difference is due to the fact that the "A" parameter for the entire shaft includes "set up" of deep sandy layers, which have lower "set up" factors. With the same procedure and using only the 120 cm hammer drop blows, the parameters "A" are smaller compared to those obtained by the Maximum Envelope, as shown in Fig. 16. Among other publications, Bilfinger (2010) obtained the parameter "A" equal to 0.61 for skin friction in the Santos Coastal Plain ("Baixada Santista") through dynamic Load Tests.

As an example of total lateral resistance "set up", Figs. 15 and 16 show that the f/f_0 ratio equals 2 in a rest period of 20 h considering only the blow of 120 cm, whereas through the Maximum Envelope method this same value would be reached in approximately 10 h.

Table 9 - Summary of the results- PC01.

No.	120 cm				Maximum envelope			
	Resistance			Quake on shaft (mm)	Resistance			Quake on shaft (mm)
	Lateral (kN)	Toe (kN)	Total (kN)		Lateral (kN)	Toe (kN)	Total (kN)	
EOD	1381	5717	7098	5.62	1381	5717	7098	5.62
3 h	3149	5533	8682	1.29	3860	5533	9393	3.25
6 h	3321	5553	8874	4.03	3908	5553	9461	3.47
24 h	4159	5009	9168	3.32	4718	5009	9727	2.66
48 h	4265	4939	9204	3.76	4877	4939	9816	3.38
216 h	4647	4912	9559	4.22	5252	4912	1016	2.99

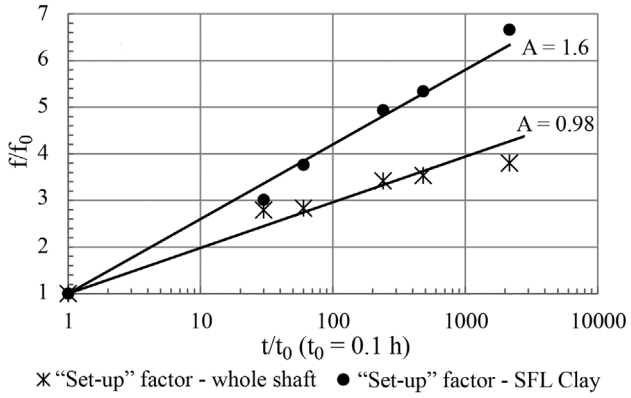

Figure 15 - Parameter A - "Set up" lateral factor - Maximum Envelope - PC01.

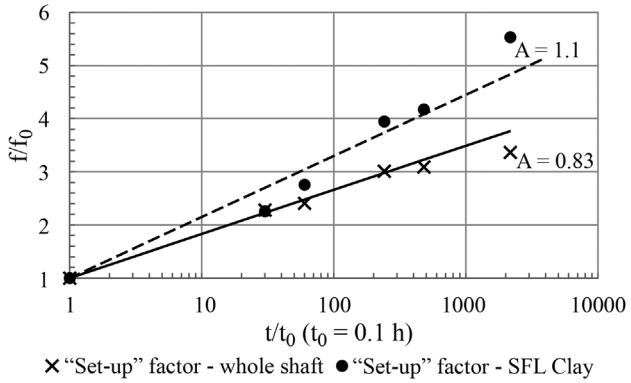

Figure 16 - Parameter A - "Set up" lateral - 120 cm - PC01.

5.5. Coyle-Reese method using the last blow (120 cm) - 216 h

The pile was divided into 8 segments, a number higher than the subsoil layers, described above. The unit skin friction values f_s along the SFL Clay layer varied along depth, in agreement with SPT increasing from 2 to 4. Therefore, this layer was divided into two parts of 10 m each, as shown in Table 10.

The toe quake is equal to 1.76 mm, the mobilized toe resistance is 4912 kN and the elastic modulus of the pile material is equal to 207 GPa. Note, in advance, that the Static Load Test (SLT) was carried out with a pile length of 36.14 m (see Table 6). Regarding Fig. 17 (a), the pile length was taken as 36.14 + 2.84 ≅ 39 m, in which 2.84 m is the distance between the PDA sensors and the soil surface. This length was used to calculate the pile elastic shortening on the Coyle-Reese method whose result shows an excellent correlation with the simulated CAPWAP curve, both associated to the last blow (120 cm) and a "set up" period of 216 h. The comparison between the Coyle-Reese curve with the Static Load Test (SLT) can be made through Fig. 17 (b). In this case, the pile length was taken equal to 36.14 m (see Table 6) and the small variation between both curves occurs mainly due to the "set up" period in which each test was performed, with a difference of 90 days.

5.6. Coyle-Reese method using the Maximum Envelope of Lateral Resistance - 216 h

The data of the load transfer functions given by the Maximum Envelope are shown in Table 11 and the resulting curve of the Coyle-Reese method is shown in Fig. 18.

Figure 18 shows remarkable correlation between the curves simulated by Coyle-Reese method and provided by the Static Load Test (SLT). The total capacity, estimated at 10164 kN by the Coyle-Reese method is indicated by the vertical dashed line. This is exactly the same value calculated by the Maximum Envelope for the 216-h rest period.

As the "set up" time increases, the toe mobilized resistances decrease. Therefore, the simulated curve by CAPWAP (120 cm and 216 h) incorporated the lowest mobilization of toe resistance, indicated as 4912 kN in Table 8. In the context of the Maximum Envelope Method, stated above, a new simulated curve by the Coyle-Reese method was done and shown in Fig. 19 considering the highest mobilization of toe resistance of 5717 kN (Table 8) with a quake of 3.1 mm, both values calculated at the end of driving (EOD). The excellent correlation is maintained and,

Table 10 - Input data for the Coyle-Reese Method - 120 cm - PC01.

No.	Soil layer	ΔH (m)	f_{max} (kPa)	y_n (mm)	$B = f_{max}/y_n$ (kPa/mm)
1	Sand earthwork	1.3	23.5	5.73	4.1
2	Clayey sand	2	26.4	5.73	4.6
3	Organic Clay (SFL)	10	18.3	5.73	3.2
4	Organic Clay (SFL)	10	37.3	5.73	6.5
5	Clayey sand (SFL)	4	52.6	5.10	10.3
6	Coarse sand	2	85.5	3.90	21.9
7	Silty sand	2	147.0	3.00	49.0
8	Sandy silt	2	150.2	2.10	71.5

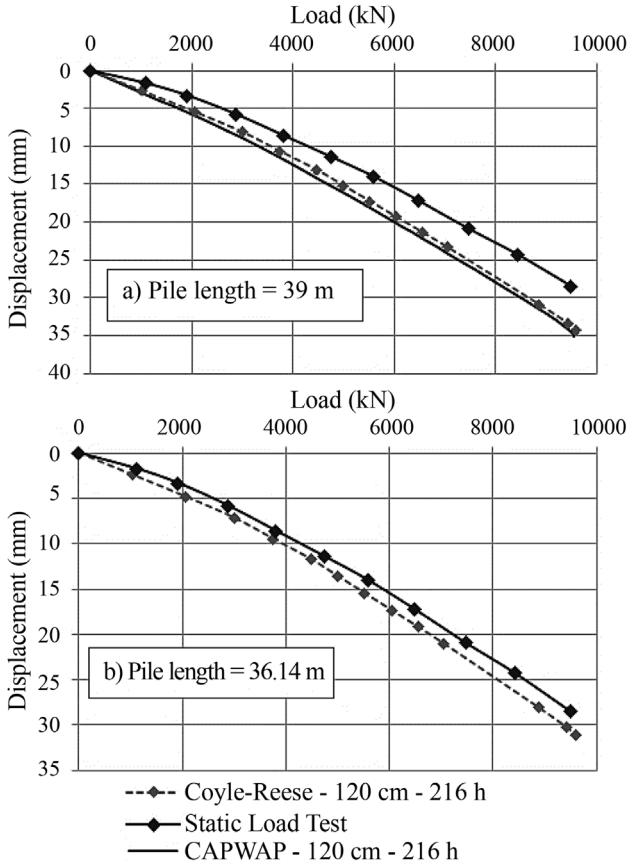

Figure 17 - Simulated load set curves *vs.* Static Load Test -PC01.

furthermore, the total capacity increased from 10164 kN to 10969 kN, as indicated by the vertical dashed line.

5.7. Summary of the results on static resistances - PC01

Table 12 summarizes the results obtained for the second case, related to mobilized static resistances. Based on these results, it is concluded that lateral resistance estimated by the Maximum Envelope associated with the Coyle-Reese Method is higher than that given solely by the CAPWAP of the last blow; the difference is 5252 - 4647 = 605 kN. Moreover, as shown above, it was possible to obtain a simulation of the load-settlement curve of

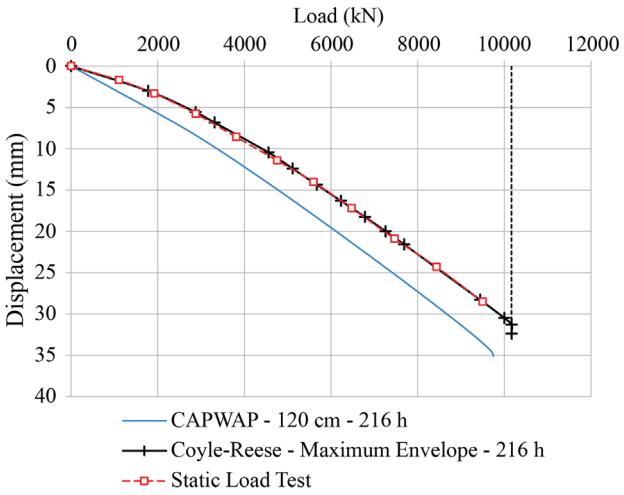

Figure 18 - Simulated load set curves *vs.* Static Load Test - PC01.

the pile top that approaches very well the Static Load Test (SLT) curve.

6. Conclusions

The application of CAPWAP only to the last blow of a dynamic increasing energy test underestimated the maximum mobilized capacity and the resistance distribution along the shaft, particularly in soils with high sensitivity, as was shown in the two studied cases. Initial blows can change the properties of the soil. This behavior is clearly seen in the curve of the lateral skin friction *vs.* displacement of the SFL Clay layer, shown in the first case study. The Maximum Envelope of Lateral Resistance made it possible to recover the lateral skin friction information lost in blows prior to that with maximum applied energy.

Compared to the load-settlement curve obtained in the Static Load Test (SLT), a set of simulated CAPWAP static curves involving all blows in the first case, like a cyclic test, revealed an equal to or better correlation than the

Table 11 - Input data for the Coyle-Reese method - Maximum Envelope - PC01

No.	Soil layer	ΔH (m)	f_{max} (kPa)	y_n (mm)	$B=f_{max}/y_n$ (kPa/mm)
1	Sand earthwork	2	25.9	5.10	5.1
2	Clayey sand	2	27.3	5.10	5.3
3	Organic Clay (SFL)	10	29.5	2.68	11.0
4	Organic Clay (SFL)	10	42.2	4.65	9.1
5	Clayey sand (SFL)	4	53.4	4.36	12.3
6	Coarse sand	2	105.3	3.07	34.3
7	Silty sand	2	147.0	3.01	48.8
8	Sandy silt	2	150.2	2.09	71.9

Table 12 - Summary of the results - PC01.

Test / Method	Static resistance (kN)		
	Lateral	Toe	Total
Static Load Test (SLT)	-	-	9497
CAPWAP - 120 cm - 216 h	4647	4912	9559
Coyle-Reese -120 cm - 216 h	4684	4912	9596
Maximum envelope - 216 h	5252	4912	10164
Coyle-Reese - Maximum envelope - 216 h	5252	4912	10164
Maximum Envelope - EOD Toe Resistance	5252	5717	10969
Coyle-Reese - Maximum envelope - EOD Toe	5252	5717	10969

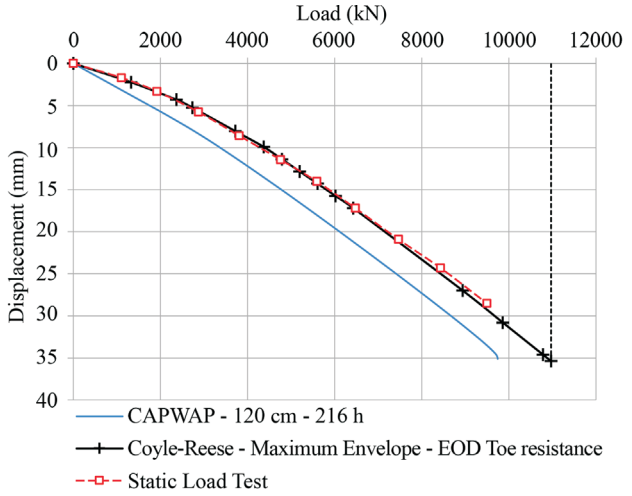

Figure 19 - Simulated load set curves *vs.* Static Load Test - PC01.

single CAPWAP simulated curve of the last blow, with the greater hammer drop height.

Moreover, the maximum lateral friction values calculated by the Maximum Envelope Method allowed the estimation of the load transfer functions for each soil layer, leading to successful applications of the Coyle-Reese Method. The load-set curves in the 2 studied cases correlated very well with the Static Load Tests (SLT). Such correlations were better in comparison with the simulated CAPWAP static analysis for only one signal, with the maximum applied energy.

The Maximum Envelope of Lateral Resistance performed in several rest periods allowed an assessment of the skin friction development over time for the second studied case. It was possible to calculate the lateral and total "set ups", particularly for the SFL Clay layer. The parameter A of Bullock *et al.* was figured out, allowing the forecast of skin friction increases on long term for the SFL Clay of Santos Coastal Plain ("Baixada Santista").

Acknowledgments

The authors acknowledge the support given by EPUSP - Escola Politécnica of University of São Paulo and would like to thank the companies PDI Engenharia and PDI-USA, for the assistance and for releasing data used in this paper, in particular to Sergio Valverde, Garland Likins and Frank Rausche.

References

ABNT (2006). Piles - Static Load Test, NBR 12131, Rio de Janeiro, Brazil (in Portuguese).

Aoki, N. (1997). The evaluation of the ultimate bearing capacity of driven piles by using increasing energy dynamic load tests. PhD thesis. Escola de Engenharia de São Carlos. Universidade de São Paulo, São Carlos.

Bilfinger, W. (2010). Set up on driven piles. Proc. V Congresso Luso Brasileiro de Geotecnia, v. 1, pp. 9-29.

Bullock, P.J.; Schmertmann, J.H. & McVay, M.C. (2005). Side shear setup. I: Test piles driven in Florida. ASCE Journal of Geotechnical Engineering, 131:292-300.

Coyle, H.M.; Reese, L.C. (1966). Load transfer for axially loaded piles in clay. Journal of Soil mech. and foundation division. Procedures of the ASCE: 1-26.

Lydon, F.D. & Balendran, R.V. (1986). Some observations on elastic properties of plain concrete. Cement and concrete research 16(3):267-459.

Massad, F. (2009). Solos Marinhos da Baixada Santista - Características e Propriedades Geotécnicas. Editora de Textos, São Paulo.

Pile Dynamics, Inc. (2006). Case Pile Wave Analysis Program - CAPWAP Manual.

Rausche, F.; Likins, G.; Liang, L. & Hussein, M. (2010). Static and dynamic models for CAPWAP signal matching. The art of foundation engineering practice. Geotechnical Special Publication, 198:534-553.

Rausche, F.; Hussein, M.; Likins, G. & Thendean, G. (1994). Static pile load-movement from dynamic measurements. Proceedings of Settlement'94. Vertical and horizontal deformations of foundations and embankments. College Station: 291-302.

Smith, E.A.L. (1960). Pile driving analysis by the wave equation. Journal of Soil Mechanics and Foundation Division, ASCE 86.

List of symbols

A: Bullock's constant, dependent on soil type
B: Coyle and Reese's elastic slope
DIET: Dynamic Increasing Energy Test
f_{max}: Coyle and Reese's maximum element skin friction
f_s: CAPWAP's element skin friction
Q: Capacity, dependent on time
Q_p: Coyle and Reese's toe resistance
q_t: Toe quake
q_{tu}: Unloading toe quake
q_u: Unloading quake
R_{lt}: Reload level
R_{nu}: Negative ultimate resistance level
R_{st}: Toe static resistance
R_{ut}: Maximum pile toe element resistance
SLT: Static Load Test
t_g: Resistance Toe Gap
U_n: Unloading multiplier
u_{px}: Maximum element displacement
u_t: Maximum pile toe displacement
y_n: Coyle and Reese's element displacement
y_t: Coyle and Reese's pile toe displacement

Technical Note

Soils and Rocks
v. 41, n. 1

Importance of the Excavation Level on the Prediction of the Settlement Pattern from Piled Raft Analyses

R.P. Cunha, H.G. Poulos

Abstract. This article analyses the effect of the excavation level on the settlement results from a standard analysis of a piled raft system. For that, a published case history that involved a house located in Gothenburg, Sweden by Hansbo (1993) was examined. This structure was founded over a soft, highly plastic marine clay of varying thickness, where the foundation was designed by using the concept of "creep piling", *i.e.*, piles in a state of full load mobilization. The analyses were carried out with the numerical tools DEFPIG and GARP, by considering a series of simplified assumptions for the load pattern, raft and pile characteristics and subsoil profile. The soil, pile and load characteristics have been considered, with analyses that allowed (or not) the effect of the excavation level. The exercise emphasizes the importance of such consideration for the assessment of the settlement pattern underneath the raft. This contribution concludes that it is not possible to precisely predict the behavior of piled rafts without a full understanding of its important input parameters, such as the excavation depth. It should be of considerable interest for those who design / simulate piled foundations and need to predict their performance in the presence of consolidating soft soils.

Keywords: foundation design, numerical analysis, piled raft, soft clay, soil excavation.

1. Introduction

In the past decade, several papers have been published with emphasis on what are now called as "piled-rafts", *i.e.*, pile groups in which the raft connecting the pile heads positively contributes to the overall foundation behavior (for example Ottaviani, 1975; Poulos, 1991; Hansbo, 1993; Burland, 1995; Ta & Small, 1996; Clancy & Randolph, 1996; Mandolini & Viggiani, 1997; Poulos, 1998 and Cunha *et al.*, 2001). The International Society for Soil Mechanics and Foundation Engineering (ISSMFE) also focused the activities of one of its Technical Committees (ITC-18) on the study of piled raft foundations. This Committee gathered valuable information on case histories and on methods of analysis, having produced comprehensive reports on these activities (O'Neill *et al.*, 1996).

In regard to the design philosophy of piled rafts, Randolph (1994) has defined the following approaches:

- The "conventional approach", in which the foundation is designed essentially as a pile group to carry the major part of the load, while making some allowance for the contribution of the raft. This is the conventional approach widely adopted in design;
- The "creep piling approach", as proposed by Hansbo & Källström (1983), in which the piles are designed to operate at a working load at which significant creep starts to occur, typically 70-80% of the ultimate load capacity. In this case, the pile cap or raft, contributes to the overall capacity;
- The "differential settlement approach", in which the piles are located strategically in order to reduce the differential settlements, rather than to substantially reduce the overall average settlement. The pile cap, or raft, also contributes to the overall capacity.

In general, the latter two approaches are more economical than the first one, but they can only be used under certain conditions, where either local standard allows or differential settlements are the key design factor. Other papers have expanded upon these ideas, such as those by Cunha & Sales (1998) and Cunha *et al.* (2000a, b). Cunha & Sales (1998) described and discussed a paper describing and discussing field loading tests carried out in small scale footings supported by a reduced number of piles. These tests were performed at the University of Brasília research site, and have confirmed that this design methodology has a large potential (although with some restrictions) to be adopted with the collapsible porous clay of the Federal District of Brazil. Cunha *et al.* (2000b) analyzed a piled raft case history in the city of Uppsala, Sweden, on a prediction exercise very close to the one presented herein. They have suggested an "optimized" parametric procedure for the preliminary design of both piled rafts and standard deep foundations. This optimization has proved that it is possible to obtain a considerable cost saving in the final design, without detriment to the original factor of safety of the foundation. The suggested procedure has been tested against another case history in Sweden (Cunha *et al.*, 2000a), al-

Renato P. Cunha, Ph.D., Full Professor, Programa de Pós Graduação em Geotecnia, Universidade de Brasília, Campus Universitário Darcy Ribeiro, Brasília, DF, Brazil. e-mail: rpcunha@unb.br.
Harry G. Poulos, D.Sc., Emeritus Professor, University of Sydney; Engineer at Coffey Geotechnics, Level 19, Tower B, Citadel Tower, 799 Pacific Highway, Chatswood, Sydney, New South Wales, Australia. e-mail: harry_poulos@coffey.com.
Submitted on August 25, 2017; Final Acceptance on March 15, 2018; Discussion open until August 31, 2018.
DOI: 10.28927/SR.411091

lowing the perception of the influence (in design) of one of the relevant variables that affect the behavior of the foundation system, *i.e.*, the number of piles underneath the raft. This latter paper established the basis of the presented numerical results, although the critical discussion and analyses have been considerably extended herein with information not available at that time. Therefore, the present exercise conveys a critical discussion on previous analyses by Cunha *et al.* (2000a), expanding their scope.

Thus this note explores the design of piled rafts, outlining the influence of the consideration (or not) of the excavation level on the proper assessment of the settlement of the piled raft system, including the excavation process in a very simplified manner. This technique is not new, and has already been adopted before by some authors as Sales *et al.* (2010) or Ibañez *et al.* (2014), among others. Sales *et al.* (2010) allowed for the influence of the variation of the stress level on the piled raft behavior in a rather complex manner, introducing the excavation sequence (stepwise) process on the numerical analyses in what has been called as a "compensated" piled raft analysis. On the other hand, Ibañez *et al.* (2014) considered the effect of the excavation with a more simplified procedure (like the one to be adopted here), simply by correcting the effective original stresses of the ground to the relief stress/reloading caused by both the extracted soil during excavation and the concrete raft molding. Both cases are simplified, and do not lead to perfect simulations of the real phenomena, but they can considerably improve the settlement pattern predicted by the numerical simulations. Of course, they cannot be precise given several other external aspects that are difficult (if not impossible) to input within the analyses, such as the stiffening and load distribution effects caused by the subsoil-superstructure interaction, the real rheological behavior of the soil upon unloading and reloading stages, the concrete placement and curing of the raft, the sequential (floor by floor) loading stages of the building, geotechnical variability of the subsoil and variable foundation geometries, concrete creep effects, and temperature effects among several others.

2. Material and Methods: Adopted Case History

Sweden is the biggest country in the Scandinavian region, covering an area of 450,000km^2. The dominant characteristics of the landscape can be attributed to glacial activity, with the rocky south-west coast along the Baltic Sea, and the Stockholm archipelago on the south-east coast, which is most notable for their fjords (as stated in the Lonely Planet web-page). Gothenburg is the Sweden's second city, being situated on the country's west coast in between Copenhagen and Oslo.

In the early 80's, two quite similar houses, one founded on conventional friction piles and the other on a "creep-piled" raft foundation were constructed in this city. These buildings, defined as "House 1" and "House 2", were located just 20 m apart. House 1 was designed in full accordance with the Swedish Building Code, meaning that the total load of the building was assumed to be carried by the piles. These piles were designed with a safety factor of 3 against a short-term (undrained) failure. House 2, on the other hand, was designed with the "creep piling" approach, as proposed by Hansbo & Källström (1983). In this approach, the piles are loaded to values close to, or equal to their creep load. They have the main purpose of reducing the settlement of the overall foundation structure, since the load of the building is partially counterbalanced by the contact pressure at the soil / raft interface (Hansbo, 1993).

House 2 was chosen to be analyzed herein. This house was designed to be an apartment house with 4 stories. It had a plan area of approximately 1000 m^2 with total dimensions of 75 *vs.* 12 m, as schematically presented in Fig. 1. It was constructed with four levels and a basement, leading to a total design load of 61.5 MN. The whole building was cast-in-situ, with basement walls uniformly spread over the base area. It was also designed to rest on a piled raft with a 0.4 m thick raft foundation, directly resting on top of the local marine clay, *i.e.*, no clear mention by Hansbo (1993) is made regarding the fact that the foundation raft was buried or not in the site although a "basement" unit has been mentioned. Nevertheless, there are some indications in this original reference that the 4 story apartment houses 1 and 2 were very similar and both had a "basement", as clearly described in the text. Besides, this reference, that indicates the ground beams for House 1, depicts what appears to be a basement space below the ground level. Hence, supported by indirect evidence, it is very probable that the foundation raft was indeed buried in the site, at least to one story level (~ 2.5 to 3 m) – and this is what it was assumed here.

In this piled raft foundation, 104 piles were used. They consisted of 0.3 m in diameter and 18 m long spliced timber "underpiles" with 8 m long 0.3 m diameter circular concrete piles on top. The total length of the composite piles was 26 m, being driven in place and uniformly spread over the building. They were placed mainly beneath the basement walls, as depicted by the filled circles of Fig. 1. It also shows the instrumentation that was placed prior to the casting of the raft. Pile load cells, contact pressure cells,

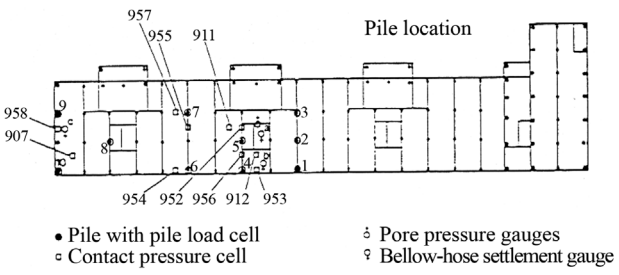

Figure 1 - House 2 – Gothenburg (modified after Van Impe, 1999).

bellows-hose (benchmark) settlement gauges, pore pressure gauges, and leveling stations were installed – as indicated in Fig. 1.

It should be pointed out that this case history was proposed by Van Impe (1999) to be one of the examples of an international exercise on the predicted behavior of piled rafts, via numerical programs. During this event, the instrumentation data was not made available to the participants, in order to characterize a "Class A" predictive exercise, although it was already known at that time that the settlement results of this case history had been previously published by Hansbo (1993). Indeed, as will be further detailed, some effort to truly perform a "Class A" prediction was made by the authors of the present contribution, by analyzing this case history solely on the basis of the data provided for the prediction exercise, together with the geotechnical characteristics of the site. Hence, "Class A" analyses are also presented and discussed in the present exercise, allowing it to highlight the importance of some of the parameters used for the numerical simulation of piled rafts, in particular the excavation level.

3. Geotechnical Characteristics of the Subsoil

The subsoil at the test site consisted of soft, highly plastic marine clay of varying thickness. The clay was relatively homogeneous and contained two layers of silty clay, one at about 12 m and one just below 30 m, as graphically depicted in Fig. 2. This clay layer extended down to a depth of 55 m beneath the two houses, and was underlain by rock.

The undrained shear strength (Su) was fairly constant along the profile, down to 10 m depth, with a mean value of about 20 kPa. It then increased linearly with depth, at an approximate rate of 2 kPa/m down to around 40 m depth. The sensitivity was quite constant, being slightly less than 20. The natural water content varied from 60 to 80%, and the liquid limit was usually somewhat higher. The plasticity index was typically about 50%, and the bulk density or total unit weight was around 16.5 kN/m^3. The clay was slightly

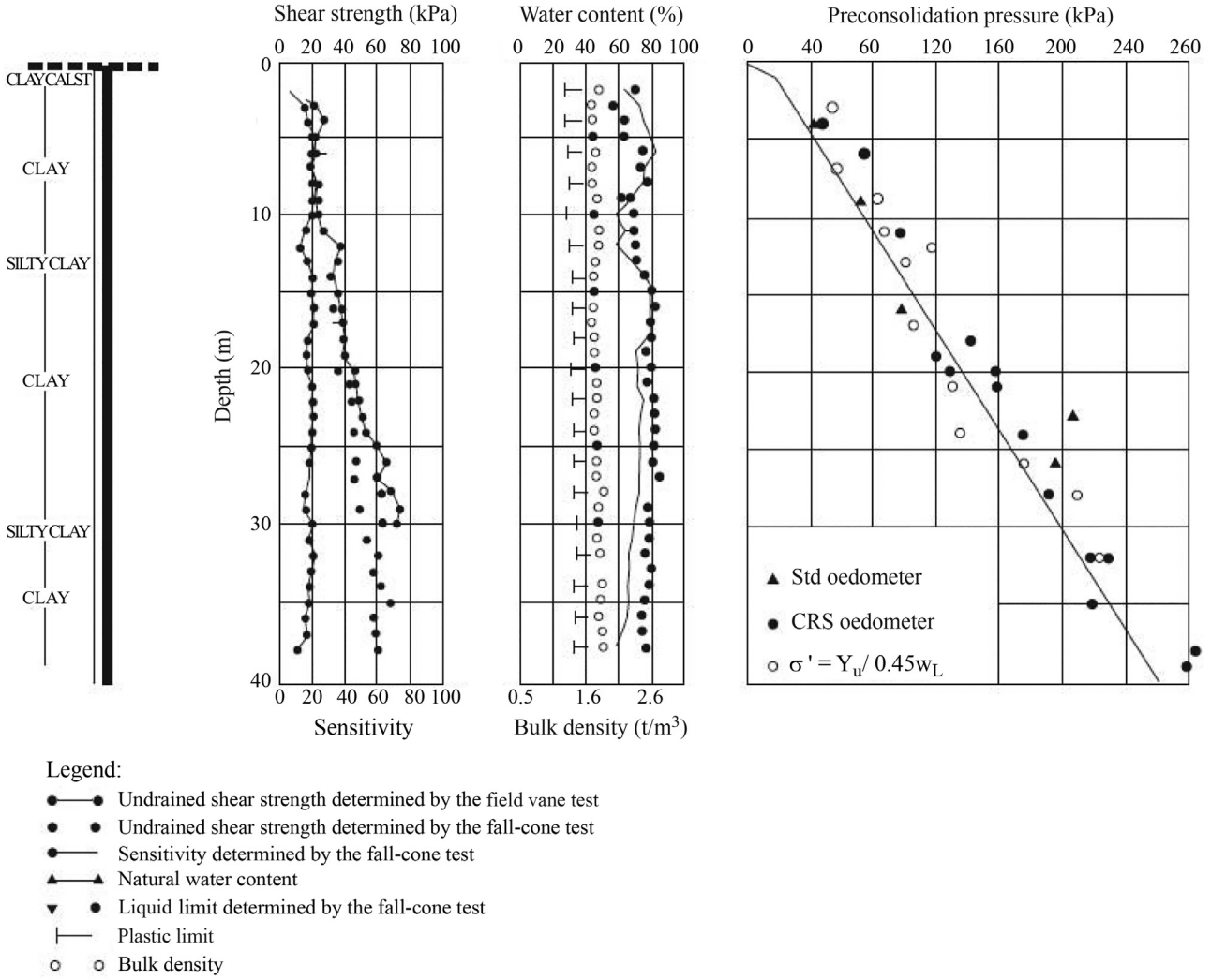

Figure 2 - Main geotechnical parameters of the subsoil (modified after Van Impe, 1999).

overconsolidated, given the fact that standard and CRS oedometer laboratory tests yielded preconsolidation pressures just above the values of vertical effective stress in the soil layer.

4. Numerical Tools and Assumptions for Analysis

The program GARP (Geotechnical Analysis of Raft with Piles, Poulos & Small, 1998) was adopted to evaluate the behavior of the rectangular piled raft foundation at Gothenburg that was subjected to a distributed vertical loading. It is based on a simplified form of a hybrid program in which the raft is represented as a linear elastic plate (via finite elements) and the soil can be modeled either as an elastic layered continuum or as a "Winkler" spring medium. The piles are represented by elastic-plastic springs that can interact with each other and with the raft. Limiting values of contact pressure (beneath the raft) and pile capacity can also be specified. By analyzing the raft using the finite element technique, rather than via finite differences, it is possible to numerically simulate irregular shaped rafts, which can also be subjected to uniform or concentrated loads.

As mentioned above, GARP also considers "interaction factors" between the springs that represent the piles. Such factors are computed via the use of another well-established software program DEFPIG (Deformation Analysis of Pile Groups, Poulos, 1990). This latter program determines the deformations and load distribution within a group of piles subjected to general loading. It was specifically written for piles designed using the "standard approach", by considering a group of identical elastic piles having axial and lateral stiffness that are constant with depth. It also allows for the eventual slippage between the piles and the surrounding soil. The stress distributions are computed from the theory of elasticity, more specifically from Mindlin's solutions for an isotropic, homogeneous, linear elastic medium. It can also consider, although in a simplified manner, the soil non-homogeneity along the length of the pile (*i.e.*, variation of the soil modulus with depth).

Both programs were used by adopting several simplified assumptions regarding the pile, raft and soil characteristics. These assumptions were necessary due to the simplified way in which these analyses were done, and also due to the lack of detailed information on this particular case history, as previously mentioned.

The following assumptions were made:

- Soil Profile: 55 m of soft to medium clay (average $Su \approx 30$ kPa varying from 20 to 60), overlying a rock surface. GARP took into consideration the soil parameters (Young's Modulus and Poisson's ratio) down to this lower limit of depth, where an extremely rigid (rock) surface was adopted. A constant drained Young's Modulus of 8200 kPa (lower limit) and 15000 kPa (upper limit) respectively were considered in the parametric analyses with the clay profile, together with a variable drained modulus ($E's$) increasing from 6600 to 11800 kPa). These values are applicable to driven piles in clay, and were estimated by adopting the correlation between shear strength and modulus expressed in Poulos and Davis (1980). A drained Young's Modulus of 5000 MPa was adopted for the rock surface. All DEFPIG and GARP analyses considered an average clay Poisson's ratio of 0.4. The water level was initially assumed to be at the ground surface, being lowered to an average level of 1.5 m below ground surface to take into consideration excavation effects (to be described below). This was based on possible range of values adopted during excavation and dewatering at this site – the real values are unknown to the authors;
- Pile Characteristics and Location: The elastic modulus of the pile was considered as constant during GARP analyses, being obtained via DEFPIG analysis with the assumed soil profile and Young's moduli, and with the given pile characteristics. The 104 composite floating piles were considered to be vertical (and uniform) with a constant diameter of 0.3 m, and length of 26 m. They were also considered to be mainly of timber, with an assumed Young's Modulus of 18000 MPa and Poisson's ratio of 0.2. In all GARP analyses the piles were assumed to apply a uniform pressure to square elements of similar area (to the pile section) in the raft;
- Raft Characteristics and Location: The Young's Modulus of the raft was assumed to be 25000 MPa, its Poisson's ratio to be 0.2, and its thickness to be 0.4 m. The base of the raft was assumed to be at the top level of the piles, with full contact with the underlying soil. An approximate dimension of 75 x 12 m (area ≈ 1000 m^2) was adopted in the analyses, with uniform pressures of 61.5, 35 and 30 kPa (parametric analyses) evenly distributed around the top surface of the raft – again, to be explained soon;
- Bearing Capacity of Pile and Raft: The long term bearing capacity of the piles was estimated and used, since the final, total settlement was desired. The point bearing capacity was calculated via a traditional effective stress approach. A drained friction angle of 25° was assumed for the clay. The shaft resistance was calculated via the "Beta" method for drained soils, using the same angle of 25° and assuming a coefficient of lateral pressure K_0 of 0.8 (OCR > 1). These are typical values found in the literature for marine clays (assuming that variations can possibly happen). The total depth of the piles was taken into consideration for the calculation of the vertical stress levels, assuming a bulk unit weight of 16.5 kN/m^3 for the soil layer. The group efficiency was estimated via the Poulos & Davis (1980) equation, which considers the sum of the ultimate capacities of individual piles and the ultimate load capacity of the "block" containing piles

and soil. An efficiency very close to 1.0 was calculated, and a unit value was therefore assumed. A drained bearing capacity was also calculated for the raft, adopting the Terzaghi (1943) equation again using a friction angle of 25° for the clay;

- Interaction Factors: These were obtained via the DEFPIG analysis, and used within GARP for pile/pile and pile/raft settlement interactions – given the lack of pile load tests on the site (none was found or apparently published). These interactions were limited to a horizontal spacing equal to the total length of the pile, *i.e.* 26 m and were assumed to be zero for greater spacings. The raft/raft and raft/pile interactions were obtained via the Boussinesq elastic equations, assuming an elastic continuum model and making approximate allowance for soil layering (*E's* variable);
- Pile and Raft Discretization: A non-symmetrical mesh with 940 nodes and 855 elements was assumed for the raft in the GARP analyses, as depicted in Fig. 3. The piles were introduced in the nodes (crossings) of this same figure, following the real disposition depicted in Fig. 1. In the DEFPIG analysis each pile was divided into 52 elements, each 0.5 m in length;
- Initial Numerical Analysis: A drained Young's Modulus of 8200 kPa and 15000 kPa was adopted for the clay. A calculated raft pressure of 61.5 kPa was adopted for the long term settlement analysis – Cases 1 and 4. These cases were followed by another analysis with a variable Young Modulus, keeping the same raft pressure – Case 6;
- Parametric Analysis: Six cases were analyzed according to Table 1. The soil Young's Modulus was considered as constant with depth (8200 and 15000 kPa – cases 1 to 5) with depth or variable (see table – case 6). The pressure on top of the raft was considered as 61.5 kPa uniformly distributed, in accordance to the published total load of the house (61.5 MN) and raft area of around 997 m^2 in accordance to cases 1, 4 and 6. The final net effective pressures of 30 and 35 kPa, adopted in cases 2, 3 and 5, were calculated by considering the excavation process;

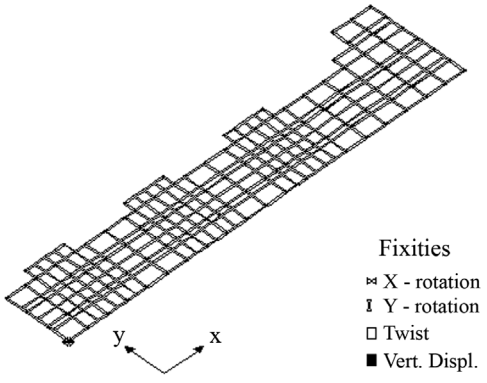

Figure 3 - Discretization of the finite element mesh of the foundation (raft and piles).

Table 1 - Parametric analyses adopted in this manuscript.

Case	*E's* (kPa)	Δ*P* raft (kPa)	Raft position
1	8200	61.5	Surface
2	8200	35	Buried
3	8200	30	Buried
4	15000	61.5	Surface
5	15000	30	Buried
6	Variable*	61.5	Surface

**E's* varying from 6600 kPa (top) to 11800 kPa (bottom of layer).

- Excavation sequence: By analyzing the accessed information of the original Hansbo (1993) paper, it appears that the raft was not cast on the deposit's surface, but rather buried on the subsoil. It was then estimated to have been constructed within an excavation of 2.5 m with the final water table at 1.5 m below ground surface. A simplified approach (hand calculation) was carried out to evaluate the net final effective pressure at raft level (as stated before, around 30 to 35 kPa). This approach adopted the same qualitative soil behavior as numerically found by Hsi & Small (1992) when simulating a 1-D excavation in a poro-elastic material. It was considered that the raft load was applied immediately after the soil excavation, *i.e.*, before any pore pressure change from negative to positive values – which is obviously another simplified assumption.

5. Results and Discussions

5.1. Overall results

The results of the numerical analyses were compared in terms of the extreme (maximum and minimum) values of settlement and moment (in both x and y directions). The load sharing between the piles and the raft was also computed and compared. These results are presented in Table 2, while Figs. 4 to 6 depict the contours of vertical settlement respectively obtained for Cases 1, 4 and 2. The discussion on the results comes in an itemized manner after that.

The contour legend represents the limits (in meters) for the obtained settlement results. For instance, in Fig. 6 the black (central) region represents the area of the raft with derived settlements between 4.5 and 5 x 10^{-2} m, *i.e.*, 4.5 to 5 cm.

The comparison in terms of absolute extreme values is useful to indicate general behavioral tendencies from the different input parameters adopted with this particular piled raft foundation.

Hence, some general observations can be drawn from the results of Table 2 and from Figs. 4 to 6:

- By increasing the Young's Modulus of the soil, while keeping all other variables constant, there is a tendency for both (max./min.) settlements and moments to de-

Table 2 - Settlement, moment and load sharing results from all the analyses.

Case	Settlement (cm)		Moments (kNm)				Load share (%)	
	max	min	Mx (max)	Mx (min)	My (max)	My (min)	Piles	Raft
1	8.3	3.0	128	-237	208	-113	75	25
2	4.7	1.7	73	-133	117	-63	75	25
3	4.1	1.5	62	-114	100	-54	75	25
4	5.3	1.9	100	-197	163	-107	66	34
5	2.6	0.9	49	-96	80	-52	66	34
6	7.4	2.6	129	-243	202	-118	77	23

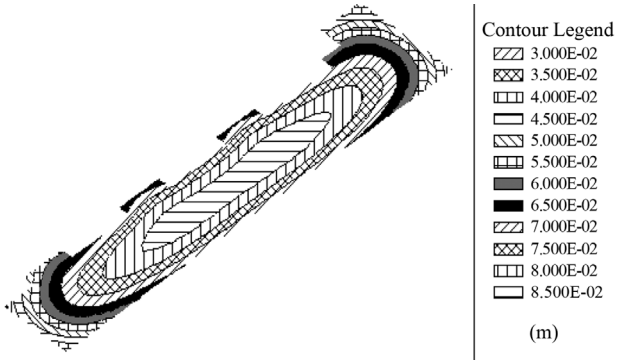

Figure 4 - Contours of vertical settlement (m) – CASE 1 – surface raft.

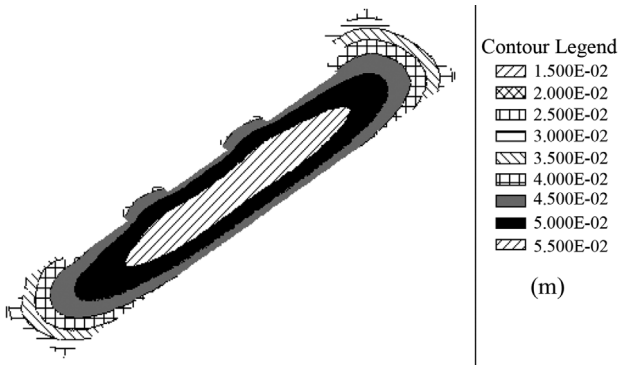

Figure 5 - Contours of vertical settlement (m) – CASE 4 – surface raft.

crease, as expected. There is also a slight tendency for the load carried by the raft to increase, reducing the load carried by the piles;

- For a variable *E's* rather than a constant *E's*, there is a tendency for the settlement values to be intermediate between those obtained with a constant *E's*. Nevertheless, similar results for moments and load division were obtained for both Cases 1 and 6;
- By decreasing the distributed pressure on top of the raft, while keeping all other variables constant, there is a tendency for both (max./min.) settlements and moments to decrease, again as expected. However, there was no variation in the load sharing between raft and piles;
- It is also noticed that similar contours of total settlement were obtained in Figs. 4 to 6 for each of the cases analyzed, although the magnitude of the settlements varied from one case to another. This indicates that all cases tended to develop similar patterns of settlement, albeit distinct values of input *E's*, raft position (buried or not) and raft pressure. Indeed, given the homogeneity of the subsoil, and linearity of loads and responses (structure and soil's modulus), such similarities were already anticipated.

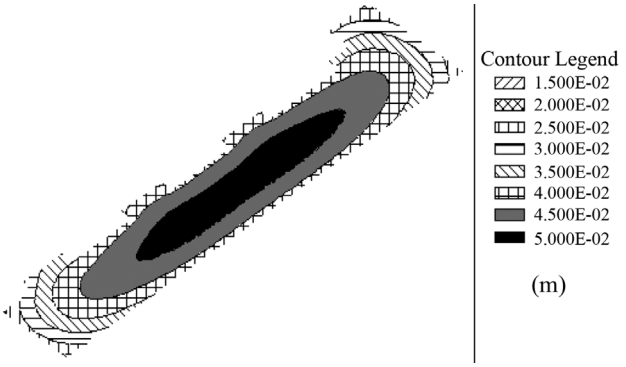

Figure 6 - Contours of vertical settlement (m) – CASE 2 – buried raft.

In summary, the analyses demonstrated the important influence of the assumed drained Young's Modulus of the clay, and the distributed load, on the predicted values of settlement and moment. The Young's Modulus has also some influence on the total load sharing between raft and piles, but to a lesser extent than the influence on the settlement.

5.2. "Class A" analyses and the assessment of the excavation

It was mentioned before that, despite the fact that this particular case history has already been published elsewhere (and the final total settlements are supposedly known), some effort has been made to characterize the numerical analyses as truly "Class A" predictions. That means, to check the predictions against the (unknown during analy-

sis) measured values. Hence, Cases 1, 4 and 6 (initial numerical analysis with the raft at surface) were analyzed solely on the basis of the information provided by Van Impe (1999) in the international exercise, without referring to the Hansbo (1993) or Hansbo & Källström (1983) papers.

The predicted settlements, presented in Table 2, varied from about 5 to 8 cm (maximum) and about 2 to 3 cm (minimum). In fact, as noted before, these settlements were strongly related to the assumed drained modulus of the clay, and the other assumptions in terms of raft pressure and position adopted for the input parameters. By comparing the predicted results with those from Hansbo (1993), depicted in Fig. 7, it was noticed that they are somewhat different from the measured "real" published settlements, which ranged from 2.5 (min.) to 4.2 cm (max.). That means, the experimental values were well below the predicted values at class A prediction from Table 2, indicating that either the model did not accomplish the nuances of the rheological phenomena or the input elastic parameters were slightly lower ("softer") than those from the real subsoil (or something else, as the actual stiffening effect of the basement beams on the overall displacement pattern).

In order to understand the possible reason for such discrepancies, the authors carefully reviewed the Hansbo (1993) paper. This extra exercise revealed that an excavation was probably carried out before the construction of the piled raft (as suspected by aforementioned comments). This excavation was not considered in the initial numerical analyses with Cases 1, 4 and 6, given the lack of detailed information about this particular case history. Indeed, the excavation process prior to the raft placement may have a large effect on the final settlement results, since it considerably changes the original stress state (see for instance Hsi & Small, 1992). According to Sales *et al.* (2010), the stress relief and preloading process that takes place during the excavation and casting of the foundation raft must be taken into account to properly simulate the loading pattern, and hence to accurately forecast the settlements at working load.

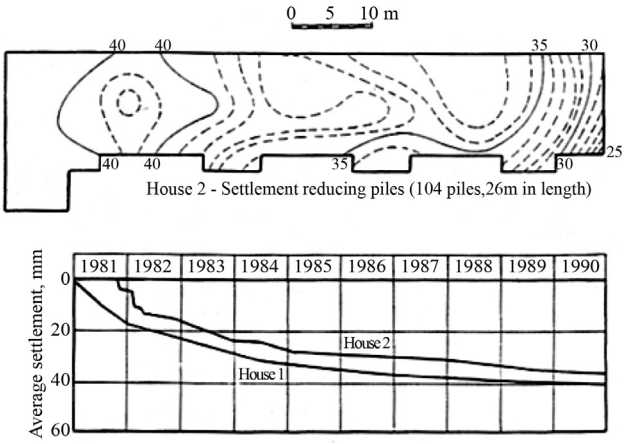

Figure 7 - Measured settlement contours in House 2 (modified after Hansbo, 1993).

In order to account for this effect, at least in a reasonable but simplified manner (as proposed by Ibáñez *et al.*, 2014), extra parametric analyses were made considering the excavation. The new assumption resulted in the final net effective pressures of 30 and 35 kPa below the raft, as adopted for Cases 2, 3 and 5 in which the raft was considered to be buried. Of course, in these particular cases, it is readily noticed that they consisted of "Class C" predictions for this particular exercise (as the authors already knew the "target" values), rather than "Class A" predictions as done before.

The new effective pressures were estimated by simple hand calculations where the effective vertical pressures below the raft were determined with the excavation effect on the groundwater pressure. That means, immediately after 2.5 m (1D) excavation the positive water pressure (with water table at ground surface) became negative in accordance to Hsi & Small (1992) advocated technique. Once the raft load is applied, by casting of the foundation, the water pressure changes again to a positive value. At this stage, it was assumed that two things took place simultaneously: The lowering of the water table from ground surface to 1.5 m below ground (dropped 1 m in height) and full dissipation of the excess pore pressures (positive excess in the previous step) to take into account long term effects. The final variation of net effective vertical pressures is simply the difference between initial and final values below the raft. Perhaps this procedure can be better visualized with the values of Table 3.

Within the context of the analyses carried out for Cases 2, 3 and 5, a reduction in the maximum settlement as high as 50% can be noticed in Table 2. It is also noticed that a variation on the effective Young's Modulus was also tried out from cases 2, 3 to 5, in order to improve even more the predictions (again, a typical "Class C" analysis since the measured results were known in advance allowing the optimization of the numerical output). The important point to note, however, relates to the fact that even by knowing beforehand the results, the present authors were unable to accurately and definitively predict the settlement pattern presented by Hansbo (1993), as depicted in Fig. 7. See, for instance, the marked differences in the pattern of vertical settlement from Figs. 6 to 7.

Although Fig. 6 presents settlement values close to the right magnitude, they were predicted to vary in a concentric "dishing" manner within the raft, which differs from the measured (real) pattern depicted in Fig. 7. This figure portrays higher settlements at the left side of the house, which could be due to some possible factors, as follows: uneven distribution of raft pressures (due to concentrated loading from existing columns), a variable clay layer profile and/or the stiffening effect of the foundation beams (in what is called as a "soil-superstructure effect"). Neither

Table 3 - Variation of pore, effective and total vertical pressures underneath the raft.

Condition	Pore pressure (kPa)	Eff. vertical pressure (kPa)	Total (*) vertical pressure (kPa)
Initial state before excavation	25	16.25	41.25
Immediately after 2.5 m excavation with GWT at surface	-16.25 (**)	16.25	0.0
Application of raft load and molding	—	—	61.5
After curing. GWT at surface	45.25	16.25	61.5
GWT at 1.5 m below surface and full consolidation	10	51.5	61.5
ΔEffective Net Vertical Pressure =		51.5 – 16.25 = ≈ 35 kPa	

*Considering a total unit weight of around 16.5 kN/m^3.
**Considering Hsi & Small (1992) approach.

conditions were considered herein, given the lack of detailed information on these parameters, as well as software capabilities.

In summary, the main observation of the final series of analyses is that the problem lacked a great deal of important information, even for a proper "Class C" prediction (see previous comment related to cases 2, 3 and 5). Besides of the shortcomings of these analyses, the present exercise was valuable in showing possible deficiencies in standard numerical design analyses, and the importance that the excavation effect, among others, has in fine tuning the settlement results. It has shown that the detailed knowledge of some input variables is essential for the proper numerical simulation of real engineering projects, and, besides all, that some extra external influential variables (nowadays considered as circumstantial aspects of the problem) should be taken into account in future numerical predictions of piled rafts.

Indeed, recently in Brazil (at its latest national geotechnical conference of 2016 – XVIII COBRAMSEG) colleagues from the geotechnical and structural area have agreed, in a special session of the event (soil-superstructure effects), that future analyses must deal somehow with this aspect (as done in a simplified manner by Cunha & Cambar, 2011), either in terms of the building structural modelling or in terms of the foundation discretization. Unfortunately, the designer is still far from reaching an agreement on how to do that in practice, and with what tools (and parameters). As a final piece of information given in this same conference, some "educated" accounts given by colleagues on the budgetary aspects of the design foresee an increase of 0.04% in the final price of the elaboration of the geotechnical design, *i.e.*, this component of the project would increase from around 0.20% of the total budget of the building construction to around 0.24%. Is the price increase worthy of the benefits of a better understanding of the whole superstructure – foundation system (hence more accurate analyses)? The future will hopefully provide answer.

6. Conclusions

The results of the present exercise highlight the fact that in practice it is extremely important to understand all input parameters which are required in the design of both piled rafts and standard (conventional) groups of piles. This is so regardless of the "accuracy" and capabilities of the numerical program in question.

This contribution has shown that it is not possible to precisely predict the behavior of piled rafts and group of piles, in both "Class A and C" analyses, without a full understanding of the problem and knowledge of its important input parameters, such as the raft geometry and load distribution (magnitude, pattern, variability with time), the excavation depth and sequence, the seasonal variability of the water level, the soil profile (depth, variability, layering), and, finally, without a comprehensive laboratory or in situ testing program. It has also allowed a clear perception of the possible influence of the lack of information of some of the above variables in the final numerical assessment of a published piled raft case history, particularly the excavation process (simulated in a simplified manner) and the soil-superstructure stiffening influence (not taken into account).

Acknowledgments

This research exercise was possible through a fruitful joint technical co-operation program from both the Universities of Sydney and Brasília, established since 1999, given the kind efforts from both Prof. Harry Poulos and John Small (now retired from the former university). The authors acknowledge their appreciation for the critical review / comments and technical papers kindly provided by Dr. K. Rainer Massarsch from Geo Risk & Vibration Scandinavia AB. The first author in particular would like to express his gratitude to the main Brazilian sponsorship organizations as the CNPq, CAPES, FINATEC and FAP-DF for all the scholarships and research grant/support he has received throughout this period in the GPFees Group (Research Group on Foundations, In Situ Testing and Retaining Struc-

tures – www.geotecnia.unb.br/gpfees) of the Geotechnical Post-Graduation Program of the University of Brasília.

References

Burland, J.B. (1995). Piles as settlement reducers. Keynote Address, 18th. Italian Conf. on Soil Mechanics, Pavia, pp. 21-34.

Clancy, P. & Randolph, M.F. (1996). Simple design tools for piled raft foundations. Géotechnique, 46(2):313-328.

Cunha, R.P. & Cambar, T.T. (2011). Numerical and experimental assessment of the soil-structure interaction effect of a building in the Brazilian central area. Proc. 14th. Pan-American Conf. on soil Mech. and Geot. Engineering, Toronto, pp. 1-7, CD-ROM.

Cunha, R.P. & Sales, M.M. (1998). Field load tests of piled footings founded on a tropical porous clay. Proc. 3rd Inter. Geot. Seminar Deep Foundation on Bored and Auger Piles, Ghent, pp. 433-438.

Cunha, R.P.; Poulos, H.G. & Small, J.C. (2001). Investigation of design alternatives for a piled raft case history. ASCE Journal of Geotechnical and Geoenvironmental Engineering, 127(8):635-641.

Cunha, R.P.; Small, J.C. & Poulos, H.G. (2000a). "Class C" analysis of a piled raft case history in Gothenburg, Sweden. Year 2000 Geotechnics – Geotechnical Engineering Conference, Bangkok, v. 1, pp. 271-280.

Cunha, R.P.; Small, J.C. & Poulos, H.G. (2000b). Parametric analysis of a piled raft case history in Uppsala, Sweden. Fourth Brazilian Seminar of Special Foundation Engineering and Geotechnics-SEFE IV, São Paulo, v. 2, pp. 381-390.

Hansbo, S. (1993). Interaction problems related to the installation of pile groups. Proc. 2nd Inter. Geot. Seminar Deep Foundation on Bored and Auger Piles, Ghent, pp. 59-66.

Hansbo, S. & Källström, R. (1983). A case study of two alternative foundation principles. Väg-och Vattenbyggaren, 7(8):23-27.

Hsi, J.P. & Small, J.C. (1992). Simulation of excavation in a poro-elastic material. Int. Journal for Numerical and Analytical Methods in Geomechanics, 16(1):25-43.

Ibáñez Mora, L.O.; Cunha, R.P. & Fernández, D.H. (2014). Analysis of foundations on compensated piled rafts. XVII Cong. Bras. Mec. Solos e Eng. Geotécnica – COBRAMSEG 2014, Goiânia, pp. 1-7. CD-ROM. (In Portuguese).

Mandolini, A. & Viggiani, C. (1997). Settlement of piled foundations. Geotechnique, (47)4:791-816.

O'Neill, M.W.; Caputo, V.; De Cock, F.; Hartikainen, J. & Mets, M. (1996). Case histories of pile-supported rafts. Report for ISSMFE TC18, Univ. of Houston, Texas.

Ottaviani, M. (1975). Three-dimensional finite element analysis of vertically loaded pile groups. Géotechnique, 25(2):159-174.

Poulos, H.G. (1990). Defpig User's Guide. Centre for Geotechnical Research, University of Sydney, 55 p.

Poulos, H.G. (1991). Foundation Economy Via Piled-Raft Systems. Piletalk International, Kuala Lumpur, pp. 97-106.

Poulos, H.G. (1998). The Pile-Enhanced Raft - An Economical Foundation System. Keynote Lecture at XI Brazilian Congress on Soil Mechanics and Geotechnical Engineering, Brasília, v. 4, pp. 27-43.

Poulos, H.G. & Davis, E.H. (1980). Pile Foundation Analysis and Design. Robert E. Krieger Publishing Co. Sydney, 397 p.

Poulos, H.G. & Small, J. C. (1998). Garp User's Manual. Coffey Partners International Pty Ltd. Sydney, 23 p.

Randolph, M. (1994). Design methods for pile groups and piled rafts. XIII Int. Conf. on Soil Mechanics and Found. Engineering, New Dehli, v. 5, pp. 61-82.

Sales, M.M.; Small, J.C. & Poulos, H.G. (2010). Compensated piled rafts in clays soils: behavior, measurements and predictions. Canadian Geotechnical Journal, 47(3):327-345.

Ta, L.D. & Small, J.C. (1996). Analysis of piled raft systems in layered soils. Int. Journal for Numerical and Analytical Methods in Geomechanics, 20(1):57-72.

Terzaghi, K. (1943). Theoretical Soil Mechanics. New York, John Wiley and Sons, 510 p.

Van Impe, W.F. (1999). International exercise on piled rafts – Sweden Examples. International Society of Soil Mechanics and Geotechnical Engineering TC-18 Committee. WVI/HDC/WIV.3.5 Report – Gent University.

Discussion

Soils and Rocks
v. 41, n. 1

Discussion

Rainfall Effects on Pore Pressure Changes in a Coastal Slope of the Serra do Mar in Santa Catarina

Discussion by:
K.V. Bicalho, C. Romanel

The writers appreciate the contributions the authors of "Rainfall Effects on Pore Pressure Changes in a Coastal Slope of the Serra do Mar in Santa Catarina" made to improving the quality of field observations involving climate/soil interaction, and would like to offer some comments addressed to the authors.

The authors present a very interesting full-scale study carried out in a densely instrumented highway slope in the South of Brazil. The slope had a history of instability movements due to intense rainfall, with debris accumulation on the highway and traffic interruption. Geotechnical instrumentation including vibrating wire piezometers, electrical tensiometers, conventional slope inclinometers, and a rain gauge was installed in the slope.

The authors investigated how rainfall causes changes in the piezometric pore pressure and soil matric suction in the monitored slope from May 2012 to March 2013. Laboratory tests classified the top soil as a silty sand. The analysis of the results showed that, during the field monitoring period, there were no heavy rains (*i.e.*, between 16 and 50 mm/h). Three monitoring periods were identified by the frequency and intensity of rainfalls, and the authors concluded that "the soil pore pressure monitoring instruments showed significant variations in the high frequency period and low intensity rainfall, and little variation in low frequency period and high intensity rainfall".

The writers would like to include additional comments on the influence of rainfall changes on the soil suction distribution observed in soil slopes. The authors mention that tensiometer measurements showed an increase in the soil suction "during the period with less rain and a decrease as the rainfall occurs". It is important to note that the infiltration capacity varies not only with the soil type and frequency and intensity of precipitation, but also with the soil water content condition. If a soil is initially dry, the infiltration capacity is high (Fetter, 1994). In an experimental embankment in the Northeast of France, rainfall events caused significant effects on the soil suction distribution in the initial period of water surplus after a long period of water deficit (Bicalho *et al.*, 2015).

It should also be observed that slope instability is affected by a combination of various factors, including intensity and duration of rainfall, duration of previous rainfall, soil initial conditions, soil permeability (or hydraulic conductivity), vegetation, slope geometry and geographical location. Among these factors, some are more significant than others, and it is not straightforward to weight the effect of any individual factor.

Numerical studies on the effect of soil permeability on soil suction distribution (Pradel & Raad, 1993, and Tsaparas *et al.*, 2002) suggest that less permeable soil slopes may fail after sufficient duration of rainfall, while failure of slopes with comparatively high permeability may take place for shorter-duration and greater-intensity rainfalls. The water hydraulic conductivity function and the water storage function for an unsaturated soil are related to the soil water retention (or characteristic) curve (SWRC), a relationship between the amount of water in the soil and the suction in the pore water. Toll *et al.* (2012) mention that the water unsaturated hydraulic conductivity can drop by 4-5 orders of magnitude relative to the saturated permeability, Ksat, as the soil desaturates. Taibi *et al.* (2009) present experimental results on two fine-grained soils showing that the effective hydraulic conductivity has a small value (≈ 0.05 Ksat) while the degree of saturation is relatively high (≈ 80%). These results are consistent with the measured hydraulic conductivity values reported by Taibi (1994) and Bicalho (1999) for fine-grained soils. As a result, knowledge of the SWRC is fundamental for application of unsaturated soil mechanics into geotechnical problems.

These issues indicate that the rainfall events may not be the only factors to explain the observed variations in soil suction with time at specified depths in the soil slope. Additional measurements of spatial and temporal changes in soil suction and corresponding water content (*i.e.*, the field

Article by A.A.M. González *et al.*, published in Soils and Rocks, 40(3):263-278 (2017), e-mail: andresmgonzaleza@gmail.com.

SWRC), as well as in-situ measurements of water hydraulic conductivity functions at predefined locations within the slope, should be continuously made in order to further understand the soil suction responses to natural climatic variations over long term periods.

References

Bicalho, K.V. (1999). Modeling Water Flow in an Unsaturated Compacted Soil. Ph.D. Thesis, University of Colorado, Boulder, Colorado, USA.

Bicalho, K.V.; Vivacqua, G.P.D.; Cui, Y.-J.; Froumentin, M.; Mercadier, D. &, Tang, A.M. (2015). Experimental investigation of soil-atmosphere interaction in an instrumented embankment constructed with two treated clays. Soils and Rocks, 38(2):149-162.

Fetter, C.W. (1994). Applied Hydrogeology, 3rd ed. Macmillan College Publishing, Inc., New York.

Pradel, D. & Raad, G. (1993). Effect of permeability on superficial stability of homogeneous slopes. Journal of Geotechnical Engineering, 119(2):315-332.

Taibi, S. (1994). Comportement Mécanique et Hydraulique des Sols Soumis à Une Pression Interstitielle Négative – Etude Expérimentale et Modélisation. Thèse de Doctorat, Ecole Centrale de Paris, France.

Taibi, S.; Bicalho, K.V.; Sayad-Gaidi, C. & Fleureau, J-M. (2009). Measurements of unsaturated hydraulic conductivity functions of two fine-grained materials. Soil and Foundation, 49(2):176-181.

Toll, D.G.; Mendes, J.; Hughes, P.N.; Glendinning, S. & Gallipoli, D. (2012). Climate change and the role of unsaturated soil mechanics. Geotechnical Engineering Journal of the SEAGS & AGSSEA, 43(1):76-82.

Tsaparas, I.; Rahardjo, H.; Toll, D.G. & Leong, E.C. (2002). Controlling parameters for rainfall-induced landslides. Comput. and Geotech., 29(1):1-27.

SOILS and ROCKS
An International Journal of Geotechnical and Geoenvironmental Engineering

Publication of
ABMS - Brazilian Association for Soil Mechanics and Geotechnical Engineering
SPG - Portuguese Geotechnical Society
Volume 41, N. 1, January-April 2018

Author index

TEIXEIRA DUARTE
ENGENHARIA E CONSTRUÇÕES, S.A.

- Head Office
  Lagoas Park – Edifício 2
  2740-265 Porto Salvo - Portugal
  Tel.:(+351) 217 912 300
  Fax: (+351) 217 941 120/21/26

- Algeria
  Parc Miremont – Rua A, Nº136 - Bouzareah
  16000 Alger
  Tel.:(+213) 219 362 83
  Fax: (+213) 219 365 66

- Spain
  Avenida Alberto Alcocer, nº24 – 7º C
  28036 Madrid
  Tel.:(+34) 915 550 903
  Fax: (+34) 915 972 834

- Angola
  Alameda Manuel Van Dunen 316/320 - A
  Caixa Postal 2857 - Luanda
  Tel.:(+34) 915 550 903
  Fax: (+34) 915 972 834

- Brazil
  Rua Iguatemi, nº488 – 14º - Conj. 1401
  CEP 01451 - 010 - Itaim Bibi - São Paulo
  Tel.: (+55) 112 144 5700
  Fax: (+55) 112 144 5704

- Mozambique
  Avenida Julyus Nyerere, 130 – R/C
  Maputo
  Tel.:(+258) 214 914 01
  Fax: (+258) 214 914 00

www.teixeiraduarte.pt

> Prospecção Geotécnica
Site Investigation
> Consultoria Geotécnica
Geotechnical Consultancy
> Obras Geotécnicas
Ground Treatment-Construction Services
> Controlo e Observação
Field Instrumentation Services and Monitoring Services
> Laboratório de Mecânica de Solos
Soil and Rock Mechanics Laboratory

Certificada ISO 9001 por

BVQi

Geocontrole

Parque Oriente, Bloco 4, EN10
2699-501 Bobadela LRS
Tel. 21 995 80 00
Fax. 21 995 80 01
e.mail: mail@geocontrole.pt
www.geocontrole.pt

Geocontrole
Geotecnia e Estruturas de Fundação SA

ENGINEERING AND ENVIRONMENTAL CONSULTANTS


COBA


GEOLOGY AND GEOTECHNICS

Hydrogeology • Engineering Geology • Rock Mechanics • Soil Mechanics • Foundations and Retaining Structures • Underground Works • Embankments and Slope Stability Environmental Geotechnics • Geotechnical Mapping

Water Resources Planning and Management
Hydraulic Undertakings
Electrical Power Generation and Transmission
Water Supply Systems and Pluvial and Wastewater Systems
Agriculture and Rural Development
Road, Railway and Airway Infrastructures
Environment
Geotechnical Structures
Cartography and Cadastre
Safety Control and Work Rehabilitation
Project Management and Construction Supervision

PORTUGAL
CENTER AND SOUTH REGION
Av. 5 de Outubro, 323
1649-011 LISBOA
Tel.: (351) 210125000, (351) 217925000
Fax: (351) 217970348
E-mail: coba@coba.pt
www.coba.pt

Av. Marquês de Tomar, 9, 6º.
1050-152 LISBOA
Tel.:(351) 217925000
Fax:(351) 213537492

NORTH REGION
Rua Mouzinho de Albuquerque, 744, 1º.
4450-203 MATOSINHOS
Tel:(351) 229380421
Fax:(351) 229373648
E-mail: engico@engico.pt

ANGOLA
Praceta Farinha Leitão, edifício nº 27, 27-A - 2º Dto
Bairro do Maculusso, LUANDA
Tel./Fax: (244) 222338 513
Cell: (244) 923317541
E-mail: coba-angola@netcabo.co.ao

MOZAMBIQUE
Pestana Rovuma Hotel. Centro de Escritórios.
Rua da Sé nº114. Piso 3, MAPUTO
Tel./Fax: (258) 21 328 813
Cell:(258) 82 409 9605
E-mail: coba.mz@tdm.co.mz

ALGERIA
09, Rue des Frères Hocine
El Biar - 16606, ARGEL
Tel.: (213) 21 922802
Fax: (213) 21 922802
E-mail: coba.alger@gmail.com

BRAZIL
Rio de Janeiro
COBA Ltd. - Rua Bela 1128
São Cristóvão
20930-380 Rio de Janeiro RJ
Tel.: (55 21) 351 50 101
Fax: (55 21) 258 01 026

Fortaleza
Av. Senador Virgílio Távora 1701, Sala 403
Aldeota - Fortaleza CEP 60170 - 251
Tel.: (55 85) 3261 17 38
Fax: (55 85) 3261 50 83
E-mail: coba@esc-te.com.br

UNITED ARAB EMIRATES
Corniche Road – Corniche Tower - 5th Floor - 5B
P. O. Box 38360 ABU DHABI
Tel.: (971) 2 627 0088
Fax: (971) 2 627 0087

Much more support to your business.

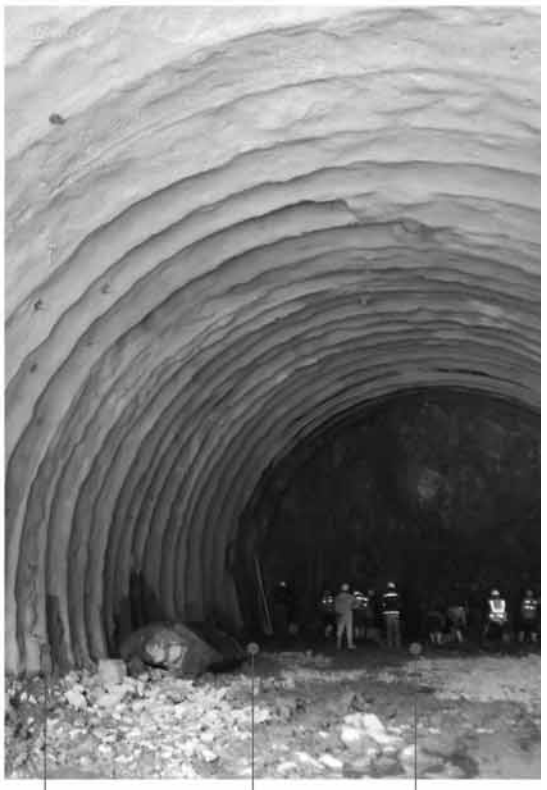

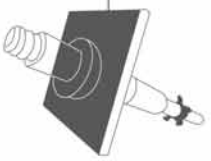

Incotep - Anchoring Systems
Incotep anchoring Systems is a division of Açotubo Group, which engaged in the development of Anchoring Systems, used in geotechnical and structural applications where high quality prestressing systems are designed to meet diverse needs.

Know our solutions for your processes

- Self Drilling Injection Hollow Bar
- Cold Rolled Thread Bars and Micropiles
- Hot Rolled Thread Bars
- Incotep Tie Rods (Port and Dike Construction)
- Umbrella Tubes Drilling System
- Pipes for Root Piles, among others

www.incotep.com.br
+55 11 2413-2000

Incotep
Sistemas de Ancoragem

A company Açotubo Group

Conheça mais:
www.geobrugg.com/pt/taludes

GEOBRUGG®
BRUGG
Safety is our nature

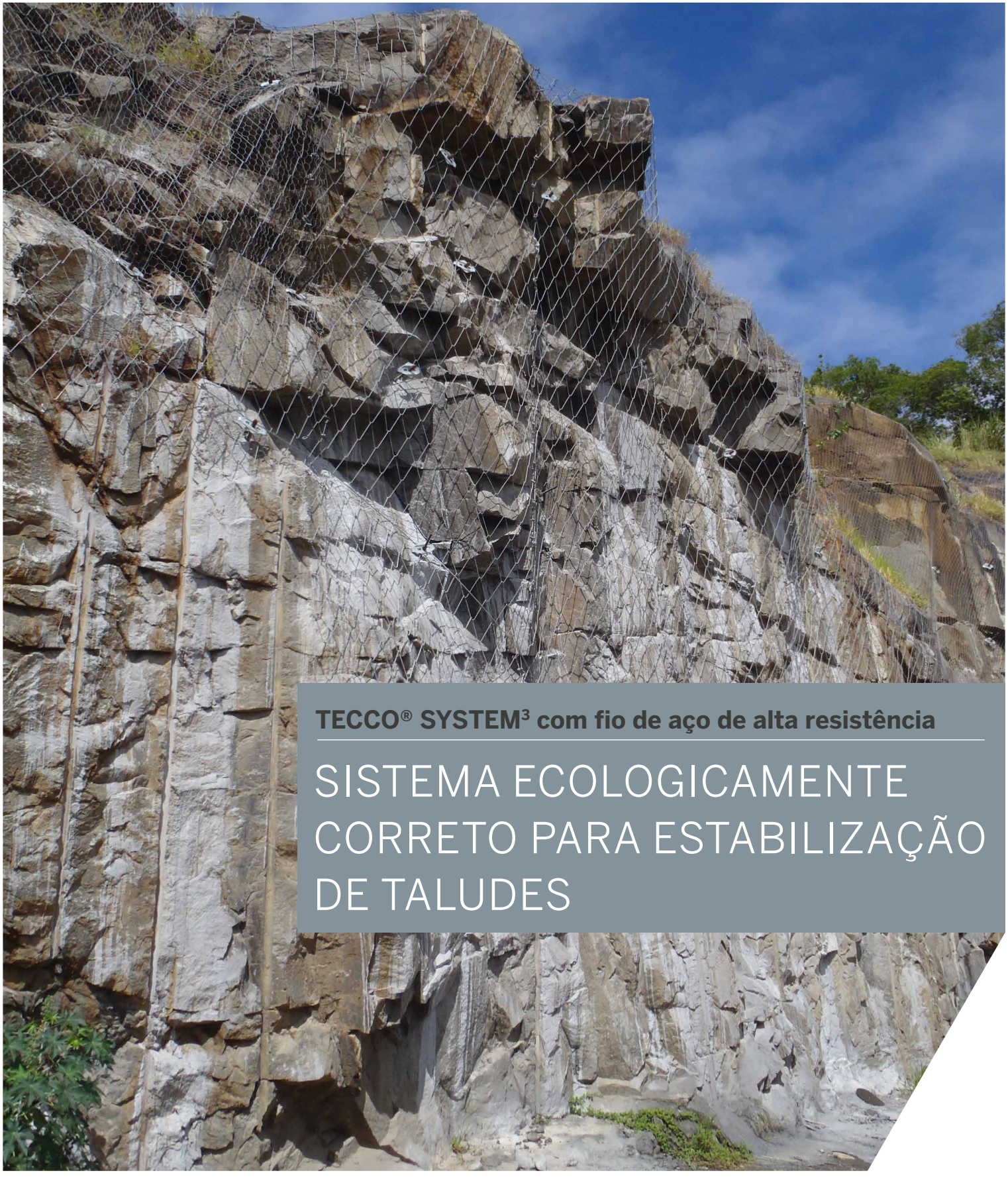

TECCO® SYSTEM³ com fio de aço de alta resistência

SISTEMA ECOLOGICAMENTE CORRETO PARA ESTABILIZAÇÃO DE TALUDES

Geobrugg AG | Rua Visconde de Pirajá, 82 sl.606 | 22410-003 - Rio de Janeiro, Brasil | Phone + 55 21 3624 1449 | www.geobrugg.com | info@geobrugg.com

A strong, lasting connection.

With a history of over 150 years of pioneering in geosynthetics, we strive to create solutions for the most diverse engineering challenges.

Our business areas:

Earthworks and Foundations

Environmental Engineering

Roads and Pavements

Hydraulic Engineering

Talk to HUESKER Brasil:
www.HUESKER.com.br
HUESKER@HUESKER.com.br
+55 (12) 3903 9300

Follow HUESKER Brasil in social media:

HUESKER
Ideen. Ingenieure. Innovationen.

Instructions for Submission of Manuscripts

Category of the Papers

Soils and Rocks is the international scientific journal edited by the Brazilian Association for Soil Mechanics and Geotechnical Engineering (ABMS) and the Portuguese Geotechnical Society (SPG). The aim of the journal is to publish (in English) original research and technical works on all geotechnical branches.

According to its content the accepted paper is classified in one of the following categories: Article paper, Technical Note, Case Study or Discussion. An article paper is an extensive and conclusive dissertation about a geotechnical topic. A paper is considered as a technical note if it gives a short description of ongoing studies, comprising partial results and/or particular aspects of the investigation. A case study is a report of unusual problems found during the design, construction or the performance of geotechnical projects. A case study is also considered as the report of an unusual solution given to an ordinary problem. The discussions about published papers, case studies and technical notes are made in the Discussions Section.

When submitting a manuscript for review, the authors should indicate the category of the manuscript, and is also understood that they:

a) assume full responsibility for the contents and accuracy of the information in the paper;

b) assure that the paper has not been previously published, and is not being submitted to any other periodical for publication.

Manuscript Instructions

Manuscripts must be written in English. The text is to be typed in a word processor (preferably MS Word), **single column**, using ISO A4 page size, left, right, top, and bottom margins of 25 mm, Times New Roman 12 font, and line spacing of 1.5. All lines and pages should be numbered. The text should be written in the third person.

The first page of the manuscript must include the title of the paper followed by the names of the authors with the abbreviation of the most relevant academic title. The affiliation, address and e-mail must appear below each author´s name. An abstract of 200 words follows after the author´s names. A list with up to six keywords at the end of the abstract is required.

Although variations on the sequence and title of each section are possible, it is suggested that the text contains the following sections: Introduction, Material and Methods, Results, Discussions, Conclusions, Acknowledgements, References and List of Symbols. A brief description of each section is given next.

Introduction: This section should indicate the state of the art of the problem under evaluation, a description of the problem and the methods undertaken. The objective of the work should be clearly presented at the end of the section.

Materials and Methods: This section should include all information needed to the reproduction of the presented work by other researchers.

Results: In this section the data of the investigation should be presented in a clear and concise way. Figures and tables should not repeat the same information.

Discussion: The analyses of the results should be described in this section.

Conclusions: The content of this section should be based on the data and on the discussions presented.

Acknowledgenments: If necessary, concise acknowledgements should be presented in this section.

References: References to other published sources must be made in the text by the last name(s) of the author(s), followed by the year of publication, similarly to one of the two possibilities below:

…while Silva & Pereira (1987) observed that resistance depended on soil density… or *It was observed that resistance depended on soil density (Silva & Pereira, 1987).*

In the case of three or more authors, the reduced format must be used, *e.g.*: Silva *et al.* (1982) or (Silva *et al.*, 1982). Two or more citations belonging to the same author(s) and published in the same year are to be distinguished with small letters, *e.g.*: (Silva, 1975a, b, c.). Standards must be cited in the text by the initials of the entity and the year of publication, *e.g.*: ABNT (1996), ASTM (2003).

Full references shall be listed alphabetically at the end of the text by the first author´s last name. Several references belonging to the same author shall be cited chronologically. Some examples are listed next:

Papers: Bishop, A.W. & Blight, G.E. (1963). Some aspects of effective stress in saturated and unsaturated soils. Geotechnique, 13(2):177-197.

Books: Lambe, T.W. & Whitman, R.V. (1979). Soil Mechanics, SI Version. John Wiley & Sons, New York, 553 p.

Book with editors: Sharma, H.D.; Dukes, M.T. & Olsen, D.M. (1990). Field measurements of dynamic moduli and Poisson's ratios of refuse and underlying soils at a landfill site. Landva, A. & Knowles, G.D. (eds), Geotechnics of Waste Fills - Theory and Practice, American Society for Testing and Materials - STP 1070, Philadelphia, pp. 57-70.

Proceedings (printed matter or CD-ROM): Jamiolkowski, M.; Ladd, C.C.; Germaine, J.T. & Lancellotta, R. (1985). New developments in field and laboratory testing of soils. Proc. 11th Int. Conf. on Soil Mech. and Found. Engn., ISSMFE, San Francisco, v. 1, pp. 57-153. (specify if CD ROM).

Thesis and dissertations: Lee, K.L. (1965). Triaxial Compressive Strength of Saturated Sands Under Seismic Loading Conditions. PhD Dissertation, Department of Civil Engineering, University of California, Berkeley, 521 p.

Standards: ASTM (2003). Standard Test Method for Particle Size Analysis of Soils - D 422-63. ASTM International, West Conshohocken, Pennsylvania, USA, 8 p.

Internet references: Soils and Rocks available at http://www.abms.com.br and downloaded on August 6th 2003.

On line first publications must also bring the digital object identifier (DOI) at the end.

Figures shall be either computer generated or drawn with India ink on tracing paper. Computer generated figures must be accompanied by the corresponding digital file (.tif, .jpg, .pcx, etc.). All figures (graphs, line drawings, photographs, etc.) shall be numbered consecutively and have a caption consisting of the figure number and a brief title or description of the figure. This number should be used when referring to the figure in text. Photographs should be black and white, sharp, high contrasted and printed on glossy paper.

Tables shall be numbered consecutively in Arabic and have a caption consisting of the table number and a brief title. This number should be used when referring to the table in the text. Units should be indicated in the first line of the table, below the title of each column. Acronyms should be avoided. When applicable, the units should come right below the corresponding column heading. Additional comments can be placed as footnotes.

Equations shall appear isolated in a single line of the text. Numbers identifying equations must be flushed with the right margin. International System (SI) units must be used. The definitions of the symbols used in the

equations must appear in the List of Symbols. It is recommended that the symbols used are in accordance with Lexicon in 8 Languages, ISSMFE (1981) and the ISRM List of Symbols.

The text of the submitted manuscript (including figures, tables and references) intended to be published as an article paper or a case history should not contain more than 30 pages, formatted according to the instructions mentioned above. Technical notes and discussions should have no more than 15 and 8 pages, respectively. Longer manuscripts may be exceptionally accepted if the authors provide proper explanation for the need of the required extra space in a cover letter.

Discussion

Discussions must be written in English. The first page of a discussion should contain:

The title of the paper under discussion;

Name of the author(s) of the discussion, followed by their position, affiliation, address and e-mail. The author(s) of the discussion should refer to himself (herself/themselves) as the reader(s) and to the author(s) of the paper as the author(s).

Figures, tables and equations should be numbered following the same sequence of the original paper. All instructions previously mentioned for the preparation of article papers, case studies and technical notes also apply to the preparation of discussions.

Editorial Review

Each paper will be evaluated by reviewers selected by the editors according to the subject of the paper. The authors will be informed about the results of the review process. If the paper is accepted, the authors will be required to submit a version of the revised manuscript with the suggested modifications. If the manuscript is rejected for publication, the authors will be informed about the reasons for rejection. In any situation comprising modification of the original text, classification of the manuscript in a category different from that proposed by the authors, or rejection, the authors can reply presenting their reasons for disagreeing with the reviewer comments.

Submission

The author(s) must upload a digital file of the manuscript to the Soils and Rocks website.

Follow Up

The online management system will provide a password to the corresponding author, which will enable him/her to follow the reviewing process of the submitted manuscript at the Soils and Rocks website.

Volume 41, N. 1, January-April 2018

Table of Contents